Investigations on the impact of cadmium on sodium selenite-induced cellular effects

Zur Erlangung des akademischen Grades eines
DOKTORS DER NATURWISSENSCHAFTEN

(Dr. rer. nat.)

Fakultät für Chemie und Biowissenschaften

Karlsruher Institut für Technologie (KIT) - Universitätsbereich

genehmigte

DISSERTATION

von

M. Sc. Nutrition

Sarah Fremgaard Risnes

aus

Oslo (Norwegen)

Dekan: Prof. Dr. Peter Roesky

Referent: Prof. Dr. Andrea Hartwig

Korreferent: Prof. Dr. Mirko Bunzel

Tag der mündlichen Prüfung: 17.07.2015

Declaration

I hereby declare that I have solely written this doctoral thesis without using other than the specified resources. Moreover, I declare that this thesis has not been used elsewhere at another university or institution.

Karlsruhe, 01.06.2015 Sarah Fremgaard Risnes

Table of contents

1 Abstract

The essential trace element selenium is an indispensable part of selenoproteins and plays a major role in cellular protection against oxidative stress. Both anti-oxidative and pro-oxidative properties have been postulated as potential cancer-preventive mechanisms of selenium. However, because of the very narrow range between deficiency and toxicity, increased intake of selenium-containing dietary supplements could pose a potential oversupply risk for this essential trace element.

Inorganic, reducible selenocompounds, such as sodium selenite, exert pro-oxidative effects. Thiol groups in zinc-binding proteins could be potential molecular targets, e.g. transcription factors or DNA repair proteins, which could possibly disturb the maintenance of genomic stability. The tumor suppressor protein p53 performs important cellular functions in maintaining genomic stability by regulating expression of target genes relevant for control of the cell cycle, DNA repair mechanisms and induction of apoptosis. Previous research in our working group has shown that sodium selenite-induced cellular responses are mediated by p53. In contrast, effects induced by the organic and fully-reduced selenomethionine seemed to be independent of cellular p53 status. The underlying carcinogenic mechanisms of cadmium are complex and not yet completely understood. Changes in the structure and function of p53 through cadmium compounds have already been reported. Concurrent cadmium exposure and dietary selenium supplementation could indeed occur, which raises the question of how these different compounds interact within the cell. In this work, a possible inhibition by cadmium chloride of sodium selenite-induced p53-mediated effects was investigated. Also the organic compound selenomethionine was examined. As a cell model system, human colon carcinoma cell lines with different p53 status were chosen. Amongst these cell lines, the p53-proficient HCT116 cells possess an intact wild-type p53, while the isogenic p53-deficient HCT116 cell line lacks the tumor-suppressive functions from p53.

In contrast to selenomethinone, pronounced cytotoxic effects over a narrow concentration range with sodium selenite were seen in the p53-proficient HCT116 cells, but not in the p53-deficient cells. Sodium selenite induced oxidative stress by generating superoxide production accompanied by depletion of GSH, which subsequently induced pro-apoptotic signaling in a p53-dependent manner. Even though superoxide and other reactive oxygen species (ROS) are important for initiating signals to activate p53, the p53 functional activity may play an important role for sustaining sodium selenite-induced ROS generation by activating pro-oxidant genes, leading to an acceleration of apoptosis.

In combination with cadmium, sodium selenite-induced cell death was modulated. Cadmium appeared to inactivate p53, which inhibited the sodium selenite-induced GSH-depletion and superoxide production and pro-apoptotic signaling of p53. Assuming that the transcription factor p53

is unfolded by cadmium exposure, protective cellular mechanisms could be disturbed, resulting in accumulation of sodium selenite-induced DNA damage. In the p53-proficient HCT116 cells, accumulation of selenium was correlated to the onset of cytotoxicity following exposure to sodium selenite. Cell cycle arrest was first induced at comparably high concentrations. Using p53-deficient cells or through inhibition of p53 by cadmium made the cells much less sensitive to sodium selenite-induced apoptosis. The role of p53 as a critical downstream mediator of ROS signaling by sodium selenite treatment was supported by the significant attenuation of overall death in the p53-deficient cells. Following exposure to the selenocompounds, the obtained gene expression profiles exhibited distinct patterns, reflecting their distinct impact on cellular processes. Sodium selenite affected expression of genes in manifold pathways in HCT116 cells, mainly mediated via p53. Sodium selenite increased oxidative stress response by induction of Nrf2 target genes and by induction of metallothioneins (MTs). Induction of genes involved in cell cycle arrest, increased DNA repair and induction of apoptosis strongly indicated a p53-mediated response to DNA damage. Cadmium attenuated on the other hand the sodium selenite-induced and p53-mediated up-regulation of the genes involved in cell cycle arrest, DNA repair and apoptosis. However, the oxidative stress response was also highly activated by cadmium alone by induction of MTs and Nrf2 target genes. On the contrary, selenomethionine had much less impact on gene expression regulation than sodium selenite, demonstrating species-specific effects. Independently of p53, selenomethionine provoked cell cycle arrest by decreasing levels of proliferative genes and repressed DNA repair factors.

Previous observations linked p53 to the cellular uptake of sodium selenite in HCT116 cells, but not the uptake of selenomethionine. Increased uptake of sodium selenite in a p53-dependent manner was confirmed in this present study. The two types of HCT116 cells exhibited different basal extracellular thiol contents, which could influence the thiol-assisted reduction of sodium selenite in the extracellular space, and thus the bioavailability of sodium selenite. The reduced cytotoxic effects of sodium selenite observed following co-exposure to cadmium was hypothesized to be explained by a potential inhibition of the cellular uptake of sodium selenite, which could not be confirmed in this work. Unexpectedly, cadmium chloride improved dramatically the uptake of sodium selenite, but not selenomethionine, independent on the cellular p53 status.

To sum up, the inhibiting effect of cadmium on sodium selenite-induced apoptosis has not been described previously in literature, to the best of our knowledge. The data obtained with HCT116 colon cancer cells may help to explain sodium selenite and cadmium interaction when present in the human gastrointestinal tract.

2 Zusammenfassung

Das essentielle Spurenelement Selen ist Bestandteil verschiedener Selenoproteine, die eine wichtige Rolle beim zellulären Schutz vor oxidativem Stress spielen. Hinsichtlich der anti-kanzerogenen Wirkung von Selen werden anti-oxidative sowie pro-oxidative Eigenschaften diskutiert. Trotzdem ist eine gesteigerte Zufuhr von Selen, insbesondere durch selenhaltige Nahrungsergänzungsmittel, kritisch anzusehen, da es so möglicherweise zu einer Überversorgung kommt.

Anorganische, reduzierbare Selenverbindungen z.B. Natriumselenit besitzen pro-oxidative Eigenschaften. Dadurch ist es ihnen möglich, Thiolgruppen in zinkbindenden Proteinen wie z.B. Transkriptionsfaktoren oder DNA-Reparaturproteinen, anzugreifen, was möglicherweise die genomische Stabilität der Zelle gefährdet. Das Tumorsuppressorprotein p53 übernimmt wichtige Funktionen innerhalb der Zelle, unter anderem die Regulation der Transkription von Zellzyklus-Genen, der DNA-Reparatur und der Apoptose. Unser Arbeitskreis konnte bereits in einer früheren Arbeit zeigen, dass p53 die durch Natriumselenit induzierte zelluläre Antwort vermittelt. Im Gegensatz dazu war die zelluläre Antwort auf die Behandlung mit vollständig reduziertem Selenomethionin vom p53-Status unabhängig. Die zu Grunde liegende karzinogene Wirkung von Cadmium beruht auf komplexen Mechanismen und ist bisher noch nicht vollständig aufgeklärt. Bereits bekannt ist, dass Cadmiumverbindungen an p53 strukturelle und somit funktionelle Änderung auslösen. Hier stellt sich die Frage, inwieweit die o.g. Selenverbindungen innerhalb der Zelle mit Cadmium in Wechselwirkung treten können. Diese Arbeit untersucht, ob und inwieweit die durch p53 vermittelte Antwort der Zelle auf die Behandlung mit Natriumselenit bzw. Selenomethionin durch Cadmium inhibiert wird. Als Modell dienten Zellen mit unterschiedlichem Tumorsuppressorprotein p53-Status aus der humanen Kolonkarzinomzelllinie HCT116.

Im Gegensatz zu Selenomethionin wirkte Natriumselenit innerhalb eines engen Konzentrationsbereiches stark zytotoxisch auf p53-profizienten HCT116-Zellen, nicht jedoch auf die p53-defizienten Zellen. Aufgrund einer gesteigerten Superoxidproduktion und einer Abnahme von GSH induzierte die anorganische Selenverbindung oxidativen Stress in den p53-profizienten Zellen. Hierdurch kam es in Abhängigkeit von p53 zu einer Aktivierung pro-apoptotischer Signalwege. Da p53 bekanntlich selbst wird u.a. durch reaktive Sauerstoffspezie (ROS) aktiviert wird, vermuten wir, dass die funktionelle Aktivität von p53 eine Rolle beim Ausmaß der Natriumselenit-induzierten ROS-Generierung spielt, indem pro-oxidative Gene von p53 aktiviert werden.

Bei Co-Inkubation der p53-profizienten Zellen mit Cadmium kam es zu einer Hemmung des durch Natriumselenit induzierten Zelltods. Zudem wurden in Anwesenheit von Cadmium in den p53-profizienten Zellen die durch Natriumselenit ausgelöste GSH-Depletion, die vermehrte Superoxidproduktion sowie die pro-apoptotische Signalwirkung von p53 stark abgeschwächt. Unsere Untersuchungen weisen darauf hin, dass Cadmium zur Inaktivierung von p53 führt. Es wird vermutet, dass das p53 von Cadmium entfaltet wird und so wichtige protektive Mechanismen innerhalb der

Zelle gestört werden. Eine mögliche Folge ist eine Akkumulation von Natriumselenit-induzierten DNA-Schäden.

Bei p53-profizienten HCT116-Zellen korrelierte die Aufnahme von Selen mit dem Beginn der Zytotoxizität nach Exposition mit Natriumselenit. Ein Zellzyklusarrest wurde erst bei Behandlung der Zellen mit hohen Konzentrationen an Natriumselenit induziert. Bei Verwendung von p53-defizienten HCT116-Zellen oder durch die Hemmung von p53 durch Cadmium nahm die Empfindlichkeit der Zellen gegenüber Natriumselenit ab, was sich in einer geringeren Apoptoserate äußerte. Das Tumorsuppressorprotein p53 gilt als sogenannter „*Downstream*"-Mediator der ROS-Signalwirkung. Dies wurde durch die signifikante Abnahme toter Zellen der p53-defizienten Zelllinie nach Behandlung mit Natriumselenit bestätigt. Nach Exposition der Zellen mit den verschiedenen Selenverbindungen zeigten sich deutliche Muster in den Genexpressionsprofilen, was die unterschiedliche Beeinflussung zellulärer Prozesse widerspiegelt. Der Einfluss von Natriumselenit auf die Expression von Genen verschiedener Signalwege in HCT116-Zellen ist vom p53-Status der jeweiligen Zelle abhängig. Durch Aktivierung von Nrf2 und Metallothioneinen (MT) verstärkte Natriumselenit die oxidative Stressantwort. Zellzyklus-Arrest, verstärkte DNA-Reparatur und Apoptose-Induktion wiesen stark auf eine p53-vermittelte Zellantwort auf DNA-Schäden hin. Cadmium wiederum hemmte die durch Natriumselenit induzierte und durch p53-vermittelte Hochregulierung derjenigen Gene, die an Zellzyklus, DNA-Reparatur und Apoptose beteiligt sind. Jedoch aktivierte Cadmium selbst bereits die oxidative Stressantwort deutlich, u.a. auch über die Induktion von MT- und Nrf2-Zielgenen. Der Einfluss von Selenomethionin auf die Genexpression war im Vergleich zu Natriumselenit allerdings deutlich schwächer. Festgestellt wurde jedoch, dass Selenomethionin durch die Herunterregulierung von proliferativen Genen sowie durch die Unterdrückung von DNA-Reparaturgenen und unabhängig vom p53-Status einen Zellzyklusarrest bewirkte.

Vorherige Untersuchungen an HCT116-Zellen weisen auf einen Zusammenhang zwischen p53 und der zellulären Aufnahme von Natriumselenit, nicht jedoch von Selenomethionin, hin. Diese Arbeit bestätigt eine gesteigerte, p53-abhängige Aufnahme von Natriumselenit in die Zelle. Zudem wurde gezeigt, dass die p53-profizienten Zellen im Vergleich zu den p53-defizienten Zellen einen höheren basalen extrazellulären Thiolgehalt aufwiesen. Die extrazelluläre thiolassistierte Reduktion von Natriumselenit wird somit als weiterer Grund für dessen gesteigerte Bioverfügbarkeit diskutiert. Die Hypothese, dass die geringere zytotoxische Wirkung von Natriumselenit bei Co-Inkubation mit Cadmium auf einer verminderten Aufnahme von Natriumselenit in die Zellen beruht, bestätigte sich allerdings nicht. Hingegen wurde unerwarteterweise festgestellt, dass Cadmium die Bioverfügbarkeit von Natriumselenit in beiden Zelllinien verbesserte. Die Bioverfügbarkeit von Selenomethionin wurde hingegen durch Cadmium nicht beeinflusst. Nach unserem besten Wissen wurde die inhibierende Wirkung von Cadmium auf die Natriumselenit-induzierte Apoptose in der Literatur bisher nicht beschrieben. Die erhaltenen Daten aus dem verwendeten Zellmodell der HCT116-Kolonkarzinomzellen können möglicherweise zu einem besseren Verständnis der Wechselwirkungen zwischen Natriumselenit und Cadmium im Magen-Darm-Trakt des Menschen beitragen.

3 Introduction

3.1 Selenium

3.1.1 Occurrence, sources and exposure to selenium

Selenium was discovered in 1817 by the Swedish chemist Jöns Jakob Berzelius. As a metalloid with the atomic number 34, it belongs to the group 16 of the oxygen family, the chalcogens. Consequently, selenium shares some of the physico-chemical properties of oxygen and sulfur (Jacob *et al.* 2003). It was originally recognized as a toxic element due to its toxicity in occupationally exposed people, while its essentiality in higher organisms was discovered only in 1957 through its role in selenoproteins. The industrial uses of selenium include, for instance, electrical components, photocopier manufacture, glass manufacture, metal alloys, as well as anti-dandruff shampoo (Johnson *et al.* 2010). While the range between deficient, essential and toxic doses of selenium is very narrow, it is indeed required in trace levels in the diet, providing crucial importance to human health (Rana 2008; Rayman 2000; Rayman 2012).

The content and species of this essential trace element in plant foods as well as animal foods depend on environmental factors, especially the quantity and species of selenium to which the animal or plant is exposed (Fairweather-Tait *et al.* 2010). Globally, selenium concentrations in soils range from 0.4 mg/kg up to 1200 mg/kg, whereby higher concentrations derive from seleniferous materials, such as sand stones and lime stones. Such seleniferous soils are widespread in parts of the United States, Canada, South America, China and Russia, while European soils as well as some parts of China are generally of low selenium concentration. Significant inputs of selenium to soils occur also from natural (e.g. volcanoes) and anthropogenic (e.g. agricultural fertilizers) sources (Fairweather-Tait *et al.* 2011; Johnson *et al.* 2010). Therefore, given the wide range of selenium content in soils, the intake of selenium varies hugely worldwide, ranging from deficient to toxic concentrations. Dietary intakes range from 7 µg per day to 4990 µg per day with the mean values of 40 µg per day in Europe and 93-134 µg per day in the USA (Rayman 2012). Selenium-containing supplements add to these intakes, especially in the USA where an estimated 50 % of the population take dietary supplements (Rayman 2012). The main food groups providing selenium are bread and cereals, meat, fish, eggs and dairy products. The amount of selenium in plant foods is generally low, except from Brazil nuts and certain vegetables which are considered to be selenium-accumulating plants, including onions, garlic, leeks, shallots, and chives (*Allium* family), and broccoli, cabbage, Brussel sprouts and cauliflower (*Brassica* family) (Fairweather-Tait *et al.* 2010).

There is an ongoing discussion whether people are sufficiently supplied with selenium or whether supplementation is recommended (Rayman 2012; Schrauzer 2001). Selenomethionine is the predominant species of selenium in most natural and non-enriched food. However, the only permitted selenium species added to foods for special nutritional use, such as baby formula milk and total parenteral nutrition products, are inorganic forms such as selenate and selenite. Worldwide, there are many different supplements with varying doses and forms of selenium, and selenium is often included in multivitamin-mineral supplements. The selenium amount in supplements analyzed in the U.S. shows that they provide between 10 and 200 µg per day (Schrauzer 2001). The German Federal Institute for risk assessment (in German, *Bundesinstitut für Risikobewertung,* (BfR)) recommends that selenium intake from dietary supplements should not exceed more than 30 µg daily. The BfR also concludes that previous studies have not shown that organic selenium compounds for use in dietary supplements are advantageous over selenite-containing supplements. A Cochrane review on antioxidant supplements concluded that consuming additional selenium from non-food sources provides no clear benefits (Bjelakovic *et al.* 2008). European populations are generally of low selenium status compared to the US population due to low concentrations in crops grown in Europe relative to North America, resulting in a more than tenfold difference in selenium concentrations between UK and US wheat (Johnson *et al.* 2010). Finland has since 1985 supplemented their soil nationwide with multi-nutrient fertilizers including selenium in the form of sodium selenate due to extremely low selenium intake in the 1970's. Monitoring the nationwide fertilization during 27 years has been shown to be effective and safe in improving animal health, increasing selenium levels in milk, eggs and the whole food chain, and thus increasing the selenium intake of the whole population. As a consequence, the average individual selenium intake in Finland has increased from about 30 µg per day to 100 µg per day (Alfthan *et al.* 2014). In a study from New Zealand, daily consumption of Brazil nuts has shown to effectively increase selenium status to the level of 100 µg selenium as selenomethionine. The inclusion of this high-selenium food in the diet could avoid the need for fortification or supplements to improve the selenium status (Thomson *et al.* 2008). However, since the selenium content of the nuts is highly dependent on the amount of selenium present in the soil, daily consumption of Brazil nuts should be limited to avoid toxicity (Dumont *et al.* 2006).

3.1.2 Absorption, metabolism and properties of selenium

Selenium absorption pathways are not yet completely characterized. Inorganic forms, e.g. selenate and selenite, seem to be well-absorbed, but not as well-retained in the body as organic forms, e.g. selenocysteine and selenomethionine (Fairweather-Tait *et al.* 2010). Most forms of selenium are absorbed efficiently, but the identification of responsible transport proteins for uptake of dietary selenium remains uncertain (Fairweather-Tait *et al.* 2011). Organic selenoamino acids appear to be

effectively transported by various intestinal amino acid transporters (Nickel *et al.* 2009), while multifunctional anion exchangers of the SLC26 family have been proposed as candidates for uptake of selenate (Fairweather-Tait *et al.* 2011). The selenite transporter remains to be identified. However, studies utilizing anion channel blockers to investigate the mechanism of selenite uptake have suggested that selenite uptake is an active process mediated by an anion transporter (Ganyc and Self 2008) or partly mediated by phosphate transporters in plants (Li *et al.* 2008). Figure 3.1 shows the chemical structures of the two investigated selenocompounds, sodium selenite and selenomethionine.

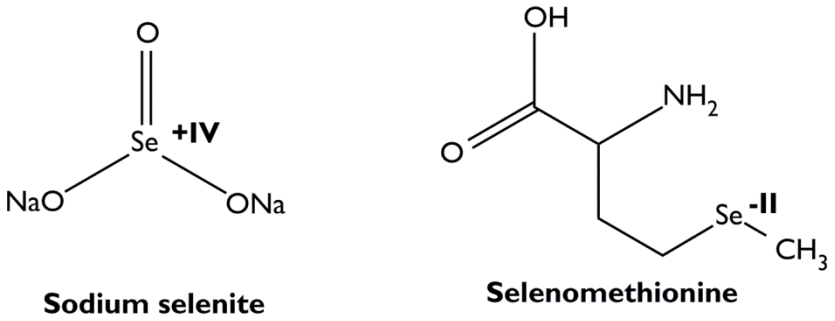

Figure 3.1: Chemical structures of sodium selenite and selenomethionine.

Absorbed dietary selenium is released from enterocytes into the portal circulation and is used for biosynthesis of intestinal selenoproteins. The further selenium metabolism depends highly on the form in which they are present in plasma. Figure 3.2 provides an overview of the metabolism of selenomethionine and sodium selenite. Hydrogen selenide (H_2Se) is the central metabolite of both organic and inorganic forms. Selenomethionine, selenocysteine, selenate and selenite enter the selenide pool by different pathways, and from this point used for synthesis of selenoproteins or excreted in the urine as selenosugars. Selenomethionine is converted via transsulfuration to selenocysteine or directly through the γ-lyase reaction into methylselenol (CH_3SeH). This is followed by a demethylation reaction and the resulting metabolite is directed into the selenide pool by selenocysteine lyase. In comparison to selenomethionine, selenite is first reduced to selenodiglutathione (GSSeSG) and then metabolized to hydrogen selenide by glutathione reductase or thioredoxin reductase under the consumption of NADPH. H_2Se can react with O_2 to form elementary selenium and superoxide ($O_2^{\bullet-}$), which has been proposed to be responsible for the induction of apoptosis by multiple selenocompounds (Brigelius-Flohe 2008). Hydrogen selenide is also phosphorylated to selenophosphate, a substrate for selenoprotein biosynthesis. Through this reductive pathway, selenocysteine, as the 21st amino acid, can finally be incorporated within the active sites of selenoproteins in response to a UGA codon in the respective mRNA (Brigelius-Flohe 2008; Brozmanova *et al.* 2010).

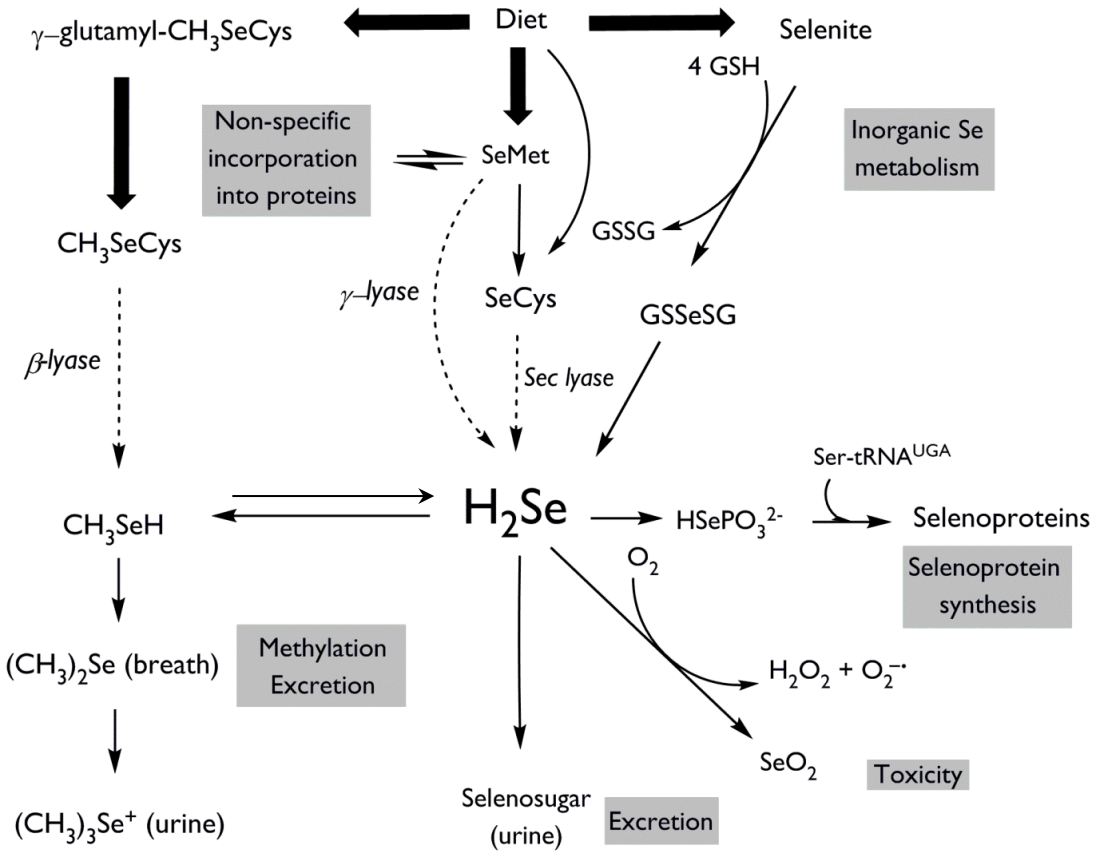

Figure 3.2: Metabolism of selenomethionine and sodium selenite. GSH: glutathione, GSSG: glutathione disulfide, GSSeSG: selenodiglutathione, CH_3SeH: methylselenol, H_2Se: hydrogen selenide, O_2•−: superoxide. Modified from (Brigelius-Flohe 2008; Fairweather-Tait *et al.* 2010; Letavayova *et al.* 2006).

Selenium plays a unique role among the essential trace elements since it is genetically encoded for incorporation into proteins, as the constitutive part of the 21st amino acid, selenocysteine. There are 25 known selenoprotein genes, and all identified selenoproteins have their selenocysteine residue in the functional catalytic site (Lu and Holmgren 2009). Two main groups of selenoproteins exist according to the location of the selenocysteine within the protein. The first group contains selenocysteine close to the C-terminal region, e.g. thioredoxin reductase (TrxRs), while selenocysteine is found close to the N terminal region in the second group, e.g. glutathione peroxidases (GPxs) (Lu and Holmgren 2009). Because the selenol is fully ionized at normal physiological pH, it is more reactive than thiol groups (Behne and Kyriakopoulos 2001). Although several selenoenzyme families, including GPxs, TrxRs and deiodinases (DIOs), are well-described (Jacob *et al.* 2003), the exact function of many selenoproteins is still unknown (Arner 2010; Brozmanova *et al.* 2010).

From a biochemical point of view, selenium substitutes for sulfur in defined cysteines present in selenoproteins. Selenium differs from sulfur by its redox potentials and stabilities of oxidation states, providing multiple catalytic potentials. Thus, it can function both as a reductant and as an oxidant. A remarkable feature of selenium consists of its ability to oxidize thiols under reducing conditions that are present in the cytosol (Jacob *et al.* 2003; Zeng and Combs, Jr. 2008). Unlike the organic forms selenomethionine and selenocysteine, in which selenium is present in the reduced state (selenide: Se 2-), the inorganic salts frequently provided as dietary supplements contain selenium in oxidized forms (selenite: Se 4+; selenate: Se 6+) (Finley 2006). Cellular effects induced by different species deserve special attention. As part of GPxs, selenium is considered as an antioxidant, but it may also exert pro-oxidative properties, depending at least in part on the selenium species under investigation. A moderate genotoxic activity of selenium compounds has been found in several *in vitro* systems (Kramer and Ames 1988), the extent varying between different selenium species investigated in our laboratory (Hall 2008; Klaus 2009). However, not only damage induction but also the cellular response to damage, for example the involvement of p53, depends on the chemical form of selenium. Zhao and co-workers showed that selenite induced apoptosis by producing superoxide, which activated p53. In turn, activation of p53 then synergistically enhanced superoxide production and apoptosis induced by selenite (Zhao *et al.* 2006).

3.1.3 Selenium in human health

Despite its very low level in humans, the micronutrient selenium is unique among the metal trace elements due to its genetically encoded incorporation via selenocysteine into selenoenzymes and position at their active catalytic center. Selenium status and the redox-protective effects of selenoproteins have potential consequences for health. While most selenoproteins participate in general antioxidant defense and redox state regulation, namely GPxs respectively TrxRs, other selenoproteins play more specific essential roles. For example, the DIOs are crucially involved in thyroid hormone metabolism, and GPx4 is essential for spermatogenesis and selenophosphate synthetase 2 (SPS2) participates in selenoenzyme biosynthesis (Roman *et al.* 2014). The immune response is affected by selenium as well, but the underlying mechanisms are poorly understood (Hoffmann and Berry 2008). A decrease in ROS from oxidative stress and the modulation of inflammatory signaling pathways via the antioxidants and redox functions of selenoproteins have been postulated (Fairweather-Tait *et al.* 2011). Selenium exhibits anti-inflammatory properties by inhibiting the NF-κB cascade that induces the production of pro-inflammatory interleukins and tumor necrosis factor-α (TNF-α) (Duntas 2009).

The range of intake between selenium deficiency and toxicity is very narrow (Fairweather-Tait *et al.* 2011). An intake of about 20 µg per day for adults is generally accepted as the minimum needed to prevent onset of Keshan disease. At low dietary intake, selenium satisfies the dietary need for selenoprotein biosynthesis, which is recommended to be 30-40 µg per day by the World Health Organization (WHO) or 55 µg of selenium per day for healthy adults recommended by the US Institute of Medicine (Dennert *et al.* 2011). In order to prevent selenosis, the US Institute of Medicine has set an upper limit of 350-400 µg per day (Dennert *et al.* 2011). However, some studies have observed selenium intake levels of 750-850 µg per day with no signs of selenium toxicity (Ramoutar and Brumaghim 2010).

Selenium deficiency can results in diseases such as hypothyroidism, weakened immune defense and cardiovascular diseases (Ramoutar and Brumaghim 2010). Keshan disease is an endemic cardiomyopathy observed in selenium-deficient areas of China, where the main clinical features are acute or chronic episodes of a heart disorder characterized by cardiogenic shock or congestive heart failure. A preventive effect of selenium supplementation against Keshan disease was identified in the 1970's in inhabitants with low selenium status (Fairweather-Tait *et al.* 2011). A disease also present in selenium-deficient areas is the Kashin-Beck disease, an endemic, chronic degenerative osteoarthropathy. The etiology of the disease is not known, but the risk factors appear to involve mycotoxins and organic substances in portable water, Coxsackie B3 virus infection and deficiency in certain trace elements, mainly iodine and selenium. Selenium supplementation seems to be effective at preventing an exacerbation of the disease and in promoting healing (Fairweather-Tait *et al.* 2011).

Selenium toxicity is much less common than deficiency, but may occur as a result of over-supplementation or through high levels in food. Acute toxic symptoms are associated with extremely high intakes of selenium (3200-7600 µg per day) (Roman *et al.* 2014). There are reports on miscalculated dietary supplements entering the market posing a health risk to users (MacFarquhar *et al.* 2010). However, only limited data regarding selenium toxicity for humans are available, which make the establishment of sound upper limit recommendations for selenium intake difficult. Clinical signs of chronic selenosis include garlic odor of the breath and skin, teeth deformation, skin lesions, brittle hair, thickened and stratified nails and loss of hair and nails in the case of dietary intake of 5 mg per day (Fairweather-Tait *et al.* 2011; Ramoutar and Brumaghim 2010).

Cancer

During the last decades, there has been an ongoing discussion on potential cancer preventive effects of higher than dietary levels of selenium and beneficial roles of dietary selenium supplementation. The landmark cancer study, Nutritional Prevention of Cancer (NPC) Trial, a randomized, double-blind,

placebo-controlled study, introduced the rationale for the use of selenium as a chemopreventive agent (Clark *et al.* 1996). Secondary results from this skin cancer prevention trial showed a significant reduction in the overall incidence of prostate cancer by selenium supplementation. Nevertheless, even though some studies point towards a reduction of, for instance, prostate tumors by selenium, the pre-terminated Selenium and Vitamin E Cancer Prevention Trial (SELECT) did not support this assumption (Lippman *et al.* 2009). The SELECT-study was the largest cancer prevention trial ever performed, randomizing more than 35 000 healthy, middle-aged men into four groups, where supplementation with selenium and vitamin E were tested separately or in combination. The primary endpoint was biopsy-confirmed prostate cancer, and the planned duration of the trial was 12 years. However, the trial was terminated after 7 years due to no observed effect on prostate cancer risk in neither of the groups. Instead, a small, non-significant increase in diabetes type 2 was indicated (Lippman *et al.* 2009). However, based on secondary findings to the SELECT follow-up, it would be more correct to report no effect in type 2 Diabetes risk (Klein *et al.* 2011). In addition, diabetes was also a secondary outcome on follow-up of the parent NPC trial (Stranges *et al.* 2007). Both studies had obvious flaws, and have met several counterarguments (Muecke *et al.* 2010; Rayman and Stranges 2013; Steinbrenner *et al.* 2013). The SELECT study results may be attributed to the relative high selenium status within the study population and to the use of selenomethionine, which may not be the most effective anti-carcinogenic form of selenium since selenomethionine is incorporated non-specifically into non-selenoenzymes due to its similarity to methionine. Therefore, choosing sodium selenite as a supplement might represent a better alternative because the effects of the supplementation can be verified by increased serum selenium or circulating selenoprotein concentrations (Fairweather-Tait *et al.* 2011; Muecke *et al.* 2010).

The mechanisms behind potential anti-cancerogenic effects of selenium are still unclear (Zhao *et al.* 2006). Postulated underlying mechanisms for effects of selenium on cancer may include regulation of cell cycle and apoptosis, antioxidant activity of selenoproteins resulting in the protection of DNA, proteins and membrane lipids, as well as immune system modulation (Fairweather-Tait *et al.* 2011). However, pro-oxidative properties of selenium, and not anti-oxidative, may best account for observed anti-cancer effects (Drake 2006). One possible mechanism might be zinc release from metallothionein via oxidation of thiol groups (Chen and Maret 2001). Nevertheless, other zinc-binding proteins could be also potential molecular targets, e.g. transcription factors, DNA repair proteins or tumor suppressors, which could possibly disturb the maintenance of genomic stability (Blessing *et al.* 2004). Increasing attention has been drawn towards polymorphisms within selenoprotein genes and their association with enhanced cancer risk (Zhuo and Diamond 2009). The effectiveness of dietary selenium supplementation depends on many factors, such as baseline selenium status, age, gender, genetic background of an individual, type of cancer, and time point of

intervention, in addition to metabolic conversion and dose of the applied selenocompound. The outcomes of human studies on cancer prevention by selenium have been, however, so far inconsistent and disappointing (Steinbrenner *et al.* 2013). Experimental human studies indicate overall that selenium does not reduce cancer risk. No convincing evidence has so far been provided that individuals with so-called low selenium intake, that is, in the order of 20-70 µg per day, may reduce cancer risk by increasing their selenium exposure (Vinceti *et al.* 2013). Vinceti and co-workers (2014) updated a Cochrane review on selenium in cancer prevention from 2011, which included 63 studies with more than one million participants. They reported that individuals with higher selenium levels or intake had a lower incidence of certain cancer types (e.g. prostate cancer), but no effect on other cancers (e.g. breast cancer) was observed. It was, however, not possible to determine whether selenium levels or intake were really the reason for the lower risk of cancer from these studies. A healthier lifestyle as well as healthier nutritional intake and overall better living conditions are important factors influencing cancer risk. Taken together, in addition to the fact that the two randomized controlled trials, NPC and SELECT, failed to provide evidence on cancer prevention by selenium supplementation in men, the authors recommended further evaluation of the effects of selenium supplements in populations according to their nutritional status as the effects may differ between low-supplied and well-supplied individuals. Currently, there is no convincing evidence that regular intake of selenium supplements is beneficial in individuals with regard to their cancer risk (Vinceti *et al.* 2014).

Type 2 Diabetes Mellitus

Epidemiological data suggests potential pro-diabetic effects of high selenium intake in humans. In well-nourished populations, high selenium exposure may be associated with type 2 diabetes or insulin resistance (Rayman and Stranges 2013). Results from *in vitro* and *in vivo* studies suggest that inorganic selenium can enhance insulin sensitivity by mediating insulin-like actions, but little information is known about insulin-like actions for selenocompounds such as selenomethionine (Stranges *et al.* 2010). Selenoproteins and selenocompounds may interfere at different stages with insulin-induced signal transduction, eventually leading to a dysregulated carbohydrate metabolism (Steinbrenner *et al.* 2011; Steinbrenner 2013). Selenium status and GPx1 expression have been reported to affect the activity of insulin-antagonistic phosphatases that are regulated by hydrogen peroxide-mediated reversible oxidation of catalytic cysteine residues. GPx1 and selenoprotein P (Sepp1) inhibited phosphorylation (activation) of key mediators in energy metabolism, such as protein kinase B (Akt) and AMP activated protein kinase (AMPK) in liver and skeletal muscle (Steinbrenner 2013). The regulation of Sepp1 as a gluconeogenic enzyme provides a likely explanation for reported cross-sectional associations of high plasma selenium/Sepp1 levels in hyperglycemia and type 2 Diabetes

(Steinbrenner 2013). However, increased plasma selenium levels might be both a consequence and a cause of diabetes. A dysregulated carbohydrate metabolism in diabetes might affect plasma selenium and Sepp1 levels, as the hepatic biosynthesis of Sepp1 is suppressed by insulin and stimulated under hyperglycemic conditions (Steinbrenner 2013).

More information is needed to identify the optimal range of selenium intake and status in order to minimize adverse effects in glucose metabolism while optimizing type 2 Diabetes prevention (Stranges *et al.* 2010). A post-hoc analysis of the NPC trial showed a significantly increased risk of type 2 Diabetes in those supplemented with selenium (200 µg per day as selenium yeast) and followed for a mean of 7.7 years (Stranges *et al.* 2007). In the SELECT study, selenium supplementation had no effect on risk of type 2 Diabetes after a median follow-up of 5.5 years (Klein *et al.* 2011). Importantly, the data from the SELECT study were not adjusted to the general increase of diabetes in the US (Muecke *et al.* 2010) seen in the context that Diabetes mellitus affected over 170 million people worldwide in 2000, and is estimated to reach 366 million people in 2030, with more than 90 % of patients suffering from type 2 Diabetes (Wild *et al.* 2004). Due to the experimental design of the SELECT trial, the study is neither adequate to prove the ineffectiveness of selenium in prevention of prostate cancer nor to estimate the risk of selenium triggering the onset of diabetes (Muecke *et al.* 2010). While a link between certain selenoproteins and glucose metabolism or insulin resistance is clear, the relationship between selenium and type 2 Diabetes is undoubtedly complex. It is possible that the relationship is U-shaped, with harm occurring both below and above the physiological range for optimal activity of some or all selenoproteins (Rayman and Stranges 2013).

3.2 Cadmium

3.2.1 Occurrence, sources and exposure to cadmium

In 1817 cadmium was discovered concurrently by the German researchers Friedrich Strohmeyer and Karl Samuel Hermann as an impurity of zinc carbonate. This chemical element with the atomic number 48 belongs to the transition metals in group 12 of the Periodic table, chemically similar to zinc and mercury. Cadmium and its compounds occur predominantly in oxidation state 2+, like zinc. It appears as a white silvery bright metal, naturally and frequently bound to zinc in zinc ores, as well as to lead and phosphate. Industrially, cadmium is primarily used in the production of nickel-cadmium batteries, alloys, in pigments such as inorganic coloring agents as well as in stabilizers for synthetic materials (Pinot *et al.* 2000). Furthermore, cadmium is present in phosphate minerals and sludge used as agricultural fertilizers. The agricultural as well as the industrial utilization of cadmium are supposed

to be the main causes of the dispersal of cadmium in the environment and in food (Satarug *et al.* 2003).

Cadmium is a heavy metal with no known biological function in humans (Pinot *et al.* 2000). Present in food and tobacco smoke it is a widespread environmental pollutant. The major sources of human exposure to cadmium are tobacco smoke and diet, as well as occupational exposure. Cadmium is taken up in the body by inhalation and ingestion, and exhibits a very long biological half-life (10-30 years) (CONTAM 2009; Waalkes 2003). The International Agency for Research on Cancer (IARC) classified cadmium in group 1 as a human carcinogen based on data from human occupational exposure delivering sufficient evidence for lung cancer and limited evidence for kidney, liver and prostate cancer (IARC 1993; WHO 2011).

Plants are known to accumulate cadmium from the soil due to a ready uptake of cadmium by the root system in plants. High consumption of cereals and vegetables is recommended due to a variety of health reasons. However, these foods are the main contributors of dietary cadmium intake and found to be most significant sources of cadmium for the non-smoking population (Satarug *et al.* 2003). Meat is also a dietary source of cadmium, but to a lower degree. Organ meats such as kidneys and liver could contain higher levels of cadmium due to its accumulation in these organs. Fish is thought to contain lower levels of cadmium, while shellfish and mollusks may accumulate larger amounts. It seems likely that vegetarians or individuals high consumption of seafood may have more cadmium accumulation than the general population (Nawrot *et al.* 2010; Satarug *et al.* 2003). Tobacco plants are known to accumulate cadmium in their leaves (Scherer and Barkemeyer 1983), which makes tobacco smoke a major exposure source to cadmium. Each cigarette is estimated to contain 1 to 2 µg cadmium, and smoking one cigarette results in a net inhalation of 0.1 to 0.2 µg cadmium (Pinot *et al.* 2000). During the burning process, cadmium oxide is formed and readily absorbed. Up to 50 % of the inhaled cadmium enters the systemic circulation of smokers (Satarug *et al.* 2003).

Gastrointestinal absorption of cadmium varies greatly between individuals, genders and foods (Satarug *et al.* 2003), however, gastrointestinal cadmium absorption is generally lower than its respiratory absorption (Nawrot *et al.* 2010). The amount of absorbed cadmium in the gastrointestinal tract is proportional to the concentration of cadmium in the food product (Nawrot *et al.* 2010). The absorption fractions are estimated to be between 5 % and 8 % (Flanagan *et al.* 1978). The uptake of cadmium is increased if the nutritional status of calcium, iron or zinc is low (Nawrot *et al.* 2010). Iron deficiency is considered to be one of the main nutritional deficiency disorders affecting large fractions of the European population (Nawrot *et al.* 2010). Iron status can significantly influence the uptake of cadmium (Flanagan *et al.* 1978; Vahter *et al.* 1996). High absorption rates of cadmium occurred during iron deficiency and iron overload due to up-regulation of the duodenal iron transporter divalent

metal transporter 1 (DMT1). Despite equal or even lower exposure levels, women absorb and accumulate cadmium to a higher extent than men (Akesson *et al.* 2002). Due to a higher prevalence of iron depletion in women than in men, low iron status is probably the main reason why cadmium is more accumulated in women (Vahter *et al.* 1996).

In 2009, the EFSA Panel on Contaminants in the Food Chain (CONTAM) established a tolerable weekly intake (TWI) for cadmium of 2.5 µg per kg body weight (CONTAM 2009). The mean exposure for European adults is close to the TWI, while subgroups such as vegetarians, children, smokers and people living in highly contaminated areas may exceed the TWI by about twofold. Although the risk for adverse effects in kidney function at an individual level is very low, the CONTAM Panel concluded that the current cadmium exposure at the population level should be reduced. The TWI from 2009 was reaffirmed in 2011 in order to ensure a high level of protection to consumers (CONTAM 2011). Moreover, in 2010 the Joint FAO/WHO Expert Committee on Food Additives (JECFA) concluded that daily ingestion of cadmium in food has a small or negligible effect on overall exposure, in spite of the long half-life of cadmium. Health risks due to cadmium exposure should be assessed over months. The Committee established therefore a monthly value of tolerable intake as provisional tolerable monthly intake (PTMI), which was set to 25 µg per kg body weight. The estimates of cadmium exposure through the diet in all age groups, including consumers with high exposure and with special dietary habits (e.g. vegetarians) were below the PTMI (FAO/WHO 2010). However, taking non-dietary exposure into account, it is anticipated that the total exposure of some subgroups of the population could exceed the JECFA PTMI as well as the CONTAM TWI (CONTAM 2011).

There are some prevention strategies to reduce exposure to a toxic metal like cadmium in order to reduce adverse health effects. Reduction of cadmium pollution must be enforced by further proper legislation. To reduce the transfer of cadmium from soil to plants, the soil cadmium bioavailability should be reduced by maintaining agricultural and garden soil close to neutral. Smoking cessation is effective in reducing the self-induced cadmium exposure, while a balanced iron intake is effective in reducing the bioavailability of cadmium present in the intestine by reducing its absorption (Nawrot *et al.* 2010).

3.2.2 Cadmium in human health

As a chemical element, cadmium cannot be degraded. Approximately 50 % of the body burden of cadmium can be found in the kidneys, whereas 15 % and 20 % are in the liver and the muscles, respectively (Nawrot *et al.* 2010). Cadmium can cross cell membranes via different mechanisms e.g. metal transporters, and once inside the cell, it binds to ligands with exceptional affinity

e.g. metallothioneins (MTs) (CONTAM 2009). Cadmium is not easily cleared by the cells, and the poor efficiency of cellular export systems explains the long storage time of cadmium in storage tissues such as the kidneys, the liver and the intestine. Because cadmium exposure induces the synthesis of MTs in several tissues, it is suggested that MT binding decreases cadmium toxicity. The ability of the liver to synthesize MT appears to be sufficient to bind all the accumulated cadmium (CONTAM 2009). Cadmium binds to albumin in the blood, and is to a large extent taken up by the liver, where it induces the synthesis of MTs. Cadmium is excreted in bile mainly bound to glutathione or released into the plasma bound to MT. The cadmium-MT complex is filtered through the renal glomeruli and then reabsorbed by proximal tubular cells until the critical concentration is reached. The critical concentration of cadmium is reached when the tubular cells are not capable of enough MT synthesis to neutralize free cadmium ions produced by lysosomal degradation of cadmium-MT complex. When the critical concentration is exceeded, tubular damage results in increased enzymuria, low molecular weight proteinuria and increased excretion of cadmium either in complex with MT or free ion (CONTAM 2009). Chronic exposure to cadmium results not only in its accumulation in the kidneys and liver, but also in the endothelium of blood vessels and vascular smooth muscle cells (Nawrot *et al.* 2010).

Cadmium has for decades been recognized as both carcinogenic and toxic. Increasing epidemiological evidence suggests that chronic low dose exposure to cadmium appears to be associated with negative effects on human health, more than previously assumed (Nawrot *et al.* 2010). Direct interactions between cadmium and DNA appear to be of minor importance. The genotoxicity of cadmium could instead be explained by indirect mechanisms (Hartwig 2010). Frequently discussed underlying mechanisms have been demonstrated in diverse experimental systems, such as generation of reactive oxygen species (ROS), inhibition of DNA repair enzymes and deregulation of cell proliferation (Hartwig 2010), but also aberrant gene expression (Joseph 2009). With respect to DNA repair processes, cadmium has been shown to disturb nucleotide excision repair (NER), base excision repair (BER) and mismatch repair (MMR). Consequences are increased susceptibility towards other DNA-damaging agents and endogenous mutagens. Furthermore, cadmium induces cell proliferation and inactivates negative growth stimuli (Giaginis *et al.* 2006; Hartwig 2010). The physicochemical properties of the divalent cadmium ion may help to explain observed biological effects. The ion easily substitutes for the calcium ion in biological systems because of equal charge and radius. In the case of the zinc ion, the radius of the cadmium ion is larger, but cadmium is still able to substitute for divalent zinc ions in many enzymes and transcription factors (Beyersmann and Hartwig 2008). In particular, cadmium interferes with the structure and function of the tumor suppressor protein p53. Zinc plays a crucial role in the structure of p53 and thereby its function by ensuring correct folding of the DNA binding domain of p53, which is essential for DNA binding and

transcriptional activity. Cadmium has been demonstrated to alter the zinc binding of p53, leading to an accumulation of p53 in cells consisting mainly of unfolded and consequently inactive p53 (Hainaut and Mann 2001; Meplan *et al.* 1999; Schwerdtle *et al.* 2010). The impairment of DNA repair by cadmium may be especially harmful in cells adapted to cadmium. Cadmium induces several genes responsible for cadmium and ROS tolerance such as those coding for metallothionein, glutathione synthesis and function, catalase and superoxide dismutase. Prolonged cell survival in combination with a tolerance of cadmium toxicity may increase the chance for accumulation of critical mutations (Beyersmann and Hartwig 2008).

3.3 Oxidative stress

Cells are able to balance the production of oxidants and antioxidants under normal physiological conditions. Oxidative stress arises when cells are subjected to either excess levels of ROS or antioxidant depletion, disturbing the cellular redox balance in favor of the pro-oxidants. Oxidative stress overwhelms antioxidant protection, which subsequently could lead to oxidative damage of cellular macromolecules. ROS are natural by-products of metabolic pathways under normal conditions, and increased ROS levels provide a major relevant function in signal transduction (Thevenod 2009). However, because ROS are highly reactive chemical species, they can cause substantial damage to tissue and cellular macromolecules. Oxidative stress may result in the accumulation of dysfunctional proteins, lipid peroxidation, damaged DNA and apoptosis caused by exogenous and endogenous sources (Ercegovac *et al.* 2010). Exogenous factors, such as ozone, UV radiation, chemicals, and also life style-related risk factors e.g. eating habits, smoking, alcohol consumption and physical activity could increase cellular oxidative stress (Willcox *et al.* 2004). During mitochondrial reduction of oxygen to water, 1-2 % of the oxygen is released, escaping general metabolism and forming superoxide anions, hydrogen peroxide and hydroxyl radicals. While hydrogen peroxide and superoxide anions cannot react with DNA, hydroxyl radicals and singlet oxygen can directly damage DNA when they are formed in close proximity to DNA (Pryor 1986). Figure 3.3 shows the major cellular forms of ROS, how they are formed and subsequently metabolized. Superoxide anion radicals can spontaneously convert to hydrogen peroxide or be converted by superoxide dismutase (SOD) to oxygen and hydrogen peroxide. From hydrogen peroxide, reactive hydroxyl radicals can be formed via catalytic effects of transition metal ions, especially Fe^{2+}. Where iron ions are present, hydroxyl radicals can form via the Fenton reaction, as hydrogen peroxide could reach all cell compartments (Halliwell and Gutteridge 1990). Hydroxyl radicals possess the ability to induce numerous types of DNA damage, such as DNA strand breaks, oxidative base modification and AP sites, while singlet oxygen reacts specifically with guanine bases and forms thereby more oxidative DNA base modifications than DNA strand breaks (Halliwell and

Aruoma 1991; Pflaum *et al.* 1994). Oxidative DNA damage could arise by direct formation of ROS, through inactivation of cellular detoxifying systems, such as GSH depletion, inhibition of anti-oxidative enzymes, or inhibition of DNA repair proteins.

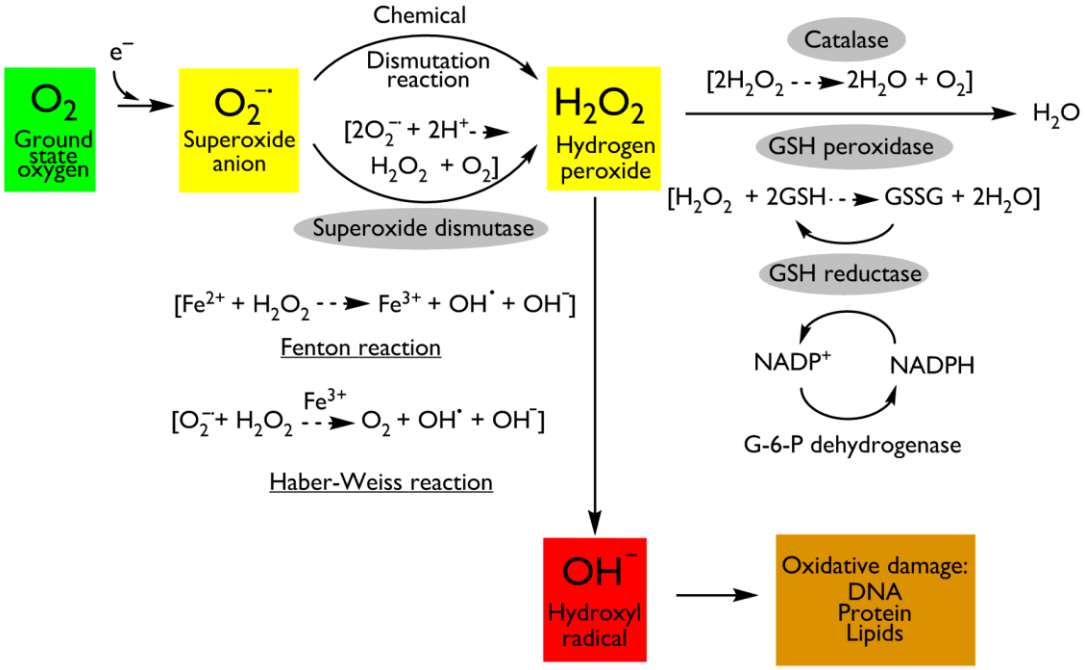

Figure 3.3: The major cellular forms of reactive oxygen species (ROS), their generation and cellular metabolism. GSH: glutathione, GSSG: glutathione disulfide, G-6-P dehydrogenase: glucose-6-phosphate dehydrogenase. Modified from (Goel and Khanduja 1998).

The sulfhydryl (-SH)-containing tripeptide glutathione (GSH) is ubiquitous in all organisms, acting as a major cellular antioxidant to maintain the cellular redox balance. The non-protein thiol consisting of γ-glutamyl-cysteinyl-glycine is synthesized from two consecutive ATP-dependent reactions following a peptide bond between glutamate and cysteine that is catalyzed by γ-glutamylcysteine synthetase. Glutathione synthetase catalyzes the condensation of the carboxyl group of cysteine with the amino group of glycine. The first reaction represents the rate-limiting synthesis step, which is inhibited by regenerated GSH and amino acid availability (Conrad and Sato 2012). When GSH is oxidized, glutathione disulfide (GSSG) is generated due to disulfide bridge formation. The glutathione reductase reduces GSSG back to GSH by consuming NADPH, representing the most important cellular redox buffer system. GSH is present in millimolar concentrations in the cell. As an electron donator, GSH is oxidized to GSSG in the enzymatic reduction of peroxides catalyzed by glutathione peroxidases, thereby protecting cells by removing hydrogen peroxides. In xenobiotic metabolism, conjugation of GSH with non-polar and electrophile xenobiotics occurs. This detoxifying reaction is catalyzed by the glutathione-S-transferase family to detoxify xenobiotics.

An important transcription factor for genes involved in the antioxidant defense and xenobiotic metabolism is the nuclear factor E2-related factor 2 (Nrf2) that binds to antioxidant responsive elements (ARE) in the promotor regions of its target genes. Activation of Nrf2 induces transcription of antioxidative and xenobiotic genes, thereby protecting cells against oxidative stress-induced cell death. Keap1 acts as a sensor of oxidative stress, functioning as a negative regulator of Nrf2. Keap1 complexes with Nrf2, which holds Nrf2 in the cytosol and ensures ubiquitination of Nrf2 and resulting in proteasomal degradation. Ubiquitin is an 8 kDa protein, which binds covalently to lysine residues of proteins in a multistep enzymatic process. A chain of poly-ubiquitin provides a signal for the proteasomal degradation of the modified protein (Haglund and Dikic 2005). The BTB (broad-complex C, Tramtrack, and Bric-a-brac), a conserved 100-residue protein motif at the N-terminal, functions as the dimerization site for Keap1 proteins. BTB binds to Cullin3, which plays an essential role for ubiquitination of Nrf2. The numerous cysteine residues in Keap1 function as optimal targets for electrophiles and oxidants. Formation of disulfide bonds through oxidation of the thiol groups changes the conformation of Keap1 and its activity. Due to the conformational change of Keap1, Keap1 can no longer bind to Nrf2, resulting in the dissociation of the two proteins, thereby Nrf2 can translocate to the nucleus. The Nrf2 signaling pathway is thus activated upon oxidative stress. The formation of heterodimers in nuclei with bZip family proteins, e.g. Maf, ensures Nrf2-regulated gene transcription (Kansanen *et al.* 2012). Figure 3.4 shows the activation of the Nrf2-Keap1 signaling pathway.

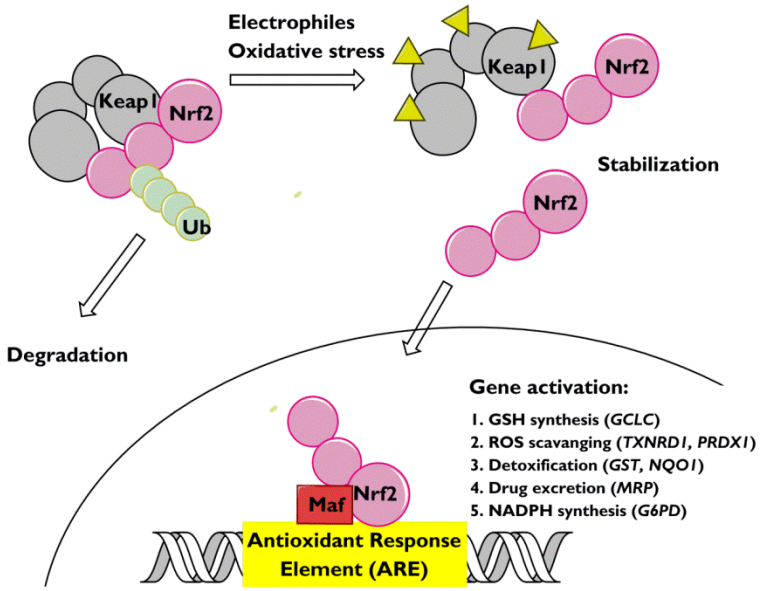

Figure 3.4: Activation of Nrf2-Keap1 pathway. Keap1 and Nrf2 associate in a complex in the cytosol, which influence the degradation of Nrf2. The stress-sensor Keap1 changes confirmation upon various stress factors, leading to the dissociation from Nrf2; thus, Nrf2 is stabilized. Nrf2 translocates to the nucleus and binds to antioxidant response elements (ARE) in promotor regions and induces numerous cytoprotective target genes. Modified from (Mitsuishi *et al.* 2012).

3.4 Tumor suppressor protein p53

The tumor suppressor protein p53 is of great importance in maintaining the genomic stability in cells and functions as a stress-responsive transcription factor. Described as the "guardian of the genome", the gene coding for the protein is frequently observed to be mutated in human cancers (Lane 1992). The observation that 50 % of all human tumors possess a mutation in the p53 gene clearly exhibits the tumor suppressive properties of the p53 protein, whereby most mutations are point mutations and occur in the region of the DNA binding domain (Martin *et al.* 2002). Consequently, when cells contain mutant p53, p53-dependent cell cycle arrest upon damaged DNA will not occur, resulting in an increased likelihood of mutations and cancer formation.

p53 is a transcription factor with a molecular weight of 53 kDa and is composed of 393 amino acids. The protein sequence can be divided into three distinct functional domains: the N-terminal transactivation domain, the DNA binding domain and the regulatory C-terminal domain. The C-terminal domain contains three functional motifs with a nuclear localization signal, a nuclear export signal regulating subcellular localization, in addition to a tetramerisation domain, responsible for the formation of the transcriptionally active tetrameric form of p53 (Hainaut and Mann 2001). In normal, non-stressed cells, p53 is maintained at low steady-state levels with a half-life of approximately 20 minutes. This short half-life is due to rapid, ubiquitin-dependent degradation of the protein shortly after its synthesis. The most important p53 regulatory protein is the E3 ubiquitin ligase MDM2, which participates in the degradation of p53. Various stress factors, such as DNA damage, could however lead to phosphorylation of the N-terminal region of p53, inhibiting binding of MDM2, and thereby leading to stabilize p53 due to increased half-life, provoking an accumulation of p53. Not only the stability of the protein itself may be altered; acetylation in the C-terminal range enhances the sequence-specific DNA-binding ability to p53-responsive elements in the promoter region of its target genes, mediating the gene expression in a multitude of genes involved in cell cycle control, apoptosis or DNA repair (Stewart and Pietenpol 2001). Figure 3.5 shows the structure of p53.

At least 3 % of all identified genes in the human genome encode for proteins with zinc-binding structures (Maret 2003). The p53 protein features also a zinc-binding protein motif, but it does not represent a classical zinc finger structure, like those in other transcription factors. Instead, one zinc ion is coordinated by three cysteine residues and one histidine residue. The zinc binding stabilizes the tertiary structure of p53 and enables the protein binding to the DNA minor grooves. The binding of p53 to specific DNA sequences is mediated through the conformation-specific structure in this central binding domain (Hainaut and Milner 1993). p53 itself is redox-sensitive because of the presence of conserved cysteine residues containing redox-sensitive thiol groups which function as cellular redox sensors. The redox status of reactive sulfhydryl residues of nuclear p53 determines its

DNA binding activity (Hainaut and Milner 1993; Kim *et al.* 2011). Human p53 contains 10 cysteine residues in the DNA binding domain and the orientation of each cysteine residue plays an important role in the redox regulation of p53 (Kim *et al.* 2011). Zinc finger structures have been shown to be sensitive targets for toxic metal compounds (Hartwig 2001). By destabilizing the conformation of these zinc-binding structures, the sequence-specific DNA binding capacity of p53 is abolished (Hainaut and Milner 1993; Meplan *et al.* 2000). Subsequently, the expression of genes involved in cell cycle regulation as well as apoptosis is affected (Chan *et al.* 2004). Exposure to cadmium has been shown to change the conformation of p53 and thereby its tumor-suppressive functions, causing p53 to function as a „mutant"-like form, meaning that p53 is not activated upon damaged DNA (Meplan *et al.* 1999; Schwerdtle *et al.* 2010).

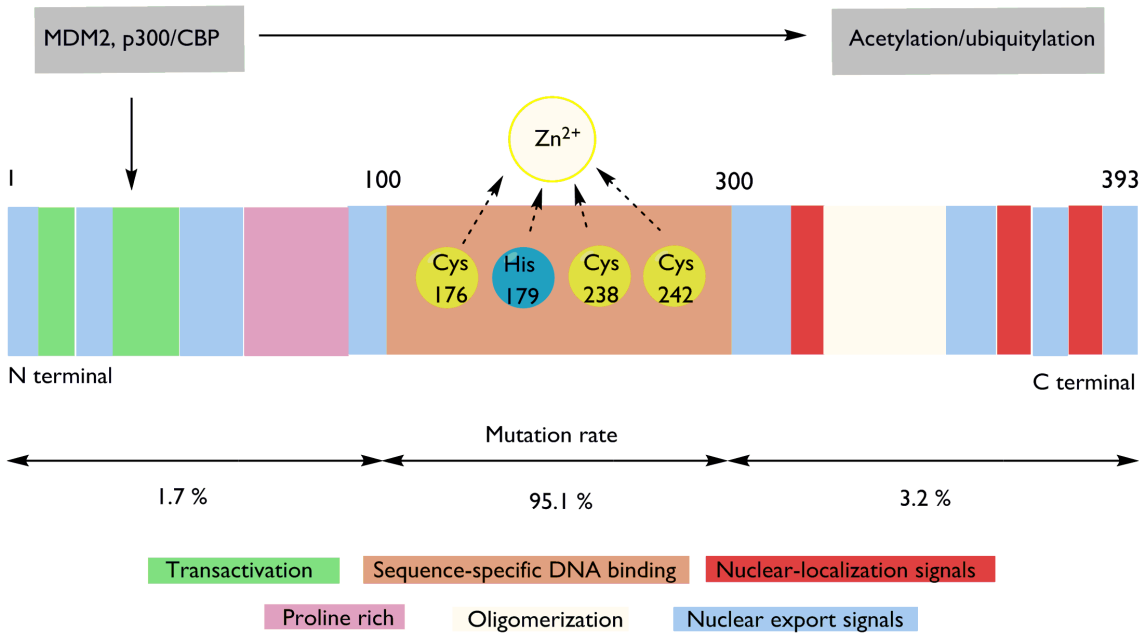

Figure 3.5: The transcription factor p53 contains several domains, including the amino (N)-terminal transactivation domain, a central sequence-specific DNA binding domain and a carboxy (C)-terminal domain that contains oligomerization sequences and nuclear-localization signals. Nuclear export of p53 is regulated by signals at both termini. Interactions with proteins e.g. MDM2 or p300/CBP with the N terminal region can lead to modifications such as ubiquitylation or acetylation in the C terminal region. Three cysteine residues and one histidine residue coordinate one zinc ion and stabilize the conformation of the DNA binding domain. In this domain, most mutations are observed. Modified from (Vousden and Lu 2002).

3.5 Cell cycle control and apoptosis

The cell cycle represents a series of tightly integrated controlled events allowing the cell to grow and proliferate. It is composed of interphase and mitosis (M) phases. The interphase includes the several gap (G) phases; the resting phase G0, the G1- and G2 phases, where the synthesis of mRNA and proteins occur, and the synthesis (S)-phase, where the DNA is replicated. This complex, interacting network is regulated by cyclins, cyclin dependent kinases (CDK) and CDK-inhibitors (CDKI) (Stewart and Pietenpol 2001) (see Figure 3.6). Eight different cyclins that are involved in the cell cycle are known, while at least 11 different CDKs are identified. Most cyclins exhibit major changes in mRNA and protein expression levels during the cell cycle course. CDKs are activated by various cyclins and provide a function in transcriptional regulation as well. Cyclin-CDK complexes are heterodimers acting as serine/threonine protein kinases, whereby their activity is regulated by phosphorylation and dephosphorylation. Active cyclin-CDK complexes phosphorylate a range of substrates, governing the course of the cell cycle. The proteins of the inhibitor of CDK4 (INK4)-family and the protein of the CDK-interacting protein/kinase inhibitor protein (CIP/KIP)-family belong to the CDKIs (Harper and Brooks 2005; Malumbres and Barbacid 2009). The retinoblastoma tumor suppressor protein (pRb) is a transcriptional master regulator, critical for G1 to S phase transition in the cell cycle (Chan *et al.* 2001). It interacts with the E2F transcription factor family to repress gene transcription required for this transition (Harbour and Dean 2000). E2F activity is regulated in a cell cycle-dependent manner, principally through its temporal association with pocket-protein family members, the prototype being pRb. Pocket proteins are, in turn, regulated through phosphorylation by CDKs, which are subject to the negative control by CDK inhibitors (CDI) (Stevens and La Thangue 2004). Deregulated cyclin activity in transformed cells contributes to accelerated cell cycle progression (Golias *et al.* 2004). Cyclin A can activate two different CDKs and function in both S phase and mitosis.

Cells are subject to permanent damage through endogenous and exogenous influences. Following DNA damage, the cell cycle can be delayed or stopped at certain checkpoints that exist at the G1-S transition and at the G2-M transition. These checkpoints sustain genomic integrity by inhibiting replication of damaged DNA and disturbances during mitosis (Iliakis *et al.* 2003). Before incorrect replication leads to mutations, different repair mechanisms can eliminate DNA damage during cell cycle arrest, allowing enough time for the damage to be repaired. If the damage is too severe, programmed cell death, known as apoptosis, will be induced.

The role of p53 in cell cycle arrest at the G1-S transition is well understood. In the event of DNA damage, the effector protein p53 is activated via a complex of signal cascades (Abraham 2001; Niida and Nakanishi 2006). Activation of p53 results in an increased expression of p21. p21 is the CDKI of

the CIP/KIP family that binds and inhibits the cyclin D-CDK4 complex. As a result, the phosphorylation of the tumor suppressor protein pRb is prevented, leaving it bound to transcription factors in the E2F family, and thereby inhibiting the expression of genes necessary for entering the S-phase (Harper and Brooks 2005). p21 can also inhibit replication and modulate repair by binding to proliferating cell nuclear antigen (PCNA) (Waga *et al.* 1994). The level of DNA damage is decisive for the fate of the cell. With low levels of damage, p53 induces p21 gene expression in order to put the cell in cell cycle arrest, which gives the cell time to repair the damage. If the level of DNA damage is too high, p53 induces expression of pro-apoptotic genes, e.g Bcl-2-associated X protein (*Bax)*, leading the cell into apoptosis due to the irreparable damage. Accumulation of the p53 protein causes a transient arrest of the cell cycle in the G1 phase, prior to DNA replication, or in the G2 phase, just before mitosis (Soussi 2000). This arrest in cell division in response to DNA damage enables the cell to activate enzymatic DNA repair processes to repair the lesions, acting as a "stop light". In cells expressing mutated p53, cell division is not arrested upon DNA damage. Mutations in the p53 gene can change the conformation of the resulting protein, making it more resistant against degradation. Regardless of the location of mutation, most p53 mutants have half-lives of 5-10 hours, and the protein accumulates in tumor cell nuclei. Cells containing a mutant p53 gene can no longer maintain the integrity of the genome since the cell does not receives the signal for a cell cycle arrest, which again can give rise to clones with greater malignant potential (Soussi 2000).

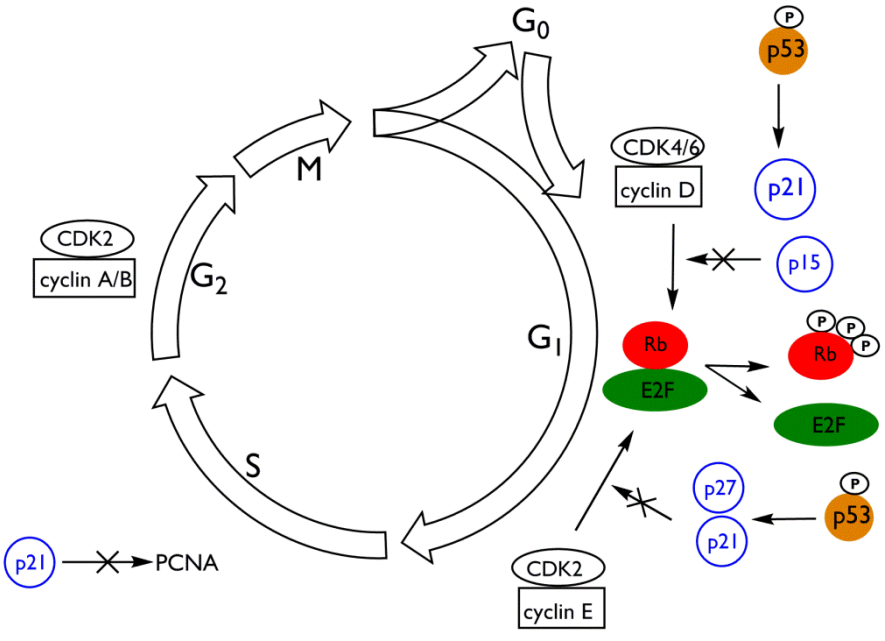

Figure 3.6: Cell cycle machinery. Schematic presentation of various factors involved in cell cycle progression and control. Modified from (Golias *et al.* 2004).

There are many different forms of cell death, including the well-known apoptosis and necrosis. Compared to necrosis, apoptosis is an active, ATP-consuming, genetically-controlled process which results in characteristic morphological changes such as cell shrinking, membrane blebbing, chromatin condensation and DNA fragmentation (Wang 2001).

Apoptosis can be induced via extrinsic (e.g. hypoxia) or intrinsic (e.g. DNA damage) signals. In the extrinsic pathway, the binding of a ligand to membrane-bound death receptors results in signaling cascades where initiator-caspases (cysteinyl-aspartate specific proteases) and subsequently, effector-caspases, are activated (Fan *et al.* 2005). Caspases are proteolytic enzymes with various functions such as deactivating anti-apoptotic proteins, activating apoptotic proteins (e.g. DNases) and degrading structural proteins (e.g. actin). The intrinsic pathway is a mitochondrial pathway. The membrane potential of the mitochondria is determined by the ratio of anti-apoptotic (e.g. Bcl-2) and pro-apoptotic (e.g. Bax) proteins of the Bcl-2 family. Reduction of the mitochondrial membrane potential accompanied by an increase of pro-apoptotic proteins makes the membrane permeable for cytochrome C, which is then released from the inner membrane into the cytosol. In the cytosol, cytochrome C forms the apoptosome together with Apaf-1 and caspase 9, which then activates the caspase cascade and the induction of apoptosis (Huerta *et al.* 2007). The intrinsic pathway also occurs independent from caspase activation through participation of the apoptosis inducing factor (AIF). AIF is released into the cytosol and translocated to the cell nuclei as DNase, where the DNase induces DNA fragmentation (Huerta *et al.* 2007). In the case of DNA damage, the p53 protein is phosphorylated and stabilized. It blocks proliferation by up-regulation of p21, which finally triggers cell cycle arrest in G1 phase. When accumulated above a certain threshold level, p53 can activate pro-apoptotic genes such as *Bax, PUMA* (p53 up-regulated modulator of apoptosis) and the FAS receptor (Roos and Kaina 2006).

4 Hypothesis

The intake of the essential trace element selenium varies widely around the globe, ranging from deficient to toxic concentrations. Because of the ongoing discussion regarding potential cancer-preventive properties of higher selenium intake levels and the beneficial roles of dietary selenium supplementation in the last decades, dietary supplements containing selenocompounds such as sodium selenite and selenomethionine add to these intakes, especially in the USA, where an estimated 50 % of the population take dietary supplements (Rayman 2012). However, at least in well-nourished populations, high selenium exposure may be associated with type 2 Diabetes or insulin resistance (Rayman and Stranges 2013). Because the range of intake between selenium deficiency and toxicity is very narrow, increased intake of selenium-containing dietary supplements could pose a potential oversupply risk for this essential trace element.

In the case of inorganic, reducible selenocompounds, like sodium selenite, pro-oxidative effects such as zinc release from metallothionein via oxidation of thiol groups are plausible (Chen and Maret 2001). Other zinc-binding proteins could also be potential molecular targets, e.g. transcription factors, DNA repair proteins or tumor suppressors, which could possibly disturb the maintenance of genomic stability (Blessing *et al.* 2004). The tumor suppressor protein p53 performs important cellular functions in order to maintain genomic stability. It acts as a redox-sensitive transcription factor, regulating expression of target genes relevant for control of the cell cycle, DNA repair mechanisms and induction of apoptosis. The native and intact conformation of p53 and thereby its function as a transcription factor is essentially coordinated by its zinc ion. Previous research in our working group has shown that sodium selenite-induced cellular effects are mediated by p53 (Klaus 2009). In contrast, effects induced by the organic and fully-reduced selenomethionine seemed to be independent of p53 status.

Cadmium is a classified carcinogen, but the underlying carcinogenic mechanisms are complex and not yet completely understood. Changes in the structure and function of p53 through cadmium compounds have already been reported (Meplan *et al.* 1999; Schwerdtle *et al.* 2010). Concurrent cadmium exposure and dietary selenium supplementation could indeed occur, which raises the question of how these compounds interact within the cell. In this work, a possible inhibition of p53-mediated effects induced by sodium selenite after co-exposure to cadmium chloride was investigated. As a cell model, human colon carcinoma cell lines with different p53 status were chosen. The p53-proficient HCT116 cells possess an intact wild-type p53, while the isogenic p53-deficient HCT116 cell line lacks the tumor-suppressive functions from p53. This present work aimed to determine sodium selenite-induced effects in the presence and absence of cadmium in these cell models, while

concurrently comparing with selenomethionine to elucidate specific selenium-species effects. The chosen endpoints were the determination of cytotoxicity, analysis of gene expression profiles, induction of oxidative stress, induction of cell cycle changes and apoptosis, and cellular uptake of the selenocompounds. We hypothesized that due to different chemical structures, and thereby different cellular metabolism of the two examined selenocompounds, varying cytotoxic effects and gene expression profiles were to be expected. One suggested mechanism in cadmium-induced carcinogenicity might involve deregulation of gene expression. It was asked whether we could observe specific selenium-species differences in the presence and absence of cadmium on the regulation of gene expression. Induction of oxidative stress by GSH depletion or by inhibition of ROS scavenging antioxidant enzymes following cadmium exposure is often reported as a mechanism in cadmium-induced cytotoxicity. The toxicity of sodium selenite is described to involve GSH in the reduction of sodium selenite, which could lead to GSH depletion and disturbance of the redox homeostasis. The questions whether cadmium could deplete GSH content in our HCT116 cells, and how the GSH content is affected by simultaneous exposure to sodium selenite and cadmium chloride, were raised. Potential targets of cadmium may be selenium-dependent enzymes, like glutathione peroxidase and thioredoxin reductase, as well as selenium-independent enzymes, such as glutathione reductase, superoxide dismutase and catalase. We asked if the selenol group in selenoproteins could be a sensitive target in cadmium-induced carcinogenicity by the specific binding of cadmium to selenol group in these antioxidant enzymes. Additionally, we asked whether the enzyme activities of antioxidant enzymes are affected by simultaneous exposure to sodium selenite and cadmium chloride.

As reported in literature, sodium selenite-induced oxidative stress could lead to DNA damage and activation of p53 (Zhao *et al.* 2006). Recognition of DNA damage provokes a DNA damage response, including cell cycle arrest, induction of DNA repair proteins or induction of apoptosis to maintain genomic stability. Determination of flow cytometric parameters, including superoxide generation, cell cycle distribution and apoptosis aimed to clarify the cellular impact of cadmium and sodium selenite in HCT116 cells, and thereby elucidate the impact of p53 status with regard to cellular response to damage. Because of a possible inhibition of p53-mediated, sodium selenite-induced cellular effects by cadmium could compromise genomic stability, and due to earlier observations in the working group regarding a possible involvement of p53 in the cellular uptake of sodium selenite, but not selenomethionine (Klaus 2009), the bioavailability of the selenocompounds in the absence and presence of cadmium was examined in order to possibly explain the impact of cadmium on induced cellular effects by selenocompounds. Determination of extracellular thiol content under the same conditions was also conducted.

5 Results and discussion

Various examinations helped elucidate the cellular effects following sodium selenite exposure. Possible interactions between sodium selenite and cadmium co-exposure were highlighted, as well as elucidating p53-mediated cellular effects in response to sodium selenite exposure and investigating selenium species specificity. Gene expression profiles were obtained in order to examine the impact of sodium selenite in combination with cadmium chloride and in comparison to selenomethionine. Other parameters such as oxidative stress markers (superoxide production, GSH content, enzymatic activity of antioxidative enzymes), as well as cell cycle distribution and apoptosis parameters (cell viability, mitochondrial membrane potential, subG1 fraction, nuclear translocation of AIF) were additionally examined after simultaneous exposure to sodium selenite and cadmium chloride. The cellular uptake of selenium after exposure to the two selenocompounds in combination with cadmium chloride was also investigated. In this chapter, the results of these investigations are presented and discussed.

5.1 Cytotoxicity

Alterations in the cytotoxicity of the two investigated selenocompounds were examined by performing colony-forming ability. The cell number provides a measure for acute cytotoxicity, while the colony number predicts the colony-forming ability of single cells, and is thereby reflecting the long-term growth inhibition and the proliferative potential after exposure to a certain compound.

5.1.1 Impact of sodium selenite and selenomethionine on the viability of HCT116 cells

Figure 5.1 and Figure 5.2 show the concentration-dependent influence on both parameters after 24 h incubation with sodium selenite or selenomethionine, respectively, in p53-proficient and p53-deficient HCT116 cells. Sodium selenite decreased both the cell number (Figure 5.1A) and the colony-forming ability (Figure 5.1B) in p53-proficient HCT116 cells, but not in p53-deficient HCT116 cells. Comparing the cell number (39 %) at the highest tested concentration (8 µM) in the wild-type cells to the colony number (8 %), the long-term proliferative potential was strongly reduced. In the p53-deficient cells, 24 h incubation with 8 µM sodium selenite caused no significant cytotoxic effect determined as cell number (87 %) or colony number (91 %), implying that the cells were not able to respond to the possible cellular damage caused by sodium selenite exposure. These results suggest that cytotoxic effects observed in sodium selenite-induced cell death might be mediated by p53.

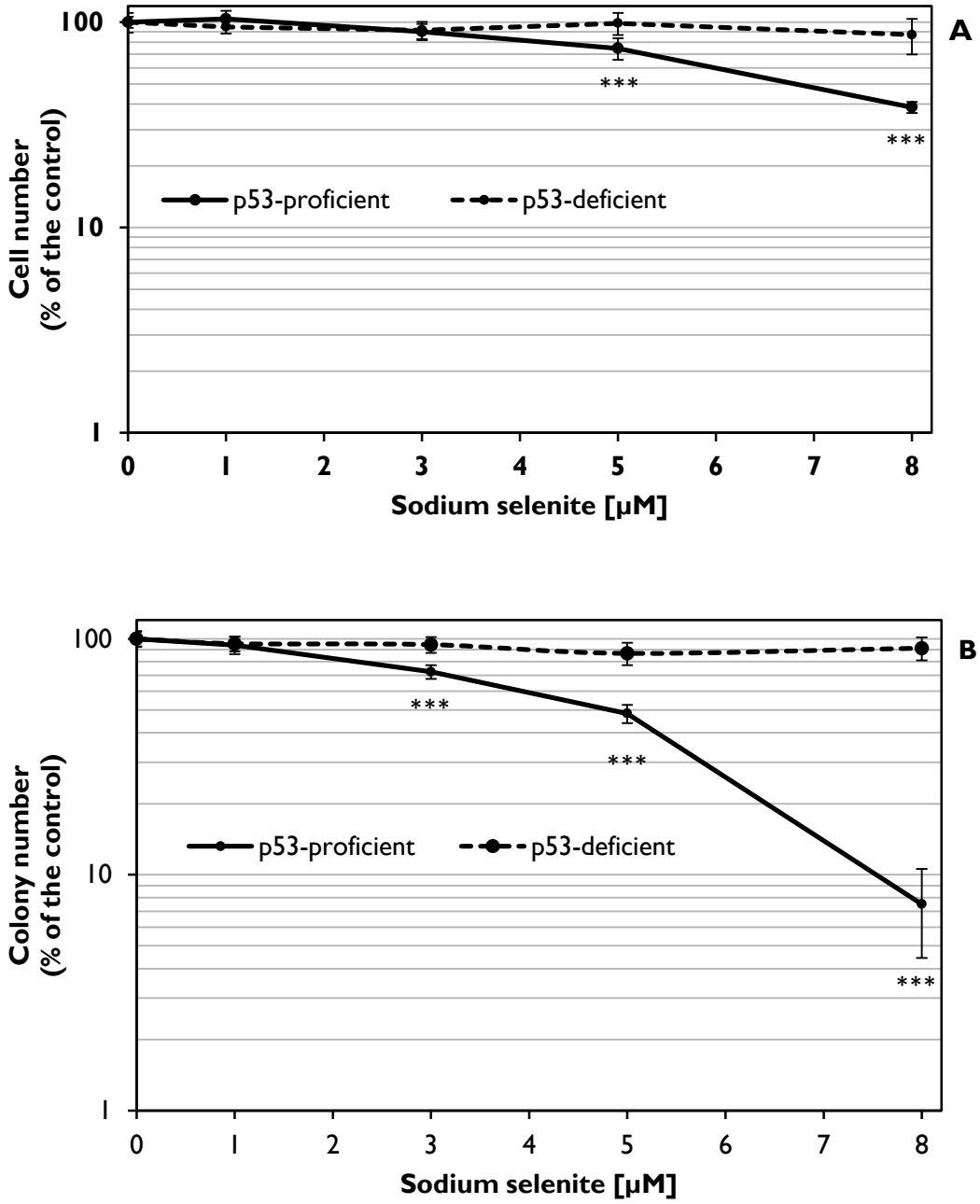

Figure 5.1: Cytotoxicity of sodium selenite in p53-proficient and p53-deficient HCT116 cells after 24 h incubations. Cytotoxicity was determined by cell number (A) and colony number (B). Mean values ± SD of three independent experiments are shown. Statistically significant differences between the cell lines tested by independent sample t-test (Mann-Whitney U test): *** = $p < 0.001$.

In the case of the reduced selenocompound, selenomethionine, we tested concentrations 100-fold higher than those of sodium selenite in the same cell models (Figure 5.2). We observed comparable effects on the cell number and colony number with increasing concentrations of selenomethionine.

Also, no significant differences in the cytotoxicity in regard to the p53-status of the cells were detected. These results imply that selenomethionine-induced cytotoxic effects are not mediated by the tumor-suppressive actions from p53, suggesting that p53 is important in selenium species specificity. Overall, sodium selenite is far more cytotoxic than selenomethionine.

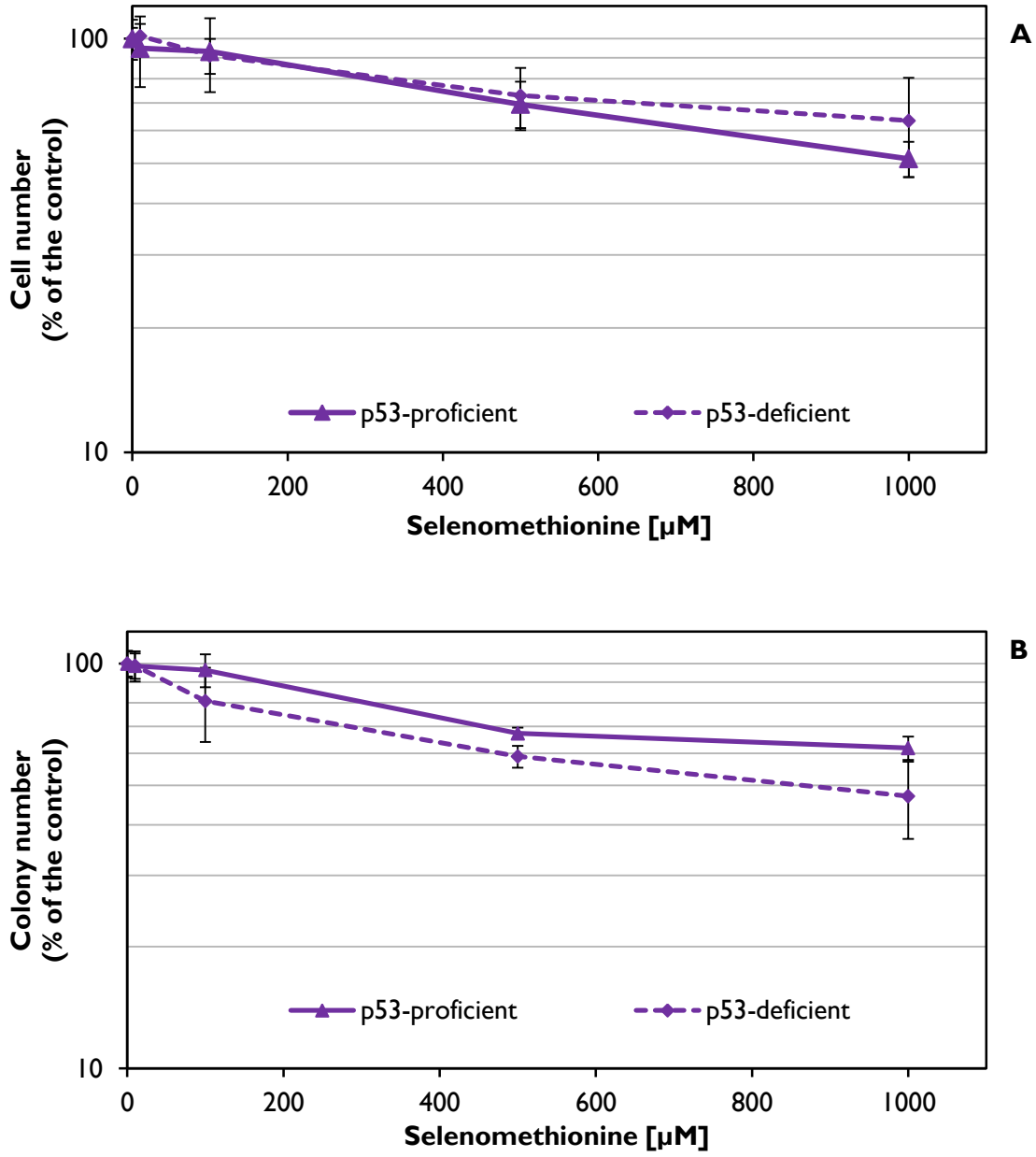

Figure 5.2: Cytotoxicity of selenomethinonine in p53-proficient and p53-deficient HCT116 cells after 24 h incubation. Cytotoxicity was determined by cell number (A) and colony number (B). Mean values ± SD of three independent experiments are shown. No statistically significant differences between the cell lines tested by independent sample t-test (Mann-Whitney U test).

Selenium is a cellular growth inhibitor in several mammalian tumor cells. Inhibition of cell proliferation and induction of cell death is induced by all forms of selenium (Lu *et al.* 1995). Kralova and co-workers showed in the same cell model that p53 sensitizes the cells towards sodium selenite. In the study by Kralova, they used proliferation tests, such as DNA synthesis measurements (BrdU-ELISA), total protein content (Coomassie Brilliant Blue Assay) or integrity of the respiratory chain (WST-1, water soluble tetrazolium) (Kralova *et al.* 2009). The WST-1 test system was insensitive in comparison to the other methods, and the differences between the cell lines were relatively low. The choice of cytotoxicity test system is decisive since different cytotoxicity tests in general provide varying results, probably due to different mechanisms of action (Schroterova *et al.* 2009). Tests that consider clonal survival are recommended (Komissarova *et al.* 2005). Goel *et al.* found no impact of the p53-status on the cytotoxicity after 24 h exposure to selenomethionine when using MTT test in the same cell model as in this present study. They showed that after longer incubation times, the cells became more sensitive (e.g. 100 µM selenomethionine after 72 h compared to untreated controls) (Goel *et al.* 2006).

A comparable cytotoxicity of selenomethionine and sodium selenite in different colon cancer cell lines is shown in only one study (Schroterova *et al.* 2009). Both selenium compounds were shown to be cytotoxic already at concentration of 1 µM in HT29 and SW480 cells, and at a concentration of 16 µM in SW620 cells. A clear difference between the compounds is however more plausible. On the one hand, the reducible sodium selenite possesses direct pro-oxidative features. These differences play a role in the metabolism. The strong accumulation of selenium in the cell after incubation with selenomethionine is due to unspecific integration into cellular proteins in exchange of methionine. Selenium is not immediately bioavailable in this storage form. Stagnation of accumulation at higher concentration may be due to storage capacity. Sodium selenite has been shown to be taken up via a passive anion transporter in keratinocyte models, while organic selenoamino acids such as selenomethionine appear to be efficiently transported by various intestinal amino acid transporters (Nickel *et al.* 2009). The uptake of sodium selenite would then greatly increase after extracellular reduction to hydrogen selenide via an active, ATP-dependent mechanism in an anion transporter (Ganyc and Self 2008). Sodium selenite cytotoxicity is determined by selenium uptake, which again is dependent on the extracellular redox state (Olm *et al.* 2009). A major part of the extracellular thiols is cysteine. Extracellular thiol production and consequently, selenium uptake and cytotoxicity, are dependent on cystine uptake through the xc^--cystine antiporter. Xc^--antiporter expression with concomitant secretion of cysteine (via MRPs) is associated with selenite sensitivity mediated via a high-affinity uptake by a reduced form of selenite (Olm *et al.* 2009).

5.1.2 Impact of sodium selenite and selenomethionine in combination with cadmium chloride on the viability of HCT116 cells

Due to the possible involvement of p53 in sodium selenite-induced cytotoxicity, as shown in Figure 5.1, we combined a simultaneous exposure to cadmium chloride and sodium selenite. Cadmium chloride has been shown to unfold the tumor suppressor protein p53 by displacing its divalent zinc ion, thereby causing a conformational change of the protein, which results in loss of functionality (Meplan *et al.* 1999; Schwerdtle *et al.* 2010). Exposure to 10 µM cadmium chloride without sodium selenite caused a reduction in the colony number to about 85 % in the proficient cell line (Figure 5.3A) and 89 % in the deficient cells (Figure 5.3B). The colony-forming ability after exposure to lower concentrations of sodium selenite (up to 3 µM) in combination with cadmium was comparable to sodium selenite incubation only. At the tested concentrations of 5 µM and 8 µM sodium selenite, the presence of cadmium attenuated the cytotoxicity caused by sodium selenite from 48 % to 65 % and 8 % to 47 %, respectively, in p53-proficient HCT116 cells (Figure 5.3A). Neither sodium selenite nor cadmium chloride co-exposure caused significant changes in the colony number in the p53-deficient HCT116 cells after 24 h incubation (Figure 5.3B).

Unexpectedly, we observed an enhancement of selenomethionine-induced cytotoxicity in combination with cadmium chloride in a p53-dependent manner (Figure 5.4A). Selenomethionine decreased indeed the colony number in the p53-deficient cells after 24 h treatment, but the presence of cadmium showed no further influence (Figure 5.4B). These data suggest an impact of p53-status on the increased selenomethionine-induced cell death when cadmium is present.

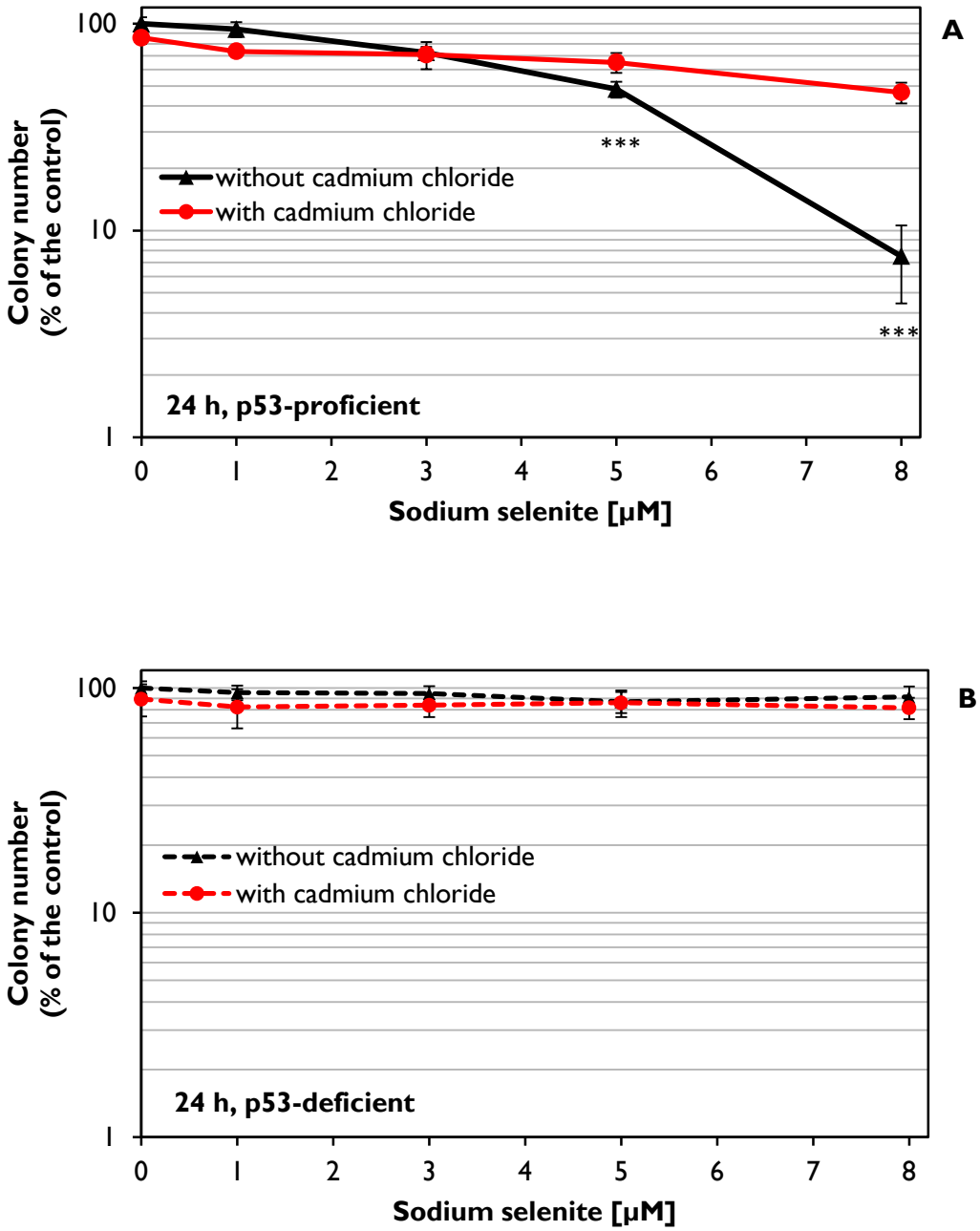

Figure 5.3: Colony-forming ability after 24 h incubation with sodium selenite in combination with cadmium chloride. p53-proficient (A) and p53-deficient (B) HCT116 cells were treated with sodium selenite (1 µM-8 µM) with or without 10 µM cadmium chloride. Cytotoxicity was determined by colony-forming ability. Mean values ± SD of three independent experiments are shown. Statistically significant differences between single and combined treatment with cadmium as tested by independent sample t-test (Mann-Whitney U test): *** = $p < 0.001$.

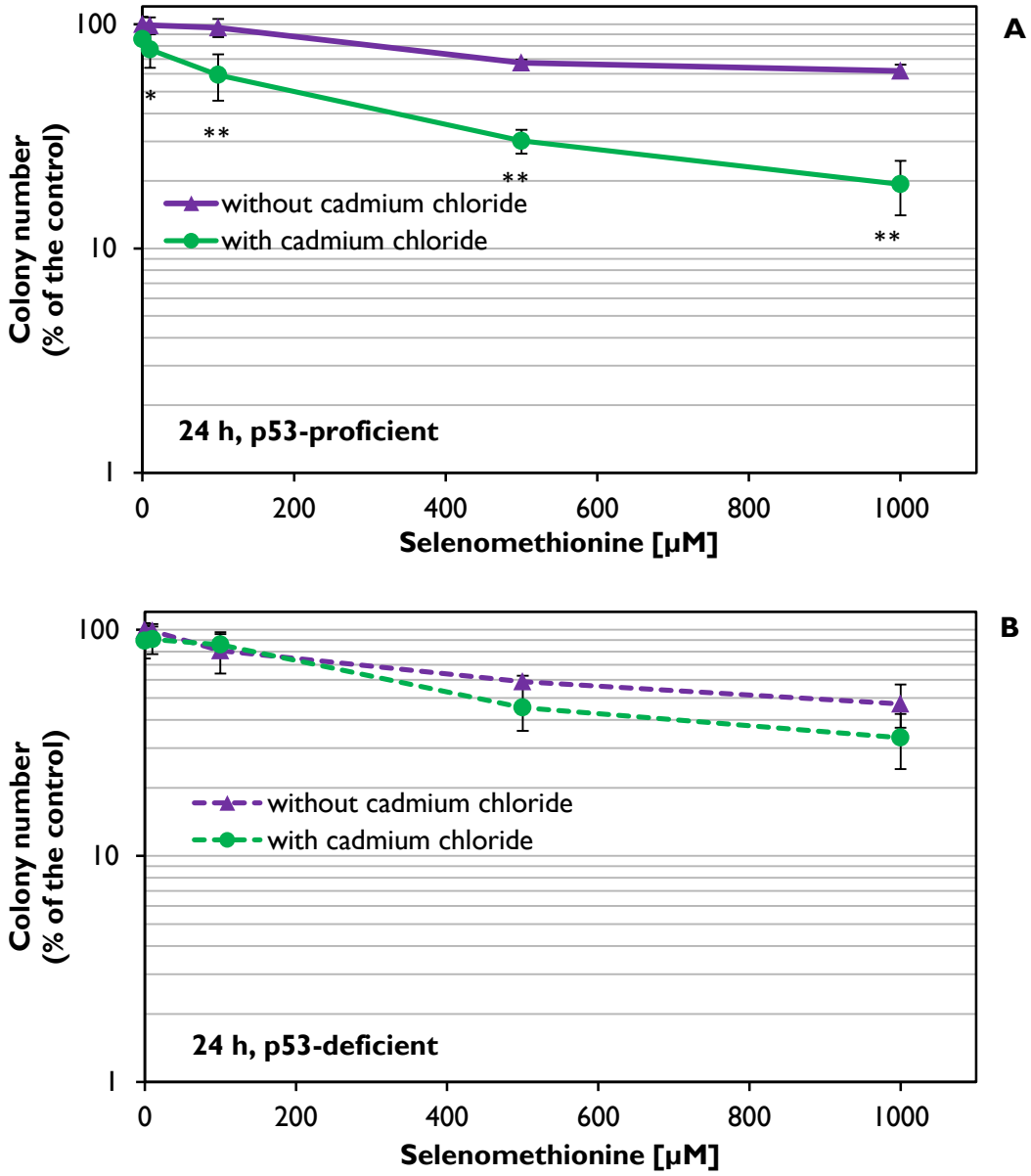

Figure 5.4: Colony-forming ability after 24 h incubation with selenomethionine in combination with cadmium. p53-proficient (A) and p53-deficient (B) HCT116 cells were treated with selenomethionine (10 µM-1000 µM) with or without 10 µM cadmium chloride co-incubation. Cytotoxicity was determined by colony-forming ability. Mean values ± SD of three independent experiments are shown. Statistically significant differences between single and combined treatment with cadmium as tested by independent sample t-test (Mann-Whitney U test): * = $p < 0.05$, ** = $p < 0.01$.

Examining the cells after 8 h sodium selenite treatment in p53-proficient HCT116 cells, a strongly reduced colony-forming ability at the highest tested concentration could be observed (Figure 5.5A), but not, however, in p53-deficient HCT116 cells (data not shown). This implies once again that

cytotoxicity following sodium selenite exposure is likely to be mediated by p53. Co-exposure to cadmium for 8 h almost completely reversed the outcome of sodium selenite incubation, again implying an impact of cadmium on p53-mediated cytotoxicity induced by sodium selenite. Figure 5.4B shows that selenomethionine only reduced the colony number to 90 % at the highest tested concentration after 8 h treatment in p53-proficient HCT116 cells, showing that the increased cytotoxicity of selenomethionine in combination with cadmium chloride seen after 24 h incubation could not be observed after 8h.

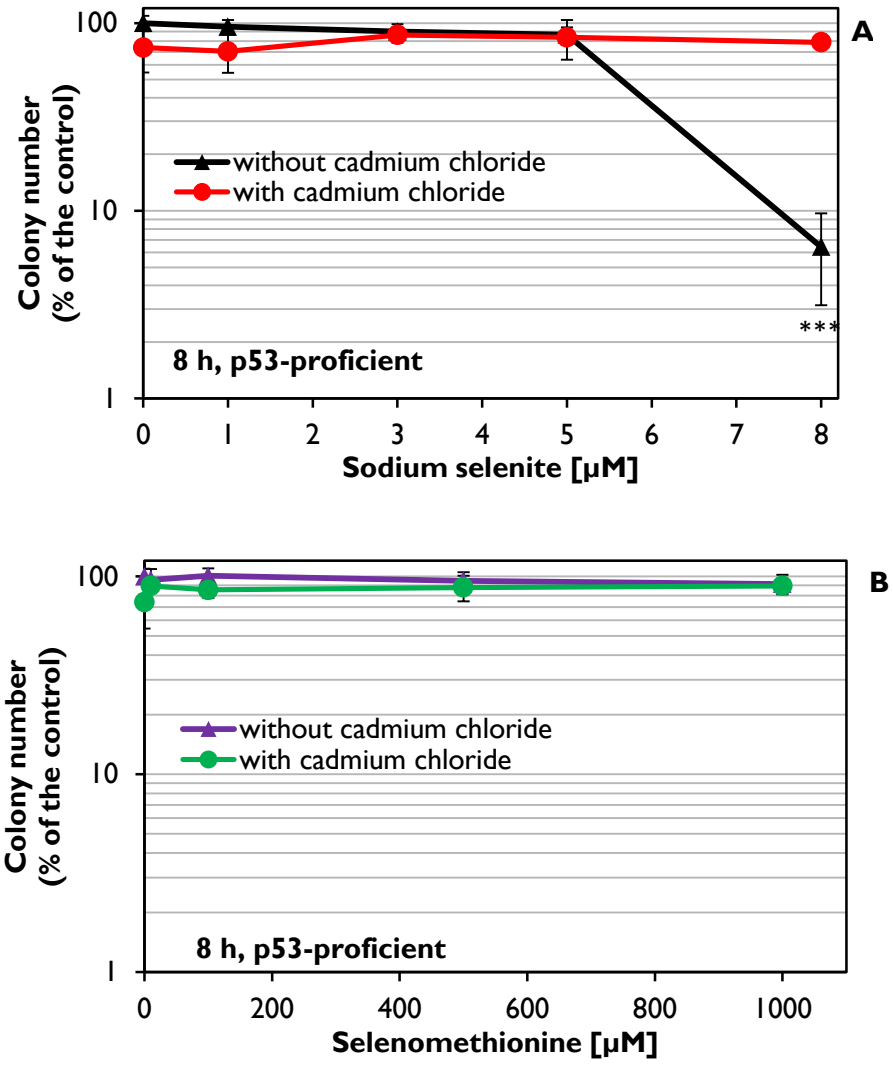

Figure 5.5: Colony-forming ability after 8 h exposure to sodium selenite or selenomethionine in combination with cadmium. p53-proficient HCT116 cells were treated with sodium selenite (A) or selenomethionine (B) with or without 10 µM cadmium chloride co-incubation. Cytotoxicity was determined by colony-forming ability. Mean values ± SD of three independent experiments are shown. Statistically significant differences between single and combined treatment with cadmium as tested by independent sample t-test (Mann-Whitney U test): *** = $p < 0.001$.

5.2 Gene expression profiling

Regulation of cellular signaling pathways and modification of gene expression occurs frequently at the transcriptional level. Analysis of transcriptional changes following exposure to a certain compound could therefore provide new insight into potential intracellular targets of compounds of interest. Whether exposure to a compound induces or represses transcription depends both on time and concentration as well as the specific compound. Employing a high throughput-RT-qPCR enabled the quantitative analysis of 96 x 96 independent PCR reactions in parallel to examine cellular responses at the transcriptional level to exposure to different selenocompounds in the combination with cadmium chloride. The gene expression profiles of sodium selenite and selenomethionine in the presence and absence of cadmium chloride could thereby be recorded, elucidating their influence on various signaling pathways. Due to the complexity of the generated data, details on genes and signaling pathways were selected and presented, in order to highlight involvement of p53 in sodium selenite-induced effects. Additionally, the possible modulation by cadmium chloride co-exposure as well as species-specific effects of selenium was examined. By arranging the genes according to highest fold change of the relative gene expression induced by sodium selenite (5 µM, 24 h) within each category, comparisons between the p53-proficient and p53-deficient HCT116 cells, and effects of co-exposure to cadmium chloride as well as exposure to selenomethionine could be obtained. More than a 2-fold gene up-regulation was considered as significant, while the cut-off for significant gene down-regulation was set to <0.5. Complete gene expression profiles of sodium selenite and selenomethionine alone and in combination with cadmium chloride, as well as concentration-dependent cadmium chloride profiles are arranged in the appendix (see Table A4-8). Also to be found in the appendix, is a summary of all examined genes together with the respective encoded proteins (Table A1-3). Because the genes *ADH, ALDH1A1, AXIN, CYP1A1, DDIT3, GADD45A, GPX2,* and *UGT1* were only marginally expressed in the applied cell lines, these genes were not considered in the data analysis.

5.2.1 Impact of sodium selenite exposure in combination with cadmium on gene expression and the role of p53 on sodium selenite-induced gene expression

In order to examine the impact of sodium selenite exposure and the possible involvement of the tumor suppressor protein p53, both p53-proficient and p53-deficient HCT116 cells were treated with sodium selenite for 24 h. In addition, p53-proficient HCT116 cells were co-incubated with sodium selenite and 10 µM cadmium chloride for 24 h to reveal the possible interaction of cadmium

on sodium selenite-induced and p53-mediated effects. Thus, their unique gene expression profiles could be analyzed and compared.

Genes involved in oxidative stress response and inflammation

Oxidative stress arises when cells are subjected to either excess levels of ROS or antioxidant depletion, disturbing the cellular redox balance in favor of the pro-oxidants. Oxidative stress overwhelms antioxidant protection, which subsequently could lead to oxidative damage of cellular macromolecules. Generated superoxide radicals are not particularly reactive, but other ROS could develop from these radicals. Superoxide dismutases convert the superoxide radical anion to molecular oxygen and hydrogen peroxide. The latter is converted to highly-reactive hydroxyl radical under the catalytic action of Fe^{2+} via the Fenton reaction (Halliwell 2006). In the case of increased ROS production, an enhanced gene expression of numerous cytoprotective antioxidants enzymes, such as heme oxygenases, catalase and glutathione peroxidases may take place.

Figure 5.6 shows the impact of 24 h exposure to sodium selenite (5 µM) on genes associated with the oxidative stress response as well as inflammation in p53-proficient- and p53-deficient HCT116 cells, as well as the impact of 24 h co-exposure to 10 µM cadmium chloride or cadmium alone in p53-proficient HCT116 cells. Transcript levels of the GSH redox system-associated genes *TXNRD, GCLC, GSR* and *G6PD*, as well as the xenobiotic genes *NQO1* and *EPHX1* were increased after sodium selenite exposure in p53-proficient HCT116 cells (Figure 5.6A). These genes are target genes of Nrf2 and possess ARE sequences in their promoter regions (Baird and Dinkova-Kostova 2011), indicating an activation by Nrf2. In the p53-deficient cell line, increased mRNA levels of *TXNRD1, GCLC* and *NQO1* were also observed: however, *GSR* and *G6PD* levels were only tendentiously induced. *EPHX1* levels were unchanged. The stronger induction of Nrf2 target genes in p53-proficient cells than p53-deficient cells could imply a partial influence of p53 in the oxidative stress response. The transcript level of *NFE2L2*, which encodes the transcription factor Nrf2, was enhanced 2-fold. The gene *KEAP1,* encoding the protein Keap1 which binds Nrf2 in cytosol leading to the proteasomal degradation of Nrf2, was however, not induced. Induction of Keap1 exerts a specific negative feedback mechanism which can turn off induced Nrf2 signal cascade (Lee *et al.* 2007). One of the most frequently induced downstream gene following Nrf2 activation is *NQO1* (summarized in Baird and Dinkova-Kostava, 2011). Induction of *NQO1* provides a protective mechanism since the oxidoreductase NQO1 catalyzes the detoxification of quinones to hydroquinones, avoiding potential formation of semichinone radical intermediates. In this way, cells are protected from quinone-induced oxidative stress. *EPHX1* encodes for the epoxide hydrolase 1, which plays an important role both in activation and inactivation of xenobiotics. Due to the ARE sequence in its promoter region, *EPHX1* activation

via Nrf2 is possible. It is difficult to evaluate which impact the induction of *EPHX1* exhibits on the cellular homeostasis in HCT116 cells since epoxide hydrolases are mainly responsible for degradation of toxic epoxides to dihydrodioles, and thereby detoxification. Glucose 6-phosphate dehydrogenase (*G6PD*), the first and rate-limiting enzyme of the pentose phosphate pathway, generates reducing equivalents in the form of NADPH, which is used to maintain GSH in its reduced form, thereby allowing detoxification reactions (Rahman *et al.* 1999). Despite Nrf2 activation, induction of all selected Nrf2 dependent genes was not observed. No expression changes in *CAT, GPX1, GSTP1, PRDX1, SOD2,* and *TXN* were seen. Gene expression induction of antioxidant enzymes could also be regulated by other less investigated mechanisms. Some studies suggest that among others kinases such as protein kinase C (PKC), phosphor-3-kinase (PI3K) and MAP kinases (MAPKs) participate in the activation of Nrf2, and thereby selectively modulate signal transduction (Huang *et al.* 2000; Keum *et al.* 2003).

Figure 5.6A shows that co-exposure to cadmium chloride also induced these Nrf2 target genes, with the exception of *EPHX1,* similar to the p53-deficient cell line in response to sodium selenite exposure. This implies a partial influence of p53 in the oxidative stress response. The transcript level of the transcription factor Nrf2 coded by *NFE2L2*, was enhanced 2-fold by sodium selenite, but co-exposure to cadmium chloride did not induce *NFE2L2* mRNA. Neither sodium selenite incubation nor co-incubation with cadmium affected the gene *KEAP1* transcript levels, which is known to be a negative cytoplasmic regulator of Nrf2 (Lee *et al.* 2007).

Exposure to cadmium only (10 µM) induced also *TXNRD1* and *GSR* mRNA levels, but only tended to up-regulate *GCLC* expression levels after 24 h (Figure 5.6A). Moreover, *TXNRD1*, *GSR* and *GCLC* mRNA levels were significantly induced already at 8 h exposure (see appendix Table A4). *ABCB1* mRNA levels were also increased following cadmium chloride exposure. *ABCB1* encodes an ABC transporter, also known as multidrug resistance P-glycoprotein 1 (Mdr1) that can function as xenobiotic efflux pump (Sabolic *et al.* 2008).The simultaneous exposure to sodium selenite and cadmium chloride, however, showed a smaller induction of the *ABCB1* gene.

Sodium selenite induced heme oxygenase 1 (*HMOX1)* transcript levels by 20-fold in the p53-proficient cell line, while an 8.5-fold increase could be observed in the p53-deficient cells (Figure 5.6B). No change in heat shock protein 1A (*HSPA1A)* was seen in any of the cell lines, indicating no activation of the transcription factor heat shock factor HSF-1. In combination with cadmium chloride, *HMOX1* mRNA was induced over 66-fold after exposure to sodium selenite. A 20-fold change could be observed after incubation with sodium selenite only, while10 µM cadmium for 24 h incubation induced the transcripts of *HMOX1* by 44-fold (Figure 5.6B), suggesting an additive effect of the co-exposure to sodium selenite and cadmium chloride on *HMOX1* expression. The early

response gene and stress response gene *HMOX1* showed a time- and concentration-dependent rise in expression levels following cadmium chloride incubation only, whereby the highest fold change (108-fold) was observed at the earliest time point of 8 h (see appendix Table A4). Induction of the early response gene *HMOX1* represents a general transcriptional response to oxidative stress, which can be induced by several transcription factors such as AP-1 (Jun), Nrf2 and HSF-1 (Alam and Cook 2003). While no change in *HSPA1A* gene expression was seen after sodium selenite incubation, co-exposure to cadmium chloride led to 30-fold higher expression levels (Figure 5.6B). The transcript levels of *HSPA1A* after 24 h incubation with 10 µM cadmium chloride were strongly induced by more than 200-fold. Like *HMOX1, HSPA1A* gene expression was also time- and concentration-dependent enhanced following cadmium chloride incubation, however, in contrast to *HMOX1* gene expression, the *HSPA1A* gene expression was higher after 24 h than 8 h. However, at a shorter incubation time (8 h), concomitant exposure to sodium selenite and cadmium chloride abolished the *HSPA1A* gene induction completely, although exposure to 10 µM cadmium chloride alone raised the *HSPA1A* mRNA levels by 59-fold after 8 h incubation (see appendix Table A4). These results would suggest an antagonistic effect of sodium selenite on cadmium-induced *HSPA1A* expression. GSH-depletion has been shown to be decrease heat shock protein mRNA levels (Belton *et al.* 2011). We observed that sodium selenite depleted intracellular GSH content (Figure 5.14), while cadmium increased the GSH levels (Figure 5.13), which might suggest that GSH-depletion could be involved in the observed antagonizing effect of sodium selenite on cadmium-induced *HSPA1A* up-regulation. Taken together, given the present results, it is likely that Nrf2 activation was involved in the cellular response to exposure to sodium selenite, as well as to cadmium and also to co-exposure to them.

Changes in the mRNA levels of *MT1X, MT2A* and *SLC30A1*, which encode for two metallothionein isoforms (MTs) and zinc transporter 1 (ZnT1), respectively, were only observed in the p53-proficient HCT116 cells, which suggest a p53-dependent effect following sodium selenite treatment (Figure 5.6C). *SLC30A1* is a target gene of metal-response element-binding transcription factor-1 (MTF-1), known to be activated by metals such as zinc, but also heavy metals like cadmium. A direct interaction with MTF1 could lead to activation of the transcription factor and induce the expression of MTs via the metal responsive element (MRE). Besides regulation by MRE, the expression of MTs can also be modified by the glucocorticoid responsive element (GRE) and ARE (Coyle *et al.* 2002). The activation through MRE occurs primarily via binding of metal to MTs. Since HCT116 cells are not hormone sensitive, activation via GRE is of little relevance. Here, we observed that sodium selenite also activated this transcription factor, possibly due to oxidative zinc release of MTs (Chen and Maret 2001). 24 h co-exposure to cadmium chloride increase the *MTX1* expression from 3-fold to 14-fold, and almost doubled the *MT2A* expression levels to 6-fold compared to sodium selenite alone (Figure 5.6C). Cadmium alone raised the *MTX1* levels 19-fold after 24 h exposure (Figure 5.6C); however, a

38-fold change was seen after 8 h (see appendix Table A4). The *MT2A* expression was increased about 8-fold after 24 h incubation. Additionally, the expression of the ZnT1 gene was 3.3-fold higher after 24 h cadmium exposure (Figure 5.6C). The mRNA levels of *ZnT1* were increased by 10-fold after 8 h cadmium exposure (see appendix Table A4). These observations point out that a strong MT expression, including zinc transporter expression, which are target genes of the metal responsive transcription factor MTF-1, were early responses to cadmium exposure. In contrast, sodium selenite-induced MT expression was first observed after 24 h, but not after 8 h incubation. However, a tendency in the up-regulation of the ZnT1 gene (1.9-fold induction) was seen after 8 h exposure to sodium selenite. The induction of these MTF-1 target genes by sodium selenite was thereby a slower response than that seen following cadmium exposure.

The inflammation marker interleukin-8 (*IL8*) gene was strongly induced 84-fold and 74-fold in p53-proficient- and deficient cells, respectively (Figure 5.6B). Cadmium alone (10 µM) increased *IL8* gene expression levels by 6-fold. Co-exposure to cadmium chloride affected sodium selenite-induced *IL8* gene expression negatively. Sodium selenite induced an 84-fold change in *IL8* mRNA levels, while in the presence of cadmium chloride only a ~6.5 fold change was observed (Figure 5.6B). While sodium selenite induced the *IL8* gene by 154-fold after 8 h (see appendix Table A5), simultaneous 8 h incubation with cadmium chloride only raised the *IL8* mRNA levels by 2.5-fold (see appendix Table A4). Concomitantly to the sodium selenite-induced up-regulation of *IL8* mRNA levels, the gene expression levels of *NFKB2* was increased by a factor of 3.7 in the p53-proficient cells, but was induced by less than 2-fold in the p53-deficient cells (Figure 5.6D). *NFKB2,* which encodes the p100 subunit of the transcription factor NF-κB, was induced also by about 2.4-fold in the presence of cadmium. Sodium selenite tended to induce transcript levels of *NFKB1A,* the NF-κB inhibitor IκBα, and *NFKB1,* the p105 subunit of NF-κB, however, co-exposure to cadmium resulted in no fold change of these two genes. The transcriptional induction of *IL8, NFKB2, NFKB1* and *NFKB1A,* is mediated by NF-κB. Another target gene of NF-κB is the gene encoding the ferritin heavy chain the intracellular iron storage protein, *FTH1,* which plays an important role in the regulation of iron homeostasis. Sodium selenite raised mRNA levels of *FTH1* mRNA levels in both cell lines by about 5-fold, independent of cadmium chloride (Figure 5.6A). This implies an activation of the transcription factor NF-κB since *IL-8* and ferritin encoded by *FTH-1* are target genes of NF-κB, in addition to the genes encoding the inactive precursor subunits of the transcription factor. Another important gene in iron homeostasis is *TFRC*, which encodes for the membrane-bound transferrin receptor. However, the expression levels of this gene were not changed after sodium selenite exposure. The change in expression of *FTH1* is presumably closely associated with the induction of *HMOX1*. Enhanced activity of the stress-responsive heme oxygenase leads to accelerated intracellular heme catabolism, which could mobilize divalent iron ions out of protoporphyrin IX ring of the heme molecule. Free iron ions

catalyze ROS formation via the Fenton reaction, thereby evoking cytotoxic effects. The ability of HMOX-1 to increase heme catabolism represents, however, a cytoprotective effect, which prevents sensitizing cells to undergo programmed cell death (Gozzelino *et al.* 2010).

Cadmium-induced oxidative stress is related to induction of overexpression of the oncogenes c-fos and c-jun, the members of the redox-sensitive AP-1 transcription factor (Joseph *et al.* 2001; Qu *et al.* 2005). Filipic and Hei showed that GSH-depletion by pretreatment with BSO resulted in increased mutagenicity of cadmium, indicating indirectly that ROS mediates a genotoxic response in mammalian cells exposed to cadmium (Filipic and Hei 2004). Exposure to cadmium consequently up-regulated genes encoding for proteins involved in defense and cellular repair including MTs, heme oxygenases, heat shock proteins and thioredoxin reductases (Nishitai and Matsuoka 2008; Valbonesi *et al.* 2008; Yamada *et al.* 2009). Suggested mechanisms are involvement of redox sensitive transcription factors such as Nrf2, AP1 and NF-κB. Direct involvement of cadmium on HMOX-1 and heat shock protein 70 has been shown to be regulated via MRE (Koizumi *et al.* 1992; Koizumi *et al.* 2007).

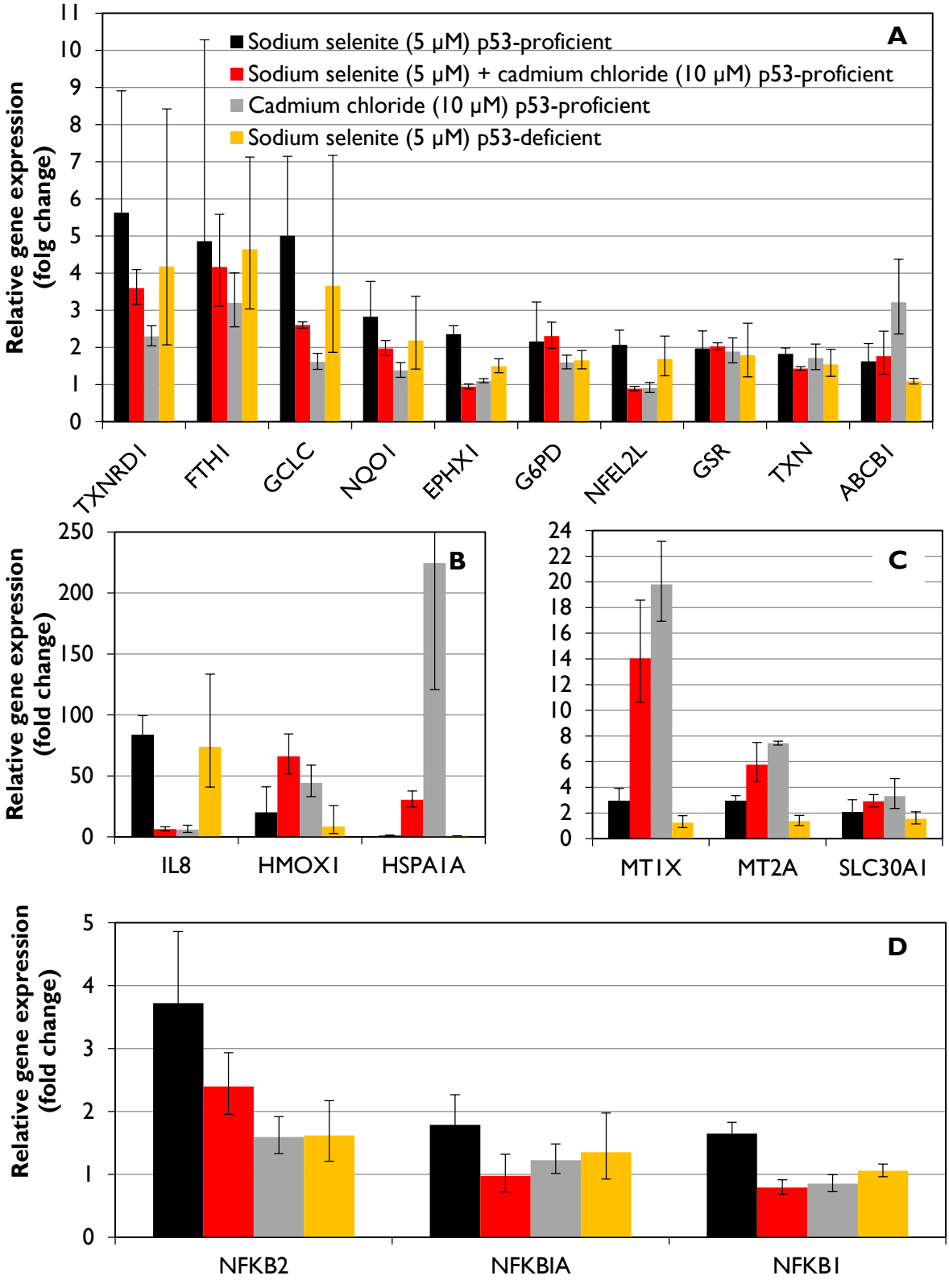

Figure 5.6: Impact of sodium selenite (5 µM) in combination with cadmium chloride (10 µM) and the role of p53 on the relative gene expression of genes associated with (A, B, C) oxidative stress response and (B, D) inflammation in p53-proficient and p53-deficient HCT116 cells after 24 h incubation Gene name abbreviations listed in Table A3. Mean values ± SD of at least two independent experiments of double or single determinations are shown.

Genes associated with cell cycle control

Relative gene expression of cell cycle control genes in p53-proficient- and p53-deficient HCT116 cells after 24 h exposure to 5 µM sodium selenite was also investigated (Figure 5.7). Sodium selenite increased mRNA levels of the cyclin-dependent kinase inhibitor *CDKN1A1* that encodes p21, by 10-fold. p21, which is mainly regulated through p53, is a major cell cycle inhibitor, leading to G1 cell arrest. In the p53-deficient cells a nearly 3-fold increased transcript amount of p21 was found, suggesting a p53-independent induction of p21. Another cyclin-dependent kinase inhibitor *CDKN2B*, known as p15, was also induced by about 3-fold upon sodium selenite treatment, however, only in p53-proficient cells. Other target genes of p53 that were only enhanced in the proficient cells were protein phosphatase *PPM1D* and serine/threonine-protein kinase *PLK3*, implying a G1/S-and G2/M arrest, respectively. The PPM1D acts as a protein phosphatase that down-regulates p38, and thereby decreasing the phosphorylation rate of p53 (Li *et al.* 2006). This feedback mechanism initiates cell cycle arrest and represses apoptotic effects. These mentioned p53 target genes were already induced after 8 h exposure to sodium selenite (see appendix Table A5). MDM2 is a negative feedback regulator of p53, and its gene expression was induced in p53-proficient cells, but not in p53-deficient cells, although p53 mRNA levels were increased in both cell lines. The enhanced transcript levels of p53 in the p53-deficient cells could possibly form a non-functional p53 protein, but thereby disabled to regulate its target genes. The cell cycle inhibitors p21 and p15 were induced in addition to the simultaneous up-regulation of *TP53* and *MDM2,* providing a marker for genotoxic stress. p53 is subject to a negative and a positive feedback mechanism as other transcription factors (Harris and Levine 2005). In this context, it is possible that p53 can induce its own expression as well as the expression of *MDM2*. The cyclin-dependent kinase regulator cyclin D (*CCND1)* was increased by 1.65-fold in the p53-proficient cells (data not shown). However, this was not significant. Cyclin D is important for the cell cycle progression by complexing with CDK4 and CDK6, which are responsible for the G1-S transition. Cyclin D also binds to the Rb protein, which leads to the release of the transcription factor E2F1, regulating genes necessary for S phase transition. In both cell lines, repressed transcript levels of the transcription factor *E2F1* important for cell cycle progression, were found, indicating prohibited cell progression and thereby cell cycle arrest. The gene expression analysis showed that the transcript levels of *EGFR* were almost doubled in the p53-proficient cells. The EGF receptor (EGFR) is activated by epidermal growth factor (EGF) that can activate, for instance, the ERK signaling pathway, leading to increased expression of cyclin D and enhanced cell proliferation. Oxidative stress-induced phosphorylation of EGFR is described in literature as an EGF-independent EGFR activation (Meves *et al.* 2001). It is therefore possible that the observed intracellular oxidative stress could activate the ERK signaling pathway through ROS and thereby affect the expression of genes involved in cell proliferation, cell differentiation and apoptosis.

An increase of *JUN* levels, which encodes activator protein AP-1, by sodium selenite was observed in both cell lines, suggesting an activated JNK/p38 MAPK signaling pathway. Originally thought to be a distinct transcription factor, AP-1 is now synonymous with the large group of homo- and heterodimeric Jun and Fos DNA-binding proteins. Jun and Fos regulate multiple cellular processes, including proliferation, differentiation, apoptosis, and the adaptive response to stress. A binding site for AP-1 is found in the promotor region of *HMOX-1* (Alam and Cook 2007). Decreased GSH levels (see Figure 5.20) and increased AP-1 and NF-κB activation seen in the gene expression profile of sodium selenite may be associated with an enhanced pro-inflammatory IL-8 release in alveolar epithelial cells, suggesting a mechanism for the pro-inflammatory effects of oxidative stress (Rahman *et al.* 2002). Another study demonstrated that NF-κB plays an essential role in the activation of wild-type p53 tumor suppressor to initiate pro-apoptotic signaling in response to generation of superoxide (Fujioka *et al.* 2004).

The impact of the simultaneous exposure of sodium selenite and cadmium chloride on the relative gene expression in cell cycle control genes in p53-proficient HCT116 cells represented a point of interest. mRNA levels of *CDKN1A1*, better known as p21, were enhanced by 10-fold by sodium selenite. However, a significant induced p21 expression was also observed to less extent in the p53-deficient cells (Figure 5.7). Co-exposure to cadmium abolished the sodium selenite-induced p21 expression completely. A G1 arrest is normally induced resulting from enhanced p21-expression. Cells were unable to raise p21 transcript levels, possibly due to an interaction between cadmium chloride and p53, since p21 is mainly regulated through p53. A 3-fold-increased expression of the CDK inhibitor p15 (*CDKN2B*) was induced upon sodium selenite treatment in a p53-dependent manner. The presence of cadmium chloride cancelled the p15 up-regulation induced by sodium selenite. Sodium selenite-enhanced expression of other target p53 genes as well such as the negative feedback regulator of p53 *MDM2*, the protein phosphatase *PPM1D* and serine/threonine-protein kinase *PLK3* was not induced when cadmium chloride was present, indicating an abolition of p53-mediated responses to sodium selenite exposure. Interactions with cell cycle checkpoints have previously been demonstrated for cadmium. In the presence of cadmium, γ-radiation-induced cell cycle arrest in G1 and G2/M phases was suppressed due to impairment of p53 caused by unfolding of its conformational structure (Meplan *et al.* 1999).

Sodium selenite-induced enhancement of *JUN* expression levels was observed in both p53-proficient and p53-deficient cells, suggesting an activated JNK/p38 MAPK signaling pathway (Figure 5.7). In the presence of cadmium chloride, a significant induction of AP1 was also observed, although sodium selenite alone induced twice the amount of *JUN* transcript levels. 24 h exposure to 10 µM cadmium chloride enhanced *JUN* expression by about 4-fold while 8 h exposure to cadmium induced a 13-fold

change of *JUN* (see appendix Table A4), suggesting that JUN might be another early response gene induced in the stress response to cadmium exposure.

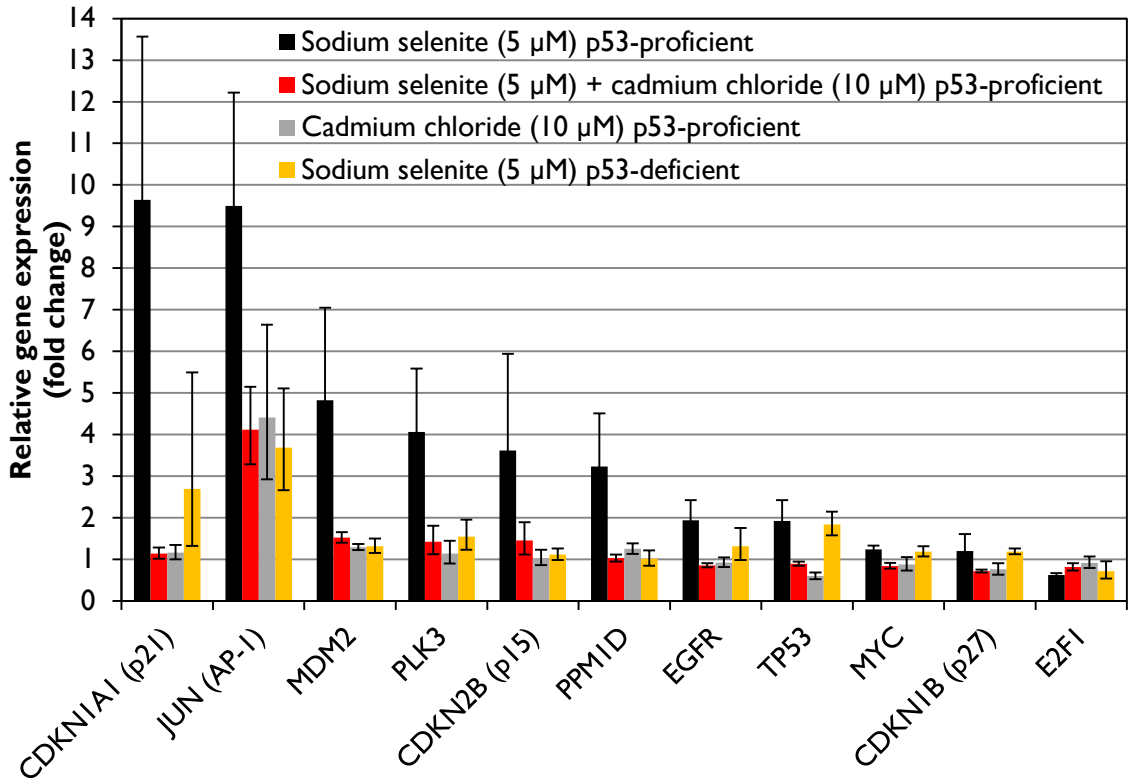

Figure 5.7: Impact of sodium selenite (5 µM) in combination with cadmium chloride (10 µM) and the role of p53 on the relative gene expression of genes associated with cell cycle control genes in p53-proficient and p53-deficient HCT116 cells after 24 h incubation. Gene name abbreviations listed in Table A3. Mean values ± SD of at least two independent experiments of double or single determinations are shown.

Genes associated with DNA repair pathways

Sodium selenite induced several p53-dependent genes involved in DNA damage response. As shown in Figure 5.8, we observed increased transcript levels of *XPC, DDB2, RRM2B,* and *ATM,* suggesting activated DNA repair mechanisms. During activated nucleotide excision repair (NER), p53 binds to p53-response elements to up-regulate the expression of the *XPC* (xeroderma pigmentosum complementation group C) and *DDB2 (*p48/DNA damage-binding protein 2) genes. XPC and p48/DDB2 recognize and bind to specific lesions on the DNA. *ERCC1, ERCC4* and *ERCC5* encode NER specific endonucleases, which bind and cleave the DNA leaving 5′ phosphate and 3′ hydroxyl-termini to the site of the damage (Sengupta and Harris 2005). Transcripts of *ERCC1, ERCC4* and *ERCC5* tended to increase following sodium selenite treatment. Together with ERCC4, also known as

XPF, ERCC1 forms the ERCC1-XPF enzyme complex in NER (Sengupta and Harris 2005). An induction of transcript levels of NER genes indicates that sodium selenite exposure causes DNA damage. *RRM2B* is generally associated with DNA repair, however not classified in a specific repair pathway due to involvement in NER, BER and MMR. *RRM2B* encodes the ATM-interacting ribonucleotide reductase M2B, and is induced to provide desoxyribonucleotides for DNA repair due to induction of other repair genes. Thus, it is essential in the DNA damage response. Marginal influence on expression of other DNA repair genes was additionally observed.

ATM and ATR play central roles in the DNA damage response with respect to cell cycle arrest and control of DNA replication. Both are serine/threonine protein kinases responsible for sensing DNA damage, activating amongst others the DNA damage checkpoint via activation of numerous targets, including p53 and checkpoint kinases (Chk1, Chk2) through phosphorylation, and thereby leading to cell cycle arrest. ATM is recruited and activated by DNA double-strand breaks, while ATR is activated in response to persistent single-stranded DNA, which may occur at stalled replication forks, and acts as an intermediate in NER and homologous recombination repair (HR) (Shiloh 2001; Shiloh 2006). Gene expression levels of NER genes were unchanged in p53-deficient HCT116 cells upon sodium selenite exposure, indicating strongly a p53-mediated response to DNA damage.

In the presence of cadmium, vertially no change in expression levels compared to the control in all selected genes in the DNA damage response was found (Figure 5.8). An inhibition of induced NER gene expression levels in response to sodium selenite exposure by cadmium suggests that sodium selenite-induced DNA damage is not being recognized and repaired due to a presumable incapability of the tumor suppressor, p53, to enhance expression levels of necessary repair proteins in response to damage. Cadmium has been shown to disturb major DNA repair processes, such as NER, BER and MMR (Hartwig 2010). There are at least 30 proteins involved in NER. Cadmium inhibits repair of UVC- and BaP-induced DNA lesions by impairing assembly and disassembly of the DNA damage recognition proteins XPC, XPA and XPG in the DNA repair complex (Fatur *et al.* 2003; Schwerdtle *et al.* 2010).

Oxidative DNA damage is repaired by DNA base excision repair (BER). No induction of BER associated genes *APEX, LIG1, LIG3, OGG1, PARP1* and *POLB* was observed after exposure to sodium selenite (data not shown). Compared to BER, p53 is assumed to affect NER to a greater extent at the transcriptional level (Seo and Jung 2004). NER repairs mainly bulky DNA adducts and helix-distorting lesions, however, NER genes such as *XPC, XPA* and *ERCC4* are shown to be up-regulated by oxidative stress (Langie *et al.* 2007). Components of the NER machinery may therefore also have a role in repair of oxidative DNA damage as a back-up mechanism to BER (Slupphaug *et al.* 2003). The

parallel induction of NER genes in addition to *ATM* and *RRM2B* represents an indicator of induced repair and synthesis of DNA.

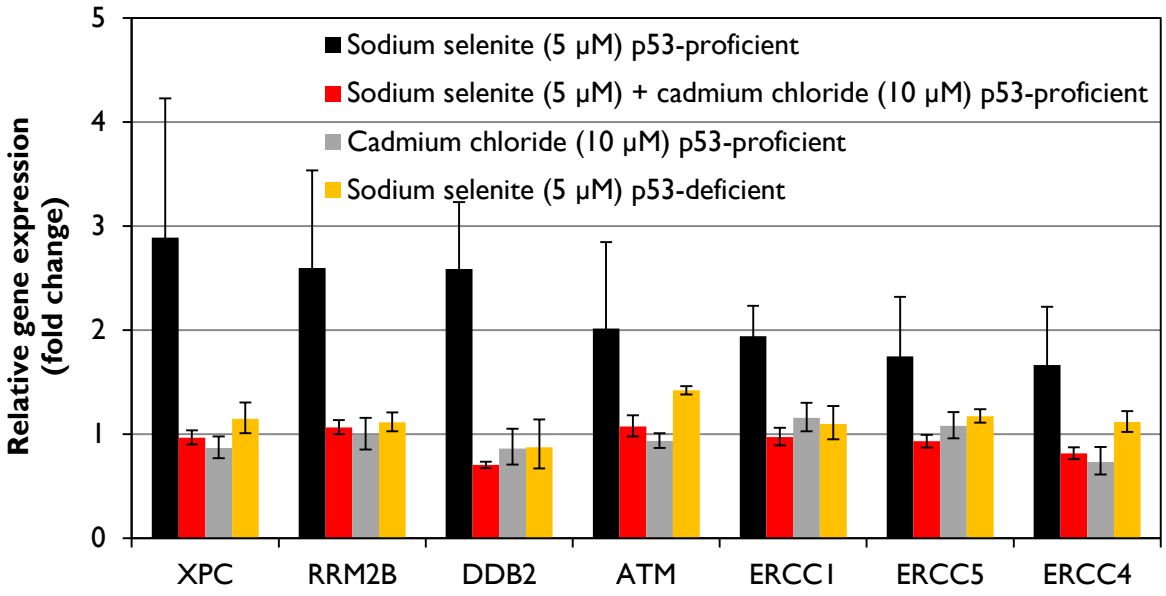

Figure 5.8: Impact of sodium selenite (5 µM) in combination with cadmium chloride (10 µM) and the role of p53 on the relative gene expression of genes associated with DNA repair in p53-proficient and p53-deficient HCT116 cells after 24 h incubation. Gene name abbreviations listed in Table A3. Mean values ± SD of at least two independent experiments of double or single determinations are shown.

Genes associated with apoptosis

The pro-apoptotic genes *BBC3, TNFRSF10B (*DR5*), PMAIP1 (*Noxa) and *BAX* were induced by sodium selenite, indicating an induction of apoptosis. However, up-regulation of the anti-apoptotic genes *XIAP* and *BCL2L1* was also observed (Figure 5.9). In p53-deficient cells, the p53-target gene *BAX* was not up-regulated after sodium selenite exposure, but *PUMA*, *Noxa* and *DR5* showed increased mRNA levels, suggesting a p53-independent response. Induction of *PMAIP1* in response to DNA damage can occur in a p53-independent manner, possibly as a downstream target of p73 (Ploner *et al.* 2008).

Co-exposure to cadmium chloride raised the Noxa gene expression levels 2-fold: however, no change in other pro-apoptotic genes was observed (Figure 5.9). Although the apoptotic transcriptional response was possibly mediated both in a p53-dependent- and independent manner, these results indicate once again that the sodium selenite-increased gene induction is attenuated by simultaneous cadmium exposure.

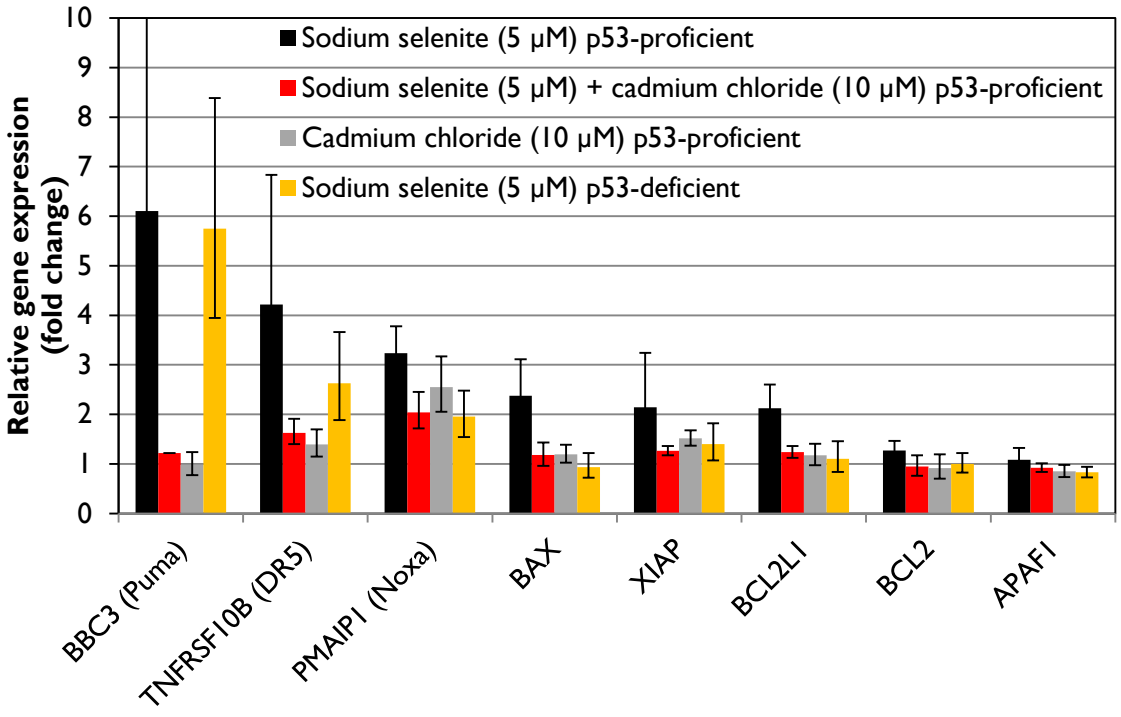

Figure 5.9: Impact of sodium selenite (5 µM) in combination with cadmium chloride (10 µM) and the role of p53 on the relative gene expression of genes associated with apoptosis in p53-proficient and p53-deficient HCT116 cells after 24 h incubation. Gene name abbreviations listed in Table A3. Mean values ± SD of at least two independent experiments of double or single determinations are shown.

The Bcl-2 family may be divided into three groups according to its Bcl-2 homology (BH) domains, its mitochondrial anchorage and its pro- or anti-apoptotic effect (Mohamad *et al.* 2005). The multi-domain pro-apoptotic *BAX* also belongs to this protein family, while the *BBC3* gene, also known as PUMA (p53 upregulated modulator of apoptosis), is a pro-apoptotic member of the BH3-only subgroup of Bcl-2 family proteins. It is a key mediator of p53-dependent and p53-independent apoptosis by binding to the inhibitory members such as anti-apoptotic members Bcl-2 and Bcl-X_L of the Bcl-2 family (Bcl-2-like proteins) via its BH3 domain (Hikisz and Kilianska 2012). *PMAIP1,* also known as Noxa, exerts its pro-apoptotic function mainly by neutralizing the anti-apoptotic Bcl-2 proteins and facilitating activation of Bax and/or Bak proteins (Ploner *et al.* 2008). Activation of death receptors (DR), which are members of the tumor necrosis factor (TNF) receptor family located at the plasma membrane, including Fas, DR4, and DR5, can be regulated by p53 as a part of the extrinsic apoptotic pathway (Sheikh *et al.* 1998; Yu and Zhang 2005).

APAF-1 is also an apoptosis initiator: however, its mRNA content remained unchanged in both cell lines. As *APAF-1* harbors p53-responsive elements in the promoter region, it represents another

target in DNA damage-induced apoptosis mediated by p53 (Robles *et al.* 2001). In mitochondria-mediated apoptosis, cytochrome C is released into the cytosol due to mitochondrial depolarization which occurs in response to DNA damage and other stimuli. APAF-1 and cytochrome C form a complex leading to the recruitment and activation of pro-caspase-9 to form the apoptosome, the first step in the caspase activation cascade that ultimately leads to chromatin degradation (Mohamad *et al.* 2005; Shi 2001).

5.2.2 Differential impact of sodium selenite and selenomethionine on transcriptional regulation

The differential gene expression profiles of the two investigated selenocompounds, sodium selenite and selenomethionine, were obtained in order to examine possible selenium species-dependent transcriptional differences following 24 h exposure to 5 µM sodium selenite and 500 µM selenomethionine in p53-proficient HCT116 cells cellular exposure. Co-exposure to selenomethionine and 10 µM cadmium chloride for 24 h were also investigated to reveal the impact of cadmium on selenomethionine-induced effects.

Genes involved in oxidative stress response and inflammation

The oxidative stress response, including inflammation markers, was highly induced by sodium selenite exposure, partially in a p53-dependent manner (Figure 5.6). Transcript levels of Nrf2 target genes remained unaffected in response to selenomethionine, unlike sodium selenite exposure, which enhanced several target genes of Nrf2 (Figure 5.10A), indicating an important specific difference between the selenium species since sodium selenite exposure enhanced several Nrf2 target genes. Figure 5.6 shows that co-exposure to cadmium chloride also induced Nrf2 target genes. However, the cadmium chloride-induced enhancement of Nrf2 target genes was less pronounced in the presence of selenomethionine (Figure 5.10). The transcript levels of the transcription factor Nrf2 coded by *NFE2L2* were neither enhanced by selenomethionine nor by co-exposure to cadmium chloride. *ABCB1* mRNA levels were repressed by 45 % after selenomethionine exposure (Figure 5.10A), but up-regulated more than 3-fold upon cadmium exposure alone (Figure 5.6A). After simultaneous exposure to selenomethionine and cadmium chloride, the *ABCB1* gene, an ABC transporter efflux pump, was more than 3-fold enhanced (Figure 5.10A). Given the present results, it is likely that induction of several Nrf2-target genes by cadmium chloride was less pronounced in the presence of selenomethionine, although expression of a few xenobiotic metabolism genes was enhanced.

The p53-dependent effects on the mRNA expression levels of *MT1X, MT2A* and *SLC30A1* following sodium selenite treatment occurred possibly due to oxidative zinc release of MTs. Exposure to selenomethionine did not affect the gene expression levels of these genes (Figure 5.10C), suggesting another differential transcriptional response to the two selenocompounds. 24 h exposure to selenomethionine and cadmium chloride increased the *MTX1* and *MT2A* expression by 47-fold and 11-fold, respectively (Figure 5.10C). Cadmium alone raised the *MTX1* levels 19-fold after 24 h exposure, while the *MT2A* expression was 8-fold increased (Figure 5.6C). The expression of the ZnT1 gene (*SLC30A1*) was unchanged upon selenomethionine incubation, but a 4.3 fold change after 24 h cadmium co-exposure was found (Figure 5.10C). This increase was most likely due to the influence of cadmium itself since cadmium alone induced a 3.3-fold change (Figure 5.6C). Target genes of the metal responsive transcription factor MTF-1, such as MTs and ZnT1, were thereby also induced in the presence of cadmium.

While sodium selenite induced *HMOX1* mRNA levels by 20-fold, a significant, but smaller (2-fold), change could be observed upon exposure to selenomethionine. Simultaneous exposure to selenomethionine and cadmium chloride led a 159-fold change of *HMOX1* gene expression (Figure 5.10B), which was much higher than the 44-fold change by 24 h incubation with 10 µM cadmium chloride alone (Figure 5.6B). Several transcription factors such as AP-1 (Jun), Nrf2 and HSF-1 may enhance the expression of the early responsive gene *HMOX1* (Alam and Cook 2003). Figure 5.11 shows that selenomethionine exposure led to an enhancement of *JUN* gene expression levels by about 3-fold, which indicates an activation of the transcription factor AP-1. *HSPA1A* mRNA levels were unchanged after exposure to selenomethionine, such as in the case of sodium selenite, implying no activation of the transcription factor heat shock factor HSF-1. However, co-exposure to cadmium chloride induced *HSPA1A* mRNA levels 139-fold. In comparison to exposure to sodium selenite in combination with cadmium chloride, a 30-fold higher *HSPA1A* gene expression was seen (Figure 5.10B). Because 24 h incubation of 10 µM cadmium chloride strongly induced *HSPA1A* mRNA levels by more 200-fold (Figure 5.6B), this could imply that *HSPA1A* transcript levels are negatively affected by co-exposure to sodium selenite, but not by co-exposure to selenomethionine.

The inflammation marker *IL8* was also induced by selenomethionine by 8-fold, which, however, was induced over 84-fold by sodium selenite in a p53-independent manner. Co-exposure to cadmium chloride led to a 16-fold change of *IL8* mRNA (Figure 5.10B). Because cadmium alone (10 µM) induced *IL8* gene expression by 6-fold, the simultaneous exposure to selenomethionine and cadmium chloride seems to act additively on the gene regulation of *IL8*. When compared to sodium selenite and cadmium chloride co-exposure, co-exposure to cadmium chloride affected sodium selenite-induced *IL8* gene negatively, as in seen in Figure 5.6B. The mRNA levels of the p100 subunit of NF-

κB, *NFKB2,* the NF-κB inhibitor IκBα *NFKB1A* or the p105 subunit of NF-κB, *NFKB1,* did not change upon selenomethionine exposure, but negatively affected by co-exposure to cadmium chloride. (Figure 5.10D). The NF-κB inhibitor IκBα *NFKB1A* was repressed by 60 % and the p105 subunit of NF-κB, *NFKB1* was more than 40 % repressed. *FTH-1* mRNA levels were, however, increased by treatment with selenomethionine by about 3-fold and by 2-fold following co-exposure to cadmium chloride (Figure 5.10A). The change in expression of *FTH1* is presumably closely associated with the induction of *HMOX1*. The genes *IL-8* and *FTH-1* are targets of the transcription factor NF-κB, and their induction after selenomethionine exposure suggests a possible activation of NF-κB, although the subunits of the NF-κB were not enhanced, and, in the case of co-exposure, repressed.

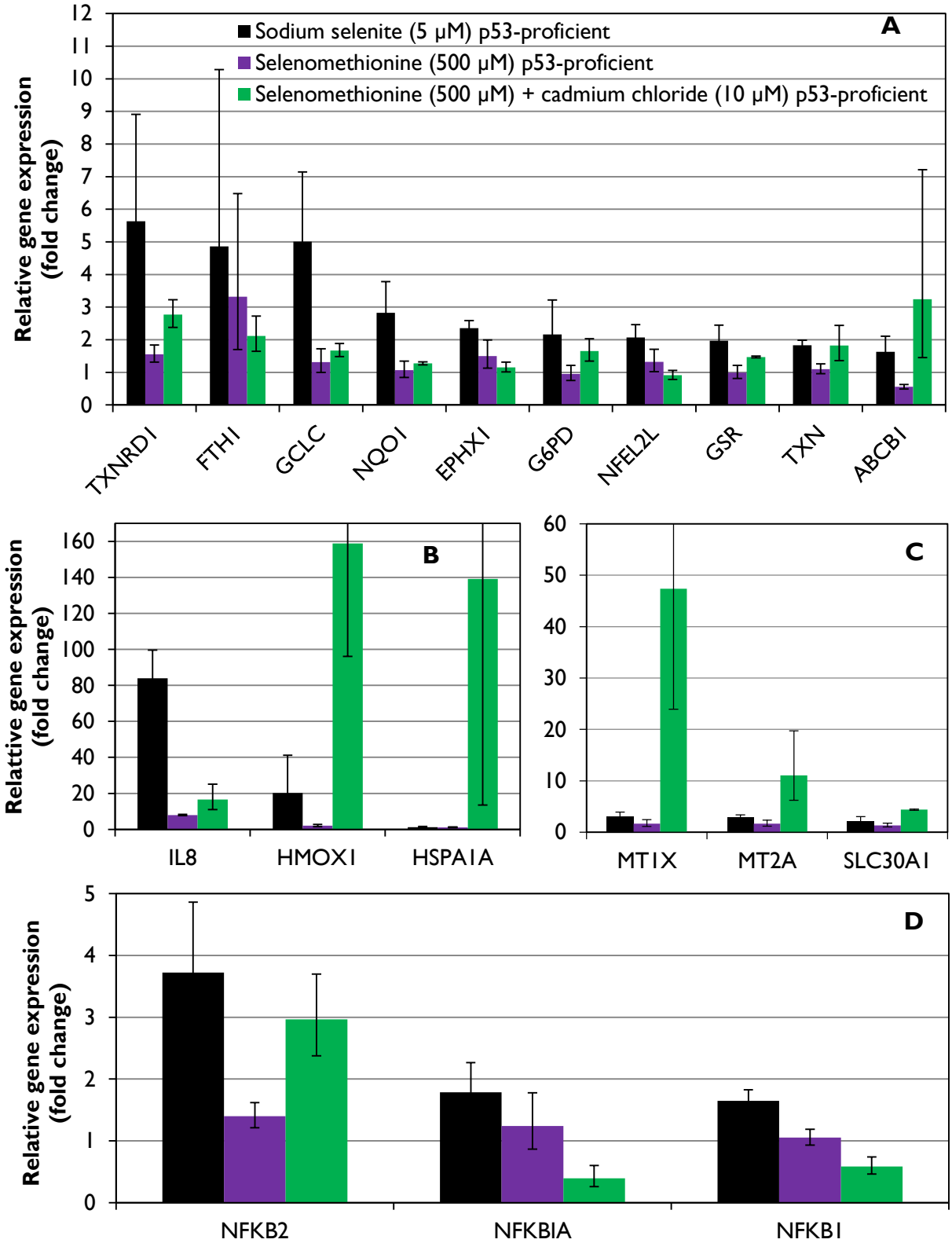

Figure 5.10: Impact of selenomethionine (500 µM) in comparison to sodium selenite (5 µM) and the impact of selenomethionine (500 µM) in combination with cadmium chloride (10 µM) regarding the relative gene expression on genes associated with oxidative stress response (A, B, D) and inflammation (C, D) in p53-proficient HCT116 cells after 24 h incubation. Gene name abbreviations listed in Table A3. Mean values ± SD of at least two independent experiments of double or single determinations are shown.

Genes associated with cell cycle control

While sodium selenite increased mRNA levels of the cyclin-dependent kinase inhibitor *CDKN1A1* (p21) by 10-fold, the p21 expression levels did not change either upon selenomethionine exposure or co-exposure to cadmium and selenomethionine (Figure 5.11). As p21 also was induced by 3-fold by sodium selenite in the p53-deficient cells, a p53-independent induction of p21 was suggested (Figure 5.8). The CDK inhibitor *CDKN2B*, p15, was however increased by about 4-fold upon selenomethionine treatment, independent of cadmium (Figure 5.11). p15 was also p53 dependently increased after sodium selenite incubation. In other words, p21 gene expression was unaffected by selenomethionine exposure and affected by sodium selenite exposure independent from p53, while p15 transcript levels were found to be affected by exposure to selenomethionine and p53 dependently raised upon exposure to sodium selenite. Another p53 target gene enhanced in response to selenomethionine independent of cadmium was the serine/threonine-protein kinase *PLK3*, indicating a possible G2/M arrest. The expression of the negative feedback regulator of p53, *MDM2* was not increased, implying no activation by p53. p53 mRNA levels were tendentiously increased (1.8-fold). However, the activity of p53 is mainly regulated by post translational modifications, and not by transcriptional regulation (Vousden and Lu 2002). Repressed transcript levels of the transcription factor *E2F1* important for cell cycle progression were found, indicating prohibited cell progression and cell cycle arrest, was observed for both selenocompounds, in addition to nearly doubled transcript levels of *EGFR*.

A more than 50 % repression of the CDK inhibitor *CDKN1B* (p27) was observed following selenomethionine exposure in combination with cadmium chloride. We observed that the gene *MYC* that encodes c-Myc, which is a multifunctional, nuclear phosphoprotein and acts as a proliferative transcription factor, was more than 65 % down-regulated after co-exposure to selenomethionine and cadmium chloride, in addition to a 55 % repression of the transcription factor *E2F1*. A tendentious down-regulation of cell cycle inhibitor p27 and the transcription factors *MYC* and *E2F1* was found after selenomethionine exposure and cadmium exposure alone (Figure 5.7), implying a possible additive repression in the simultaneous incubation of selenomethionine and cadmium chloride. E2F1 promoter contains c-MYC responsive elements (Oswald *et al.* 1994). Inhibition of E2F1 expression could result in decreased formation of the E2F1-DP1 complex, and, thereby in relatively low activation of DNA synthesis genes.

An activation of the transcription factor AP-1 was assumed due to the selenomethionine-induced enhancement of *JUN* gene expression levels about 3-fold. An 11-fold increase in *JUN* gene induction was observed upon co-exposure to cadmium chloride (Figure 5.11). After 24 h exposure to cadmium

alone, a 4-fold change of *JUN* expression was found (Figure 5.7), suggesting an additive induction of *JUN* gene expression after co-exposure to selenomethionine and cadmium chloride.

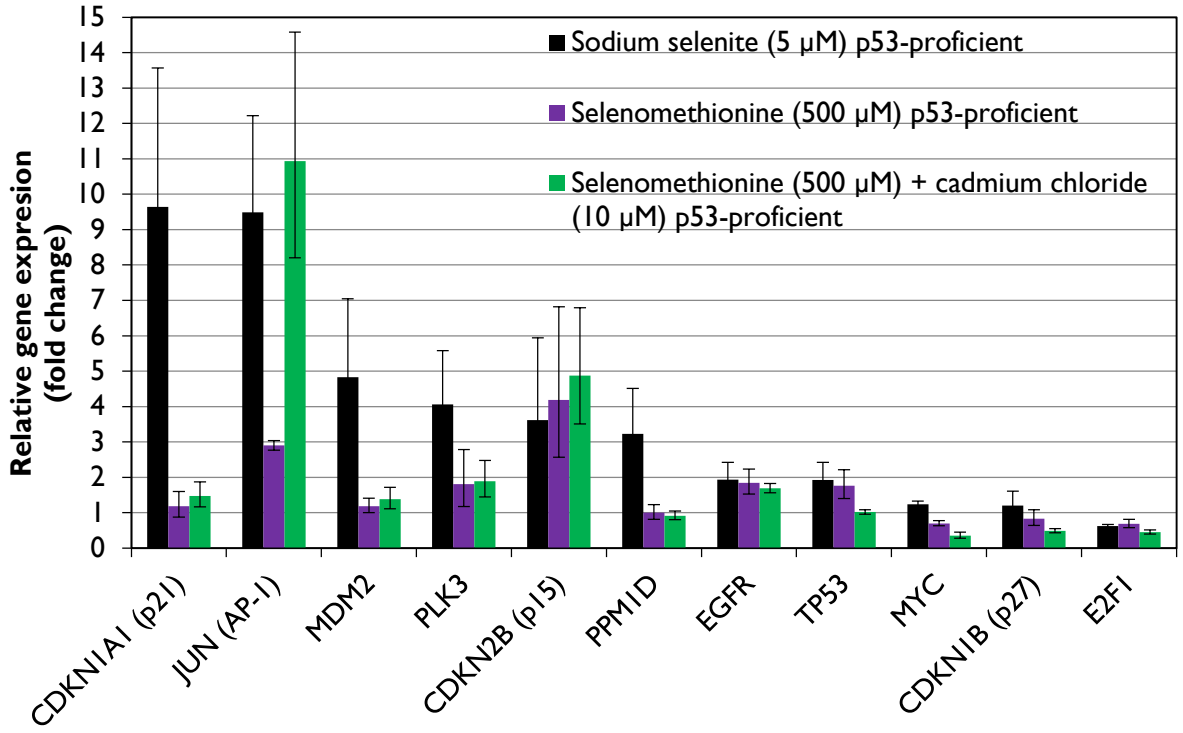

Figure 5.11: Impact of selenomethionine (500 µM) in comparison to sodium selenite (5 µM) and the impact of selenomethionine (500 µM) in combination with cadmium chloride (10 µM) regarding the relative gene expression on cell cycle control associated genes in p53-proficient HCT116 cells after 24 h incubation. Gene name abbreviations listed in Table A3. Mean values ± SD of at least two independent experiments of double or single determinations are shown.

Genes associated with DNA repair pathways and apoptosis

Sodium selenite induced several p53-dependent genes involved in NER and DNA damage response, in a p53-dependent fashion (Figure 5.8). Oxidative DNA damage is repaired by DNA base excision repair. Like in the case of sodium selenite, no enhancement of BER associated genes *APEX, LIG3, OGG1,* and *POLB* was observed after exposure to selenomethionine. However, mRNA levels of *PCNA* and *LIG1* were repressed by about 50 %, indicating a possible inhibition of DNA repair processes. Repression of *LIG1*, a gene encoding for a DNA ligase and necessary for the conjunction of two DNA strands to one DNA strand, indicates a possible inhibition of DNA ligation. *PCNA* (proliferating cell nuclear antigen) suppresses the activation of DNA polymerase δ (*POLD1*), thereby playing a role in replication inhibition. Overall, it is evident that the two different selenocompounds clearly influence DNA damage gene regulatory patterns, and that this effect was selenium species-specific.

No significant induction of DNA damage response-associated genes could be found after co-exposure to selenomethionine and cadmium chloride due to relatively high standard deviations (Figure 5.12A). Down-regulation of several repair genes was, however, observed in response to treatment, especially to co-treatment of selenomethionine and cadmium chloride. Selenomethionine repressed *LIG1* both in the presence and absence of cadmium. *LIG1* is a gene encoding for a DNA ligase 1, and its repression might result in an inhibition of DNA ligation. The gene expression of *PCNA*, which is the co-factor of DNA polymerase δ by suppressing the activation of the polymerase, was even further repressed from 48 % down to 33 % in the presence of cadmium, which could imply a possible replication inhibition. The expression of the p53-dependent NER-associated gene *DDB2 (*p48/DNA damage-binding protein 2) was down-regulated to 40 % in the presence of cadmium.

The *APEX* gene encodes the major apurinic/apyrimidinic (AP) endonuclease, which is especially involved in DNA base excision repair. This gene was also repressed by 60 % upon simultaneous treatment of selenomethionine and cadmium chloride. Down-regulation of this important AP endonuclease, which initiates repair by cleaving the occurring AP site, could therefore impair the repair process. A 60 % down-regulation of the repair gene *RAD51* was also found after co-exposure to cadmium. The gene product of *RAD51* is a recombinase that transiently binds to both single-stranded and double-stranded DNA during the recombination reaction, being essential in homologous recombination (HR) of DNA during double strand break repair. Taken together, exposure to selenomethionine alone and in combination with cadmium chloride could possibly inhibit DNA repair processes due to down-regulation of several central genes involved in these mechanisms.

While sodium selenite enhanced induction of the pro-apoptotic genes *BBC3* (Puma), *TNFRSF10B* (DR5), *PMAIP1 (*Noxa) and *BAX*, an indication of apoptosis induction, exposure to selenomethionine also led to an activation of DR5 and Noxa, which would suggest an induction of apoptosis (Figure 5.12B). This effect occurred also in the presence of cadmium. No significant changes in mRNA levels of the pro-apoptotic factors *BBC3* (Puma) and *BAX* were observed. The anti-apoptotic gene *XIAP*, which encodes the X-linked inhibitor of apoptosis protein, doubled its transcript levels in response to co-exposure to cadmium and selenomethionine, while the anti-apoptotic *BCL2* gene was down-regulated by 45 %. In addition, the mRNA content of the apoptosis initiator *APAF-1* was repressed by about 40 %. The complex formed by APAF-1 and cytochrome C known as the apoptosome recruits and activates procaspase-9 initiating the first step in the cascade of caspase activation that ultimately leads to chromatin degradation (Mohamad et al. 2005; Shi 2001). Down-

regulation of *APAF1* could therefore lead to decreased formation of the apoptosome, and thus apoptosis.

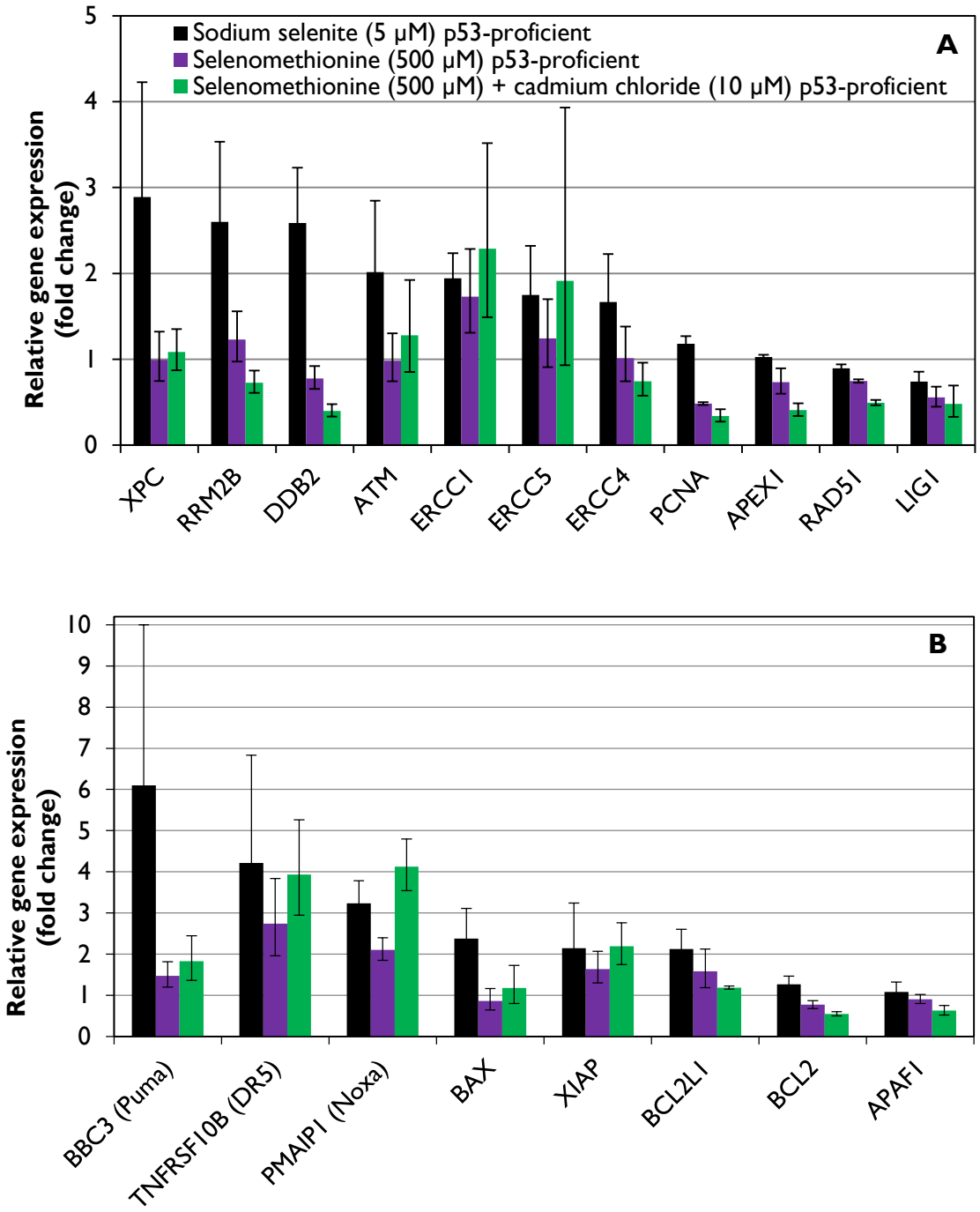

Figure 5.12: Impact of selenomethionine (500 µM) in comparison to sodium selenite (5 µM) and the impact of selenomethionine (500 µM) in combination with cadmium chloride (10 µM) regarding the relative gene expression on (A) DNA repair and (B) apoptosis associated genes in p53-proficient HCT116 cells after 24 h incubation. Gene name abbreviations listed in Table A3. Mean values ± SD of at least two independent experiments of double or single determinations are shown.

5.2.3 Summary of the gene expression profiling

The oxidative stress response was strongly induced by sodium selenite, partially dependent of p53 cellular status. Enhanced pro-inflammatory *IL-8* levels suggest a mechanism for pro-inflammatory effects of sodium selenite-induced oxidative stress. Sodium selenite induced p53 target genes in cell cycle control, DNA repair and apoptosis, indicating strongly a p53-mediated response to DNA damage. The parallel induction of NER genes in addition to *ATM* and *RRM2B* represents an indicator of induced DNA repair – and synthesis. *PUMA, Noxa* and *DR5* showed increased mRNA levels in both cell lines, suggesting a p53-independent response. Cadmium attenuated the sodium selenite-induced and p53-mediated up-regulation of genes involved in cell cycle, DNA repair and apoptosis. Moreover, the oxidative stress response was highly activated by cadmium alone. Selenomethionine had to less extent impact on gene expression regulation than sodium selenite, demonstrating species-specific effects. The DNA damage response, especially BER, was however negatively affected by selenomethionine, which was further repressed in the presence of cadmium. Table 5.1 summarizes the obtained gene expression profiles.

Table 5.1: Summary of obtained gene expression profiles of selenocompounds alone or in combination with cadmium chloride. Na_2SeO_3: sodium selenite, SeMet: selenomethionine, $CdCl_2$: cadmium chloride

	Na_2SeO_3 ($p53^{+/+}$)	Na_2SeO_3 ($p53^{-/-}$)	Na_2SeO_3 + $CdCl_2$ ($p53^{+/+}$)	SeMet ($p53^{+/+}$)	SeMet + $CdCl_2$ ($p53^{+/+}$)	$CdCl_2$ ($p53^{+/+}$)
MTs	↑	-	↑↑	-	↑↑↑	↑↑↑
Heat-shock	-	-	↑	-	↑↑↑	↑↑↑
Oxidative stress response	↑↑	↑	↑↑↑	↑	↑↑	↑↑↑
Inflammation	↑↑↑	↑↑↑	↑	↑	↑	↑
Redox-sensitive transcription factors	↑↑↑	↑	↑	-	-	↓↑
Cell cycle progression	-	-	-	↓	↓	↑↑
Cell cycle arrest	↑↑↑	↑	-	↑	↑	-
DNA damage response	↑↑	-	-	↓	↓	-
NER	↑↑	-	-	(↓)	↓	-
BER	-	-	-	↓	↓↓	-
Pro-apoptotic signaling	↑↑↑	↑↑	↑	↑	↑	↑
Anti-apoptotic signaling	↑	-	-	-	-	↑

5.3 Oxidative stress

Potential mechanisms in induction of oxidative stress include GSH-depletion or inhibition of ROS-scavenging antioxidant enzymes, which are often proposed as mechanisms in cadmium-induced cytotoxicity. We investigated the possible depletion of GSH by cadmium in our cell model of HCT116 cells. Since the toxicity of sodium selenite may involve GSH in the reduction of sodium selenite, which could in turn lead to GSH-depletion and disturbance of the redox homeostasis by the production of superoxide, we examined the effect of simultaneous exposure to sodium selenite and cadmium chloride on GSH content and superoxide generation. Other potential targets of cadmium may be selenium-dependent enzymes like glutathione peroxidase and thioredoxin reductase as well as selenium-independent enzymes, such as glutathione reductase, superoxide dismutase and catalase. Selenoproteins could be a sensitive target in cadmium-induced carcinogenicity by specific binding to selenol group in these antioxidative enzymes. Examinations of enzyme activities of antioxidant enzymes after simultaneous exposure to sodium selenite and cadmium chloride were performed.

5.3.1 Impact of sodium selenite in combination with cadmium chloride on GSH content

GSH is the most prevalent low-molecular-weight thiol in mammalian cells and essential in the regulation of disulfide bonds of proteins and the detoxification of electrophiles and oxidants. Thus, it belongs to the major components in the cellular antioxidative defense. A reduced content of GSH or a shift towards GSSG are associated with intracellular oxidative stress. In non-stressed cells more than 99 % of GSH is maintained in its reduced state (Deneke and Fanburg 1989). The quantification of total GSH content was determined by Tietze's enzymatic recycling assay using the thiol reagent DTNB (Tietze 1969).

The intracellular GSH pool following exposure to increasing cadmium chloride concentrations at a series of time point was studied (Figure 5.13). At the earliest examined time points (2 h and 4 h), no changes in the intracellular GSH were observed after incubation with cadmium chloride in the concentration range from 1 µM to 50 µM. The lowest investigated cadmium chloride concentration (1 µM) had no influence on intracellular GSH levels at any of the studied time points. Increased intracellular GSH levels were, however, seen after 6 h exposure to cadmium chloride at a concentration of 5 µM, reaching a peak level after 12 h with 10 µM cadmium chloride. Neither longer incubation time (24 h) nor higher cadmium chloride concentration (50 µM) further increased the GSH pool. Cells growing under sodium selenite supplementation upon cadmium exposure showed similar patterns (data not shown). Buthionine sulfoximine (BSO) was used as a positive control to specifically deplete GSH due to its irreversible inhibition of γ-glutamyl-cysteine synthetase and

thereby *de novo* GSH synthesis. 1h exposure to 100 µM BSO depleted the total GSH level to 4.7 % compared to the untreated control, which contained on average 6.7 mM total GSH (data not shown).

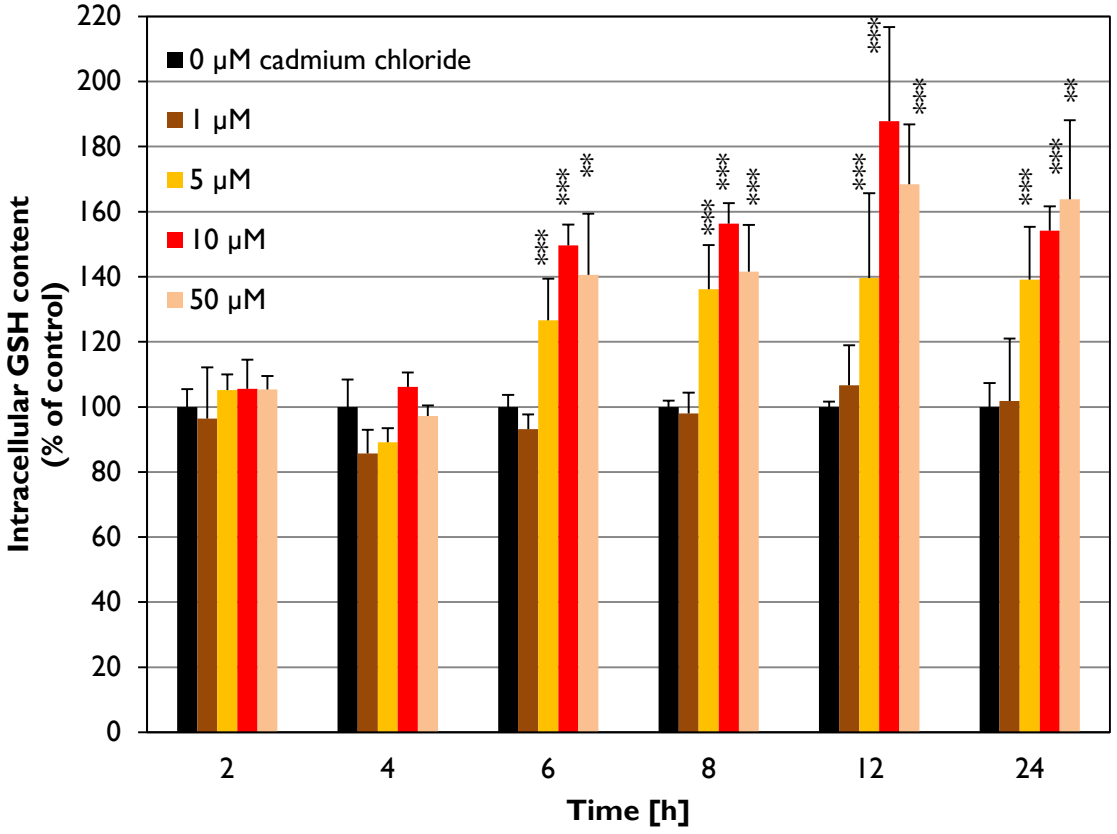

Figure 5.13: Impact of cadmium on intracellular GSH content. p53-proficient HCT116 cells were treated with increasing cadmium chloride concentrations (1 µM-50 µM) after several incubation time (2 h, 4 h, 6 h, 8 h, 12 h and 24 h). The total content of GSH was determined after the method of Tietze. Mean values ± SD of three independent experiments are shown. Statistically significant differences from the corresponding untreated control at each time point were tested by ANOVA with Dunnett's T3 Post-Hoc test: ** = $p < 0.01$, *** = $p < 0.001$.

In p53-proficient HCT116 cells, sodium selenite reduced the cellular GSH level at cytotoxic concentrations (8 µM) after 8 h as well as after 24 h to about 65 % and 37.6 %, respectively. Increasing concentrations from 1 µM to 5 µM sodium selenite did not result in any significant changes in the cellular GSH content (Figure 5.14A). However, with similar conditions in p53-deficient cells, 8 µM sodium selenite only diminished the GSH pool to 85.7 % of the control after 24 h exposure, implying a p53 dependent effect on the GSH-depletion provoked by sodium selenite (Figure 5.14B).

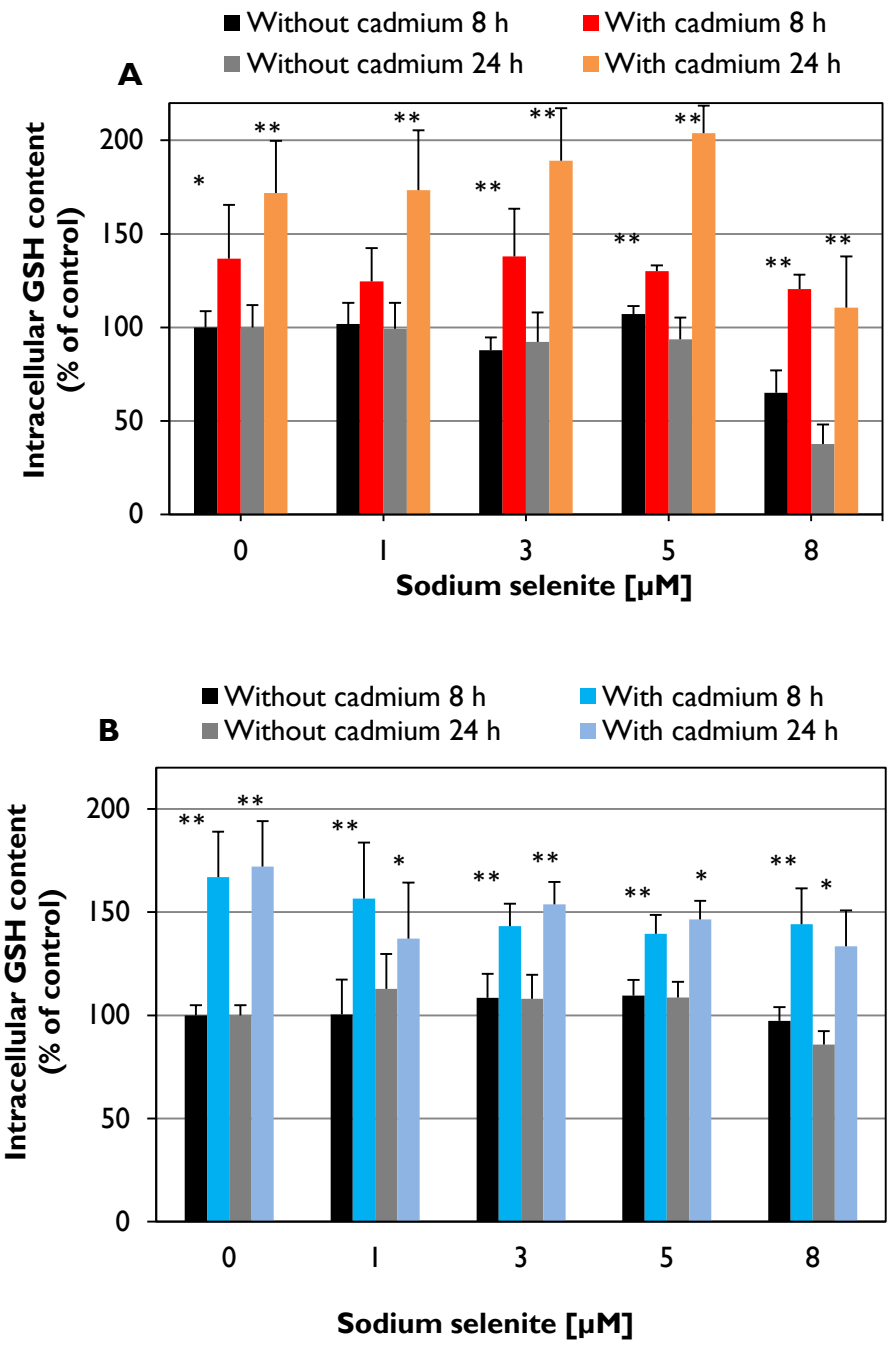

Figure 5.14: Impact of sodium selenite in combination with cadmium chloride on intracellular GSH content. p53-proficient HCT116 cells (A) or p53-deficient HCT116 cells (B) were treated with sodium selenite (1 µM-8 µM) in combination with 10 µM cadmium chloride for 8 h and 24 h incubation The total content of GSH was determined after the method of Tietze (Tietze 1969). Mean values ± SD of three independent experiments are shown. Statistically significant differences between single and combined treatments with cadmium chloride as tested by independent sample t-test (Mann Whitney U test): * = $p < 0.05$, ** = $p < 0.01$.

Other studies have shown that cytotoxic effects followed by GSH-depletion are mediated, at least in part, through activation of p53 (Du *et al.* 2008). Incubation with cadmium chloride (10 µM) alone in p53-proficient HCT116 cells increased the glutathione content significantly compared to the untreated control. Sodium selenite in combination with cadmium chloride remained similar compared to cadmium chloride alone (Figure 5.14A). The same could be observed in p53-deficient HCT116 cells (Figure 5.14B). Only at 8 µM sodium selenite, the GSH pool in the presence of cadmium chloride was dropped to control levels after 8 h and 24 h co-exposure in the p53-proficient cells.

The rapid rise in GSH levels in response to only short exposure to cadmium might be due to the induction of newly synthesized GSH. Intensified regeneration of GSSG to GSH could also play a role. Based on the gene expression profile following cadmium chloride, increased gene expression levels of GSH-synthesizing γ-glutamyl cysteine ligase (*GCLC*) and the GSSG reducing GR were induced, which supports the effect of cadmium chloride on the increased GSH content. These results are in agreement with other studies showing that exposure to cadmium results in the induction of *GCLC,* facilitating enhanced GSH synthesis (Bannai *et al.* 1991; Eneman *et al.* 2000). GSH might be the primary detoxifying mechanism against cadmium for the cell due to the fact that its cysteine thiol group, which reduces the heavy metal by generating a stable glutathione-cadmium complex (Delalande *et al.* 2010). Cadmium has a high affinity for thiols, and thus the highly abundant GSH is a primary target for free cadmium ions in cells. GSH acts by scavenging cadmium to prevent its interaction with critical cellular targets. Reports show that during acute cadmium exposure GSH levels undergo a rapid depletion, and cadmium-induced depletion of the GSH pool, thus disturbing the redox balance and leading to an oxidative environment (Lopez *et al.* 2006). Chronic exposure to cadmium produces an elevation in tissue GSH content, which in turn decreases oxidative damage, which could be explained by the initial cadmium-induced GSH depletion counteracted immediately via an increased GSH synthesis (Cuypers *et al.* 2010). A significant rapid increase of GSH levels in the protective response to cadmium exposure through Nrf2 signaling in Jurkat T-cells is also reported (Ogasawara *et al.* 2014). Their findings suggest that cadmium-induced activation of GSH synthesis is initiated as an acute response for cadmium detoxification. They found that MT expression induced by cadmium occurred much later. The study indicates that the rapid increase in GSH is an essential defense response, with the subsequent induction of MT potentially chelating the remaining cadmium retained within the cell, and thereby leading to continued suppression of cadmium toxicity.

5.3.2 Impact of sodium selenite in combination with cadmium chloride on superoxide generation

We determined the induction of superoxide radicals after exposure to increasing concentrations of sodium selenite in the presence and absence of 10 µM cadmium chloride for 6 h. The redox cycler menadione was used as a positive control to induce superoxide. 15 min incubation of 100 µM menadione increased superoxide levels dramatically to 345 % in the p53-proficient HCT116 cells compared to the untreated control (Figure 5.15A). The whole concentration range of sodium selenite from 3 µM to 9 µM induced significantly the superoxide levels in p53-proficient cells, while concomitant exposure to cadmium chloride suppressed sodium selenite-enhanced superoxide generation. At the concentration 5 µM sodium selenite, the superoxide induction was increased to 161 %, while 7 µM and 9 µM sodium selenite caused an increase to 216 % and 238 %, respectively. Figure 5.15A shows also that the same concentration range of sodium selenite failed to generate significant levels of superoxide in the p53-deficient HCT116 cells, indicating a p53-dependent effect on superoxide induction when the cells are exposed to sodium selenite. In contrast, exposure to the fully-reduced selenomethionine did not induce superoxide in either set of HCT116 cells (Figure 5.15B). These results indicate that superoxide generation is presumably p53-mediated due to p53 activation upon sodium selenite exposure, which might play an important role in pro-apoptotic signaling induced by sodium selenite in HCT116 cells.

Cadmium did not induce formation of superoxide in HCT116 cells under the given conditions. Appearing in its +2 oxidation state, cadmium belongs to the transition metal group, however, cadmium is not redox-active, being unable to induce ROS in Fenton or Haber Weiss like reactions (Casalino *et al.* 1997; Eneman *et al.* 2000). As an exogenous source cadmium is demonstrated to indirectly produce ROS in various cell lines (Price and Joshi 1983; Szuster-Ciesielska *et al.* 2000; Watanabe *et al.* 2003). Production and accumulation of ROS inhibits the electron transfer chain in mitochondria (Wang *et al.* 2004). Cadmium has been shown to generate ROS, producing a breakdown of the mitochondrial membrane potential (Lopez *et al.* 2006).

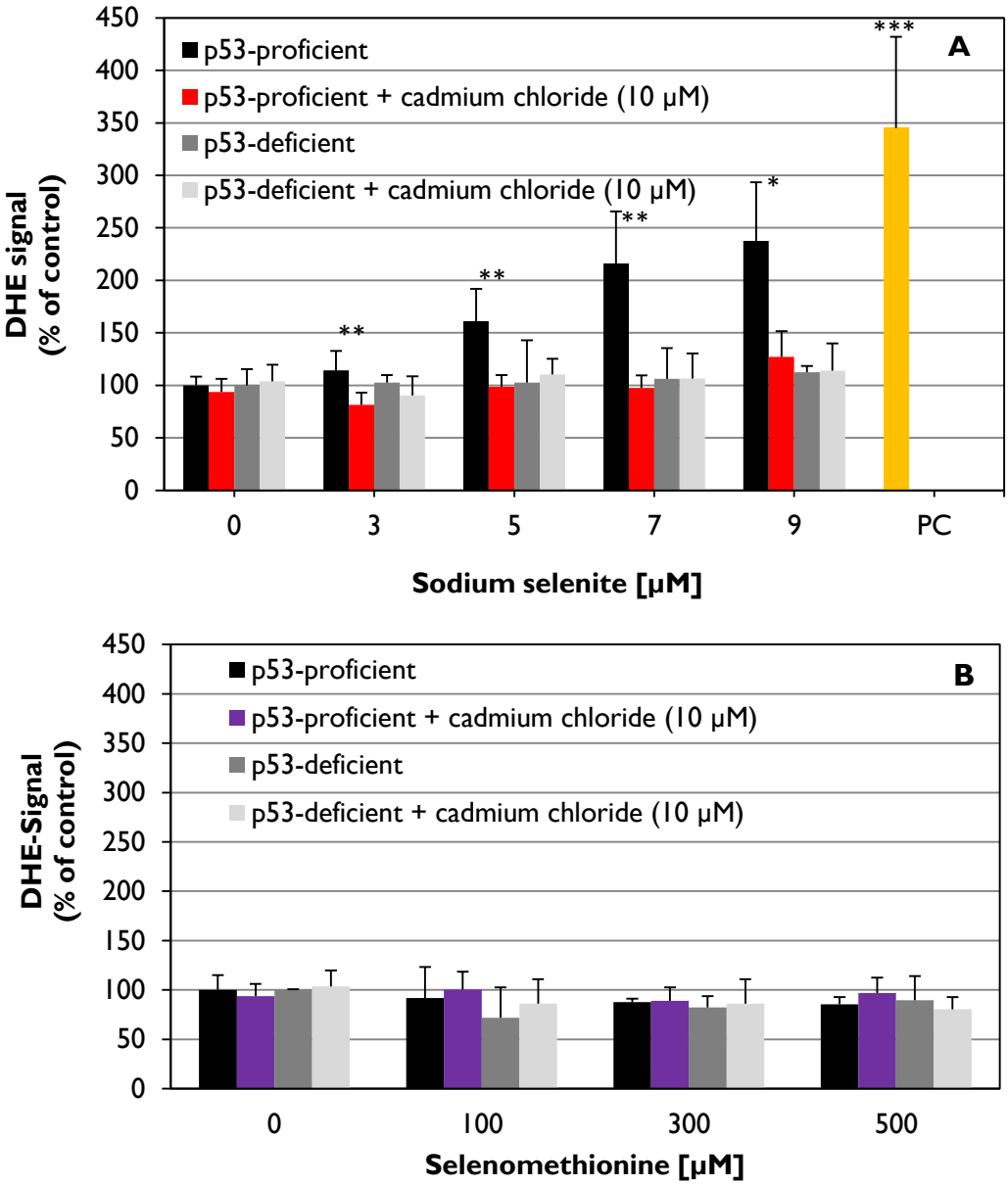

Figure 5.15: Impact of sodium selenite or selenomethionine in combination with cadmium on superoxide generation. p53-proficient and p53-deficient HCT116 cells were treated with (A) sodium selenite (3 µM-9 µM) or (B) selenomethionine (100 µM-500 µM) in combination with cadmium chloride (10 µM) for 6 h. 15 min incubation with 100 µM menadione was used as the positive control (PC). The level of superoxide was detected by the dye indicator dihydroethidium (DHE) using flow cytometry. Mean values ± SD of three independent experiments are shown. Statistically significant differences between single and combined treatment with cadmium chloride as tested by independent sample t-test (Mann-Whitney U test): * = $p < 0.05$, ** = $p < 0.01$. Statistically significant differences between untreated control and positive control tested by ANOVA with Dunnett's T3 Post-Hoc test: *** = $p < 0.001$.

5.3.3 Impact of cadmium chloride on enzymatic activities of isolated antioxidant enzymes

Selenoproteins could be potential targets of cadmium due to their selenol group in the catalytic active site. Figure 5.16A shows that the enzyme activity of isolated GPx from bovine erythrocytes is strongly reduced after incubation with cadmium. About 50 % of the inhibition occurred already after incubation with 5 µM cadmium. At the highest tested concentration (50 µM), the remaining GPx activity was about 9 %. The enzyme activity of isolated TrxR from rat liver was concentration-dependently inhibited after incubation with cadmium chloride (Figure 5.16B). Furthermore, the concentration of TrxR incubated with cadmium chloride was decisive in the observed activity inhibition. GR is structurally homologous to TrxR: both are members of pyridine nucleotide-disulphide oxidoreductase family, but are differentiated by the SeCys in the active catalytic center of TrxR and Cys residue of GR (Zhong *et al.* 2000). We investigated whether cadmium could also inhibit GR enzyme activity due to this homology. Figure 5.16C shows that GR activity decreased with increasing cadmium concentrations. About 50 % of the inhibition occurred, like in the case with GPx, already after incubation with only 5 µM cadmium. These data suggest that cadmium is able to interact with both the thiol group in GR and selenol in TrxR and GPx, thus inhibiting their enzyme activity in a subcellular context.

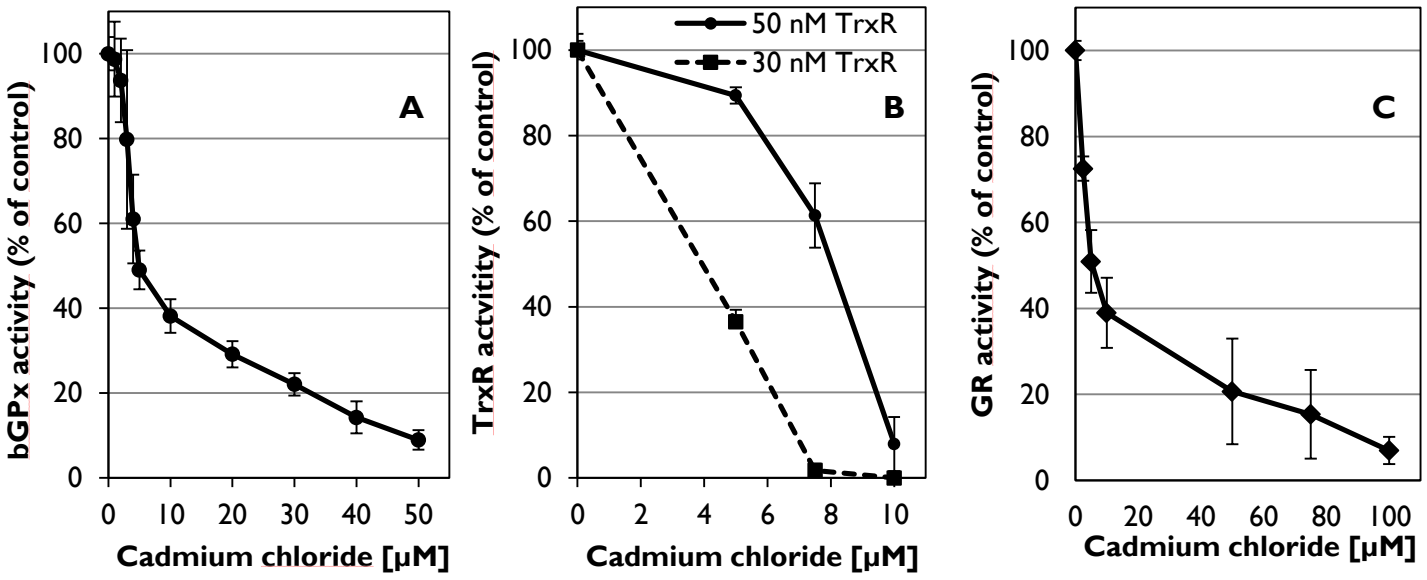

Figure 5.16: Impact of cadmium on enzyme activity. Isolated GPx (100 mU/ml) from bovine erythrocytes (A), isolated TrxR (30 or 50 nM) from rat liver (B), and isolated GR (2,5 U/ml) from Baker's yeast (C) were incubated with increasing cadmium chloride concentration for 5 min. Total GPx activity was determined indirectly by GR coupled assay with reduction of GSH. Total TrxR activity was determined with the DTNB reduction assay. Total GR activity was determined by NADPH consumption in regeneration of GSH. Mean values ± SD of at least two experiments are shown.

5.3.4 Impact of sodium selenite in combination with cadmium chloride on enzymatic activities of antioxidant enzymes

We determined the impact of our treatments on antioxidant enzyme activities originating from the same cell extracts from HCT116 cells. Figure 5.17A shows that sodium selenite increased thioredoxin reductase activity, also in the p53-deficient cells as in the presence of cadmium, which reflects the results from the gene expression analysis. Only a marginal increase of GR activity to 130 % was observed after sodium selenite treatment, however, increased GR activity (165 %) in the presence of cadmium was seen (Figure 5.17B). No significant change in GPx activity after sodium selenite exposure was seen in neither cell lines, regardless of co-exposure to cadmium (Figure 5.17C). The selenocysteine residue in the active center of the selenoproteins GPx and TrxR seemed to be a less sensitive target of cadmium in the cellular context. Complexation of cadmium within the cells could be a possible explanation why enzyme activity inhibition could not be shown in cells exposed to cadmium, thereby unable to reach the level an intracellular concentration of free cadmium required for enzyme activity inhibition.

These three antioxidant enzymes play important roles in the antioxidative defense. Together with thioredoxin (Trx) and NADPH, thioredoxin reductase is an essential part of the thioredoxin system which exists in nearly all living cells. Trx is a small redox active protein sustaining a wide range of functions in many different organisms. The oxidized Trx possesses an active site disulfide that has to be reduced to a dithiol for Trx to exert most of its functions. This reduction is catalyzed by TrxR using NADPH. The different functions of Trx are thereby entirely dependent upon the activity of TrxR (Arner 2009). Glutathione reductase catalyzes the reduction of glutathione disulfide (GSSG) to the sulfhydryl form glutathione (GSH), which is essential in maintaining the reducing environment of the cell (Seefeldt *et al.* 2009). Glutathione peroxidases reduce lipid hydroperoxides to their corresponding alcohols by oxidation of the selenol of its selenocysteine residue by hydrogen peroxide, and thereby using GSH as substrate free hydrogen peroxide can be reduced to water (Brigelius-Flohe 2008).

Under standard cell culture conditions selenium is deficient in the growth medium (Muller *et al.* 2010). We cultivated HCT116 cells also by supplementing the growth medium with 50 nM sodium selenite already in freshly thawed cells, providing time for the cells to express and induce selenoproteins. Basal GPx activity was more than 200 % higher in selenite supplemented cells, while basal TrxR activity was not significantly higher under selenite supplementation (data not shown). We further investigated whether Se supplementation could potentially enhance overall cellular antioxidative capacity by modulating catalase and SOD enzyme activities. However, sodium selenite supplementation did not alter their basal enzyme activities (data not shown).

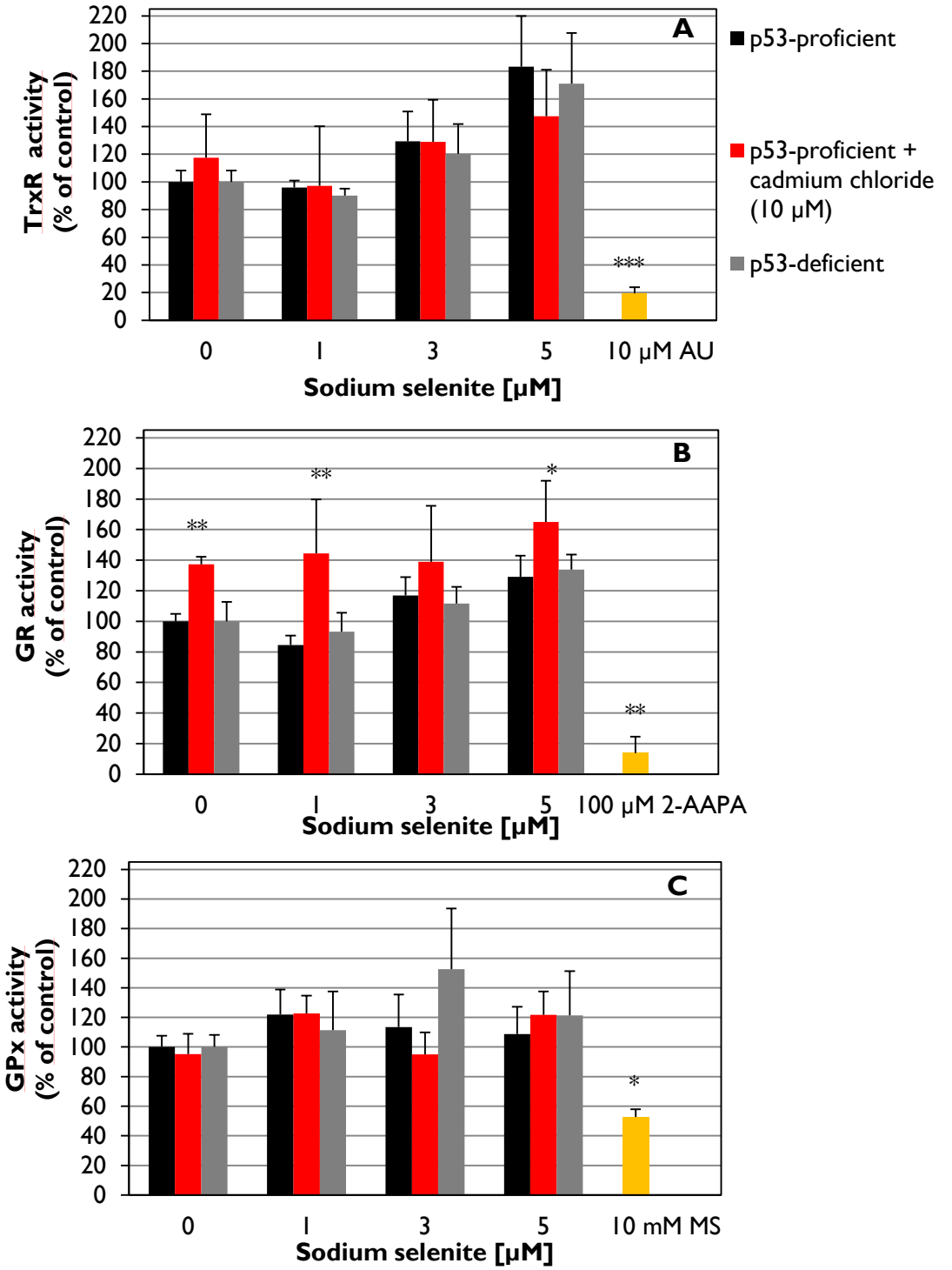

Figure 5.17: Impact of sodium selenite in combination with cadmium chloride on (A) TrxR enzyme activity (B) GR activity and (C) GPx activity in p53-proficient and p53-deficient HCT116 cells after 24 h incubation. 10 µM auranofin (AU) (6 h) served as TrxR positive control. TrxR activity was determined by the DTNB reduction assay. 100 µM 2-AAPA (20 min) served as GR positive control. Total GR activity was determined by NADPH consumption in regeneration of GSH. 10 mM mercaptosuccinate (MS) (5,5h) served as GPx positive control. Total GPx activity was determined indirectly by GR coupled assay with reduction of GSH. Mean values ± SD of three independent experiments are shown. Statistically significant differences between single and combined treatment with cadmium chloride as tested by independent sample t-test (Mann Whitney U test): * = $p < 0.05$, ** = $p < 0.01$. Statistically significant differences from the negative control and positive control tested by ANOVA with Dunnett's T3 Post-Hoc test: * = $p < 0.05$, ** = $p < 0.01$, *** = $p < 0.001$.

Neither catalase activity (see appendix Figure A1A) nor SOD activity was significantly decreased (see appendix Figure A1B) following cadmium exposure. Sodium selenite decreased catalase activity in both cell lines in the absence of cadmium, but not significantly (see appendix Figure A1A). Gene expression data showed, however, that catalase mRNA levels tended to be decreased upon sodium selenite exposure. Total SOD activity was not significantly changed following exposure to sodium selenite (see appendix Figure A1B). The catalase enzyme contains four heme groups per tetramer, whereby the N triangle of the His 74 imidazole residue is the functional catalytic site (Casalino *et al.* 2002). This essential enzyme protects against oxidative stress by detoxifying hydrogen peroxides to water and oxygen. The mechanisms suggested for decreased catalase activity are interactions between cadmium and the catalytic subunit of the enzyme, as well as iron deficiency due to cadmium exposure (Cuypers *et al.* 2010). Reduced enzyme activity is linked to pH-sensitive reduction of nitrogen in the imidazole residue of His 74. At physiological pH, this nitrogen is unprotonated, making it possible for cadmium to interact with the active site. Casalino *et al.* showed that cadmium-induced inhibition of liver mitochondrial MnSOD activity was completely restored when adding Mn^{2+} ions, suggesting that the activity-reducing effect on this enzyme was probably due to the substitution of cadmium by manganese (Casalino *et al.* 2002). However, reduced activity of the enzyme did not seem to be due to the replacement of zinc by cadmium, nor to the peroxides formed. Ikediobo *et al.* demonstrated that cadmium exposure in CRL-1439 normal rat liver cells led to loss of SOD, catalase, GR and GPx enzyme activities after 4 h (Ikediobi *et al.* 2004). However, the concentrations chosen were very high and possibly toxic concentrations (100-300 µM). SOD and GPx activities increased after 8 h exposure, while catalase and GR were significantly decreased. One possible underlying mechanism of cadmium-induced effects on GPx activities might be selenium depletion arising from the formation of Cd-Se-Cys complex at the active site of GPx. It is well established that cadmium is able to form covalent attachments with various cellular thiols (e.g. GSH, MTs as well as proteins). The impact of total SOD activity as well as catalase activity following cadmium exposure has been intensively studied, resulting in descriptions of increases and decreases of their activities depending on exposure conditions and target system studied (Cuypers *et al.* 2010).

5.4 Cell cycle distribution and apoptosis

Different types of DNA lesions occur due to DNA damage, leading to changes of the course of cell cycle, a complicated, interacting network of various regulatory factors involved in the control of cell growth and genomic stability. Repair of DNA damage is often connected with the cell cycle arrest to ensure sufficient time for recovering to the original undamaged condition. If repair is not possible, another controlled mechanism, programmed cell death, is induced. In addition to the analysis of transcript levels of genes associated with apoptosis, examination of involvement of apoptosis in the observed cytotoxic effects of sodium selenite, several parameters were investigated, including increase of sub-diploid cells (sub-G1 fraction), cell viability, mitochondrial membrane potential, and translocation of AIF.

The obtained gene expression profiles showed induction of several p53 target genes, such as the cell cycle inhibitors *CDKN1A* and *CDKN2B* as well as pro-apoptotic genes PUMA, NOXA, DR5 and *BAX* after treatment with sodium selenite, which indicates that sodium selenite induced genotoxic stress, cell cycle arrest and induction of apoptosis. Therefore, cell cycle distribution and cell viability was examined from the same sample using increasing concentrations of sodium selenite in combination with 10 µM cadmium chloride for 24 h. Floaters and attached cells were combined for the analysis. The cell cycle phases were analyzed by flow cytometry and DNA staining with DAPI. Figure A3 in the appendix illustrates how the single phases are distributed according to DNA content: Cells in the G2/M phase contain double DNA content compared to cells in the G1 or G0 phases, while cells in S-phase have DNA contents between those cells in G1 and G2/M phase. Classification of cell viability was analyzed by simultaneous three color staining with propidium iodide (PI) and FITC-conjugated Annexin-V, which indicate membrane integrity and phosphatidylserine (PS) exposure, respectively, in addition to DiIC1(5), which determines mitochondrial membrane potential by accumulating in mitochondria with active membrane potential (see appendix Figure A4).

5.4.1 Impact of sodium selenite in combination with cadmium chloride on cell cycle distribution and sub-G1 fraction

The impact of sodium selenite on cell cycle distribution was dependent on the p53 status of the HCT116 cells (Figure 5.18). The effects induced by 7 µM sodium selenite in p53-proficient cells treated for 24 h were significantly different from the untreated control. Cells in the G1 phase declined from 45.2 % in untreated cells to 33.3% in treated cells, increased from 22.3 % to 30.6 % in the S phase, declined from 31.7 % to 25.1 % at G2/M phase, and increased from 0.4 % to 11.3 % sub-G1 fraction, characteristic of apoptotic cells. Even though the G1 phase arrest was not observed, the sub-G1 fraction of sub-diploid cells was significantly increased in the higher tested concentrations of

sodium selenite and accompanied by S phase arrest (Figure 5.18A), suggesting that the cells are arrested in G1 phase but have already initiated programmed cell death. Lower concentrations than 6 µM sodium selenite did not produce such effects. These results clearly showed that sodium selenite could significantly affect the cell cycle distribution of HCT116 cells and induce apoptosis. However, these effects were abolished in the presence of cadmium chloride (Figure 5.18B). Results from the flow cytometry showed that p53-deficient HCT116 cells treated for 24 h by sodium selenite had a similar cell cycle distribution as untreated cells, whereby cells in the G1 phase comprised about 47 % of the total cell population, S phase 24 %, and G2/M phase 28 %. Moreover, no increased sub-G1 fraction was observed (Figure 5.18C). Cao and co-workers performed cell cycle analysis and gene expression profiling with different doses of sodium selenite, which inhibited cell proliferation in NB4 cells (Cao *et al.* 2006). They showed an increased G0/G1 cell cycle arrest in addition to enhanced sub-G1 peak, accompanied with up-regulation of pro-apoptotic genes, such as *BAX* and *CASP8*. Exposure to 500 µM selenomethionine affected the cell cycle by depleting S phase, independent of p53, as well as a concomitant G2 phase arrest, independent of cadmium (data not shown).

In human DU145 prostate cancer cells, expressing mutant p53, S phase arrest was detected after sodium selenite incubation. This arrest was independent from p53, and p21 also did not play a role (Jiang *et al.* 2002). Our working group has previously shown that sodium selenite induced p21 first of all p53 dependently at the protein level (Klaus 2009). Data on cell cycle analysis in colon cancer cell lines focusing on the influence of sodium selenite have been studied. Cytotoxic levels of sodium selenite led to arrest in the S- and G1 phases and induction of p21 at mRNA level in HAT-29 cells, which express mutant p53 (Zeng and Davis 2003). The expression of cell cycle control genes in p53-deficient cells presented in this current work was increased, but whether the induction of *p21* compared to the p53-proficient cell line was enhanced at the protein level needs to be investigated.

Based on the transcriptional activation of p53 target genes, *CDKN1A* and *CDKN2B*, we expected to see an effect on the cell cycle. In principle, activation of kinase inhibitors can serve as a protective mechanism following genotoxic stress. *CDKN1A* encodes for the cyclin-dependent kinase inhibitor, p21, which following its activation leads to cell cycle arrest in the G1/S, as well as G2/M phases and to cellular senescence (Abbas and Dutta 2009). p21 belongs to the so-called stress response gene family. The protein p21 is activated by p53 and binds to cyclin-CdK complex. As a downstream gene of p53, p21 is a part of p53-mediated apoptotic signaling. *CDKN2B* encodes the cyclin-dependent kinase inhibitor p15, which like p21 induces G1 phase cell arrest. A p53-dependent prevention of cell cycle arrest upon co-exposure to cadmium was also expected in regard to the observed reduced cytotoxicity and deregulated gene expression. Meplan and co-workers investigated the impact of

cadmium on p53 conformation, DNA-binding and transcriptional activity (Meplan *et al.* 1999). They showed that sub-toxic concentrations of cadmium (10-30 µM) disturbed the folding of p53 and abolished binding of DNA to the protein. Moreover, cadmium impaired the induction of p53 by a DNA-damaging agent and down-regulated the transcriptional activity. Cell cycle arrest in response to γ-irradiation was prevented in the presence of cadmium.

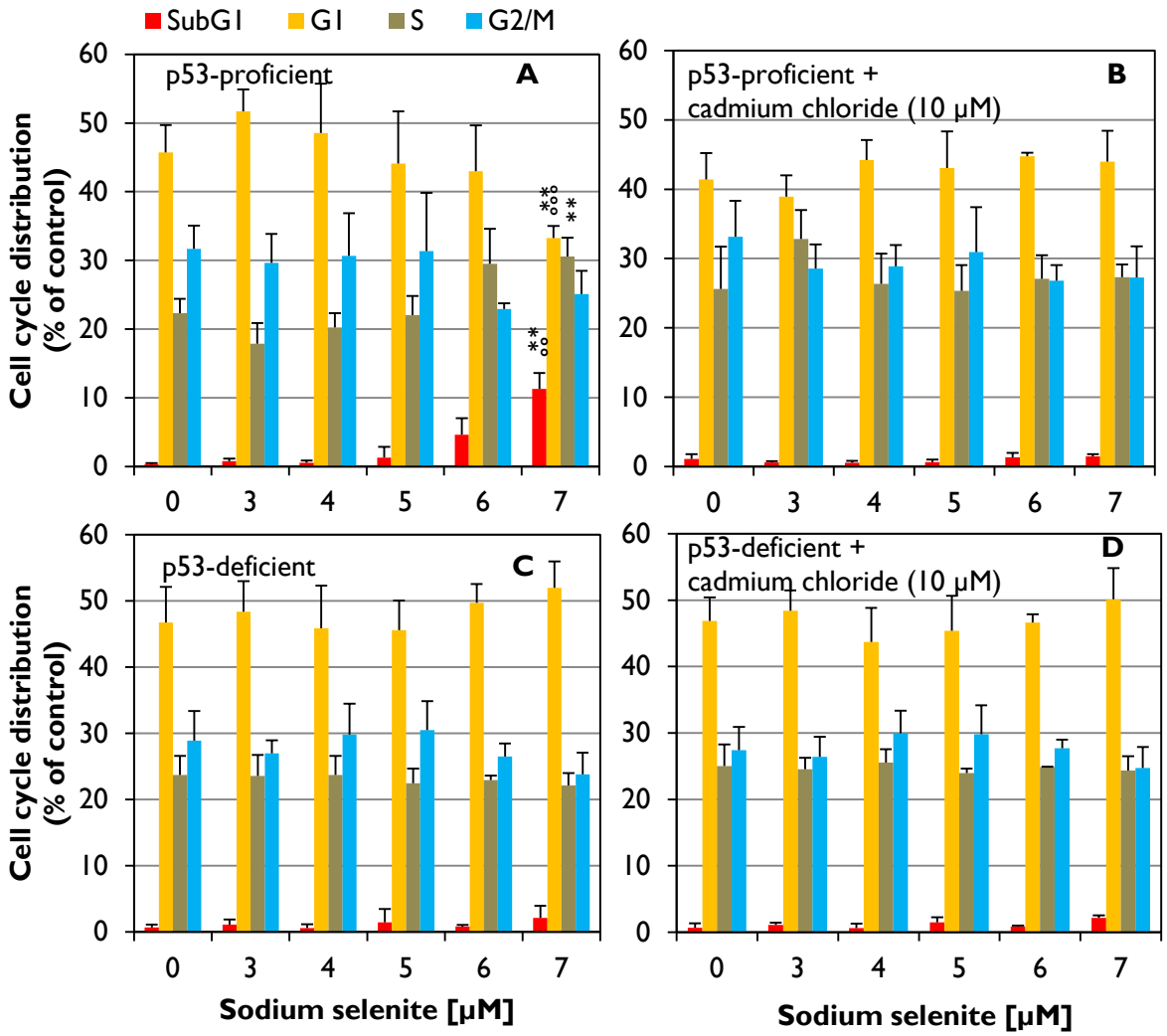

Figure 5.18: Impact of sodium selenite in combination with cadmium on cell cycle distribution. p53-proficient HCT116 cells (A, B) and p53-deficient HCT116 cells (C, D) were treated with sodium selenite (3 µM-7 µM) in combination with cadmium chloride (10 µM) for 24 h incubation. Cell cycle distribution was determined by flow cytometry using the DNA dye 4', 6-diamidino-2-phenylindole (DAPI). Mean values ± SD of least three independent experiments are shown. Statistic significant differences between single and combined treatment with cadmium chloride as tested by independent sample t-test (Mann Whitney U test): ** = $p < 0.01$. Statistically significant differences from the corresponding negative control tested by ANOVA with Dunnett's T3 Post-Hoc test: °° = $p < 0.01$, °°° = $p < 0.001$.

5.4.2 Flow cytometric analysis of cell viability

HCT116 cells with different p53 status were incubated with increasing amounts of sodium selenite for 24 h with or without cadmium chloride (Figure 5.19 and Figure 5.20). At the end of treatment, trypsin-detached cells as well as floaters in the incubation medium were stained simultaneously by three dyes: the nucleic acid dye PI, phosphatidylserine marker FITC-conjugated Annexin-V, and mitochondrial membrane potential dye DiIC1(5). Cells that are AnnexinV-positive and PI-negative are in early apoptosis, as PS translocation has already occurred, although the plasma membrane remains intact. By gating the stained cells into sub-populations according to staining patterns, the degree of cell viability could be determined. Cells that are positive for both Annexin-V and PI are either in the late stages of apoptosis or are already dead, as PS translocation has occurred, and the loss of plasma membrane integrity is visible.

Figure 5.19A shows that sodium selenite caused loss of membrane integrity and PS translocation, as well as increased loss of mitochondrial membrane potential in a dose-dependent manner, indicating induction of apoptotic as well as necrotic cell death. These staining patterns were strongly suppressed in p53-deficient cells (Figure 5.20) and by co-exposure to cadmium chloride (Figure 5.19B). However, this method cannot discriminate between late apoptotic and primary necrotic cells, since both of these groups of cells are Annexin V-positive/PI-positive, whereas late apoptotic cells exhibit same staining patterns due to a loss of plasma membrane integrity. In addition, reliable apoptotic quantification in adherent cell cultures by flow cytometry is difficult and unreliable given the fact that during the process of cell harvesting and manipulation before and during flow cytometry assays many apoptotic cells undergo secondary necrosis (Oropesa-Avila *et al.* 2014).

According to the gene expression data, the pro-apoptotic *BAX* gene was induced in p53 dependent manner, but suppressed by the presence of cadmium. Bax is an initiator in mitochondrial apoptotic pathway. Direct activation of Bax mediates mitochondrial membrane permeabilization, releasing cytochrome C into the cytoplasm to mitochondria, which triggers subsequent activation of executer caspases and leads to apoptosis (Zhang *et al.* 2000). Sodium selenite induced p53-mediated activation of *Bax* transcription, which can translocate into the mitochondria, and trigger loss of mitochondrial membrane integrity. Sodium selenite induced apoptosis by producing superoxide to activate p53, whose activation in turn synergistically enhanced superoxide production and apoptosis induced by sodium selenite (Zhao *et al.* 2006). Inorganic selenium sensitizes prostate cancer cells TRAIL-induced apoptosis through superoxide/p53/Bax-mediated activation of mitochondrial pathway (Hu *et al.* 2006).

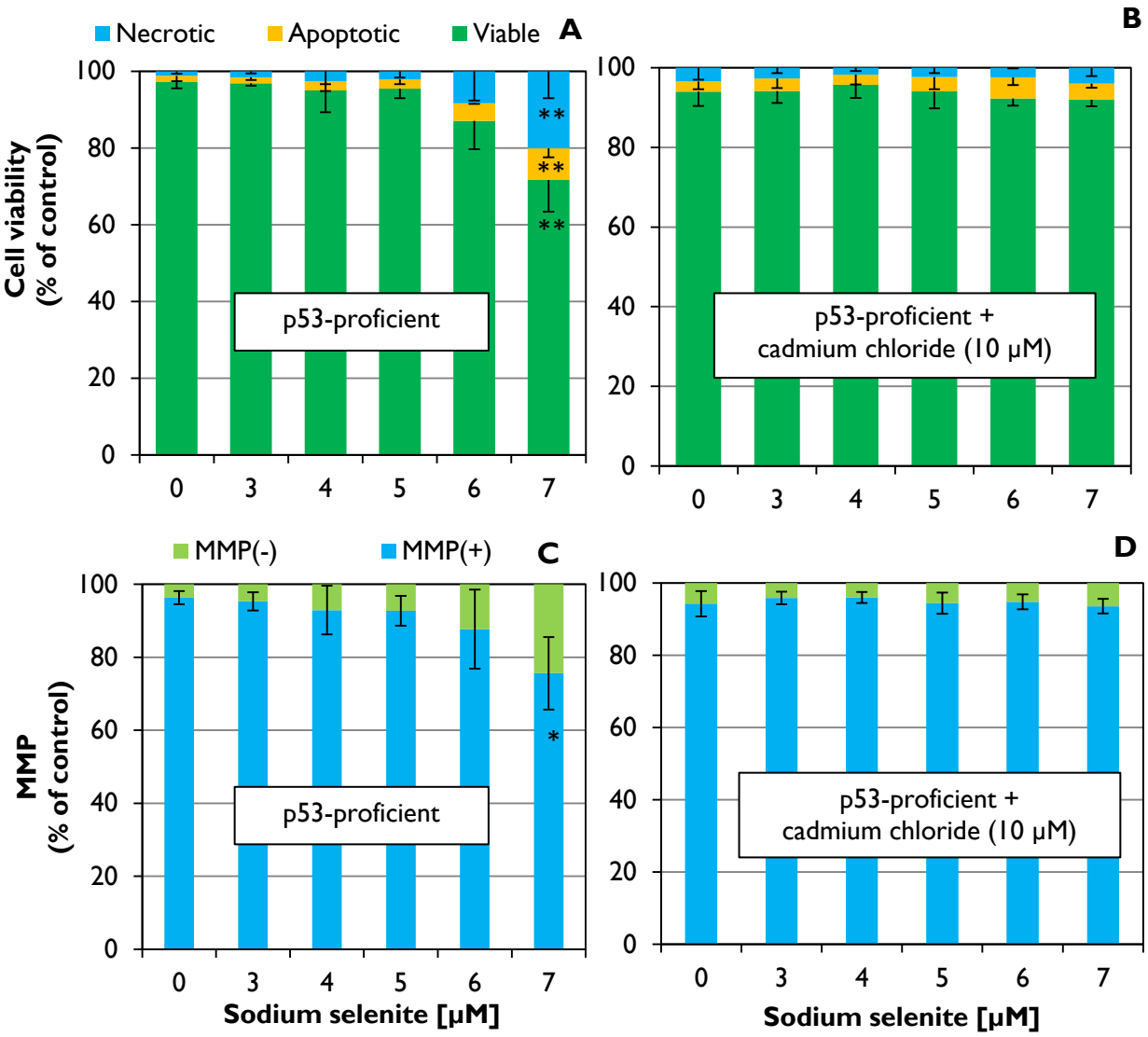

Figure 5.19: Impact of sodium selenite in combination with cadmium on cell viability of p53-proficient HCT116 cells determined by flow cytometric analysis. Cells were treated with sodium selenite (3 µM-7 µM) alone (A, B) in combination with cadmium chloride (10 µM) (C, D) for 24 h incubation. Necrotic cells: propidium iodide (PI) positive/annexin positive, apoptotic cells: PI negative/annexin positive, viable cells: PI negative/annexin negative. Mitochondrial membrane potential (MMP); MMP+: active MMP, MMP-: decreased MMP. Mean values ± SD of three independent experiments are shown. Statistically significant differences between single and combined treatment with cadmium chloride as tested by independent sample t-test (Mann Whitney U test): * = $p < 0.05$, ** = $p < 0.01$.

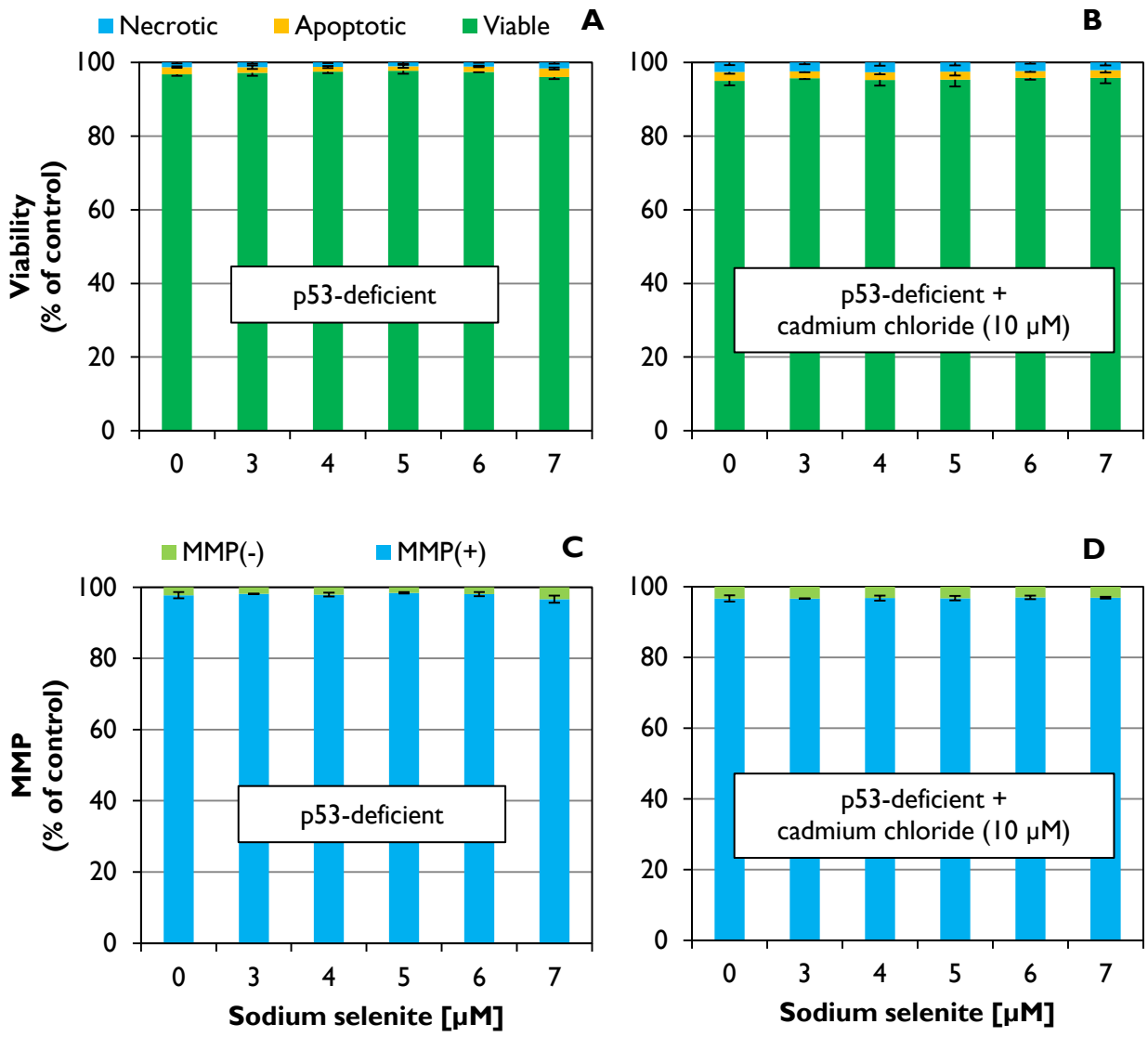

Figure 5.20: Impact of sodium selenite in combination with cadmium on cell viability of p53-deficient HCT116 cells determined by flow cytometric analysis. Cells were treated with sodium selenite (3 µM-7 µM) alone (A, B) in combination with cadmium chloride (10 µM) (C, D) for 24 h incubation. Necrotic cells = propidium iodide (PI) positive/annexin positive, apoptotic cells = PI negative/annexin positive, viable cells = PI negative/annexin negative. Mitochondrial membrane potential (MMP); MMP + = active MMP, MMP - = decreased MMP. Mean values ± SD of three independent experiments are shown.

5.4.3 AIF translocation

Apoptosis-inducing factor (AIF) is released into the cytosol in mitochondria-mediated apoptosis and further translocated to the cell nuclei, where it accumulates and in turn induces apoptosis. We observed that sodium selenite induced nuclear translocation of AIF to 130 %, which was significant compared to negative control cells (Figure 5.21A). The sodium selenite-induced AIF translocation was significantly decreased by cadmium. No translocation of AIF was also seen in p53-deficient HCT116 cells (data not shown). The apoptosis-inducer staurosporine (STS) (400 nM) served as the positive control and increased the AIF fluorescence signal to 146 %. With regard to selenomethionine, no nuclear translocation of AIF could be detected (data not shown). Detection of AIF by the means of immunofluorescence microscopy normally exhibits a punctuated cytoplasmic staining pattern with some preference for the perinuclear area, which is typical for mitochondrial localization (Daugas *et al.* 2000). This pattern was seen in the untreated HCT116 cells in both cell lines. After treatment with STS and sodium selenite, apoptotic cells, in which DNA condensation took place, were visible, with an increase in the fluorescence signal intensity within the cell nuclei.

Apoptotic cells are characterized by various morphological, molecular and biochemical properties, e.g. cell shrinkage, membrane "blubbing", chromatin condensation and DNA fragmentation. Detection of several parameters of apoptosis is essential for identifying definitely apoptotic cells (Rahman *et al.* 2002). In this present work, sodium selenite affected the normal cell cycle distribution and generated a detectable fraction of late apoptotic cells with subdiploid DNA, which was not found after co-exposure to cadmium chloride. The amount of AIF located in the nuclei was increased in p53-proficient HCT116 cells, while co-exposure to cadmium or selenomethionine alone did not produce apoptotic outcomes.

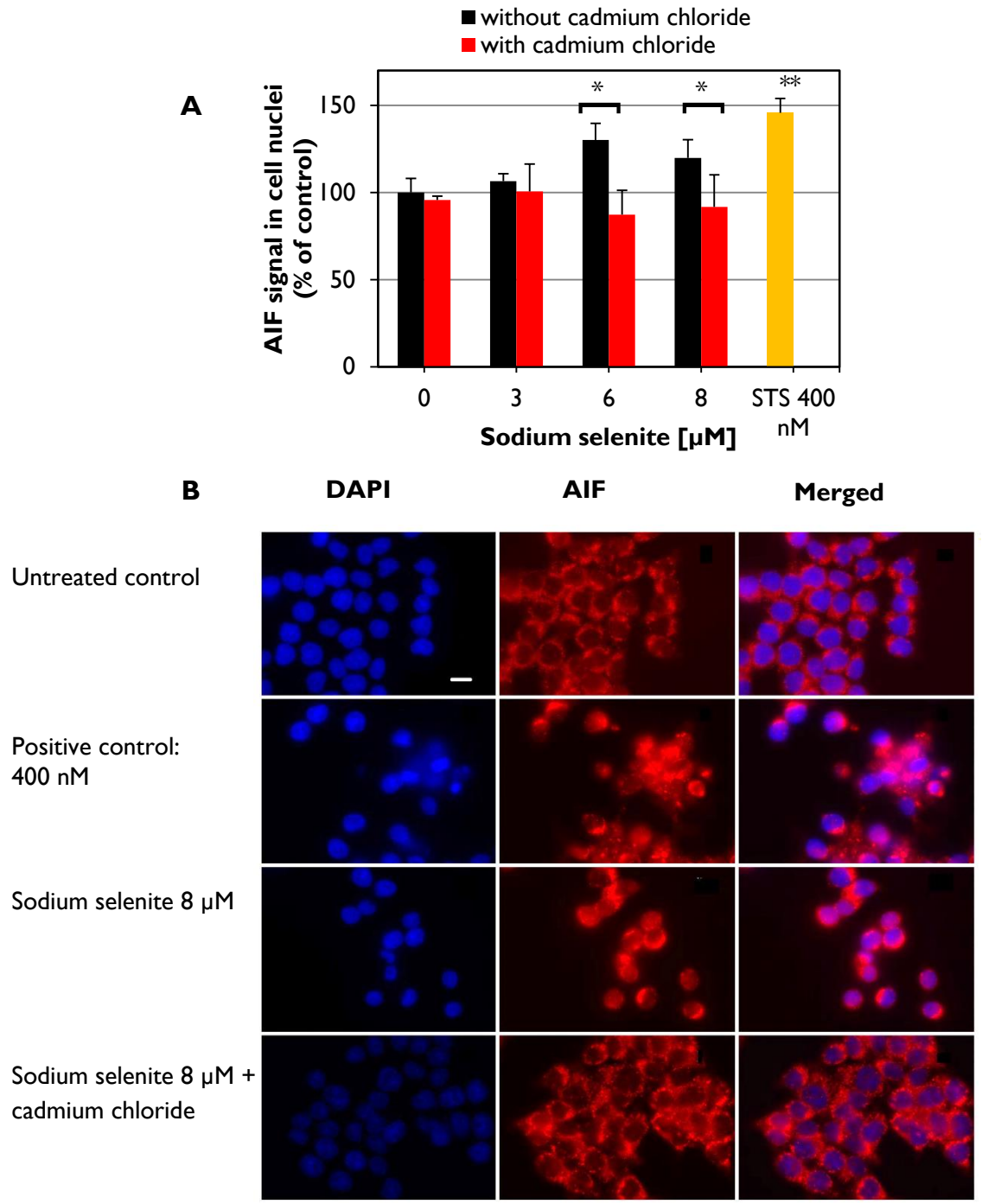

Figure 5.21: Impact of sodium selenite on nuclear AIF translocation in combination with cadmium chloride as well as impact of selenomethionine on nuclear AIF translocation. p53-proficient HCT116 cells were incubated for (A) 24 h with sodium selenite alone and in combination with cadmium chloride (15 µM, 2 h pretreatment). (B) Shown are representative immunofluorometric images from three experiments. Scale bar = 32 µM, magnification of the pictures = 63x. The nuclear translocation of AIF was visualized by indirect immunofluorescence microscopy The DNA dye 4', 6-diamidino-2-phenylindole (DAPI) was used to stain the nuclei. Staurosporine (STS) 400 nM was used as positive control. Mean values ± SD of three experiments are shown. Statistically significant differences between single and combined treatment with cadmium chloride as tested by independent sample t-test (Mann-Whitney U): * = $p < 0.05$. Statistically significant differences between the positive control and the corresponding negative control tested by independent sample t-test (Mann-Whitney U): ** = $p < 0.01$.

5.5 Bioavailability

To investigate if the observed cytotoxic effects by the two selenocompounds are associated to bioavailability, the total cellular uptake of selenium was quantified. Bioavailability is characterized as the relationship between the applied and the resorbed amount of a substance. Previous work in this working group showed that cellular uptake of sodium selenite in HCT116 cells was p53 dependent, but not selenomethionine (Klaus 2009). Therefore, the question concerning a possible interaction of cadmium chloride with the uptake of sodium selenite in a p53 dependent matter was raised. Could cadmium co-exposure affect the bioavailability of sodium selenite by inhibiting the cellular uptake of the element, and thus reduce the cytotoxic effects observed after sodium selenite exposure? With regard to selenomethionine, would cadmium exert no influence on the fully-reduced selenomethionine due to its presumably p53 independent cellular uptake?

The basal contents of selenium in untreated cells were 1.4 µM and 2.3 µM in the p53-proficient and the p53-deficient cells, respectively (Figure 5.22A). Under standard cell culture conditions, cells are grown under selenium deficient conditions. Previous investigations showed that the content of selenium in the cell culture growth medium was 2 nM (Klaus 2009). Exposure to 7 µM sodium selenite reached 44.4 µM intracellular selenium concentration in the p53-proficient cells and 40.5 µM intracellular selenium concentrations in the p53-deficient cells (Figure 5.22A). The uptake of selenium as sodium selenite was, however, significantly higher in the p53-proficient HCT116 cells than in the p53-deficient cell line at lower tested concentrations, confirming the observation previously seen in our working group.

To address the question whether cadmium co-exposure could decrease the uptake of sodium selenite, cells were co-incubated with sodium selenite and cadmium chloride for 24 h. Cadmium exposure alone did not significantly change the basal content of selenium in either cell line. Unexpectedly, simultaneous exposure to cadmium chloride led to a dramatically increased content of intracellular selenium over the whole concentration range in both cell lines (Figure 5.22B). These results show that cadmium chloride improves the bioavailability of sodium selenite independently of the cellular p53 status. Indeed, there was a significant higher absolute uptake of selenium in the p53-proficient HCT116 cells in the lower concentration range of sodium selenite than in the p53-deficient cells. In the p53-proficient cells, from 5 µM sodium selenite, the uptake of selenium reached a plateau around 700 µM in the simultaneous presence of cadmium chloride. In the p53-deficient cell line, a concentration-dependent increase of intracellular selenium was observed, reaching a concentration of 886 µM intracellular selenium when co-exposed to 7 µM sodium selenite and 10 µM cadmium chloride for 24 h.

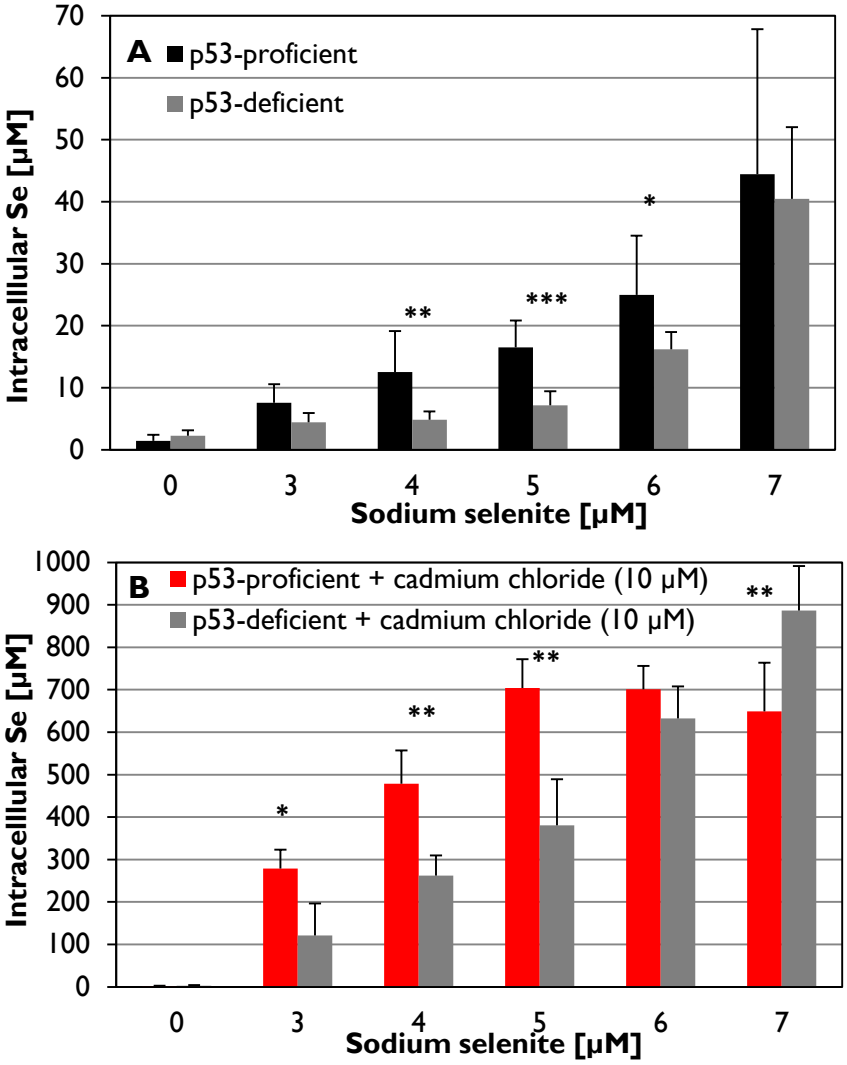

Figure 5.22: Cellular uptake of sodium selenite in p53-proficient- and p53-deficient HCT116. Cells were incubated with (A) sodium selenite (3 µM-7 µM) without cadmium chloride, (B) or in combination with cadmium chloride (10 µM) for 24 h. The total cellular selenium content was determined by graphite furnace atomic absorption spectroscopy (GF-AAS). Mean values ± SD of three independent experiments are shown. Statistically significant differences between the cell lines as tested by independent sample t-test (Mann Whitney U test): * = $p < 0.05$, ** = $p < 0.01$, *** = $p < 0.001$.

The intracellular selenium concentration after 24 h exposure to selenomethionine produced a different picture compared to sodium selenite exposure. After incubation with 10 µM selenomethionine in the p53-proficient HCT cells, 79.1 µM intracellular selenium was measured (Figure 5.23), which exerted no cytotoxic effects. In contrast, exposure to 7 µM sodium selenite increased the intracellular concentration to only 44.4 µM selenium (Figure 5.22A), however, which was sufficient to strongly induce cell death.

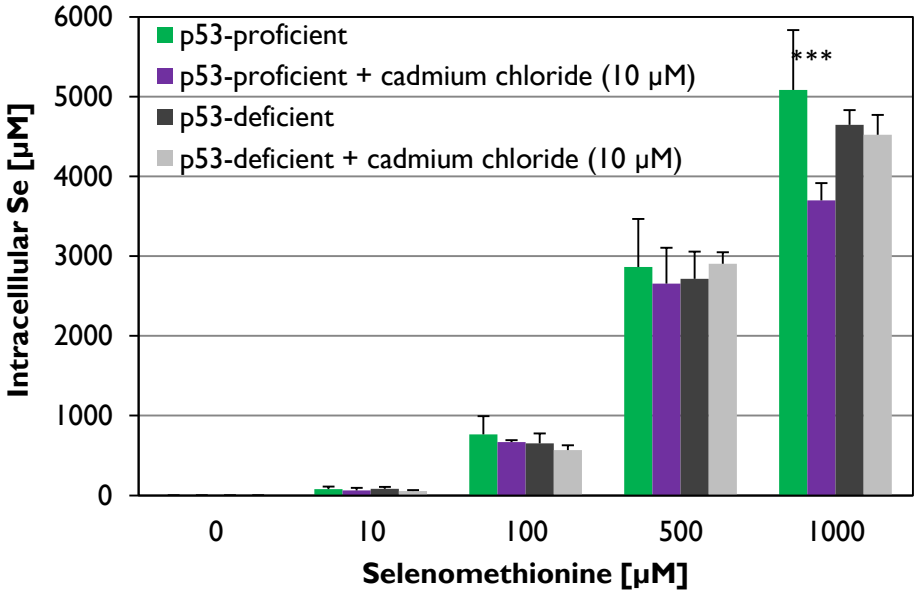

Figure 5.23: Cellular uptake of selenomethionine in p53-proficient and p53-deficient HCT116 cells. Cells were incubated with selenomethionine (10 µM-1000 µM) without cadmium chloride or in combination with 10 µM cadmium chloride for 24 h. The total cellular selenium content was determined by graphite furnace atomic absorption spectroscopy (GF-AAS). Mean values ± SD of at least two independent experiments are shown. Statistically significant differences between single and combined treatment with cadmium chloride as tested by independent sample t-test (Mann Whitney U test): *** = $p < 0.001$.

Increasing the selenomethionine incubation concentration from 10 to 100 µM resulted in an approximately 10-fold increase in the intracellular selenium level. Further increasing the selenomethionine incubation concentration to 500 µM raised the intracellular content of selenium by 36-fold to about 2900 µM. Raising the incubation concentration of selenium to 1000 µM further enhanced the intracellular selenium content almost by 64-fold (5100 µM). Compared to basal levels, with increasing selenomethionine concentrations, a nearly linear uptake of selenium was observed (correlation coefficient >0.99). Simultaneous exposure to selenomethionine (up to 500 µM) and 10 µM cadmium chloride, no difference in the intracellular level of selenium was found compared to

selenomethionine exposure in the absence of cadmium chloride. However, at 1000 µM selenomethionine in the presence of cadmium, the intracellular level of selenium reached about 3700 µM compared to 5100 µM without co-exposure in the proficient cell line. Selenomethionine and other selenoamino acids appear to be effectively transported by various intestinal amino acid transporters (Nickel *et al.* 2009), which do not seem to be affected by the presence of cadmium.

What could explain the strongly enhanced uptake of selenium after exposure to sodium selenite in the presence of cadmium? Several studies have shown that selenium uptake in the form of selenite increases after extracellular thiol-assisted reduction (Ganyc and Self 2008; Olm *et al.* 2009; Tarze *et al.* 2007). Tarze *et al.* (2007) demonstrated that millimolar tolerance to selenite in yeast can be reduced to the micromolar range in the presence of excessive thiols in the growth medium through high-affinity uptake of a more reduced form of selenite. All assayed thiols were shown to drastically enhance selenite toxicity, resulting in entry of selenium inside the cell possibly under the form of hydrogen selenide. Ganyc and Self (2007) used a human keratinocyte model to determine whether reduction of selenite to the more reduced form, selenide, would affect uptake. They showed a high-affinity uptake of selenium even in the nanomolar range of selenite through the addition of extracellular thiols. Selenium uptake was prevented in keratinocytes by an anion channel blocker in the presence and absence of GSH, suggesting that both selenite and selenide were taken up through these pathways but with different affinities. Olm *et al.* (2009) showed that selenite cytotoxicity is determined by its cellular uptake and not by intrinsic cellular differences. Selenite uptake and consequently its cytotoxic effects were dependent on the extracellular redox state. By oxidizing or reducing compounds the extracellular state was modulated, and thus able to sensitize or desensitize cells towards selenite. The sensitivity of malignant cells to selenite was decreased by extracellular glutamate, while higher extracellular cysteine concentrations facilitated the reduction of selenite to hydrogen selenide, which was rapidly taken up into the cells and thus highly cytotoxic. This study by Olm demonstrated that high extracellular cysteine levels in the selenite-sensitive cells must be linked with high system xc^--activity. The transporter system xc^- consists of two protein components: the 4F2 heavy chain, necessary for membrane location of the heterodimer and the xCT protein, responsible for transport activity. The system transports one molecule of cystine, the oxidized form of cysteine, into cells and releases one molecule of glutamate into the extracellular space (Conrad and Sato 2012). Importantly, xCT expression can be triggered in response to increased oxidative stress to stimulate GSH biosynthesis. In this way, the supply of cysteine for protein synthesis and GSH biosynthesis is ensured by this transporter system. The system is unaffected by the highly specific and irreversible inhibitor of γ-glutamylcysteine synthetase, BSO, suggesting that this transporter system may independently of GSH sustain a redox cycle across the plasma membrane. The features of this redox cycle are cystine uptake, intracellular reduction to cysteine and secretion

of the surplus cysteine into the extracellular space (Conrad and Sato 2012). The xc^- antiporter expression has been shown to be regulated by ARE and is therefore an Nrf2 target gene associated with other phase II proteins, in addition to MRPs and enzymes regulating intracellular redox homeostasis (Sasaki *et al.* 2002). The role of the xc^- exchanger among the ARE-regulated proteins is to facilitate uptake of cystine, increasing intracellular cysteine availability and thereby enhancing GSH levels in the cellular defense against oxidative stress. The reductive microenvironment is dependent on cystine uptake via system xc^-, intracellular reduction of NADPH-dependent redox protein systems and secretion of cysteine to the extracellular environment by MRPs. The gene induction of xCT gene and the activity of system xc^- is induced by various stimuli, including electrophilic agents and heavy metals like cadmium (Sasaki *et al.* 2002). Bannai *et al. (*1991) showed that cadmium caused an increase of cellular GSH due to the enhanced uptake of cystine, a protective mechanism related to the induced cellular stress. We demonstrated in this work that cadmium increased the intracellular GSH levels, in addition to activating Nrf2 target genes. Thus, it is likely that cadmium could cause an enhancement of extracellular cysteine concentration, which could lead to an extracellular reduction of the present sodium selenite to a more reduced form of selenite, possibly hydrogen selenide. This form of selenium is then taken up more efficiently than selenite, which would explain the enhanced uptake of selenium in sodium selenite-treated cells in the presence of cadmium chloride.

We determined therefore the total extracellular thiol content after exposure to increasing concentrations of sodium selenite with or without cadmium chloride for 24 h in p53-proficient HCT116 cells (Figure 5.24). The data showed that the extracellular thiol content was decreased by raising sodium selenite concentrations, which may indicate that sodium selenite is reduced by the present cysteine in the culture media, and thus enhanced the uptake of sodium selenite. Cadmium alone did not increase the extracellular thiol content as might expected due to the presumed increased GSH biosynthesis and cystin/cysteine cycle, however, the simultaneous incubation of sodium selenite and cadmium chloride did not deplete the thiol levels in the extracellular space, like observed by sodium selenite exposure only. Upon co-exposure, the transport of cysteine across the cell membrane into the extracellular compartment might perhaps provide an increased supply of cysteine in order to sustain a reductive extracellular environment. In this way, sodium selenite molecules could be reduced without depleting the present thiols. The extracellular thiol content in untreated, p53-deficient HCT116 cells was more than half the basal levels in the p53-proficient cell line (data not shown). These observations might explain the reason why the uptake of selenium following sodium selenite incubation is higher in the p53-proficient cells than in the p53-deficient cells due to the potential thiol-assisted reduction of sodium selenite, and thereby increasing the bioavailability of the element.

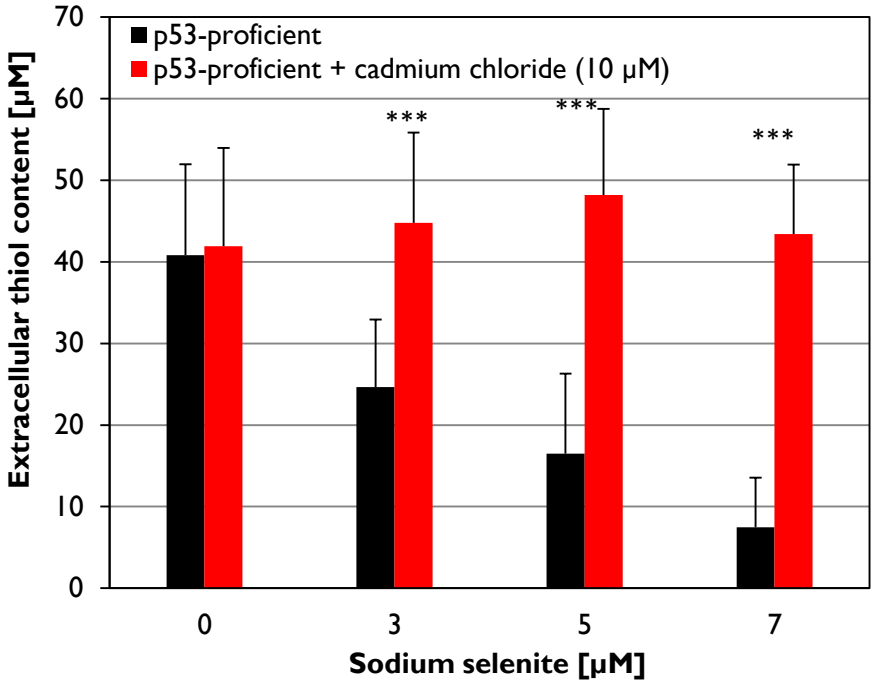

Figure 5.24: Impact of sodium selenite in combination with cadmium on extracellular thiol content. p53-proficient HCT116 cells were treated with sodium selenite (3 µM-7 µM) in combination with 10 µM cadmium chloride for 24 h incubation. The total extracellular thiol content was determined by the thiol reagent 5.5'-dithiobis-(2-nitrobenzoic acid) (DTNB) using L-cysteine as standard. Mean values ± SD of three independent experiments are shown. Statistically significant differences between single and combined treatment with cadmium chloride as tested by independent sample t-test (Mann Whitney U test): *** = $p < 0.001$.

Preliminary data have shown that pre-incubation of thiols (GSH, L-Cysteine) and sodium selenite (3 µM) before addition to the culture media for further 24 h co-incubation (with no presence of cadmium chloride), increased cytotoxicity by reducing colony-forming ability, and thereby confirming the assumption that thiol-assisted reduction of sodium selenite occurs in the extracellular compartment of HCT116 cells. However, the presumed enhanced uptake of intracellular selenium following thiol-treated sodium selenite incubation has not been demonstrated by us so far.

The cytotoxic effects of sodium selenite were significantly reduced when the cells were co-exposed to cadmium chloride. This appeared to involve an inactivation of p53 and thereby an inhibition of sodium selenite-induced and p53-mediated effects. The high intracellular concentration of selenium after sodium selenite exposure in combination with cadmium chloride did not cause cell death, as we would have expected. The more reduced form of sodium selenite that is absorbed could be elemental selenium and thereby induce less cytotoxic effects. However, elemental selenium has a much lower bioavailability than hydrogen selenide (Tarze *et al.* 2007), which makes this explanation less plausible. Interactions between selenite and other elements have been reported for copper.

Zeng and Botnen showed that copper may interact with sodium selenite extracellularly in cultured HT-29 cells (Zeng and Botnen 2004). Their results indicated that copper might specifically interact with inorganic, but not organic forms of selenium by strongly suppressing selenite-induced cell cycle arrest. Selenite-catalyzed generation of superoxide has been shown to be inhibited by copper in another study (Davis and Spallholz 1996). However, simultaneous incubation with copper and selenite in culture media significantly reduced intracellular selenium content, providing direct evidence that copper ions can interact with selenite extracellularly and block selenite from getting through the cell membrane (Zeng and Botnen 2004). A possible mechanism behind inhibition by cadmium of sodium selenite-induced cytotoxicity might be the complexation of cadmium ions by selenite molecules. Metal ions, including cadmium ions protect cells against selenium toxicity by formation of insoluble colloids with selenide in yeast cells, believed to provide cross-protection against the toxicities of both metals and selenocompounds (Dauplais *et al.* 2013). This explanation needs, however, further investigations.

6 Summary and conclusions

Selenium is an essential trace element, which presents a very narrow range between deficient, essential and toxic doses. Dietary intake of this essential trace element is not just provided by consumption of foods, such as dairy products, bread and cereals, fish and meat, but also by consumption of selenium-containing dietary supplements. During the last decades, selenium has raised significant expectations of the prevention of chronic diseases, such as several forms of cancer, due to the potential of selenoproteins to protect against oxidative stress (Stranges *et al.* 2010). Thus, selenium is marketed as a dietary supplement for optimal health and is therefore commonly added to multivitamin-mineral supplements consumed in many Western countries. However, optimum selenium dietary requirements are still a matter of debate, and concerns have been brought up about potential toxicities from long-term intake of selenium supplementation (Vinceti *et al.* 2014). Most beneficial effects from selenium supplementation are limited to initially inadequate selenium status, which means that care should be taken when using supplements because high selenium intake could lead to toxic effects (Roman *et al.* 2014). Despite the lack of definitive evidence on the efficacy of selenium for disease prevention, the use of selenium-enriched foods, fertilizers, and supplements has increased considerably in the US and other Western countries in recent years (Stranges *et al.* 2010). The indiscriminate use of selenium supplements in individuals and populations with adequate to high selenium status cannot be justified, posing a potential health risk (Rayman and Stranges 2013).

A central role in the maintenance of genomic stability belongs to the tumor suppressor protein p53. An appropriate cellular response to DNA damage is important; otherwise errors could lead to incorrect replication which can then manifest in mutations. Mutations in p53 are closely associated with cancer development, and more than 50 % of human primary tumors possess a mutated p53 (Greenblatt *et al.* 1994). The tumor suppressor protein p53 is intrinsically sensitive to oxidative stress, but also to transition metals, e.g. zinc and toxic metals (Hartwig 2001). Furthermore, ROS play important regulatory roles in the p53 signaling pathways as well as the fine-tuning of p53 itself (Meplan *et al.* 2000). Moreover, superoxide is produced by several selenocompounds e.g. sodium selenite, which are able to interact with thiols, which could subsequently activate p53 (Zhao *et al.* 2006). In fact, pro-oxidant effects have been proposed to be one of the mechanisms where selenium provides anticancer effects. On the other hand, as an oxidizing agent, sodium selenite is capable of compromising genetic stability by inducing DNA damage through the generation of ROS (Drake 2006). Structural and functional changes of the p53 protein may also be induced by toxic metal compounds, which are already shown for cadmium compounds (Meplan *et al.* 1999; Schwerdtle *et al.* 2010). One possible explanation is the interaction with the zinc-binding structure of the tumor

suppressor protein due to high affinity to sulfhydryl groups, also known as thiol reactivity (Hartwig 2013).

Because cadmium affects multiple cellular functions, our studies aimed to elucidate the impact of cadmium on cellular effects induced by two different selenocompounds. With respect to sodium selenite, pronounced cytotoxic effects over a narrow concentration range were seen in p53-proficient cells. In contrast, in combination with cadmium, the colony-forming ability was increased, implying an inhibition of sodium selenite-induced cell death. The p53-deficient HCT116 cells were still viable after both treatment conditions, indicating that this effect was restricted to p53-proficient cells, and displaying p53 dependence of the cellular response to sodium selenite. Subsequently, the genomic integrity may be endangered upon sodium selenite exposure, underlining the importance of p53 as a tumor suppressor. In the case of selenomethionine exposure, whose concentration was 100-fold higher than for sodium selenite, there was no observed p53 dependence or effect of cadmium on the acute toxicity determined by cell number. However, the presence of cadmium resulted in a significant reduction on long-term toxicity estimated by colony-forming ability in all tested concentrations of selenomethionine in p53-proficient cells, but not in the p53-deficient cells. Taken together, cadmium mitigated the cytotoxicity of high sodium selenite concentrations, while it enhanced the cytotoxicity of selenomethionine in a p53-dependent manner.

Underlying mechanisms in cadmium carcinogenicity are complex and not yet completely understood (Hartwig 2010). Despite the inability of cadmium to directly generate free radicals under physiological conditions, lipid peroxidation and removal of iron from cell membranes have long been considered to be primary mechanisms for cadmium toxicity (Casalino *et al.* 1997; Eneman *et al.* 2000). "Free" redox active metals directly enhance hydroxyl radical production via the Fenton reaction, followed by reduction of the oxidized metal achieved by the Haber-Weiss reaction with superoxide radicals as substrate (Winterbourn 1979). Although cadmium exposure increased the intracellular GSH levels in our cell culture model rather than depleting total GSH and did not increase the formation of superoxide, the gene expression profile analysis of cadmium indicated that the oxidative stress response was activated. Stress-responsive gene transcripts were strongly upregulated, such as *HMOX-1, HSPA1A, MT1A, MT2X* as well as Nrf2 target genes in phase I and phase II metabolism. The cadmium-induced up-regulation of cytoprotective enzymes, activation of GSH synthesis and MT expression is presumably a cellular attempt to initiate an acute response towards cadmium detoxification. This detoxification mechanism effectively suppresses the toxic action of cadmium ions in the cell. The induction of MT and GSH activity suppresses the action of free Cd^{2+} by converting it to a stable, chelated form, thus preventing the associated adverse effects of cadmium, such as impaired cell growth (Delalande *et al.* 2010). The high basal level of GSH in the

examined cells might also be a specific reason why inhibition of cellular GPx activity could not be observed. Enhanced cellular levels of GSH, increased availability of enzymes involved in GSH-mediated detoxification and removal of cadmium and its toxic by-products could potentially prevent their interaction with key cellular targets and reduce toxicity and carcinogenesis (Eneman *et al.* 2000).

Sodium selenite induced oxidative stress by generating superoxide production accompanied by depletion of GSH, which subsequently induced pro-apoptotic signaling in a p53-dependent manner. The intracellular GSH levels were, however, enhanced after exposure to sodium selenite in combination with cadmium chloride. The sodium selenite concentration, which decreased the GSH content in the absence of cadmium, also lowered the cadmium-induced glutathione increase to control levels. In addition to inactivating p53, cadmium appeared to attenuate the sodium selenite-induced GSH depletion, and thereby also superoxide production as well as pro-apoptotic signaling of p53. The dependence of sodium selenite-induced apoptosis on p53-mediated ROS generation was found by another studies (Zhao *et al.* 2006), showing that sodium selenite induced apoptosis by producing superoxide, which then activated p53. In turn, the activation of p53 synergistically enhanced superoxide production and apoptosis induced by sodium selenite. These results suggest that superoxide may be a mediator for p53 phosphorylation/activation following sodium selenite exposure (Zhao *et al.* 2006). Generation of ROS is a key event in sodium selenite-induced apoptosis in different cancer cells, and sodium selenite-induced generation of ROS is blocked by antioxidants (NAC, catalase, SOD) protecting cells from sodium selenite-induced apoptosis (Jiang *et al.* 2002; Li *et al.* 2007; Shen *et al.* 1999; Stewart *et al.* 1997; Wang *et al.* 2002). DNA strand breaks result in stabilization of p53 and an initiation of p53-dependent signal transduction (Nelson and Kastan 1994). Sodium selenite induces DNA-strand breaks via generation of ROS, such as H_2O_2 and superoxide (Drake 2006; Kim *et al.* 2001; Li *et al.* 2007). Studies by several working groups have shown that sodium selenite-induced apoptosis involves the rapid induction of single-stranded DNA breaks in a variety of cell types (Jiang *et al.* 2004; Lu *et al.* 1994; Lu *et al.* 1995). These results suggest that even though ROS are important for initiating signals which activate p53, the p53 functional activity may play an important role for sustaining the ROS generation induced by sodium selenite, leading to an acceleration of apoptosis. Up-regulation of p53-induced ROS-generating enzymes could eventually contribute to the oxidative stress and consequently apoptosis (Liu *et al.* 2008). Assuming that the transcription factor p53 is unfolded by cadmium chloride exposure, protective cellular mechanisms could be disturbed, resulting in accumulation of sodium selenite-induced DNA damage. In the p53-proficient HCT116 cells, accumulation of selenium was correlated to the onset of cytotoxicity following exposure to sodium selenite. Cell cycle arrest was only induced at comparably high concentrations. As expected, the data presented here indicate that attenuating p53 activity by cadmium chloride or using p53-deficient cells led to a lower sensitivity towards sodium selenite-

induced apoptosis. The role of p53 as a critical downstream mediator of ROS signaling and DNA damage by sodium selenite treatment was supported by the significant attenuation of overall death in the p53-deficient cells.

Previous work in our working group examined the induction of DNA-strand breaks and Fpg-sensitive base modification via different selenium compounds in relation to p53 status (Klaus 2009). A 45 h-exposure to sodium selenite led to a strikingly different accumulation of oxidative damage in the HCT116 cell lines. The p53-deficient HCT116 cells accumulated high levels of DNA-strand breaks already at non-cytotoxic concentrations of sodium selenite, while p53-proficient cells exhibited marginal DNA damage even in the cytotoxic range. Fpg-sensitive lesions were first observed at 5 µM sodium selenite in the p53-deficient cells. Exposure to 8 µM sodium selenite resulted in comparable high levels of DNA damage in both cell lines. Appearance of DNA damage was independent of p53 status following exposure to selenomethionine. At 500 µM selenomethionine, the level of single-stranded DNA breaks was raised. The impact of sodium selenite exposure in combination with cadmium chloride on the induction of oxidative DNA damage was also investigated, however, only over a 24 h period. The degree of DNA damage caused by sodium selenite was higher in the presence of cadmium chloride than induced in the absence of the heavy metal cadmium (Klaus 2009). Cadmium chloride alone generated a similar number of DNA-strand breaks as the co-exposure to sodium selenite and cadmium chloride, indicating that the formed oxidative damage was induced by cadmium chloride with no additive effects by sodium selenite. Cadmium itself induced similar levels of DNA damage without highly reducing colony-forming ability, suggesting possible impairment of p53 functions. Inactivation of p53 by cadmium chloride due to conformational changes in its zinc-binding domain could possibly explain the observed effects, since divalent metal ions, such as cadmium could unfold the zinc-binding DNA binding domain, via a possible displacement of zinc ions by cadmium ions (Meplan *et al.* 1999; Schwerdtle *et al.* 2010). Inhibition of p53-mediated processes through cadmium represents a possible underlying mechanism in its cancerogenic potential.

Cadmium is also suggested to activate the nuclear translocation of Nrf2 to prevent apoptosis, possibly through induction of ROS or by increasing Nrf2 stability by direct binding of Cd^{2+} to cysteine residues on Keap1 (Chen and Shaikh 2009). Sodium selenite has been shown to activate Nrf2 via superoxide production, which consequently leads to apoptosis (Park *et al.* 2012). Chen and co-workers suggested that p53 controls a biphasic Nrf2 response, depending on the level of ROS and thereby the expression of p53 (Chen *et al.* 2012). Nrf2 is proposed to act as another key player in p53's tumor suppression. Since cadmium has been shown to activate Nrf2 while inactivating p53, what is the proposed cross-link between p53 and Nrf2 responding to high levels of ROS production from sodium selenite exposure? In this work, we attempted to answer this question in p53-proficient

and p53-deficient HCT116 cells exposed to sodium selenite exposure with or without cadmium co-exposure by using antibody-coupled immunofluorescence microscopy, which detects Nrf2's nuclear location and by live-cell imaging followed by stable transfection with GFP-Nrf2 in HeLaS3 cells (Furukawa and Xiong 2005; Ott 2014). However, the Nrf2 activation methods did not provide optimal confirmation from positive control substances (e.g. sulphoraphane), and the stable GFP-Nrf2 transfected cells only showed a cytoplasmic green signal, which was highly dependent on cell cycle stage, making it very difficult to distinguish a potential nuclear translocation signal. Therefore, a possible Nrf2 activation by sodium selenite and cadmium chloride dependent on p53 status was only investigated at the transcriptional level by gene expression analysis.

Previous work in this working group showed that cellular uptake of sodium selenite, but not the uptake of selenomethionine in HCT116 cells, was p53-dependent (Klaus 2009). Therefore, the question of a potential interaction of cadmium chloride concerning the uptake of sodium selenite in a p53-dependent matter was raised. It would be possible that cadmium co-exposure affected the bioavailability of sodium selenite by inhibiting the cellular uptake of the element, and in this way reduce the cytotoxic effects observed after sodium selenite exposure. Unexpectedly, simultaneous exposure to cadmium chloride led to a dramatically increased content of intracellular selenium over the whole concentration range in both cell lines. The results show overall that cadmium chloride improves the bioavailability of sodium selenite independent on the cellular p53 status. With simultaneous exposure to selenomethionine and cadmium chloride, no difference in the intracellular level of selenium was found compared to selenomethionine exposure in the absence of cadmium chloride. Most selenium compounds can be converted to one or more metabolites: hydrogen selenide, methylselenol and selenomethionine. Hydrogen selenide can redox cycle, deplete GSH and produce ROS such as superoxide and hydrogen peroxide (Jackson and Combs, Jr. 2008). Different chemical forms of selenium are metabolized differently *in vivo*, activate distinct molecular mechanisms and exhibit varying degrees of anti-carcinogenicity in different cancer types (Jiang *et al.* 2002; Li *et al.* 2007; Meuillet *et al.* 2004). Olm and co-workers demonstrated that the extracellular environment is a key factor specific to sodium selenite cytotoxicity, and that sodium selenite uptake depends on extracellular reduction. Extracellular reduction is mediated by cysteine, and the efficacy is determined by the uptake of cystine by the xc$^-$-antiporter and secretion of cysteine by multidrug resistance proteins (Olm *et al.* 2009). A major mechanism of sodium selenite cytotoxicity is thought to be the generation of oxidative stress through intracellular redox cycling of the selenium metabolite selenide with oxygen and cellular thiols, producing superoxide and cellular disulfides. The induction of oxidative stress and consequent apoptosis has been demonstrated in numerous cancer cell lines (Nilsonne *et al.* 2006; Rudolf *et al.* 2008; Zou *et al.* 2008). This occurs mainly in malignant cells. A cancer-specific, high-affinity selenium uptake mechanism could possibly explain cancer-specific sodium

selenite cytotoxicity (Olm *et al.* 2009). The xc-antiporter expression is regulated by ARE and is thereby an Nrf2 target gene and associated with other phase II proteins, in addition to MRPs and enzymes regulating intracellular redox homeostasis. The gene induction of xCT gene and the activity of system xc- is induced by various stimuli, including electrophilic agents and heavy metals such as cadmium (Sasaki *et al.* 2002). Bannai *et al. (*1991) showed that cadmium caused an increase of cellular GSH due to the enhanced uptake of cystine, a protective mechanism related to the induced cellular stress. The reductive microenvironment is dependent on cystine uptake via system xc-, intracellular reduction of NADPH dependent redox protein systems and secretion of cysteine to the extracellular environment by MRPs. In this work, we demonstrated that cadmium increased the intracellular GSH levels in addition to activating Nrf2 target genes, and therefore possibly the xCT gene. Thus, it is likely that cadmium would cause an enhancement of extracellular cysteine concentration, which could lead to an extracellular reduction of the present sodium selenite to a more reduced form of selenite, possibly hydrogen selenide. This form of selenium could then be taken up more efficiently than selenite, which would explain the enhanced uptake of selenium in sodium selenite treated cells in the presence of cadmium chloride. The cytotoxic effects of sodium selenite were significantly reduced when the cells were co-exposed to cadmium chloride, suggested to involve an inactivation of p53 and thereby an inhibition of sodium selenite-induced, p53-mediated effects. Cytotoxic effects were clearly attenuated despite the dramatically higher intracellular concentration of selenium after sodium selenite exposure in combination with cadmium chloride. It is also possible that the absorbed form of selenium could be another form than hydrogen selenide, and accumulates in the cell without acting as cytotoxic as sodium selenite and hydrogen selenide. Another possible mechanism behind cadmium's inhibition of sodium selenite-induced cytotoxicity might be a complexation of cadmium ions with selenite molecules. Metal ions, including cadmium ions protect cells against selenium toxicity by formation of insoluble colloids with selenide in yeast cells, believed to provide cross-protection against the toxicities of both metals and selenocompounds (Dauplais *et al.* 2013). Extracellular interactions between sodium selenite and copper have been reported (Zeng and Botnen 2004). The authors suggested that copper interacts specifically with inorganic, but not organic forms of selenium by strongly suppressing selenite-induced cell cycle arrest. Generation of superoxide by sodium selenite has shown to be inhibited by copper in another study (Davis and Spallholz 1996). In contrast to our results, which showed that cadmium enhances the bioavailability of selenium in the form of sodium selenite, they demonstrated that the extracellular interaction between copper and sodium selenite significantly reduced intracellular selenium content. Altogether, the observed increased bioavailability of selenium by cadmium following sodium selenite exposure needs further investigations. Taken together, Figure 6.1 provides a summary of the impact of cadmium on sodium selenite-induced cellular effects.

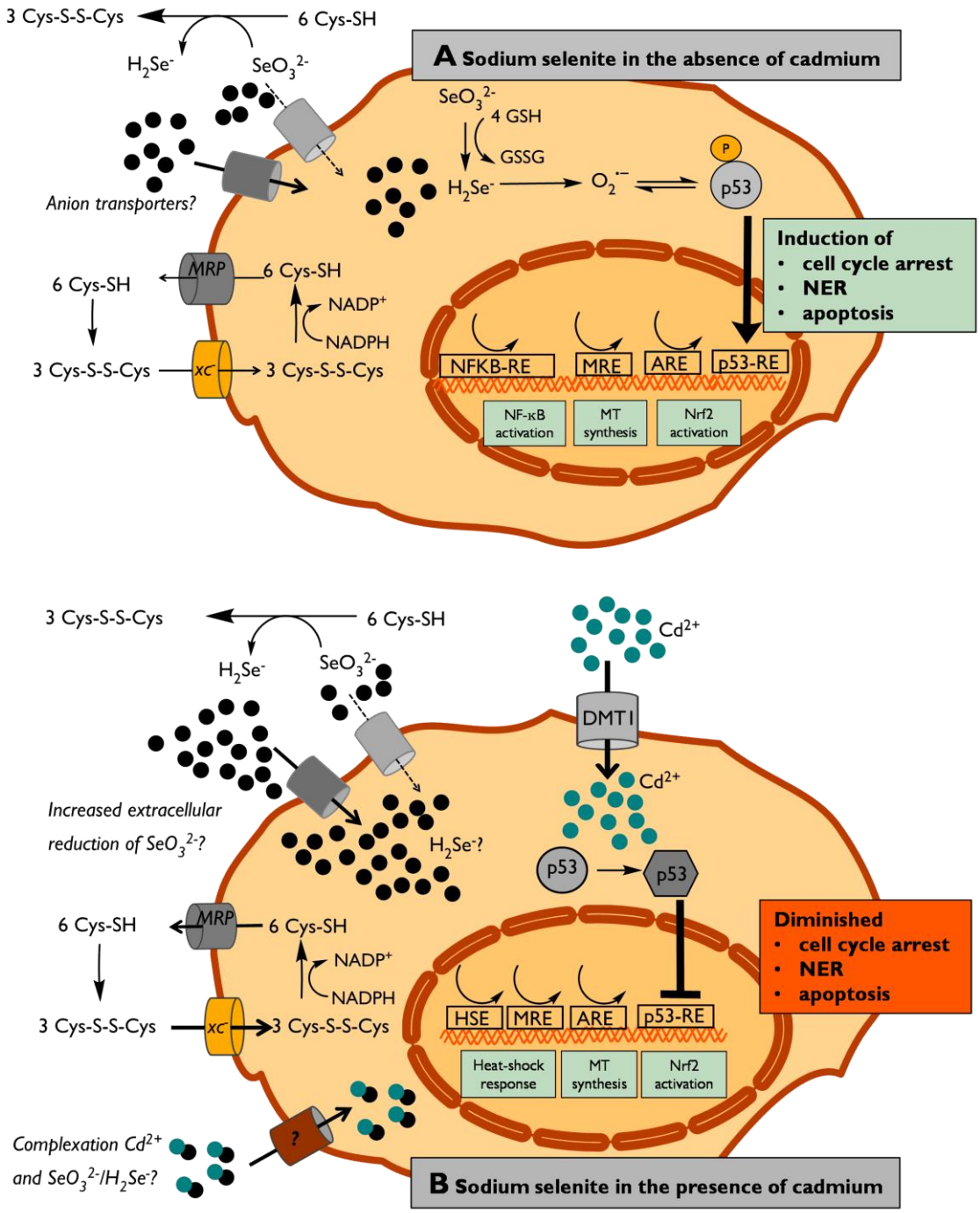

Figure 6.1: (A) Cellular uptake of sodium selenite and the following GSH-depletion and superoxide generation. Tumor suppressor protein p53 is thus activated, leading to cell cycle arrest and apoptosis, which provides protection against genotoxic DNA damage. Other redox-sensitive transcription factors are also activated. (B) In the presence of cadmium, oxidative stress occurs along with the conformational alteration of p53, causing the protein to function similar to a mutant p53. The conformational alteration induced by cadmium prevents cells to undergo normal p53-dependent responses to sodium selenite. This continued cell proliferation might allow the expansion of clones of genetic unstable cells increasing the risk of critical mutations. An improved bioavailability of sodium selenite was observed, hypothesized to be due to increased extracellular thiol-assisted reduction of sodium selenite as a result of enhanced cystine/cysteine redox cycling. Complexation by cadmium ions and selenite/selenide ions is also discussed, but further investigation is needed. DMT1: divalent metal transporter 1, MRP: multidrug resistance-related protein, xc-: xc^--antiporter.

The comparison of sodium selenite and selenomethionine showed that sodium selenite exhibits higher cytotoxicity at much lower concentrations, while selenomethionine accumulates more strongly in the cell because of unspecific integration into proteins following incubation at higher concentration before cytotoxic effects occur. Selenomethionine induced DNA damage only at comparably high, cytotoxic concentrations independent of the p53 status (Klaus 2009). On the other hand, sodium selenite produced a p53-dependent response. Therefore, due to different chemical properties of selenocompounds and differing interactions with other metals, such as cadmium, it is important to be precise when discussing the respective selenium compounds instead of using "selenium" as a general term, particularly when it comes to dietary supplements. Which selenocompound is preferable for supplementation must be further discussed. Sodium selenite is critical due to its pro-oxidative and cytotoxic effects. On the other hand, a possible chronic toxicity through the strong accumulation of selenomethionine should not be underestimated. For this reason the Federal Institute of Risk Assessment (BfR) in Germany advised against supplementation with selenomethionine (BfR 2004).

To the best of our knowledge, the inhibiting effect of cadmium on sodium selenite-induced apoptosis has not been described previously in literature. The data obtained with HCT116 colon cancer cells may help to explain sodium selenite and cadmium interaction when present in the gastrointestinal tract. The presented results of this work help to illustrate that indiscriminate consumption of selenium-containing dietary supplements may possibly be a risk for individuals at particularly high risk of cadmium exposure (e.g. vegetarians, children, females). Although smoking exposes the lung tissue by inhalation, the selenite-cadmium interaction could be an additional risk for smokers, as smokers are remarkably more exposed to cadmium due to the fact that a single cigarette contains 1-2 µg cadmium. Inactivation of tumor suppressive responses could lead to accumulation of mutations and eventually to increased genomic instability. However, conclusions from *in vitro* studies must be drawn with caution as they do not fully reflect *in vivo* situations. Until these effects are well understood, it is important to establish safe supplementation and exposure levels for selenium and its compounds, in order to maximize health benefits while avoiding potential chronic toxic effects. Additionally, the contamination of soil, plants and animals by cadmium must be reduced and controlled in order to achieve a minimum exposure for individuals at high risk.

7 Materials and methods

7.1 Cell culture

7.1.1 Cell lines

As cell culture models for our investigations, adherent cell lines growing under sterile conditions, and cultivated at 37 °C in 5 % CO_2 and 100 % humidity were used. The human colon cancer cell line HCT116 and the isogenic p53-deficient cell line (Bunz *et al.* 1998) were originally established by Prof. Vogelstein (John Hopkins University, Baltimore, USA) and kindly given as a gift from Prof. Schönfelder (Charité, Universitätsmedizin, Berlin). The cell lines were grown in DMEM with the addition of 10 % fetal bovine serum (FBS), 100 U/mL penicillin and 100 µg/mL streptomycin. Sub-cultivation of the HCT116 cells followed every 2-3 days. Prior to sub-cultivation, all necessary solutions were preheated to 37 °C and cells were observed microscopically to inspect their morphology. To detach the cells, cells were first washed with PBS and then with 0.25 % trypsin/EDTA solution (~30 s) followed by 1,5-2 min in the incubator before fresh medium was added to detach the cells. To quantify the cell number, aliquots of the cell suspension were measured using an electronic cell number device (Counter coulter ®, Beckmann). Both HCT116 cell lines were measured in size range of 9-30 µM. Appropriate aliquots of the cell suspension were finally diluted in new cell culture dishes.

7.1.2 Incubations

Stock solutions of cadmium chloride (100 mM), sodium selenite (100 mM) and selenomethionine (100 mM) in bidistilled water were prepared, sterile-filtered and stored at 4 °C until use. Prior to the experiment the stock solutions were further diluted and defined aliquots were pipetted into the cell culture medium. The volume of the cell culture medium was determined before by using the scaling of a glass pipette.

7.1.3 Colony-forming ability

To determine colony-forming ability, cells were trypsinised after treatment with the respective compounds, counted, and 300 cells were seeded in 60 mm cell culture dishes in triplicate. Following 9 days in the incubator, the medium was removed, plates were washed once with cold PBS and the

colonies were fixed with ice-cold 96 % ethanol. The colonies were subsequently stained with Giemsa, washed with distilled water and counted.

7.2 Gene expression profiling

Determination of relative gene expression was performed using high throughput-RT-qPCR. 5 x 10^5 cells were seeded in 60 mm culture dishes to grow for 24 h. Cells were treated with selenocompounds in the presence or absence of cadmium chloride, or by cadmium chloride only. After incubation, the cells were detached with trypsin, harvested in PBS/FBS (10 % FBS) and centrifuged at 1300 rpm and 4 °C for 4 min. The cell pellet was washed again with 1 ml PBS, transferred to an Eppendorf tube and centrifuged at 1300 rpm and 4 °C for 3 min. The supernatant was removed, and the pellets were stored at -20 °C.

RNA isolation was performed using NucleoSpin RNA II Kit (Macherey Nagel). This kit uses a silica-based membrane which selectively binds RNA molecules longer than 200 nucleotides. mRNA are usually longer than 200 nucleotides, while other types of RNA, such as rRNA, 5S rRNA and tRNA are mostly less than 200 nucleotides in length and are therefore excluded.

The pellets were thawed and resuspended in 100 µL sterile PBS. For cell lysis, 350 µL lysis buffer (RAI) and 3.5 µL mercaptoethanol were added and thoroughly mixed. The samples were aspirated five times by a needle (0.9 mm) and liquefied through shearing. After adding 350 µL of ethanol (70 %) and further mixing, the samples were transferred to the columns and centrifuged at 8600 x g for 30 s. The columns were washed with 350 µL of membrane-desalting-buffer (MDB). After 1 min centrifugation at 12 900 x g, DNA was digested by the addition of 95 µl DNase solution (1:10 diluted with DNase reaction buffer) to the columns and incubation for 15 min at room temperature. After adding 200 µl wash buffer (RA2) to the columns, they were centrifuged for 30 s at 8600 x g. A washing step with 600 µl wash buffer (RA3) was followed by centrifugation for 30 s at 8600 x g. The washing step was repeated with another 250 µl at 18 000 x g for 2 min. 30 µl RNase free water was added to the columns, which were centrifuged at 18 000 x g, followed by a second centrifugation step with the 30 µL elute. The eluted RNA was stored at -80 °C.

The isolated mRNA was quantified prior to cDNA synthesis by measuring the absorption of an undiluted aliquot (2 µl) in duplicate at 260 nm a using a multi-plate reader with NanoQuant plate (Infinite M200, Tecan). The ratio of the absorbance at 260 nm and 280 nm (maximum absorption of proteins) was also measured to determine the purity of the mRNA. A ratio of A260:A280 >1.8 indicates high RNA purity.

RNA integrity of HCT116 cells was previously confirmed in the working group (Neumann 2014). By the means of gel electrophoresis, electrophoretic separation of ribosomal RNA, which represents a major part of total RNA (85-90 %), was performed. At high RNA quality the ribosomal RNA separates in two bands, 28 S and 18 S bands, producing a 28S/18S rRNA ratio of 2:1 in the electrical field. By densitometric quantification of the two bands with Aida software the 28S/18S rRNA ratio of 2.2:1 was detected, confirming proper RNA integrity (Neumann 2014). An automated capillary electrophoresis by the means of Lab-on-Chip technology on a Bioanalyzer was performed to verify the confirmation from the agarosis gel electrophoresis results. In an electrogram, individual rRNA fractions, mRNA and fragmented RNA are visualized. A RNA integrity number (RIN) of 10 was detected, which represented intact, but not degraded or fragmented, RNA (Neumann 2014).

cDNA synthesis was performed in duplicate using the qScript™ cDNA Synthesis Kit (BioRad). 1 µg RNA was mixed with 4 µL reaction mix and 1 µL iScript reverse transcriptase in PCR strip tubes in a total reaction volume of 20 µL with RNase free water. The reaction was initiated using a temperature program (1 cycle 25 °C for 5 min, 1 cycle 42 °C for 30 min, 1 cycle 85 °C for 5 min) conducted by a Thermocycler iCycler (BioRad).

To guarantee sufficient cDNA amount for the RT-qPCR a pre-amplification of the samples was performed with the specific primer pairs. 2.5 µL TaqMan® PreAmp Master Mix (2x) was mixed with 0.5 µM of 500 nM mix for each primer pair, 0.75 µL water and 1.25 µl of the sample were mixed together and preamplified in the thermo cycler (Temperature programme: 1 cycle 95 °C for 10 min, 12 looped cycles at 95 °C for 15 s and 60 °C for 4 min). A non-template control (NTC) (water) and untranscribed RNA samples as –Reverse Transcriptase (-RT) control served as controls. After the preamplification an exonuclease digestion was also performed to remove residual, unbound primers. 2 µL of an exonuclease solution (4 U/µL) was added to each sample and incubated at 37 °C (40 min). The exonuclease was inactivated by heating (80 °C for 15 min), and the entire sample set was diluted 1:5 with TE buffer and stored at -20 °C.

Before the RT-qPCR analysis 2.25 µl of each pre-amplified sample was combined with 2.5 µL SsoFast EvaGreen® Supermix (2 x with low ROX) and 0.25 µL DNA Binding Dye Sample Loading Reagent (20x). Another NTC was included. The primer pairs were diluted with DNA Suspension buffer (1x) and Assay Loading Reagent (2x), obtaining a primer concentration of 5 µM. The final primer concentration was accordingly 500 nM. The RT-qPCR analysis was performed on a Biomark™-RT-qPCR instrument, allowing simultaneous analysis of 96 x 96 independent PCR reactions using a chip. The Dynamic Array of the chip was primed with a control liquid in Integrated Fluidic Circuits (IFC) Controller HX to fill the channels of the Dynamic Array. Afterwards, 5 µL of each sample and primer solutions were pipetted in the respective cavities and the chip was loaded with the solutions in the

IFC Controller HX. In the following RT-qPCR, amplification of each separate sample to each of the 95 primer pairs took place (temperature program: 1 cycle 70 °C for 40 min, 1 cycle 60 °C for 30 s, 1 cycle 95 °C for 1 min, 30 looped cycles at 96 °C for 5 s and 60 °C for 20 s, 1 cycle from 60 to 95 °C for 3 min).

The analysis of the obtained data was performed using Fluidigm Real Time PCR Analysis software. By using the passive reference dye, ROX, the correct loading of all reaction chambers was confirmed. The amplificates were quantified using the intercalating fluorescence dye EvaGreen, whereby the specificity of each PCR reaction was monitored by assessing the respective melting curves. The GenEx software (MultiD Analyses) was used to obtain Cq values. The samples were normalized to the reference genes *ACTB, B2M, GAPDH, GUSB* and *HPRT*.

7.3 Detection of superoxide generation

The superoxide indicator dihydroethidium (DHE), also called hydroethidine, exhibits blue-fluorescence in the cytosol until oxidized to the fluorescent molecule ethidium bromide by $O_2^{\bullet -}$, where it intercalates with DNA in the cell, staining its nucleus a bright fluorescent red. The oxidation of DHE is rapid when the oxidant is $O_2^{\bullet -}$, but considerably slower in the presence of O_2, H_2O_2, HOCl or $ONOO^-$. Consequently, DHE is considered a good detector of intracellular superoxide (Carter *et al.* 1994).

2.5 x 10^5 HCT116 cells were seeded out in 40 mm culture dishes for 42 h before 6 h incubation time with selenocompounds in the presence or absence of cadmium chloride. 15 min treatment with 100 µM menadione was used as positive control. After treatment, cells were trypsinized and 1 ml fresh medium was added to each dish, then 500 µl was transferred to conical tubes (suitable for flow cytometer) and centrifuged at 1300 rpm for 3 min. After centrifugation, the medium supernatant was removed. Next, 400 µl of a mixture of DHE dye and PBS (1:100 from 1 mM DHE frozen aliquot; final concentration 10 µM DHE) was added to each tube, briefly vortexed and incubated at 37 °C for 45 min. The stained samples were again centrifuged to remove the dye and resuspended with 300 µl PBS before being measured in the flow cytometer.

Flow cytometry data were acquired with LSRII Fortessa (BD Sciences). Excitation for PE was at 488 nm and the emission of 10 000 cells per sample was recorded at FL-1sensor (575/28 nm BP). Data analysis was performed with BD FACSDiva™ software and expressed as the percentage of the untreated control cells, which was set to 100 %.

7.4 Thiol determination

7.4.1 Intracellular quantification of total GSH

Quantification of the total intracellular GSH content was performed by the recycling assay as described by Tietze (Tietze 1969). Here, Ellman's reagent (5.5'-dithio-bis-(2-nitrobenzoic acid), DTNB) is reduced by GSH to the yellow-colored 5-thio-2-nitrobenzoic acid (TNB). Through addition of GR/NADPH, GSSG is reduced back to GSH in a redox cycle. The GR-driven GSSG recycling leads to a persistent increase in TNB, and quantified via absorbance at 412 nm.

3.5 x 10^5 HCT116 cells were seeded out in 60 mm culture dishes for 24 h before the desired incubation time with selenocompounds in the presence or absence of cadmium chloride, or by cadmium chloride alone. After each treatment, cells were trypsinized to measure cell number as well as mean cell volume before transferring 2 ml of cell suspension in micro-reaction vessels. Cells were centrifuged at 640 g to pellets at 4 °C for 4 min, supernatant was removed and potassium phosphate puffer added giving a cell concentration of 2.5 x 10^5 cells per 120 µL solution.

For cell lysis, cells were stored at -80 °C for at least 24 h. After thawing, sonification followed for 5 min in an ultra sound bath before a second freeze/thaw/sonification cycle. 6.5 % 5-sulfo salicyl acid (5-SSA) solution (final concentration 1.3 %) was added for protein precipitation, followed by 10 min on ice after thoroughly mixing. The protein precipitate was separated from the supernatant at 2000 x g at 4 °C, using the supernatant directly for the recycling assay.

The measurement of the total GSH content was performed in 96 microwell plates in a microplate reader (Tecan). 20 µL supernatant was added per cavity as well as 40 µL phosphate potassium buffer and 100 µL DTNB/NADPH mixture (final concentrations in mixture 2 mM DTNB and 0.3 mM NADPH). The reaction was initiated by addition of 40 µL GR (4 U/mL). The formed TNB was measured in 30 s intervals for a 4 min reaction time (8 cycles). The total GSH content of the samples as well as an external control (20 µM GSSG) were determined using an external calibration curve (GSH 5-50 µM).

To calculate the intracellular total GSH content, the extinction difference (ΔE) between cycle 1 and cycle 5 was determined ($\Delta E = E_{Cycle\ 5} - E_{Cycle1}$). Relative GSH content of the samples could be determined by the external calibration curve ($E = \Delta E_{Sample} - \Delta E_{Background}$). The GSH data was normalized to the actual mean cell volumes in order to obtain molar intracellular concentrations.

7.4.2 Extracellular quantification of total thiols

Quantification of the total extracellular thiol content was performed by using the thiol reagent DTNB, which is reduced by present thiols to the yellow-colored TNB. The conversion of DTNB to TNB was quantified via the absorbance at 412 nm.

2.5 x 10^5 HCT116 cells were seeded out in 40 mm culture dishes for 24 h before the desired incubation time with selenocompounds in the presence or absence of cadmium chloride. Directly after addition of compounds, culture medium (200 µl) was transferred in micro reaction tubes (1.5 ml) in order to determine the thiol levels at 0 h incubation time, as well as after 24 h treatment. Detached cells and debris from culture medium was separated by centrifugation (2 min, 1500 rpm). A medium blank (growth medium only) was included for each time point to subtract the background from the samples. L-cysteine was used as standard. The calibration curve ranged from 7.8 µM to 1000 µM cysteine, prepared by serial dilutions (1:2) starting from a stock solution of 2 mM cysteine, which was dissolved in 400 mM Tris-HCl (pH 8.0). 50 µl standard or incubated medium supernatant was transferred in 96 well plates (in triplicate). 150 µl buffer (400 mM Tris HCl pH (8.0) was added to each well followed by addition of 10 µl DTNB (10 mM) to the wells to initiate the thiol reaction, and the absorption measured at 412 nm. The untreated control was set to 100 %.

7.5 Enzymatic activities of antioxidant enzymes

1.7 x 10^6 HCT116 cells were seeded out in 100 mm culture dishes to grow for 24 h before incubation with selenocompounds in the presence or absence of cadmium chloride. After each treatment, cells were trypsinized to determine cell number before transferring 2 ml cell suspension in micro reaction vessels. Cells were centrifuged at 640 x g to pellets at 4 °C for 4 min, the supernatant was removed and 0.1 M potassium phosphate puffer (pH 7.0), including 1 % reduced Triton X-100 (Fluka) was added (final cell concentration of 3.0 x 10^6 cells/150 µL solution). For cell lysis, cells were centrifuged at 16600 x g for 10 min at 4°C. The supernatants were transferred into new micro reaction vessels and stored at -20°C until assay measurement.

All the enzyme activity measurements were performed in 96 microwell plates with a microplate reader (Tecan).

Thioredoxin Reductase (TrxR) Assay (DTNB reduction):

The quantification of the intrinsic TrxR enzyme activity was modified after the method of Smith (Smith *et al.* 2001). The assay buffer used was 0.1 M KH_2PO_4 (pH 7.0). Rat liver TrxR (IMCO, Sweden) was stored at -20 °C in aliquots of 2.64 µM (50 µl in 50 mM TE, pH 7.5). 50 nM TrxR was

used as a positive assay control. Cellular samples treated with the gold compound auranofin (Sigma) was used to inhibit cellular TrxR activity, and served as a positive inhibition control. A specific TrxR inhibitor, aurothiomalate (Sigma) (final concentration 20 µM), was added to sample wells, allowing correction of non-thioredoxin reductase-independent DTNB reduction (e.g. presence of glutathione) (Smith *et al.* 1999). The difference between samples with or without the inhibitor aurothiomalate obtained the DTNB reduction due to TrxR activity. 120 to 160 µL assay buffer was added to all wells, depending on the activity in the lysates. 2.5 mM DTNB in assay buffer (final concentration 0.25 mM) was added and the absorbance (412 nm) was measured for 8 cycles of 20 s intervals to obtain the background. Addition of 2 mM NADPH (final concentration 0.2 mM) initiated the reaction. The NADPH-dependent disappearance of DTNB, the conversion into TNB, was recorded at the absorbance at 412 nm using a kinetics program with 31 cycles of 20 s intervals obtaining the reaction rate.

The TNB extinction coefficient is 13.6 mM^{-1} cm^{-1}. The path length of the solution in the well (0.6 cm) was adjusted for the activity calculation. The change in absorbance per min (ΔA/min) was determined, and the A values plotted as a function of time to obtain the slope of the linear part of the curve ($\Delta A/min = (A_2-A_1)/(t_2-t_1)$). The background value was subtracted from the sample values, as well as the values from samples containing the TrxR specific inhibitor. One unit is defined as the NADPH-dependent production of 2 µmol of TNB from DTNB per min. TrxR activity (µmol/min) in samples was calculated using this equation: ((ΔA/min)/ 6.756 mM^{-1}). The untreated control was set to 100 %.

Glutathione Reductase (GR) Assay (NADPH consumption):

Quantification of the intrinsic GR enzyme activity was modified after the method of Carlberg and Mannervik (Carlberg and Mannervik 1985). The assay buffer used was 0.1 M KH_2PO_4 (pH 7.0). The isolated GR enzyme (Baker's yeast) served as the positive assay control (0.25 U/mL, final concentration 5 mU per well). Cellular samples treated with the specific cellular GR inhibitor, 2-AAPA (Sigma) was used as positive inhibitor control (Seefeldt *et al.* 2009). A stock solution of 100 mM oxidized GSH (GSSG) was stored at -20°C. 90 µl assay buffer and 10 µL of sample, positive control or lysis buffer were added to each cavity. 100 µl of the GSSG-NADPH mixture prepared in assay buffer (final concentrations in mixture 1 mM GSSG/0.4 mM NADPH) was added to start the reaction. The absorbance (A) was measured immediately at 340 nm with a kinetics program with 16 cycles of 20 s intervals.

The NADPH extinction coefficient is 0.00622 μM^{-1} cm^{-1}. The path length of the solution in the well (0,6 cm) was adjusted for the activity calculation. The change in absorbance per min (ΔA/min) was

determined, and the A values plotted as a function of time to obtain the slope of the linear part of the curve ($\Delta A/min = (A_2-A_1)/(t_2-t_1)$). The background value was subtracted from the test values. One unit is defined as the amount of enzyme which will cause the oxidation of 1 nmol of NADPH to $NADP^+$ per min. GR activity (nmol/min) in the samples was calculated using this equation: $((\Delta A/min)/0.00373\ \mu M^{-1})$). The untreated control was set to 100 %.

Glutathione Peroxidase (GPx) Assay (indirect GR-coupled):

Quantification of the intrinsic GPx enzyme activity was modified after the method of Sharov (Sharov *et al.* 1999). The assay buffer used was 0.1 M KH_2PO_4 (pH 7.0) and isolated bovine erythrocytes GPx (Sigma) used as positive assay control (1U/mL). Bovine erythrocytes GPx was stored at -80 °C in aliquots of 100 U/mL (20 µl in 10 mM Na_2HPO_{4+} in 1 mM DTT). Cellular samples treated with mercaptosuccinate (Sigma) was used to inhibit cellular GPx and served as a positive inhibitor control (Michiels and Remacle 1988). A reaction mix (RM) of 100 µL per cavity was prepared, including 10 mM GSH (final concentration 1 mM), 6 U/ml GR (final concentration 0,6 U/mL), and 3.3 mM DETAPAC/0.166 M KH_2PO_4 (final concentration 1 mM DETAPAC). 20 to 60 µL of sample or positive control was added depending on the activity in the cell lysate. 1 mM NADPH (final concentration 0.1 mM) was added before addition of 12 mM tertbutyl hydroperoxide (t-BOOH, final concentration 1.2 mM) was used to initiate the reaction. The absorbance (A) was measured immediately at 340 nm with a kinetics program with 16 cycles of 20 s intervals, thus obtaining the reaction rate of the conversion to NADP+ from NADPH.

The NADPH extinction coefficient is 0.00622 $\mu M^{-1}\ cm^{-1}$. The path length of the solution in the well (0.6 cm) was adjusted for the activity calculation. The change in absorbance per min ($\Delta A/min$) was determined, and the A values plotted as a function of time to obtain the slope of the linear part of the curve ($\Delta A/min = (A_2-A_1)/(t_2-t_1)$). The background value was subtracted from the test values. One unit is defined as the amount of enzyme which will cause the oxidation of 1 nmol of NADPH to $NADP^+$ per min. GPx activity (nmol/min) in samples was calculated using this equation: $((\Delta A/min)/0.00373\ \mu M^{-1})$. The untreated control was set to 100 %.

Catalase Assay:

Quantification of the intrinsic catalase enzyme activity was modified after the method of Li and Schellhorn (Li and Schellhorn 2007). In this assay, 96 well UV micro plates were used to measure decomposition of H_2O_2 from the catalase present in the samples. Isolated catalase from bovine erythrocytes (Sigma), as well as cellular samples treated with sodium azide, served as positive controls (Sorg *et al.* 1997). 10 µL of sample or positive controls were pipetted into the cavities,

followed by 200 µL 5.25 mM H_2O_2 (final concentration 5 mM H_2O_2) to start the reaction. The decomposition of H_2O_2 was measured immediately at 240 nm using a kinetics program with 16 cycles of 20 s intervals to obtain the reaction rate.

The H_2O_2 extinction coefficient is 39.4 mM^{-1} cm^{-1}. The path length of the solution in the well (0.6 cm) was adjusted for the activity calculation. The change in absorbance per min (ΔA/min) was determined, and the A values plotted as a function of time to obtain the slope of the linear part of the curve ($\Delta A/min = (A_2-A_1)/(t_2-t_1)$). The background value was subtracted from the sample values. One unit is defined as the amount of enzyme which will cause the decomposition of 1 µmol of H_2O_2 per min. Catalase activity (µmol/min) in samples was calculated using this equation: ((ΔA/min)/ 23.64 mM^{-1}). The untreated control was set to 100 %.

Superoxide dismutase (SOD) Assay:

This assay is based on the published assay from Peskin and Winterbourn (Peskin and Winterbourn 2000). Cells were treated with the positive control sodium diethyl dithio carbamate (DDC). Assay buffer used in the assay and reaction mix was 0.1 M KH_2PO_4 (pH 8.0), including 0.1 mM DETAPAC and 0.1 mM hypoxanthine. The superoxide radical WST-1 (Dojindo) was kept in aliquots (10 mM in water) at -20 °C, and added immediately before use in reaction mixture (final concentration 50 µM), including 10 U/mL catalase (final concentration 0.06 U/ml). As the samples had high SOD activity, the samples were diluted prior to the assay. 10 µl of diluted samples, lysis buffer (background) and SOD standard, as well as 200 µl reaction mixture were added to all wells. 20 µL 100 mU/ml xanthine-oxidase (XO) (final concentration per well 8.7 mU/mL) was quickly added to initiate the reactions, the plate was covered and incubated for 20 min at 37 °C in the dark, and measured at 450 nm. One unit is defined as the amount of enzyme needed to exhibit 50 % dismutation of the superoxide radical. Relative SOD content of the samples could be determined by the external calibration curve from SOD standards (from bovine erythrocytes).

7.6 Cell cycle distribution and apoptosis

To examine if apoptosis is involved in the observed cytotoxic effects, several parameters were investigated. In addition to the analysis of transcript levels of genes associated with apoptosis (see section for gene expression profiling), cell death analysis and mitochondrial membrane potential were simultaneously detected by flow cytometry, as well as determination of concurrent increase of sub-diploid cells (sub-G1 fraction) in the cell cycle distribution. Immunofluorescence microscope analysis of nuclear AIF translocation was also performed.

7.6.1 Single tube flow cytometric cell death analysis

Cell death classification can be provided by staining cells with different dyes from one single tube (Munoz *et al.* 2013). The common markers AnnexinV-FITC and propidium iodide (PI) stain for phosphatidylserin (PS) exposure and plasma membrane damage, respectively. Mitochondrial membrane potential could be determined by the dye 1,1',3,3,3',3'-hexamethylindodicarbocyanine iodid (DiIC1(5)), which accumulates in mitochondria with active membrane potential. Morphological alterations in cell size and cell granularity are provided by scatter changes in forward scatter (FSC) and side scatter (SSC). Apoptotic cells are detected as a cell population with decreased FSC and increased SSC due to cellular shrinkage and an increased cytoplasmic granularity (Hagenhofer *et al.* 1998).

5.0 x 10^5 HCT116 cells were seeded out in 60 mm culture dishes for 24 h before another 24 h incubation time with selenocompounds in the presence or absence of cadmium chloride. After treatment, 150 µl incubation medium containing detached cells was transferred to conical FACS tubes for cell death classification. The rest of the incubation medium was transferred to conical tubes for a separate measurement of cell cycle distribution. Attached cells were trypsinized and collected in 1 ml fresh medium. 150 µl was transferred to respective tubes for the cell viability test, while the remaining cell suspension was transferred to the respective tube for cell cycle measurement. 200 µl fresh master mix (containing 200 µl Ringers solution (calcium-containing puffer), 5 µl PI (50 µg/µl), 1 µl AnnexinV-FITC and 1 µl DiIC1(5) (3 µM)) for each tube was added and briefly vortexed followed by 30 min incubation in the dark at 4 °C. The samples were immediately measured in the flow cytometer.

Flow cytometry data were acquired with LSRII Fortessa (BD Sciences). Excitation for FITC and PI was at 488 nm, the FITC fluorescence was recorded on the FL-1 sensor (530/30 nm BP), the PI fluorescence on the FL-3 sensor (695/40 nm BP). FITC signal (X axis) was set up against the PI signal (Y axis), allowing gating of PI negative/Annexin V negative (viable), PI negative/Annexin V positive (apoptotic), PI positive/Annexin V positive (necrotic) cell populations. DiIC1(5) fluorescence was excited at 640 nm and recorded with the FL-2 sensor (670/14 nm BP). The DiIC1(5) signal was displayed as a histogram, and a decreased signal compared to the viable cell population was interpreted as apoptotic or already dead cells. The dyes were compensated in advance to reduce fluorescence overlap. 10 000 cells per sample were recorded and analyzed. Data analysis was performed with BD FACSDiva™ software.

7.6.2 Cell cycle distribution and sub-G1 fraction

Flow cytometry allows the investigation of DNA content in cells. Specific markers of DNA, such as 4', 6-diamidino-2-phenylindole (DAPI), can be used. DAPI binds preferentially to AT-rich regions of the minor grooves of DNA, resulting in a 20-fold fluorescence enhancement (Karlsson *et al.* 2003; Kubista *et al.* 1987). The absorbed amount of dye is proportional to the DNA content. By excitation of the dye, the emitted fluorescent signal can be examined and quantified. The distribution of cells can be separated into cell cycle phases, based on the DNA content. Cells containing less DNA than a cell in the G1-phase are cells in late apoptosis due to DNA fragmentation and can be detected due to their appearance as the so-called sub-G1 fraction in the histogram.

During the 30 min incubation time for cell viability test (see 7.6.1), the cell samples for cell cycle analysis were centrifuged at 1300 rpm for 3 min at 4 ° C. The pellet was resuspended in 1 ml cold PBS and fixed with dropwise addition of another 3 ml of ice-cold ethanol (96 %) while vortexing. The samples were stored at -20 °C until the day of measurement. On the day of measurement the samples were centrifuged, and the supernatant removed followed by resuspension of 250 µL DAPI staining solution (CyStainDNA, Partec, Münster, Germany). Samples were incubated for 30 min at 4 °C before measurement. 30 000 cells per sample were examined and analyzed by LSRII and the Diva software.

7.6.3 AIF translocation

Apoptosis is triggered by two possible pathways. The first pathway is receptor-mediated, and the second one is mediated by the mitochondria. Cytochrome C and apoptosis inducing factor (AIF) are anchored at the inner mitochondrial membrane. The mitochondria-mediated apoptotic pathway is triggered through certain apoptotic stimuli, and thereby cytochrome C and AIF can detach from the membrane and be released into cytosol. From the cytosol, AIF is further translocated to the cell nuclei, where it accumulates and in turn induces chromatin condensation as well as DNA fragmentation (Norberg *et al.* 2010). By means of a specific primary antibody against AIF detected by a red fluorescence-coupled secondary antibody, the localization of the AIF was examined. The nuclei were stained with DAPI, a fluorescent dye that binds to A-T rich regions in DNA.

1.5 x 10^5 cells were seeded and grown on sterile cover slips (12 mm Ø) placed in 60 mm culture dishes. After 24 h, cells were incubated with sodium selenite, selenomethionine or staurosporine for 24 h. In combination with cadmium, cells were co-incubated with cadmium chloride for 26 h. At the end of the incubation, the medium was removed from the culture dishes. The cells were washed twice in ice-cold PBS-UVC solution, ice-cold methanol was quickly added to fix the cells for 10 min

according to Chen *et al.* (Chen *et al.* 2008). The cover slips covered with cells were taken from the dishes and coated with blocking solution (5 % FBS in PBS/UVC) for at least 30 min to block unspecific binding sites. After removing the blocking solution, 70 µl of the primary antibody (anti-AIF-antibody H300 (rabbit), diluted 1:300 in blocking solution) were applied and incubated for 1 h at 37 °C to reduce background signal. Afterwards, the cover slips were washed several times with PBS followed by another blocking step for 10 min. Next, the cells were incubated with 70 µl of the secondary antibody (anti-rabbit-antibody Cy3, diluted 1:300 in blocking solution) under the same conditions as for the primary antibody. Finally, after another three washing steps, coverslips were placed on microscope slides with a drop of Vectashield mounting medium containing DAPI. Labeled AIF location was visualized and recorded using an Axio Imager.M1 fluorescence microscope with an AxioCam MRm camera (Zeiss). The red AIF fluorescence signal intensity of at least 100 cells per slide (15-30 pictures) was analyzed by the AxioVision 4.8 software (Zeiss). Only signals in DAPI-stained nuclei were quantified. The untreated control was set to 100 %.

7.7 Bioavailability

To investigate if the observed different cytotoxic effects following exposure to selenocompounds in combination of cadmium chloride are associated with bioavailability, the uptake of total selenium was quantified by graphite furnace atomic absorption spectroscopy (GF-AAS).

1.0 x 10^6 HCT116 cells were seeded out for 24 h. To assess cellular uptake of sodium selenite and selenomethionine in combination with cadmium chloride, logarithmically growing HCT116 cells were treated for 24 h with the respective selenocompound in the presence of cadmium chloride (10 µM) or by cadmium chloride alone. After treatment, cells were trypsinized, collected in 5 ml 5 % FBS in PBS and centrifuged (1250 rpm, 5 min, 4 °C) before determination of cell number and mean cell volumes. Next, the pellets were washed twice with ice-cold PBS and stored at -20 °C. For the cell disruption, the pellets were resuspended in a 1:1 mixture of HNO_3 (69 %) and H_2O_2 (30 %) (suprapure quality) (so-called nitrohydrochloric acid) before incinerated in a thermo mixer at 65 °C for 1 h and stepwise by 10 °C per hour until reaching 95 °C for about 7 h. The ash was collected in 1 ml double-distilled water. Next, selenium was determined by GF-AAS (Perkin-Elmer, PinAAcle 900 T). The measurements and signal analysis were performed using Software AA Winlab32. The peak areas were quantified. Argon was used as protective gas. For the AAS measurements, 20 µl of sample or dilution was applied together with 5 µl Pd/Mg modifier in the graphite furnace, and analyzed by optimized temperature program for Se (Table 7.1). The wave length for analysis of Se was 196.03 nm. We used a 5-point calibration curve in the range of 2-20 µg Se/l in a dilution of a selenium atom spectroscopy standard solution (cSe = 1 g/l; Roth) with 0.2 % HNO_3. The blank limit

for Se was 0.53 µg/l, the limit of detection was 1.05 µg/land the quantification limit was 1.58 µg/l. External recovery using the AAS standard solution (10 µg Se/l) for each test series was determined in order to verify a constant measuring performance of the GF-AAS. The external recovery of Se was in average 102.4 % ± 10.7 %. It is thereby assumed that the determination of Se by GF-AAS identified correct measurement data. Additionally, for each cell disruption procedure by nitrohydrochloric acid, another external recovery with 10 µg Se/l was performed. This external standard yielded in average 89.1 % ± 11.8 %, by which a marginal loss of selenium might have occurred during the cell disruption and ashing.

Table 7.1: Temperature program of the AAS analysis of Se

Se	Temp (°C)	Ramp (sec)	Hold (sec)	Internal Flow (ml/min)
Drying	110	1	30	250
Drying	130	15	30	250
Pyrolysis	1200	10	20	250
Atomisation	1800	0	5	0
Clean-out	2450	1	3	250

7.8 Statistical analysis

Besides descriptive statistics, data were analyzed by the Levene's test for equality of variances. Differences between the mean values compared to the untreated control were examined by one-way factorial analysis of variance (ANOVA). In the case of equal variance post hoc Dunnett's T-test was used. In the case of unequal variance, Dunnett's T3 Post-Hoc test was used. Identification of statistical significant differences ($p<0.05$) between the treatments in the different cell lines or with the respective selenocompounds alone and in combination with cadmium in the HCT116 cells was revealed by using a non-parametric independent samples t-test. The Mann-Whitney U test was chosen to compare differences between two not normally distributed and independent groups with the dependent continuous variable. Data from at least two sets of independent experiments are shown as arithmetic mean ± SD.

Statistical analysis was performed with SPSS (PASW Statistics 19; IBM, Armonk, USA) and Microsoft Excel 2010 (Microsoft Deutschland GmbH, Unterschleisheim, Germany).

8 Reference list

Abbas, T., and Dutta, A. (2009). p21 in cancer: intricate networks and multiple activities. *Nat. Rev. Cancer* **9**(6), 400-414.

Abraham, R. T. (2001). Cell cycle checkpoint signaling through the ATM and ATR kinases. *Genes Dev.* **15**(17), 2177-2196.

Akesson, A., Berglund, M., Schutz, A., Bjellerup, P., Bremme, K., and Vahter, M. (2002). Cadmium exposure in pregnancy and lactation in relation to iron status. *Am. J. Public Health* **92**(2), 284-287.

Alam, J., and Cook, J. L. (2003). Transcriptional regulation of the heme oxygenase-1 gene via the stress response element pathway. *Curr. Pharm. Des* **9**(30), 2499-2511.

Alam, J., and Cook, J. L. (2007). How many transcription factors does it take to turn on the heme oxygenase-1 gene? *Am J Resp Cell Mol Biol* **36**(2), 166-174.

Alfthan, G., Eurola, M., Ekholm, P., Venalainen, E. R., Root, T., Korkalainen, K., Hartikainen, H., Salminen, P., Hietaniemi, V., Aspila, P., and Aro, A. (2014). Effects of nationwide addition of selenium to fertilizers on foods, and animal and human health in Finland: From deficiency to optimal selenium status of the population. *J. Trace Elem. Med. Biol.*, doi:10.1016/j.itemb.2014.04.009.

Arner, E. S. (2009). Focus on mammalian thioredoxin reductases--important selenoproteins with versatile functions. *Biochim. Biophys. Acta* **1790**(6), 495-526.

Arner, E. S. (2010). Selenoproteins-What unique properties can arise with selenocysteine in place of cysteine? *Exp. Cell Res.* **316**(8), 1296-1303.

Baird, L., and Dinkova-Kostova, A. T. (2011). The cytoprotective role of the Keap1-Nrf2 pathway. *Arch. Toxicol.* **85**(4), 241-272.

Bannai, S., Sato, H., Ishii, T., and Taketani, S. (1991). Enhancement of glutathione levels in mouse peritoneal macrophages by sodium arsenite, cadmium chloride and glucose/glucose oxidase. *Biochim. Biophys. Acta* **1092**(2), 175-179.

Behne, D., and Kyriakopoulos, A. (2001). Mammalian selenium-containing proteins. *Annu. Rev. Nutr.* **21**, 453-473.

Belton, M., Prato, F. S., and Carson, J. J. (2011). Effect of Glutathione Depletion, Hyperthermia, and a 100-mT Static Magnetic Field on an hsp70/luc Reporter System. *Bioelectromagnetics* **32**(6), 453-462.

Beyersmann, D., and Hartwig, A. (2008). Carcinogenic metal compounds: recent insight into molecular and cellular mechanisms. *Arch. Toxicol.* **82**(8), 493-512.

BfR. (2004). Bundesinstitut für Risikobewertung, Selenverbindungen in Nahrungsergänzungsmitteln. Report. 015/2005

Bjelakovic, G., Nikolova, D., Gluud, L. L., Simonetti, R. G., and Gluud, C. (2008). Antioxidant supplements for prevention of mortality in healthy participants and patients with various diseases. *Cochrane. Database. Syst. Rev.*(2), CD007176.

Blessing, H., Kraus, S., Heindl, P., Bal, W., and Hartwig, A. (2004). Interaction of selenium compounds with zinc finger proteins involved in DNA repair. *Eur. J. Biochem.* **271**(15), 3190-3199.

Brigelius-Flohe, R. (2008). Selenium compounds and selenoproteins in cancer. *Chem. Biodivers.* **5**(3), 389-395.

Brozmanova, J., Manikova, D., Vlckova, V., and Chovanec, M. (2010). Selenium: a double-edged sword for defense and offence in cancer. *Arch. Toxicol.* **84**(12), 919-938.

Bunz, F., Dutriaux, A., Lengauer, C., Waldman, T., Zhou, S., Brown, J. P., Sedivy, J. M., Kinzler, K. W., and Vogelstein, B. (1998). Requirement for p53 and p21 to sustain G2 arrest after DNA damage. *Science* **282**(5393), 1497-1501.

Cao, T. M., Hua, F. Y., Xu, C. M., Han, B. S., Dong, H., Zuo, L., Wang, X., Yang, Y., Pan, H. Z., and Zhang, Z. N. (2006). Distinct effects of different concentrations of sodium selenite on apoptosis, cell cycle, and gene expression profile in acute promyeloytic leukemia-derived NB4 cells. *Ann Hematol* **85**(7), 434-442.

Carlberg, I., and Mannervik, B. (1985). Glutathione reductase. *Methods Enzymol.* **113**, 484-490.

Carter, W. O., Narayanan, P. K., and Robinson, J. P. (1994). Intracellular Hydrogen-Peroxide and Superoxide Anion Detection in Endothelial-Cells. *J Leukocyte Biol* **55**(2), 253-258.

Casalino, E., Calzaretti, G., Sblano, C., and Landriscina, C. (2002). Molecular inhibitory mechanisms of antioxidant enzymes in rat liver and kidney by cadmium. *Toxicology* **179**(1-2), 37-50.

Casalino, E., Sblano, C., and Landriscina, C. (1997). Enzyme activity alteration by cadmium administration to rats: the possibility of iron involvement in lipid peroxidation. *Arch. Biochem. Biophys.* **346**(2), 171-179.

Chan, H. M., Smith, L., and La Thangue, N. B. (2001). Role of LXCXE motif-dependent interactions in the activity of the retinoblastoma protein. *Oncogene* **20**(43), 6152-6163.

Chan, W. M., Siu, W. Y., Lau, A., and Poon, R. Y. (2004). How many mutant p53 molecules are needed to inactivate a tetramer? *Mol. Cell Biol.* **24**(8), 3536-3551.

Chen, J., and Shaikh, Z. A. (2009). Activation of Nrf2 by cadmium and its role in protection against cadmium-induced apoptosis in rat kidney cells. *Toxicol. Appl. Pharmacol.* **241**(1), 81-89.

Chen, T. H., Pan, S. L., Guh, J. H., Chen, C. C., Huang, Y. T., Pai, H. C., and Teng, C. M. (2008). Denbinobin induces apoptosis by apoptosis-inducing factor releasing and DNA damage in human colorectal cancer HCT-116 cells. *N-S Arch. Pharmacol.* **378**(5), 447-457.

Chen, W., Jiang, T., Wang, H., Tao, S., Lau, A., Fang, D., and Zhang, D. D. (2012). Does Nrf2 contribute to p53-mediated control of cell survival and death? *Antioxid. Redox. Signal.* **17**(12), 1670-1675.

Chen, Y., and Maret, W. (2001). Catalytic oxidation of zinc/sulfur coordination sites in proteins by selenium compounds. *Antioxid. Redox. Signal.* **3**(4), 651-656.

Clark, L. C., Combs, G. F., Jr., Turnbull, B. W., Slate, E. H., Chalker, D. K., Chow, J., Davis, L. S., Glover, R. A., Graham, G. F., Gross, E. G., Krongrad, A., Lesher, J. L., Jr., Park, H. K., Sanders, B. B., Jr., Smith, C. L., and Taylor, J. R. (1996). Effects of selenium supplementation for cancer prevention in patients with carcinoma of the skin. A randomized controlled trial. Nutritional Prevention of Cancer Study Group. *JAMA* **276**(24), 1957-1963.

Conrad, M., and Sato, H. (2012). The oxidative stress-inducible cystine/glutamate antiporter, system x (c) (-) : cystine supplier and beyond. *Amino. Acids* **42**(1), 231-246.

CONTAM (2009). Scientific opinon of the panel on contaminants in the food chan in a request from the European Commission on cadmium in food. *EFSA J*(980), 1-139.

CONTAM (2011). Scientific Opinion on tolerable weekly intake for cadmium. *EFSA J* **9**(2), 1975.

Coyle, P., Philcox, J. C., Carey, L. C., and Rofe, A. M. (2002). Metallothionein: The multipurpose protein. *Cell Mol. Life Sci.* **59**(4), 627-647.

Cuypers, A., Plusquin, M., Remans, T., Jozefczak, M., Keunen, E., Gielen, H., Opdenakker, K., Nair, A. R., Munters, E., Artois, T. J., Nawrot, T., Vangronsveld, J., and Smeets, K. (2010). Cadmium stress: an oxidative challenge. *Biometals* **23**(5), 927-940.

Daugas, E., Susin, S. A., Zamzami, N., Ferri, K. F., Irinopoulou, T., Larochette, N., Prevost, M. C., Leber, B., Andrews, D., Penninger, J., and Kroemer, G. (2000). Mitochondrio-nuclear translocation of AIF in apoptosis and necrosis. *FASEB J.* **14**(5), 729-739.

Dauplais, M., Lazard, M., Blanquet, S., and Plateau, P. (2013). Neutralization by Metal Ions of the Toxicity of Sodium Selenide. *Plos One* **8**(1).

Davis, R. L., and Spallholz, J. E. (1996). Inhibition of selenite-catalyzed superoxide generation and formation of elemental selenium (Se degrees) by copper, zinc, and aurintricarboxylic acid (ATA). *Biochem. Pharmacol.* **51**(8), 1015-1020.

Delalande, O., Desvaux, H., Godat, E., Valleix, A., Junot, C., Labarre, J., and Boulard, Y. (2010). Cadmium-glutathione solution structures provide new insights into heavy metal detoxification. *FEBS J.* **277**(24), 5086-5096.

Deneke, S. M., and Fanburg, B. L. (1989). Regulation of Cellular Glutathione. *Am J Physiol.* **257**(4), L163-L173.

Dennert, G., Zwahlen, M., Brinkman, M., Vinceti, M., Zeegers, M. P., and Horneber, M. (2011). Selenium for preventing cancer. *Cochrane. Database. Syst. Rev.* **5**, CD005195.

Drake, E. N. (2006). Cancer chemoprevention: selenium as a prooxidant, not an antioxidant. *Med. Hypotheses* **67**(2), 318-322.

Du, T., Ciccotosto, G. D., Cranston, G. A., Kocak, G., Masters, C. L., Crouch, P. J., Cappai, R., and White, A. R. (2008). Neurotoxicity from glutathione depletion is mediated by Cu-dependent p53 activation. *Free Radic. Biol. Med.* **44**(1), 44-55.

Dumont, E., De Pauw, L., Vanhaecke, F., and Cornelis, R. (2006). Speciation of Se in Bertholletia excelsa (Brazil nut): A hard nut to crack? *Food Chem.* **95**(4), 684-692.

Duntas, L. H. (2009). Selenium and inflammation: underlying anti-inflammatory mechanisms. *Horm. Metab Res.* **41**(6), 443-447.

Eneman, J. D., Potts, R. J., Osier, M., Shukla, G. S., Lee, C. H., Chiu, J. F., and Hart, B. A. (2000). Suppressed oxidant-induced apoptosis in cadmium adapted alveolar epithelial cells and its potential involvement in cadmium carcinogenesis. *Toxicology* **147**(3), 215-228.

Ercegovac, M., Jovic, N., Simic, T., Beslac-Bumbasirevic, L., Sokic, D., Djukic, T., Savic-Radojevic, A., Matic, M., Mimic-Oka, J., and Pljesa-Ercegovac, M. (2010). Byproducts of protein, lipid and DNA oxidative damage and antioxidant enzyme activities in seizure. *Seizure.* **19**(4), 205-210.

Fairweather-Tait, S. J., Bao, Y., Broadley, M. R., Collings, R., Ford, D., Hesketh, J. E., and Hurst, R. (2011). Selenium in human health and disease. *Antioxid. Redox. Signal.* **14**(7), 1337-1383.

Fairweather-Tait, S. J., Collings, R., and Hurst, R. (2010). Selenium bioavailability: current knowledge and future research requirements. *Am. J. Clin. Nutr.* **91**(5), 1484S-1491S.

Fan, T. J., Han, L. H., Cong, R. S., and Liang, J. (2005). Caspase family proteases and apoptosis. *Acta Biochim. Biophys. Sin. (Shanghai)* **37**(11), 719-727.

FAO/WHO (2010). Joint FAO/WHO Expert Commitee on Food Additives. Seventy-third meeting, Geneva, 8-17 June 2010.Evaluation of certain food additive and contaminants. *World Health Organ Tech. Rep. Ser.*(960), 1-226.

Fatur, T., Lah, T. T., and Filipic, M. (2003). Cadmium inhibits repair of UV-, methyl methanesulfonate- and N-methyl-N-nitrosourea-induced DNA damage in Chinese hamster ovary cells. *Mutat. Res.* **529**(1-2), 109-116.

Filipic, M., and Hei, T. K. (2004). Mutagenicity of cadmium in mammalian cells: implication of oxidative DNA damage. *Mutat. Res.* **546**(1-2), 81-91.

Finley, J. W. (2006). Bioavailability of selenium from foods. *Nutr. Rev.* **64**(3), 146-151.

Flanagan, P. R., McLellan, J. S., Haist, J., Cherian, G., Chamberlain, M. J., and Valberg, L. S. (1978). Increased dietary cadmium absorption in mice and human subjects with iron deficiency. *Gastroenterology* **74**(5 Pt 1), 841-846.

Fujioka, S., Schmidt, C., Sclabas, G. M., Li, Z. K., Pelicano, H., Peng, B., Yao, A., Niu, J. G., Zhang, W., Evans, D. B., Abbruzzese, J. L., Huang, P., and Chiao, P. J. (2004). Stabilization of p53 is a novel mechanism for proapoptotic function of NF-kappa B. *J. Biol. Chem.* **279**(26), 27549-27559.

Furukawa, M., and Xiong, Y. (2005). BTB protein Keap1 targets antioxidant transcription factor Nrf2 for ubiquitination by the Cullin 3-Roc1 ligase. *Mol. Cell Biol.* **25**(1), 162-171.

Ganyc, D., and Self, W. T. (2008). High affinity selenium uptake in a keratinocyte model. *FEBS Lett.* **582**(2), 299-304.

Giaginis, C., Gatzidou, E., and Theocharis, S. (2006). DNA repair systems as targets of cadmium toxicity. *Toxicol. Appl. Pharmacol.* **213**(3), 282-290.

Goel, A., Fuerst, F., Hotchkiss, E., and Boland, C. R. (2006). Selenomethionine induces p53 mediated cell cycle arrest and apoptosis in human colon cancer cells. *Cancer Biol. Ther.* **5**(5), 529-535.

Goel, R., and Khanduja, K. L. (1998). Oxidative stress-induced apoptosis - An overview. *Curr Sci. India* **75**(12), 1338-1345.

Golias, C. H., Charalabopoulos, A., and Charalabopoulos, K. (2004). Cell proliferation and cell cycle control: a mini review. *Int. J. Clin. Pract.* **58**(12), 1134-1141.

Gozzelino, R., Jeney, V., and Soares, M. P. (2010). Mechanisms of Cell Protection by Heme Oxygenase-1. *Annu Rev Pharmacol Toxicol* **50**, 323-354.

Greenblatt, M. S., Bennett, W. P., Hollstein, M., and Harris, C. C. (1994). Mutations in the p53 tumor suppressor gene: clues to cancer etiology and molecular pathogenesis. *Cancer Res.* **54**(18), 4855-4878.

Hagenhofer, M., Germaier, H., Hohenadl, C., Rohwer, P., Kalden, J. R., and Herrmann, M. (1998). UV-B irradiated cell lines execute programmed cell death in various forms. *Apoptosis.* **3**(2), 123-132.

Haglund, K., and Dikic, I. (2005). Ubiquitylation and cell signaling. *Embo J* **24**(19), 3353-3359.

Hainaut, P., and Mann, K. (2001). Zinc binding and redox control of p53 structure and function. *Antioxid. Redox. Signal.* **3**(4), 611-623.

Hainaut, P., and Milner, J. (1993). Redox modulation of p53 conformation and sequence-specific DNA binding in vitro. *Cancer Res.* **53**(19), 4469-4473.

Hall, C. (2008). Untersuchungen zur direkten und indirekten Genotoxizität von Natriumselenit und Selenomethionin. Dissertation. Department of Food Technology and Chemistry, Technical University Berlin.

Halliwell, B. (2006). Reactive species and antioxidants. Redox biology is a fundamental theme of aerobic life. *Plant Physiol* **141**(2), 312-322.

Halliwell, B., and Aruoma, O. I. (1991). Dna Damage by Oxygen-Derived Species - Its Mechanism and Measurement in Mammalian Systems. *FEBS Letters* **281**(1-2), 9-19.

Halliwell, B., and Gutteridge, J. M. C. (1990). Role of Free-Radicals and Catalytic Metal-Ions in Human-Disease - An Overview. *Methods Enzymol.* **186**, 1-85.

Harbour, J. W., and Dean, D. C. (2000). The Rb/E2F pathway: expanding roles and emerging paradigms. *Gene Dev* **14**(19), 2393-2409.

Harper, J. V., and Brooks, G. (2005). The mammalian cell cycle: an overview. *Method Mol Biol* **296**, 113-153.

Harris, S. L., and Levine, A. J. (2005). The p53 pathway: positive and negative feedback loops. *Oncogene* **24**(17), 2899-2908.

Hartwig, A. (2001). Zinc finger proteins as potential targets for toxic metal ions: differential effects on structure and function. *Antioxid. Redox. Signal.* **3**(4), 625-634.

Hartwig, A. (2010). Mechanisms in cadmium-induced carcinogenicity: recent insights. *Biometals* **23**(5), 951-960.

Hartwig, A. (2013). Metal interaction with redox regulation: an integrating concept in metal carcinogenesis? *Free Radic. Biol. Med.* **55**, 63-72.

Hikisz, P., and Kilianska, Z. M. (2012). Puma, a critical mediator of cell death - one decade on from its discovery. *Cell Mol Biol Lett* **17**(4), 646-669.

Hoffmann, P. R., and Berry, M. J. (2008). The influence of selenium on immune responses. *Mol. Nutr. Food Res.* **52**(11), 1273-1280.

Hu, H., Jiang, C., Schuster, T., Li, G. X., Daniel, P. T., and Lu, J. (2006). Inorganic selenium sensitizes prostate cancer cells to TRAIL-induced apoptosis through superoxide/p53/Bax-mediated activation of mitochondrial pathway. *Mol. Cancer Ther.* **5**(7), 1873-1882.

Huang, H. C., Nguyen, T., and Pickett, C. B. (2000). Regulation of the antioxidant response element by protein kinase C-mediated phosphorylation of NF-E2-related factor 2. *Proc. Natl. Acad. Sci. U. S. A* **97**(23), 12475-12480.

Huerta, S., Goulet, E. J., Huerta-Yepez, S., and Livingston, E. H. (2007). Screening and detection of apoptosis. *J. Surg. Res.* **139**(1), 143-156.

IARC. (1993). Beryllium, cadmium, mercury, and exposures in the glass manufacturing industry IARC monographs on the evaluation of carcinogenic risks to humans. 58, 119-237. Lyon, France, World Health Organisation.

Ikediobi, C. O., Badisa, V. L., Ayuk-Takem, L. T., Latinwo, L. M., and West, J. (2004). Response of antioxidant enzymes and redox metabolites to cadmium-induced oxidative stress in CRL-1439 normal rat liver cells. *Int. J. Mol. Med.* **14**(1), 87-92.

Iliakis, G., Wang, Y., Guan, J., and Wang, H. (2003). DNA damage checkpoint control in cells exposed to ionizing radiation. *Oncogene* **22**(37), 5834-5847.

Jackson, M. I., and Combs, G. F., Jr. (2008). Selenium and anticarcinogenesis: underlying mechanisms. *Curr. Opin. Clin. Nutr. Metab Care* **11**(6), 718-726.

Jacob, C., Giles, G. I., Giles, N. M., and Sies, H. (2003). Sulfur and selenium: the role of oxidation state in protein structure and function. *Angew. Chem. Int. Ed Engl.* **42**(39), 4742-4758.

Jiang, C., Hu, H., Malewicz, B., Wang, Z., and Lu, J. (2004). Selenite-induced p53 Ser-15 phosphorylation and caspase-mediated apoptosis in LNCaP human prostate cancer cells. *Mol. Cancer Ther.* **3**(7), 877-884.

Jiang, C., Wang, Z., Ganther, H., and Lu, J. (2002). Distinct effects of methylseleninic acid versus selenite on apoptosis, cell cycle, and protein kinase pathways in DU145 human prostate cancer cells. *Mol. Cancer Ther.* **1**(12), 1059-1066.

Johnson, C. C., Fordyce, F. M., and Rayman, M. P. (2010). Symposium on 'Geographical and geological influences on nutrition': Factors controlling the distribution of selenium in the environment and their impact on health and nutrition. *Proc. Nutr. Soc.* **69**(1), 119-132.

Joseph, P. (2009). Mechanisms of cadmium carcinogenesis. *Toxicol. Appl. Pharmacol.* **238**(3), 272-279.

Joseph, P., Muchnok, T. K., Klishis, M. L., Roberts, J. R., Antonini, J. M., Whong, W. Z., and Ong, T. (2001). Cadmium-induced cell transformation and tumorigenesis are associated with transcriptional activation of c-fos, c-jun, and c-myc proto-oncogenes: role of cellular calcium and reactive oxygen species. *Toxicol. Sci.* **61**(2), 295-303.

Kansanen, E., Jyrkkanen, H. K., and Levonen, A. L. (2012). Activation of stress signaling pathways by electrophilic oxidized and nitrated lipids. *Free Radic. Biol. Med.* **52**(6), 973-982.

Karlsson, H. J., Lincoln, P., and Westman, G. (2003). Synthesis and DNA binding studies of a new asymmetric cyanine dye binding in the minor groove of [poly(dA-dT)](2). *Bioorgan Med Chem* **11**(6), 1035-1040.

Keum, Y. S., Owuor, E. D., Kim, B. R., Hu, R., and Kong, A. N. T. (2003). Involvement of Nrf2 and JNK1 in the activation of antioxidant responsive element (ARE) by chemopreventive agent phenethyl isothiocyanate (PEITC). *Pharmaceut Res* **20**(9), 1351-1356.

Kim, D. H., Kundu, J. K., and Surh, Y. J. (2011). Redox Modulation of p53: Mechanisms and Functional Significance. *Mol. Carcinog.* **50**(4), 222-234.

Kim, T., Jung, U., Cho, D. Y., and Chung, A. S. (2001). Se-methylselenocysteine induces apoptosis through caspase activation in HL-60 cells. *Carcinogenesis* **22**(4), 559-565.

Klaus, V. (2009). Die Rolle von p53 in der zelluläre Antwort auf Natriumselenit und Selenomethionin. Dissertation. Department of Food Technology and Chemistry, Technical Unviersity Berlin.

Klein, E. A., Thompson, I. M., Jr., Tangen, C. M., Crowley, J. J., Lucia, M. S., Goodman, P. J., Minasian, L. M., Ford, L. G., Parnes, H. L., Gaziano, J. M., Karp, D. D., Lieber, M. M., Walther, P. J., Klotz, L., Parsons, J. K., Chin, J. L., Darke, A. K., Lippman, S. M., Goodman, G. E., Meyskens, F. L., Jr., and Baker, L. H. (2011). Vitamin E and the risk of prostate cancer: the Selenium and Vitamin E Cancer Prevention Trial (SELECT). *JAMA* **306**(14), 1549-1556.

Koizumi, S., Gong, P., Suzuki, K., and Murata, M. (2007). Cadmium-responsive element of the human heme oxygenase-1 gene mediates heat shock factor 1-dependent transcriptional activation. *J. Biol. Chem.* **282**(12), 8715-8723.

Koizumi, S., Suzuki, K., and Otsuka, F. (1992). A nuclear factor that recognizes the metal-responsive elements of human metallothionein IIA gene. *J. Biol. Chem.* **267**(26), 18659-18664.

Komissarova, E. V., Saha, S. K., and Rossman, T. G. (2005). Dead or dying: the importance of time in cytotoxicity assays using arsenite as an example. *Toxicol. Appl. Pharmacol.* **202**(1), 99-107.

Kralova, V., Brigulova, K., Cervinka, M., and Rudolf, E. (2009). Antiproliferative and cytotoxic effects of sodium selenite in human colon cancer cells. *Toxicol. In Vitro* **23**(8), 1497-1503.

Kramer, G. F., and Ames, B. N. (1988). Mechanisms of mutagenicity and toxicity of sodium selenite (Na2SeO3) in Salmonella typhimurium. *Mutat. Res.* **201**(1), 169-180.

Kubista, M., Akerman, B., and Norden, B. (1987). Characterization of Interaction Between Dna and 4',6-Diamidino-2-Phenylindole by Optical Spectroscopy. *Biochemistry* **26**(14), 4545-4553.

Lane, D. P. (1992). Cancer - P53, Guardian of the Genome. *Nature* **358**(6381), 15-16.

Langie, S. A. S., Knaapen, A. M., Houben, J. M. J., van Kempen, F. C., de Hoon, J. P. J., Gottschalk, R. W. H., Godschalk, R. W. L., and van Schooten, F. J. (2007). The role of glutathione in the regulation of nucleotide excision repair during oxidative stress. *Toxicol. Lett.* **168**(3), 302-309.

Lee, O. H., Jain, A. K., Papusha, V., and Jaiswal, A. K. (2007). An auto-regulatory loop between stress sensors INrf2 and Nrf2 controls their cellular abundance. *J Biol Chem* **282**(50), 36412-36420.

Letavayova, L., Vlckova, V., and Brozmanova, J. (2006). Selenium: from cancer prevention to DNA damage. *Toxicology* **227**(1-2), 1-14.

Li, D. W. C., Liu, J. P., Schmid, P. C., Schlosser, R., Feng, H., Liu, W. B., Yan, Q., Gong, L., Sun, S. M., Deng, M., and Liu, Y. (2006). Protein serine/threonine phosphatase-1 dephosphorylates p53 at Ser-15 and Ser-37 to modulate its transcriptional and apoptotic activities. *Oncogene* **25**(21), 3006-3022.

Li, G. X., Hu, H., Jiang, C., Schuster, T., and Lu, J. (2007). Differential involvement of reactive oxygen species in apoptosis induced by two classes of selenium compounds in human prostate cancer cells. *Int. J. Cancer* **120**(9), 2034-2043.

Li, H. F., McGrath, S. P., and Zhao, F. J. (2008). Selenium uptake, translocation and speciation in wheat supplied with selenate or selenite. *New Phytol.* **178**(1), 92-102.

Li, Y., and Schellhorn, H. E. (2007). Rapid kinetic microassay for catalase activity. *J. Biomol. Tech.* **18**(4), 185-187.

Lippman, S. M., Klein, E. A., Goodman, P. J., Lucia, M. S., Thompson, I. M., Ford, L. G., Parnes, H. L., Minasian, L. M., Gaziano, J. M., Hartline, J. A., Parsons, J. K., Bearden, J. D., III, Crawford, E. D., Goodman, G. E., Claudio, J., Winquist, E., Cook, E. D., Karp, D. D., Walther, P., Lieber, M. M., Kristal, A. R., Darke, A. K., Arnold, K. B., Ganz, P. A., Santella, R. M., Albanes, D., Taylor, P. R., Probstfield, J. L., Jagpal, T. J., Crowley, J. J., Meyskens, F. L., Jr., Baker, L. H., and Coltman, C. A., Jr. (2009). Effect of selenium and vitamin E on risk of prostate cancer and other cancers: the Selenium and Vitamin E Cancer Prevention Trial (SELECT). *JAMA* **301**(1), 39-51.

Liu, B., Chen, Y. M., and Clair, D. K. S. (2008). ROS and p53: A versatile partnership. *Free Radic. Biol. Med.* **44**(8), 1529-1535.

Lopez, E., Arce, C., Oset-Gasque, M. J., Canadas, S., and Gonzalez, M. P. (2006). Cadmium induces reactive oxygen species generation and lipid peroxidation in cortical neurons in culture. *Free Radic. Biol. Med.* **40**(6), 940-951.

Lu, J., and Holmgren, A. (2009). Selenoproteins. *J. Biol. Chem.* **284**(2), 723-727.

Lu, J., Jiang, C., Kaeck, M., Ganther, H., Vadhanavikit, S., Ip, C., and Thompson, H. (1995). Dissociation of the genotoxic and growth inhibitory effects of selenium. *Biochem. Pharmacol.* **50**(2), 213-219.

Lu, J., Kaeck, M., Jiang, C., Wilson, A. C., and Thompson, H. J. (1994). Selenite induction of DNA strand breaks and apoptosis in mouse leukemic L1210 cells. *Biochem. Pharmacol.* **47**(9), 1531-1535.

MacFarquhar, J. K., Broussard, D. L., Melstrom, P., Hutchinson, R., Wolkin, A., Martin, C., Burk, R. F., Dunn, J. R., Green, A. L., Hammond, R., Schaffner, W., and Jones, T. F. (2010). Acute selenium toxicity associated with a dietary supplement. *Arch. Intern. Med.* **170**(3), 256-261.

Malumbres, M., and Barbacid, M. (2009). Cell cycle, CDKs and cancer: a changing paradigm. *Nat. Rev. Cancer* **9**(3), 153-166.

Maret, W. (2003). Cellular zinc and redox states converge in the metallothionein/thionein pair. *J. Nutr.* **133**(5 Suppl 1), 1460S-1462S.

Martin, A. C., Facchiano, A. M., Cuff, A. L., Hernandez-Boussard, T., Olivier, M., Hainaut, P., and Thornton, J. M. (2002). Integrating mutation data and structural analysis of the TP53 tumor-suppressor protein. *Hum. Mutat.* **19**(2), 149-164.

Meplan, C., Mann, K., and Hainaut, P. (1999). Cadmium induces conformational modifications of wild-type p53 and suppresses p53 response to DNA damage in cultured cells. *J. Biol. Chem.* **274**(44), 31663-31670.

Meplan, C., Richard, M. J., and Hainaut, P. (2000). Redox signalling and transition metals in the control of the p53 pathway. *Biochem. Pharmacol.* **59**(1), 25-33.

Meuillet, E., Stratton, S., Prasad, C. D., Goulet, A. C., Kagey, J., Porterfield, B., and Nelson, M. A. (2004). Chemoprevention of prostate cancer with selenium: an update on current clinical trials and preclinical findings. *J. Cell Biochem.* **91**(3), 443-458.

Meves, A., Stock, S. N., Beyerle, A., Pittelkow, M. R., and Peus, D. (2001). H2O2 mediates oxidative stress-induced epidermal growth factor receptor phosphorylation. *Toxicol. Lett.* **122**(3), 205-214.

Michiels, C., and Remacle, J. (1988). Use of the inhibition of enzymatic antioxidant systems in order to evaluate their physiological importance. *Eur. J. Biochem.* **177**(2), 435-441.

Mitsuishi, Y., Motohashi, H., and Yamamoto, M. (2012). The Keap1-Nrf2 system in cancers: stress response and anabolic metabolism. *Front Oncol.* **2**, 200.

Mohamad, N., Gutierrez, A., Nunez, M., Cocca, C., Martin, G., Cricco, G., Medina, V., Rivera, E., and Bergoc, R. (2005). Mitochondrial apoptotic pathways. *Biocell* **29**(2), 149-161.

Muecke, R., Schomburg, L., Buentzel, J., Kisters, K., and Micke, O. (2010). Selenium or no selenium--that is the question in tumor patients: a new controversy. *Integr. Cancer Ther.* **9**(2), 136-141.

Muller, M., Banning, A., Brigelius-Flohe, R., and Kipp, A. (2010). Nrf2 target genes are induced under marginal selenium-deficiency. *Genes Nutr.* **5**(4), 297-307.

Munoz, L. E., Maueroder, C., Chaurio, R., Berens, C., Herrmann, M., and Janko, C. (2013). Colourful death: six-parameter classification of cell death by flow cytometry--dead cells tell tales. *Autoimmunity* **46**(5), 336-341.

Nawrot, T. S., Staessen, J. A., Roels, H. A., Munters, E., Cuypers, A., Richart, T., Ruttens, A., Smeets, K., Clijsters, H., and Vangronsveld, J. (2010). Cadmium exposure in the population: from health risks to strategies of prevention. *Biometals* **23**(5), 769-782.

Nelson, W. G., and Kastan, M. B. (1994). DNA strand breaks: the DNA template alterations that trigger p53-dependent DNA damage response pathways. *Mol. Cell Biol.* **14**(3), 1815-1823.

Neumann, D. (2014). Untersuchungen zum Einfluss von Glucosinolat-Hydrolyseprodukten auf die Genexpression in HCT 116-Zellen mittels *high-throughput* RT-qPCR. Disseration. Department of Food Chemistry and Toxicology, Karlsruhe Institute of Technology.

Nickel, A., Kottra, G., Schmidt, G., Danier, J., Hofmann, T., and Daniel, H. (2009). Characteristics of transport of selenoamino acids by epithelial amino acid transporters. *Chem. Biol. Interact.* **177**(3), 234-241.

Niida, H., and Nakanishi, M. (2006). DNA damage checkpoints in mammals. *Mutagenesis* **21**(1), 3-9.

Nilsonne, G., Sun, X., Nystrom, C., Rundlof, A. K., Fernandes, A. P., Bjornstedt, M., and Dobra, K. (2006). Selenite induces apoptosis in sarcomatoid malignant mesothelioma cells through oxidative stress. *Free Radic. Biol. Med.* **41**(6), 874-885.

Nishitai, G., and Matsuoka, M. (2008). Differential regulation of HSP70 expression by the JNK kinases SEK1 and MKK7 in mouse embryonic stem cells treated with cadmium. *J. Cell Biochem.* **104**(5), 1771-1780.

Norberg, E., Karlsson, M., Korenovska, O., Szydlowski, S., Silberberg, G., Uhlen, P., Orrenius, S., and Zhivotovsky, B. (2010). Critical role for hyperpolarization-activated cyclic nucleotide-gated channel 2 in the AIF-mediated apoptosis. *EMBO J.* **29**(22), 3869-3878.

Ogasawara, Y., Takeda, Y., Takayama, H., Nishimoto, S., Ichikawa, K., Ueki, M., Suzuki, T., and Ishii, K. (2014). Significance of the rapid increase in GSH levels in the protective response to cadmium exposure through phosphorylated Nrf2 signaling in Jurkat T-cells. *Free Radic. Biol. Med.* **69**, 58-66.

Olm, E., Fernandes, A. P., Hebert, C., Rundlof, A. K., Larsen, E. H., Danielsson, O., and Bjornstedt, M. (2009). Extracellular thiol-assisted selenium uptake dependent on the x(c)- cystine transporter explains the cancer-specific cytotoxicity of selenite. *Proc. Natl. Acad. Sci. U. S. A* **106**(27), 11400-11405.

Oropesa-Avila, M., Andrade-Talavera, Y., Garrido-Maraver, J., Cordero, M., de la Mata, M., Cotan, D., Paz, M., V, Pavon, A., Alcocer-Gomez, E., de lavera, I., Lema, R., Zaderenko, A., Rodriguez-Moreno, A., and Sanchez-Alcazar, J. (2014). Stabilization of apoptotic cells: generation of zombie cells. *Cell Death & Disease* **5**.

Oswald, F., Lovec, H., Moroy, T., and Lipp, M. (1994). E2F-Dependent Regulation of Human Myc - Transactivation by Cyclin-D1 and Cyclin-A Overrides Tumor-Suppressor Protein Functions. *Oncogene* **9**(7), 2029-2036.

Ott, D. (2014). Etablierung einer Reportergen-Zelllinie zur Untersuchung des Keap1/Nrf2 Systems. Diploma Thesis. Department of Food Chemistry and Toxicology, Karlsruhe Institute of Technology.

Park, S. H., Kim, J. H., Chi, G. Y., Kim, G. Y., Chang, Y. C., Moon, S. K., Nam, S. W., Kim, W. J., Yoo, Y. H., and Choi, Y. H. (2012). Induction of apoptosis and autophagy by sodium selenite in A549 human lung carcinoma cells through generation of reactive oxygen species. *Toxicol. Lett.* **212**(3), 252-261.

Peskin, A. V., and Winterbourn, C. C. (2000). A microtiter plate assay for superoxide dismutase using a water-soluble tetrazolium salt (WST-1). *Clin. Chim. Acta* **293**(1-2), 157-166.

Pflaum, M., Boiteux, S., and Epe, B. (1994). Visible-Light Generates Oxidative Dna-Base Modifications in High Excess of Strand Breaks in Mammalian-Cells. *Carcinogenesis* **15**(2), 297-300.

Pinot, F., Kreps, S. E., Bachelet, M., Hainaut, P., Bakonyi, M., and Polla, B. S. (2000). Cadmium in the environment: sources, mechanisms of biotoxicity, and biomarkers. *Rev. Environ. Health* **15**(3), 299-323.

Ploner, C., Kofler, R., and Villunger, A. (2008). Noxa: at the tip of the balance between life and death. *Oncogene* **27**, S84-S92.

Price, D. J., and Joshi, J. G. (1983). Ferritin. Binding of beryllium and other divalent metal ions. *J. Biol. Chem.* **258**(18), 10873-10880.

Pryor, W. A. (1986). Oxyradicals and Related Species - Their Formation, Lifetimes, and Reactions. *Annu Rev Physiol* **48**, 657-667.

Qu, W., Diwan, B. A., Reece, J. M., Bortner, C. D., Pi, J., Liu, J., and Waalkes, M. P. (2005). Cadmium-induced malignant transformation in rat liver cells: role of aberrant oncogene expression and minimal role of oxidative stress. *Int. J. Cancer* **114**(3), 346-355.

Rahman, I., Gilmour, P. S., Jimenez, L. A., and MacNee, W. (2002). Oxidative stress and TNF-alpha induce histone acetylation and NF-kappa B/AP-1 activation in alveolar epithelial cells: Potential mechanism in gene transcription in lung inflammation. *Mol. Cell Biochem.* **234**(1), 239-248.

Rahman, Q., Abidi, P., Afaq, F., Schiffmnn, D., Mossman, B. T., Kamp, D. W., and Athar, M. (1999). Glutathione redox system in oxidative lung injury. *Crit Rev. Toxicol.* **29**(6), 543-568.

Ramoutar, R. R., and Brumaghim, J. L. (2010). Antioxidant and anticancer properties and mechanisms of inorganic selenium, oxo-sulfur, and oxo-selenium compounds. *Cell Biochem. Biophys.* **58**(1), 1-23.

Rana, S. V. (2008). Metals and apoptosis: recent developments. *J. Trace Elem. Med. Biol.* **22**(4), 262-284.

Rayman, M. P. (2000). The importance of selenium to human health. *Lancet* **356**(9225), 233-241.

Rayman, M. P. (2012). Selenium and human health. *Lancet* **379**(9822), 1256-1268.

Rayman, M. P., and Stranges, S. (2013). Epidemiology of selenium and type 2 diabetes: can we make sense of it? *Free Radic. Biol. Med.* **65**, 1557-1564.

Robles, A. I., Bemmels, N. A., Foraker, A. B., and Harris, C. C. (2001). APAF-1 is a transcriptional target of p53 in DNA damage-induced apoptosis. *Cancer Res.* **61**(18), 6660-6664.

Roman, M., Jitaru, P., and Barbante, C. (2014). Selenium biochemistry and its role for human health. *Metallomics.* **6**(1), 25-54.

Roos, W. P., and Kaina, B. (2006). DNA damage-induced cell death by apoptosis. *Trends Mol. Med.* **12**(9), 440-450.

Rudolf, E., Rudolf, K., and Cervinka, M. (2008). Selenium activates p53 and p38 pathways and induces caspase-independent cell death in cervical cancer cells. *Cell Biol. Toxicol.* **24**(2), 123-141.

Sabolic, I. s. h., Breljak, D., Herak-Kramberger, C. M., Ljubojevic, M., and Thevenod, F. (2008). Expression of multidrug resistance P-glycoprotein Mdr1 (Abcb1) in rat kidney proximal tubules is up-regulated by nephrotoxic metals. *Metal Ions Biol Med*, 315-321.

Sasaki, H., Sato, H., Kuriyama-Matsumura, K., Sato, K., Maebara, K., Wang, H., Tamba, M., Itoh, K., Yamamoto, M., and Bannai, S. (2002). Electrophile response element-mediated induction of the cystine/glutamate exchange transporter gene expression. *J. Biol. Chem.* **277**(47), 44765-44771.

Satarug, S., Baker, J. R., Urbenjapol, S., Haswell-Elkins, M., Reilly, P. E., Williams, D. J., and Moore, M. R. (2003). A global perspective on cadmium pollution and toxicity in non-occupationally exposed population. *Toxicol. Lett.* **137**(1-2), 65-83.

Scherer, G., and Barkemeyer, H. (1983). Cadmium concentrations in tobacco and tobacco smoke. *Ecotoxicol. Environ. Saf* **7**(1), 71-78.

Schrauzer, G. N. (2001). Nutritional selenium supplements: product types, quality, and safety. *J. Am. Coll. Nutr.* **20**(1), 1-4.

Schroterova, L., Kralova, V., Voracova, A., Haskova, P., Rudolf, E., and Cervinka, M. (2009). Antiproliferative effects of selenium compounds in colon cancer cells: comparison of different cytotoxicity assays. *Toxicol. In Vitro* **23**(7), 1406-1411.

Schwerdtle, T., Ebert, F., Thuy, C., Richter, C., Mullenders, L. H., and Hartwig, A. (2010). Genotoxicity of soluble and particulate cadmium compounds: impact on oxidative DNA damage and nucleotide excision repair. *Chem. Res. Toxicol.* **23**(2), 432-442.

Seefeldt, T., Zhao, Y., Chen, W., Raza, A. S., Carlson, L., Herman, J., Stoebner, A., Hanson, S., Foll, R., and Guan, X. (2009). Characterization of a novel dithiocarbamate glutathione reductase inhibitor and its use as a tool to modulate intracellular glutathione. *J. Biol. Chem.* **284**(5), 2729-2737.

Sengupta, S., and Harris, C. C. (2005). p53: Traffic cop at the crossroads of DNA repair and recombination. *Nat. Rev. Mol. Cell Biol.* **6**(1), 44-55.

Seo, Y. R., and Jung, H. J. (2004). The potential roles of p53 tumor suppressor in nucleotide excision repair (NER) and base excision repair (BER). *Exp. Mol. Med.* **36**(6), 505-509.

Sharov, V. S., Briviba, K., and Sies, H. (1999). Peroxynitrite diminishes gap junctional communication: protection by selenite supplementation. *IUBMB. Life* **48**(4), 379-384.

Sheikh, M. S., Burns, T. F., Huang, Y., Wu, G. S., Amundson, S., Brooks, K. S., Fornace, A. J., and El-Deiry, W. S. (1998). p53-dependent and -independent regulation of the death receptor KILLER/DR5 gene expression in response to genotoxic stress and tumor necrosis factor alpha. *Cancer Res.* **58**(8), 1593-1598.

Shen, H. M., Yang, C. F., and Ong, C. N. (1999). Sodium selenite-induced oxidative stress and apoptosis in human hepatoma HepG2 cells. *Int. J. Cancer* **81**(5), 820-828.

Shi, Y. G. (2001). A structural view of mitochondria-mediated apoptosis. *Nat Struct Biol* **8**(5), 394-401.

Shiloh, Y. (2001). ATM and ATR: networking cellular responses to DNA damage. *Curr Opin Genet Dev* **11**(1), 71-77.

Shiloh, Y. (2006). The ATM-mediated DNA-damage response: taking shape. *Trends Biochem. Sci.* **31**(7), 402-410.

Slupphaug, G., Kavli, B., and Krokan, H. E. (2003). The interacting pathways for prevention and repair of oxidative DNA damage. *Mutat Res-Fund Mol M* **531**(1-2), 231-251.

Smith, A. D., Guidry, C. A., Morris, V. C., and Levander, O. A. (1999). Aurothioglucose inhibits murine thioredoxin reductase activity in vivo. *J. Nutr.* **129**(1), 194-198.

Smith, A. D., Morris, V. C., and Levander, O. A. (2001). Rapid determination of glutathione peroxidase and thioredoxin reductase activities using a 96-well microplate format: comparison to standard cuvette-based assays. *Int. J. Vitam. Nutr. Res.* **71**(1), 87-92.

Sorg, O., Horn, T. F., Yu, N., Gruol, D. L., and Bloom, F. E. (1997). Inhibition of astrocyte glutamate uptake by reactive oxygen species: role of antioxidant enzymes. *Mol. Med.* **3**(7), 431-440.

Soussi, T. (2000). The p53 tumor suppressor gene: from molecular biology to clinical investigation. *Ann. N. Y. Acad. Sci.* **910**, 121-137.

Steinbrenner, H. (2013). Interference of selenium and selenoproteins with the insulin-regulated carbohydrate and lipid metabolism. *Free Radic. Biol. Med.* **65**, 1538-1547.

Steinbrenner, H., Speckmann, B., Pinto, A., and Sies, H. (2011). High selenium intake and increased diabetes risk: experimental evidence for interplay between selenium and carbohydrate metabolism. *J. Clin. Biochem. Nutr.* **48**(1), 40-45.

Steinbrenner, H., Speckmann, B., and Sies, H. (2013). Toward understanding success and failures in the use of selenium for cancer prevention. *Antioxid. Redox. Signal.* **19**(2), 181-191.

Stevens, C., and La Thangue, N. B. (2004). The emerging role of E2F-1 in the DNA damage response and checkpoint control. *DNA Repair (Amst)* **3**(8-9), 1071-1079.

Stewart, M. S., Davis, R. L., Walsh, L. P., and Pence, B. C. (1997). Induction of differentiation and apoptosis by sodium selenite in human colonic carcinoma cells (HT29). *Cancer Lett.* **117**(1), 35-40.

Stewart, Z. A., and Pietenpol, J. A. (2001). p53 Signaling and cell cycle checkpoints. *Chem. Res. Toxicol.* **14**(3), 243-263.

Stranges, S., Marshall, J. R., Natarajan, R., Donahue, R. P., Trevisan, M., Combs, G. F., Cappuccio, F. P., Ceriello, A., and Reid, M. E. (2007). Effects of long-term selenium supplementation on the incidence of type 2 diabetes: a randomized trial. *Ann. Intern. Med.* **147**(4), 217-223.

Stranges, S., Navas-Acien, A., Rayman, M. P., and Guallar, E. (2010). Selenium status and cardiometabolic health: state of the evidence. *Nutr. Metab Cardiovasc. Dis.* **20**(10), 754-760.

Szuster-Ciesielska, A., Stachura, A., Slotwinska, M., Kaminska, T., Sniezko, R., Paduch, R., Abramczyk, D., Filar, J., and Kandefer-Szerszen, M. (2000). The inhibitory effect of zinc on cadmium-induced cell apoptosis and reactive oxygen species (ROS) production in cell cultures. *Toxicology* **145**(2-3), 159-171.

Tarze, A., Dauplais, M., Grigoras, I., Lazard, M., Ha-Duong, N. T., Barbier, F., Blanquet, S., and Plateau, P. (2007). Extracellular production of hydrogen selenide accounts for thiol-assisted toxicity of selenite against Saccharomyces cerevisiae. *J. Biol. Chem.* **282**(12), 8759-8767.

Thevenod, F. (2009). Cadmium and cellular signaling cascades: to be or not to be? *Toxicol. Appl. Pharmacol.* **238**(3), 221-239.

Thomson, C. D., Chisholm, A., McLachlan, S. K., and Campbell, J. M. (2008). Brazil nuts: an effective way to improve selenium status. *Am. J. Clin. Nutr.* **87**(2), 379-384.

Tietze, F. (1969). Enzymic Method for Quantitative Determination of Nanogram Amounts of Total and Oxidized Glutathione - Applications to Mammalian Blood and Other Tissues. *Anal. Biochem.* **27**(3), 502-&.

Vahter, M., Berglund, M., Nermell, B., and Akesson, A. (1996). Bioavailability of cadmium from shellfish and mixed diet in women. *Toxicol. Appl. Pharmacol.* **136**(2), 332-341.

Valbonesi, P., Ricci, L., Franzellitti, S., Biondi, C., and Fabbri, E. (2008). Effects of cadmium on MAPK signalling pathways and HSP70 expression in a human trophoblast cell line. *Placenta* **29**(8), 725-733.

Vinceti, M., Crespi, C. M., Malagoli, C., Del Giovane, C., and Krogh, V. (2013). Friend or Foe? The Current Epidemiologic Evidence on Selenium and Human Cancer Risk. *J Environ Sci Heal C* **31**(4), 305-341.

Vinceti, M., Dennert, G., Crespi, C. M., Zwahlen, M., Brinkman, M., Zeegers, M. P., Horneber, M., D'Amico, R., and Del, G. C. (2014). Selenium for preventing cancer. *Cochrane. Database. Syst. Rev.* **3**, CD005195.

Vousden, K. H., and Lu, X. (2002). Live or let die: The cell's response to p53. *Nat. Rev. Cancer* **2**(8), 594-604.

Waalkes, M. P. (2003). Cadmium carcinogenesis. *Mut Res-Fund Mol M* **533**(1-2), 107-120.

Waga, S., Hannon, G. J., Beach, D., and Stillman, B. (1994). The P21 Inhibitor of Cyclin-Dependent Kinases Controls Dna-Replication by Interaction with Pcna. *Nature* **369**(6481), 574-578.

Wang, H. T., Yang, X. L., Zhang, Z. H., Lu, J. L., and Xu, H. B. (2002). Reactive oxygen species from mitochondria mediate SW480 cells apoptosis induced by Na2SeO3. *Biol. Trace Elem. Res.* **85**(3), 241-254.

Wang, X. (2001). The expanding role of mitochondria in apoptosis. *Genes Dev.* **15**(22), 2922-2933.

Wang, Y., Fang, J., Leonard, S. S., and Rao, K. M. (2004). Cadmium inhibits the electron transfer chain and induces reactive oxygen species. *Free Radic. Biol. Med.* **36**(11), 1434-1443.

Watanabe, M., Henmi, K., Ogawa, K., and Suzuki, T. (2003). Cadmium-dependent generation of reactive oxygen species and mitochondrial DNA breaks in photosynthetic and non-photosynthetic strains of Euglena gracilis. *Comp Biochem. Physiol C. Toxicol. Pharmacol.* **134**(2), 227-234.

WHO (2011). Evaluation of certain food additive and contaminants. *World Health Organ Tech. Rep. Ser.*(960), 1-226, back.

Wild, S., Roglic, G., Green, A., Sicree, R., and King, H. (2004). Global prevalence of diabetes - Estimates for the year 2000 and projections for 2030. *Diabetes Care* **27**(5), 1047-1053.

Willcox, J. K., Ash, S. L., and Catignani, G. L. (2004). Antioxidants and prevention of chronic disease. *Crit Rev Food Sci* **44**(4), 275-295.

Winterbourn, C. C. (1979). Comparison of superoxide with other reducing agents in the biological production of hydroxyl radicals. *Biochem. J.* **182**(2), 625-628.

Yamada, H., Uenishi, R., Suzuki, K., and Koizumi, S. (2009). Cadmium-induced alterations of gene expression in human cells. *Environ. Toxicol. Pharmacol.* **28**(1), 61-69.

Yu, J., and Zhang, L. (2005). The transcriptional targets of p53 in apoptosis control. *Biochem. Biophys. Res. Co.* **331**(3), 851-858.

Zeng, H., and Combs, G. F., Jr. (2008). Selenium as an anticancer nutrient: roles in cell proliferation and tumor cell invasion. *J. Nutr. Biochem.* **19**(1), 1-7.

Zeng, H., and Davis, C. D. (2003). Down-regulation of proliferating cell nuclear antigen gene expression occurs during cell cycle arrest induced by human fecal water in colonic HT-29 cells. *J. Nutr.* **133**(8), 2682-2687.

Zeng, H. W., and Botnen, J. H. (2004). Copper may interact with selenite extracellularly in cultured HT-29 cells. *J. Nutr. Biochem.* **15**(3), 179-184.

Zhang, L., Yu, J., Park, B. H., Kinzler, K. W., and Vogelstein, B. (2000). Role of BAX in the apoptotic response to anticancer agents. *Science* **290**(5493), 989-992.

Zhao, R., Xiang, N., Domann, F. E., and Zhong, W. (2006). Expression of p53 enhances selenite-induced superoxide production and apoptosis in human prostate cancer cells. *Cancer Res.* **66**(4), 2296-2304.

Zhong, L. W., Arner, E. S. J., and Holmgren, A. (2000). Structure and mechanism of mammalian thioredoxin reductase: The active site is a redox-active selenolthiol/selenenylsulfide formed from the conserved cysteine-selenocysteine sequence. *Proc. Natl. Acad. Sci. U. S. A* **97**(11), 5854-5859.

Zhuo, P., and Diamond, A. M. (2009). Molecular mechanisms by which selenoproteins affect cancer risk and progression. *Biochim. Biophys. Acta* **1790**(11), 1546-1554.

Zou, Y., Niu, P., Yang, J., Yuan, J., Wu, T., and Chen, X. (2008). The JNK signaling pathway is involved in sodium-selenite-induced apoptosis mediated by reactive oxygen in HepG2 cells. *Cancer Biol. Ther.* **7**(5), 689-696.

9 Appendix

9.1 List of Abbreviations

ActD	Actinomycin D
AIF	Apoptosis inducing factor
AP	Apurinic/apyrimidinic
ARE	Antioxidant response element
ATM	Aurothiomalate
ATP	Adenosine triphosphate
Bax	Bcl-2-associated protein
BER	Base excision repair
BfR	Bundesinstitut für Risikobewertung, The German Federal Institute for risk assessment
BH	Bcl-2 homology
Bp	Base pairs
Caspase	Cysteinyl-aspartate specific protease
CDK	Cyclin-dependent kinase
CDKI	Cyclin-dependent kinase inhibitor
cDNA	Complementary DNA
CONTAM	EFSA Panel on Contaminants in the Food Chain
C_q	quantification cycle
Cys	Cysteine
DAPI	4`, 6-Diamidino-2-phenylindol
DiIC1(5)	1,1',3,3,3',3'-hexamethylindodicarbocyanine iodid
DIO	Deiodinase
DMEM	Dulbeccos Modified Eagle Medium
DMSO	Dimethyl sulphoxide
DMT1	Divalent metal transporter 1
DNA	Deoxyribonucleic acid
dsDNA	Double stranded DNA
DTNB	5.5'-dithiobis-(2-nitrobenzoic acid)
EDTA	Diethylenediamine tetraacetic acid
EFSA	European Food Safety Authority
FBS	Fetal bovine serum
FITC	Fluoresceinisothiocyanat
FSC	Forward scatter
GAPDH	Glycerinaldehyde-3-phophate dehydrogenase
GF-AAS	Graphite furnace atomic absorption spectroscopy
GPx	Glutathione peroxidase
GRE	Glucocortoid responsive element
GSH	Glutathione (reduced form)
GSSG	Glutathione disulfid (oxidized form)
GST	Glutathione-S-transferase
HCT116	Human colon cancer cell line
His	Histidine
HPRT	Hypoxanthine phosphoribosyltransferase 1
IARC	International Agency for Research on Cancer
IFC	Integrated fluidic circuit
IL	Interleukin
kDa	Kilo dalton

Keap1	Kelch-like ECH-associated protein 1
MAPK	Mitogen-activated protein kinase
MDB	Membrane desalting buffer
MDR1	Multidrug-resistance protein 1
MMR	Mismatch repair
MRE	Metal response element
mRNA	Messenger RNA
MRP	Multidrug resistance related protein
MT	Metallothionein
MTF-1	Metal-regulatory transcription factor 1
MTT	[3 – (4,5-dimethylthiazol-2-yl) -2,5-diphenyl tetrazolium bromide
NER	Nucleotide excision repair
NF-kB	nuclear factor kappa-light-chain-enhancer of activated B cells
NF-κB	Nuclear factor kappa B
NPC	Nutritional Prevention of Cancer Trial
Nrf2	Nuclear factor-E2-related factor 2
NTC	No template control
PARP	Poly (ADP-ribose)-polymerase
PBS	Phosphate buffered saline
PCR	Polymerase chain reaction
PI	Propidium iodide
PS	Phosphatidylserine
RIN	RNA integrity number
RNA	Ribonucleic acid
ROS	Reactive oxygen species
RT-PCR	Reverse transcriptase polymerase chain reaction
SD	Standard deviation
SELECT	Selenium and Vitamin E Cancer Prevention Trial
Sepp	Selenoprotein P
SOD	Superoxide dismutase
SPS2	Selenophosphate syntethase 2
SSC	Side scatter
Sub-G1-fraction	Cells containing subdiploid DNA
TNB	5-thio-2-nitrobenzoic acid
TNF	Tumor Necrosis Factor
TRAIL	Tumor necrosis factor-related apoptosis-inducing ligand
TrxR	Thioredoxin reductase
WHO	World Health Organization
WST-1	Water-soluble tetrazolium-1
ZnT	Zinc export protein

9.2 Applied chemicals

Chemical	Manufacture (Location)
1,1',3,3,3',3'-hexamethylindodicarbocyanine iodide (DilC1(5))	Invitrogen (Darmstadt, DE)
1.4-Dithiothreitol (DTT), (≥99% p.a.)	Roth (Karlsruhe, DE)
2-acetylamino-3-[4-(2-acetylamino-2-carboxyethylsulfanylthiocarbonylamino)phenylthiocarbamoylsulfanyl]propionic acid (2-AAPA) (≥95 %)	Sigma-Aldrich (Steinheim, DE)
2-mercaptoethanol	Serva (Heidelberg, DE)
5.5'-dithiobis-(2-nitrobenzoic acid) (DTNB) (≥99 % p.a.)	Roth (Karlsruhe, DE)
5-sulfo salicyl acid (SSA) (≥99 %)	Roth (Karlsruhe, DE)
Annexin-V (FITC conjugated)	Biolegend (London, UK)
Anti-AIF-antibody (H300) (rabbit polyclonal)	Santa Cruz Biotechnology (Heidelberg, DE)
Anti-rabbit-antibody (Cy3) (goat)	Jackson Immuno Research Laboratories
Assay Loading Reagent 2x	Fluidigm (San Francisco, USA)
Auranofin	Sigma-Aldrich (Steinheim, DE)
Cadmium chloride (99.9 %) ($CdCl_2$)	Sigma-Aldrich (Steinheim, DE)
Catalase (bovine liver)	Sigma-Aldrich (Steinheim, DE)
Coulter Isoton II Diluent	Beckman Coulter (Krefeld, DE)
D, L-Buthionine-[S, R]-Sulfoximine (BSO) (≥97 %)	Sigma-Aldrich (Steinheim, DE)
DAPI staining solution (Cystain DNA/Protein)	Partec (Münster, DE)
Diethylenetriaminepentaacetic acid (DETAPAC)	Sigma-Aldrich (Steinheim, DE)
Dihydroethidium	Sigma-Aldrich (Steinheim, DE)
Dimethylsulfoxid (DMSO)	Sigma-Aldrich (Steinheim, DE)
Dipotassium phosphate (K_2HPO_4)	Roth (Karlsruhe, DE)
Disodium hydrogen phosphate (Na_2HPO_4)	Roth (Karlsruhe, DE)
DNA Away	Molecular BioProducts (San Diego, USA)
DNA Binding Dye Sample Loading Reagent (20x)	Fluidigm (San Francisco, USA)
DNA suspension buffer	Teknova (Hollister, USA)
Dulbecco's Modified Eagel's Medium (DMEM)	Sigma-Aldrich (Steinheim, DE)
Ethanol, 96 %, denatured	Sigma-Aldrich (Steinheim, DE)
Ethylenediaminetetraacetic acid (EDTA, ≥99 %)	Roth (Karlsruhe, DE)
Exonuclease I (20 U/µl)	New England BioLabs (Frankfurt am Main, DE)
Exonuclease reaction buffer	New England BioLabs (Frankfurt am Main, DE)
FACS-Flow	BD (Heidelberg, DE)
Fetal bovine serum (FBS)	Gibco, Invitrogen (Darmstadt, DE)
Giemsa (Azure Eosin Methylene Blue) solution	Roth (Karlsruhe, DE)
Glutathione peroxidase (bovine erythrocytes)	Sigma-Aldrich (Steinheim, DE)
Glutathione reductase (Baker's yeast, *S. cerevisiae*)	Sigma-Aldrich (Steinheim, DE)
Hydrogen chloride (HCl, 0.1 N, 4 N)	Roth (Karlsruhe, DE)
Hydrogen peroxide (H_2O_2, 30 %), suprapure	Merck (Darmstadt, DE)
Hypoxanthine	Sigma-Aldrich (Steinheim, DE)
L (+)-Selenomethionine (99 %)	Acros Organics (Geel, BE)
L-Cysteine (≥98 %)	Roth (Karlsruhe, DE)
L-Glutathione, oxidized (≥98 %)	Sigma-Aldrich (Steinheim, DE)
L-Glutathione, reduced (≥98 %)	Sigma-Aldrich (Steinheim, DE)
Magnesium Matrix modifier	Merck (Darmstadt, DE)
Menadione	Sigma-Aldrich (Steinheim, DE)
Mercaptosuccinate	Sigma-Aldrich (Steinheim, DE)
Methanol	Roth (Karlsruhe, DE)
Monopotassium phosphate (KH_2PO_4)	Roth (Karlsruhe, DE)
Nicotinamide adenine dinucleotide phosphate	Roth (Karlsruhe, DE)

(NADPH) tetrasodium salt (≥97 %)	
Nitric acid (HNO_3, 65 %)	Merck (Darmstadt, DE)
NucleoSpin RNA II (RNA Isolation Kit)	Macherey-Nagel (Düren, DE)
Palladium Modifier	Merck (Darmstadt, DE)
PCR Certified Water	Teknova (Hollister, USA)
Penicillin (5.000 U/ ml) - Streptomycin (5 mg/l) solution	Sigma-Aldrich (Steinheim, DE)
Potassium chloride (KCl)	Merck (Darmstadt, DE)
Potassium dihydrogen phosphate (KH_2PO_4, ≥99 %)	Merck (Darmstadt, DE)
Primer	Eurofins (Hamburg, DE)
Primer (Gene Expression Design)	Fluidigm (San Francisco, USA)
Propidium iodide (1 mg/ml)	Sigma-Aldrich (Steinheim, DE)
qScript™ cDNA Synthesis Kit	Quanta Biosciences via VWR (Dresden, DE)
RNase Away	Molecular BioProducts (San Diego, USA)
Single Element AAS Standard solution selenium (1g/L)	Roth (Karlsruhe, DE)
Sodium aurothiomalate	Sigma-Aldrich (Steinheim, DE)
Sodium azide (NaN_3)	Sigma-Aldrich (Steinheim, DE)
Sodium chloride (NaCl)	AppliChem (Darmstadt, DE)
Sodium diethyl dithio carbamate (DDC) trihydrate (≥98 %)	Alfa Aesar (Karlsruhe, DE)
Sodium hydroxide (NaOH 0.1 N, 4 N)	Roth (Karlsruhe, DE)
Sodium selenite (Na_2SeO_3, 99 %)	Sigma-Aldrich (Steinheim, DE)
SsoFast EvaGreen® Supermix with low ROX	BioRad (München, DE)
Staurosporine	Sigma-Aldrich (Steinheim, DE)
Superoxide dismutase (bovine erythrocytes)	Sigma-Aldrich (Steinheim, DE)
TaqMan® PreAmp Master-Mix 2x	Life Technologies (Darmstadt, DE)
TE buffer (10 mM Tris, 1 mM EDTA, pH 8.0)	Teknova (Hollister, USA)
Tertbutyl hydroperoxide (t-BOOH)	Fluka (buchs, CH)
Thioredoxin reductase (rat liver)	IMCO (Solna, SE)
Tris -(hydroxymethyl)-aminomethan	Roth (Karlsruhe, DE)
Triton™ X-100 (reduced form, Fluka)	Sigma-Aldrich (Steinheim, DE)
Trypsin (10x)	Sigma-Aldrich (Steinheim, DE)
Vectashield Mounting Medium (DAPI)	Vector Laboratories (Burlingame, USA)
WST-1	Dojindo (Kumamoto, JP)
Xanthine-oxidase (from bovine milk)	Sigma-Aldrich (Steinheim, DE)

9.3 Applied solutions and buffers

Culture medium for HCT116 cells	DMEM 10 % FBS 100 U pencillin/ml, 10 µg streptomycin/ml
PBS (pH 7.4)	100 mM NaCl, 4.5 mM KCl 7 mM Na_2HPO_4, 3 mM KH_2PO_4
PBS-EDTA	0,5 mM EDTA in PBS
Trypsin solution (1x)	0.25 % trypsin in PBS-EDTA
Potassium phosphate buffer (pH 7.4) (total intracellular GSH determination)	Solution A: 0.1 M K_2HPO_4, 1 mM EDTA Solution B: 0.1 M KH_2PO_4, 1 mM EDTA Solution B is added to solution A to set pH 7.4
Tris-HCl 400 mM (pH 8.0) (total extracellular thiol determination)	400 mM Tris, pH 8.0 set with 1 N HCl
Potassium phosphate buffer (0.1 M) (pH 7.0) (enzyme activity assays)	0.1 M KH_2PO_4
PBS-UVC (pH 7.4) (indirect immunofluorescence)	137.1 mM NaCl, 2.15 mM KCl 8.5 mM Na2HPO4, 2.35 mM KH_2PO_4
Blocking solution	5 % FBS in PBS-UVC, 2 % FBS in PBS-UVC

9.4 Applied materials

Material	**Manufacturer (Location)**
96 well plates, transparent	TPP (Trasadingen, CH)
96 well plates, UV-star	Greiner BioOne (Frickenhausen, DE)
Accuvette cups	Beckmann Coulter (Krefeld, DE)
Cell culture dishes (40, 60, 100 mm)	TPP (Trasadingen, CH)
Cell culture flasks (25 cm^2)	TPP (Trasadingen, CH)
Centrifuge tubes, 15 and 50 ml	Sarstedt (Nümbrecht, DE)
Cover glass, 12 mm	Roth (Karlsruhe, DE)
Cover slides, 75 x 25 mM	VWR (Darmstadt, DE)
Cryo tubes with screw cap	Roth (Karlsruhe, DE)
Glass pipettes (1, 2, 5, 10, 20 ml)	Roth (Karlsruhe, DE)
Micro tubes, 1.5 and 2 ml	Sarstedt (Nümbrecht, DE)
Needles 0.4 x 20 mm	Terumo (Eschborn, DE)
PCR reaction tubes	Sarstedt (Nümbrecht, DE)
Pipette tips for multipette (1, 5 ml)	Eppendorf (Hamburg, DE)
Pipette tips, 0.1-10 µl	Sarstedt (Nümbrecht, DE)
Pipette tips, 100-1000 µl	Brand (Wertheim, DE)
Pipette tips, 10-200 µl	Roth (Karlsruhe, DE)
Pipette tips, 500-5000 µl	Eppendorf (Hamburg, DE)

9.5 Applied instruments and software

Instrument	Manufacturer (Location)
Atom absorption spectrometer PinAacle 900T	Perkin Elmer (Rodgau, DE)
Autoclave D-150	Systec (Linden, DE)
Axio Imager Z2	Carl Zeiss (Oberkochen, DE)
Biofreezer Herafreeze top	Thermo Scientific (Langenselbold, DE)
Biofuge pico	Heraeus (Hanau, DE)
Biomark HD System	Fluidigm (San Francisco, USA)
Centrifuge 5810R	Eppendorf (Hamburg, DE)
Colony Counter BZG-30	WTW (Weilheim, DE)
Coulter counter Z2	Beckman Coulter, Inc (Krefeld, DE)
Drying cabinet Heraeus T6	Heraeus (Hanau, DE)
Galaxy Mini Centrifuge	VWR (Darmstadt, DE)
Gas burner Gas Profi 1 SCS micro	Roth (Karlsruhe, DE)
Hera Cell 150 incubator	Heraeus (Hanau, DE)
HERAsafeKS (Sterile bench)	Thermo Scientific (Langenselbold, DE)
iCycler	BioRad (München, DE)
IFC Controlle HX	Fluidigm (San Francisco, USA)
Infinite M200	Tecan (Crailsheim, DE)
LSRII Fortessa	BD Sciences (Heidelberg, DE)
Megafuge 1.0	Heraeus (Hanau, DE)
Microscope Axiovert 40C	Carl Zeiss (Oberkochen, DE)
Mini Rocker MR-1	PeqLab (Erlangen, DE)
Multichannel pipette (1-10 µl)	Mettler-Toledo (Gießen, DE)
Multipette®	Eppendorf (Hamburg, DE)
NanoQuant plate	Tecan (Crailsheim, DE)
PCR Workstation Pro	PeqLab (Erlangen, DE)
pH meter 3210	WTW (Weilsheim, DE)
Pipetus Akku	Hirschmann (Eberstadt, DE)
Professional laboratory dish washer G7883	Miele (Gütersloh, DE)
Real-Time System CFX96	BioRad (Hercules, USA)
Refrigerators and freezers	Bosch (Stuttgart, DE)
Software AA Winlab32	Perkin Elmer (Rodgau, DE)
Software BD FACSDiva™	BD Sciences (Heidelberg, DE)
Software Data Collection	Fluidigm (San Francisco, USA)
Software GenEx	MultiD (Göteborg, SE)
Software IBM Statistics 19	SPSS Statistics (Chicago, USA)
Software Real-Time PCR Genetic Analysis	Fluidigm (San Francisco, USA)
Software Tecan i-Control	Tecan (Crailsheim, DE)
Software ZEN	Carl Zeiss (Oberkochen, DE)
Thermomixer MKR 13	HLC BioTech (Bovenden, DE)
Thermomixer SH 26	CAT (Staufen, DE)
Ultra precision scale	Sartorius (Göttingen, DE)
Ultra sound bath Sonifier 250	Branson (Danbury, USA)
Ultrapure water purification system Milli-Q	Millipore (Darmstadt, DE)
Vortex Genie 2T	Scientific Industries (New York, USA)
Water bath	Memmert (Schwabach, DE)

9.6 Supplementary data

9.6.1 Gene expression analysis

Table A1: The 95 genes of the assay setup classified in various signaling pathways

Reference genes	Redox-sensitive transcription factors	DNA damage response	Apoptosis	Cell cycle control	Oxidative stress response	Xenobiotic metabolism
ACTB	*AXIN2*	*APEX1*	*APAF1*	*CCND1*	*CAT*	*ABCB1*
B2M	*BTRC*	*ATM*	*BAX*	*CDKN1A*	*FTH1*	*ABCC1*
GAPDH	*JUN*	*ATR*	*BBC3*	*CDKN1B*	*G6PD*	*ADH1B*
GUSB	*KEAP1*	*BRCA1*	*BCL2*	*CDKN2B*	*GCLC*	*ALDH1A1*
HPRT1	*MAP3K5*	*BRCA2*	*BCL2L1*	*E2F1*	*GPX1*	*CYP1A1*
	MDM2	*DDB1*	*PMAIP1*	*EGFR*	*GPX2*	*EPHX1*
	NFE2L2	*DDB2*	*TNFRSF10B*	*IL8*	*GSR*	*GSTP1*
	NFKB1	*DDIT3*	*XIAP*	*MYC*	*HMOX1*	*NAT1*
	NFKB2	*ERCC1*		*PLK3*	*HSPA1A*	*NQO1*
	NFKBIA	*ERCC2*		*PPM1D*	*MT1X*	*SULT1A1*
	TP53	*ERCC4*		*SIRT2*	*MT2A*	*UGT1A*
	SLC30A1	*ERCC5*			*PRDX1*	
	VEGFA	*GADD45A*			*SEPP1*	
		LIG1			*SOD1*	
		LIG3			*SOD2*	
		MGMT			*TFRC*	
		MLH1			*TXN1*	
		MSH2			*TXNRD1*	
		OGG1				
		PARP1				
		PCNA				
		POLB				
		POLD1				
		RAD50				
		RAD51				
		RRM2B				
		XPA				
		XPC				
		XRCC5				

Table A2: Forward and reverse primer sequences of the 95 genes for the RT-qPCR analysis

Gene	Forward Primer (5`→3´)	Reverse Primer (5´→3´)
ABCB1	AACACCACTGGAGCATTGAC	ACAGCAAGCCTGGAACCTA
ABCC1	CCTGTTCTCGGAAACCATCC	AAGGTGATCCTCGACAGGAA
ACTB	CCAACCGCGAGAAGATGAC	TAGCACAGCCTGGATAGCAA
ADH1	CCCTCAAGACTACAAGAAA	CAGTCAGTAGCAGCATAG
ALDH1A1	CTTATCAGCAGGAGTGTT	GACCTCTGTATATTCATGGA
APAF1	AAATCTGGGCTTCTGATG	CTCTTGTCTCTGGTTGTAA
APEX1	GGATTAGATTGGGTAAAGGA	CCTATGCCGTAAGAAACT
ATM	TACCAAGCAGCATGGAGGAA	GATTCATGGTAACTGGTTCCTTCTAC
ATR	CATTCCAAAGCGCCACTGAA	CGCTGCTCAATGTCAAGAACA
AXIN2	CTTGAATGAAGAAGAGGAGT	CCTGTATCCACTGTCAAC

B2M	CGCTACTCTCTCTTTCTG	CAGTGTAGTACAAGAGATAGA
BAX	GGGTTGTCGCCCTTTTCTAC	TCTTGGATCCAGCCCAACA
BBC3	GACCTCAACGCACAGTAC	GTATGCTACATGGTGCAG
BCL2	TGACAGAGGATCATGCTGTACTTA	TCCAATTCCTTTCGGATCTTTATTTCA
BCL2L1	AAGCGTAGACAAGGAGAT	TCCCATAGAGTTCCACAA
BRCA1	AGTATGGGCTACAGAAAC	CACAGTTCCAAGGTTAGA
BRCA2	ATGCAGCAGACCCAGCTTA	TCCATGGCCTTCCTAATTTCCA
BTRC	CTGCTATGAAGACTGAGAA	TTCCACTTGATCTGACTC
CAT	AGAAGTGCGGAGATTCAACAC	CCTCATTCAGCACGTTCACA
CCND1	AGAGGCGGAGGAGAACAAA	AGGGCGGATTGGAAATGAAC
CDKN1A	CAGCATGACAGATTTCTAC	CACACAAACTGAGACTAAG
CDKN1B	AGGAAGCGACCTGCAACC	TTGGGGAACCGTCTGAAACA
CDKN2B	TTACGGCCAACGGTGGATTA	GGCATGCCCTTGTTCTCC
CYP1A1	TTTGAGAAGGGCCACATC	CCAGGAGATAGCAGTTGT
DDB1	ATCATCATTGGACAGGAG	AGGTATCTTGAGCCATTAG
DDB2	ACACTCTGGATTCTTACC	ACTGGTTGGTATTGAGAG
DDIT3	TTAAGTCTAAGGCACTGAG	GGTGTGGTGATGTATGAA
E2F1	AGCTCATTGCCAAGAAGTCCAA	TCCTGGGTCAACCCCTCAA
EGFR	GAACCCCGAGGGCAAATACA	CACGAGCCGTGATCTGTCA
EPHX1	GAGATCCACGACTTACAC	AATTCATTCCGCCAGTAG
ERCC1	GCCGACTGCACATTGATCC	TCCGCTGGTTTCTGCTCATA
ERCC2	TGAGAAGGTGATTGAAGAG	GGCATCAAATTCCTCATAGA
ERCC4	CTTCTGGAATCTCTGAGAGCAA	GAGGTGCTGGAGTCAAGAAA
ERCC5	TTGATGGGGATGCTCCACTA	TGGAGTCACTGGACGCTAA
FTH1	TTACCTGTCCATGTCTTAC	CATCACAGTCTGGTTTCT
G6PD	GCCGTCACCAAGAACATTCA	CTCCCGAAGGGCTTCTCC
GADD45A	GCTCCTGCTCTTGGAGAC	CAGGATCCTTCCATTGAGATGAA
GAPDH	ACACCATGGGGAAGGTGAAG	GTGACCAGGCGCCCAATA
GCLC	TGGATGCCATGGGATTTGGAA	CTCAGATATACTGCAGGCTTGGAA
GPX1	CACCCTCTCTTCGCCTTCC	GAGCTTGGGGTCGGTCATAA
GPX2	AGGAGAACTGTCAGAATG	GGGTCATCATAAGGGTAG
GSR	CGTGAATGTTGGATGTGTA	GGACTTGGTGAGATTGTT
GSTP1	CTCCGCTGCAAATACATC	CACAATGAAGGTCTTGCC
GUSB	CATCGATGACATCACCGTCAC	ACAGGTTACTGCCCTTGACA
HMOX1	CAGTCAGGCAGAGGGTGATA	GCTCCTGCAACTCCTCAAA
HPRT1	GCTTTCCTTGGTCAGGCAGTA	ACTTCGTGGGGTCCTTTTCAC
HSPA1A	TCCTGTGTTTGCAATGTTGAA	CTGCATGTAGAAACCGGAAAA
IL8	CACTCCATAAGGCACAAA	GCACTGACATCTAAGTTCT
JUN	GGTAGCAGATAAGTGTTGA	CAGTTAGAGAGAAGGTGAAA
KEAP1	CTTCGCTGAGCAGATTGG	GTAGAACCGTCGCTGTTC
LIG1	TGGGAAGTACCCGGACATCA	GCTTCGGTGTCCAGGATGAA
LIG3	TCCAGGACTTCCTTCGGAAA	CAGCAGCAGCTTCACTGTTA
MAP3K5	ATCATTCGGAAGGCGGTACA	ACTCTCAGATGCAAGGCTGAA
MDM2	CCATGATCTACAGGAACTTGGTA	GACACCTGTTCTCACTCACA
MGMT	TGTGAAATTCGGAGAAGTGA	GAGGATGGGGACAGGATT
MLH1	TACTTCACCCAGACTTTG	GCATAGACCTTATCACTACT
MSH2	CCAGCAGCAAAGAAGTGCTA	TGTTTCACCTTGGACAGGAAC
MT1X	TTCTCCTTGCCTCGAAAT	GGTTGCTCTATTTACATCTG
MT2A	AACCTGTCCCGACTCTAG	GAAGTCGCGTTCTTTACA
MYC	ACTGGAACTTACAACACC	GTAGTCGAGGTCATAGTTC
NAT1	GCAATCTGTCTTCTGGAT	CAATGGATGTTAAGGTTCTC
NFE2L2	CCTGAGTTACAGTGTCTTAA	GTGGACTACAGTTACCTAC
NFKB1	TCAGAATGGCAGAAGATG	CCATCTGTGGTTGAAATAC
NFKB2	TGACTTTGAGGGACTGTA	ATCTCTGTGGCTAGATGC
NFKBIA	ACTTTCGAGGAAATACCC	GATAGAGGCTAAGTGTAGAC
NQO1	TCGGACCTCTATGCCATGAAC	AAAGTTCGCAGGGTCCTTCA
OGG1	ATCAAGTATGGACACTGAC	CACACCTTGGAATTTCTG
PARP1	TTCTGGAGGACGACAAGGAA	GTTGCTACCGATCACCGTAC
PCNA	TCTGAGGGCTTCGACACCTA	CATTGCCGGCGCATTTTAGTA

PLK3	ACTGTCCAGGTGAACTTC	GAAGCGAGGTAAGTACAAG
PMAIP1	TGTGTAGTTGGCATCTCC	CTGAGTTGAGTAGCACAC
POLB	AAGTACAATGCTTACAGAAAAG	GTATCATCCTGCCGAATC
POLD1	TTACAACATCCAGAACTTCG	GCTTGGACTGGAATGAAG
PPM1D	AGCCAGAACTTCCCAAGGAAA	ACTACACGATTCACCCCAGAC
PRDX1	GCTGATAGGAAGATGTCT	GTGAAGTCAAGAGGGTAA
RAD50	TCCCTCCTGGAACCAAAGGAA	AGACGAATCTGGGCTCTCACA
RAD51	GGGAAGACCCAGATCTGTCA	ATGTACATGGCCTTTCCTTCAC
RRM2B	AGAATGTTCACTCAGAGATG	GCCAGAATATAGCAGCAA
SEPP1	CCAATGCTAAACTCCAATG	GAGAAGAGATTCCTTGATGA
SIRT2	GCTATTTCAAGAAACATCCG	TATTCGCTCCAGGGTATC
SLC30A1	GGTTCAGTGATTGTAGTAGT	GCAGATTCCTTAAGTAATGG
SOD1	GAGTTTGGAGATAATACAGC	CAACATGCCTCTCTTCAT
SOD2	AGGATCCACTGCAAGGAACA	GTGCTCCCACACATCAATCC
SULT1A	GAGACTCTGAAAGACACA	AACATAGACCACCTTGAC
TFRC	GTTGATAAGAACGGTAGACT	CTGCTCTGACAATCACTAT
TNFRSF10B	GTGATTCAGGTGAAGTGG	TCTTTGTGGACACATTCG
TP53	TTCGAGATGTTCCGAGAG	AGAAGTGGAGAATGTCAGT
TXN	TAAGAAGGGACAAAAGGTG	AGCTATTCAGACATGAGAC
TXNRD1	GCATCCCTGGTGACAAAGAA	CCAACAACCAGGGTCTTACC
UGT1A	CTCAGAAATTCCAGAGAAGA	GTGTTGTTCGCAAGATTC
VEGFA	TACATCTTCAAGCCATCC	CTGTAGGAAGCTCATCTC
XIAP	ACACCATCACTAACTAGAAG	TCTGACTTGACTCATCTTG
XPA	ACATCATTCACAATGGGGTGATA	ACCCCAAACTTCAAGAGACC
XPC	TAAAGGGGTCCATGAGGACACA	CTGGCTGGCTGCAGATGTTA
XRCC5	CAGTATCAGAACATCACAGT	CAATATGCCTCTTCTCAAAC

Table A3: Overview of the investigated genes and their encoded proteins

Gene	Coding protein
ABCB1	ATP-binding cassette, Multidrug resistance protein 1, ABCB1 = MDR1
ABCC1	ATP-binding cassette, Multidrug resistance-associated protein 1, ABCC1 = MRP1
ACTB	Actin, cytoplasmic 1
ADH1	Alcohol dehydrogenase 1B
ALDH1A1	Aldehyde dehydrogenase 1
APAF1	Apoptotic peptidase activating factor 1
APEX1	APEX nuclease (multifunctional DNA repair enzyme) 1
ATM	ATM serine/threonine kinase
ATR	ATR serine/threonine kinase
AXIN2	Axin 2
B2M	Beta-2-microglobulin
BAX	BCL2-associated X protein
BBC3	BCL2 binding component 3
BCL2	B-cell CLL/lymphoma 2
BCL2L1	BCL2-like 1
BRCA1	breast cancer 1 susceptibility protein
BRCA2	breast cancer 2 susceptibility protein
BTRC	beta-transducin repeat containing E3 ubiquitin protein ligase
CAT	catalase
CCND1	cyclin D1, G1/S specific
CDKN1A	cyclin-dependent kinase inhibitor 1A (p21, Cip1)
CDKN1B	cyclin-dependent kinase inhibitor 1B (p27, Kip1)
CDKN2B	cyclin-dependent kinase inhibitor 2B (p15, inhibits CDK4)
CYP1A1	cytochrome P450 family 1
DDB1	damage-specific DNA binding protein 1, XPE = DDB1
DDB2	damage-specific DNA binding protein 2

DDIT3	DNA-damage-inducible transcript 3
E2F1	E2F transcription factor 1
EGFR	epidermal growth factor receptor
EPHX1	epoxide hydrolase 1
ERCC1	excision repair cross-complementing rodent repair deficiency, complementation group 1
ERCC2	excision repair cross-complementing rodent repair deficiency, complementation group 2, XPD = ERCC2
ERCC4	excision repair cross-complementing rodent repair deficiency, complementation group 4, XPF = ERCC4
ERCC5	excision repair cross-complementing rodent repair deficiency, complementation group 5, XPG = ERCC5
FTH1	Ferritin, heavy chain
G6PD	glucose-6-phosphate dehydrogenase
GADD45A	growth arrest and DNA-damage-inducible protein, alpha
GAPDH	glyceraldehyde-3-phosphate dehydrogenase
GCLC	glutamate-cysteine ligase (catalytic subunit)
GPX1	glutathione peroxidase 1
GPX2	glutathione peroxidase 2 (gastrointestinal)
GSR	glutathione reductase
GSTP1	glutathione S-transferase pi 1
GUSB	glucuronidase, beta
HMOX1	heme oxygenase 1
HPRT1	hypoxanthine phosphoribosyltransferase 1
HSPA1A	heat shock 70kDa protein 1A
IL8	interleukin 8
JUN	Jun Proto-Oncogene (AP-1)
KEAP1	kelch-like ECH-associated protein 1
LIG1	DNA ligase 1
LIG3	DNA ligase III
MAP3K5	mitogen-activated protein kinase kinase kinase 5
MDM2	E3 ubiquitin protein ligase MDM2 (proto-oncogene)
MGMT	O-6-methylguanine-DNA methyltransferase
MLH1	DNA mismatch repair protein, mutL homolog 1
MSH2	DNA mismatch repair protein, mutS homolog 2
MT1X	metallothionein 1X
MT2A	metallothionein 2A
MYC	MYC proto-oncogene protein
NAT1	arylamine N-acetyltransferase 1
NFE2L2	NF-E2-related factor 2, nuclear factor, erythroid 2-like 2 (Nrf2)
NFKB1	nuclear factor of kappa light polypeptide gene enhancer in B-cells 1, p105 subunit
NFKB2	nuclear factor of kappa light polypeptide gene enhancer in B-cells 2, p100 subunit
NFKBIA	nuclear factor of kappa light polypeptide gene enhancer in B-cells inhibitor, alpha
NQO1	NAD(P)H dehydrogenase, quinone 1;
OGG1	8-oxoguanine DNA glycosylase, HOGG1 = OGG1,
PARP1	poly (ADP-ribose) polymerase 1
PCNA	proliferating cell nuclear antigen
PLK3	serine/threonine kinase, polo-like kinase 3
PMAIP1	phorbol-12-myristate-13-acetate-induced protein 1
POLB	DNA polymerase beta
POLD1	DNA polymerase delta 1 (catalytic subunit)
PPM1D	protein phosphatase 1D (Mg2+/Mn2+ dependent)
PRDX1	peroxiredoxin 1
RAD50	DNA repair protein RAD50 (homolog (S. cerevisiae))
RAD51	DNA repair protein RAD51 (recombinase)
RRM2B	ribonucleotide reductase M2 B (TP53 inducible)
SEPP1	selenoprotein P 1 (plasma)
SIRT2	NAD dependent protein deacetylase sirtuin 2
SLC30A1	solute carrier family 30 1 (zinc transporter = ZNT1)
SOD1	superoxide dismutase 1

SOD2	superoxide dismutase 2
SULT1A	sulfotransferase 1A (cytosolic)
TFRC	transferrin receptor 1
TNFRSF10B	tumor necrosis factor receptor superfamily member 10b
TP53	tumor protein p53
TXN	thioredoxin
TXNRD1	thioredoxin reductase 1
UGT1A	UDP glucuronosyltransferase 1A
VEGFA	vascular endothelial growth factor A
XIAP	E3 ubiquitin protein ligase X-linked inhibitor of apoptosis
XPA	DNA repair protein xeroderma pigmentosum, complementation group A
XPC	DNA repair protein xeroderma pigmentosum, complementation group C
XRCC5	X-ray repair complementing defective repair in Chinese hamster cells 5

Table A4: mRNA levels in p53-proficient HCT 116 cells: Exposure to cadmium chloride (24h:1 µM-50 µM. 16h: 10 µM-50 µM; 8h 10 µM-50 µM)

	$CdCl_2$ (24 h)												$CdCl_2$ (16 h)						$CdCl_2$ (8 h)					
	1 µM			**5 µM**			**10 µM**			**50 µM**			**10 µM**			**50 µM**			**10 µM**			**50 µM**		
	Mean	SD err+	SD err-	**Mean**	SD err+	SD err-	**Mean**	SD err+	SD err-	**Mean**	SD err+	SD err-	**Mean**	SD err+	SD err-	**Mean**	SD err+	SD err-	**Mean**	SD err+	SD err-	**Mean**	SD err+	SD err-
ABCB1	0.94	0.18	0.15	**1.86**	0.20	0.18	**2.86**	0.59	0.49	**4.49**	0.39	0.36	**3.67**	1.95	1.27	**5.10**	1.80	1.33	**2.93**	1.55	1.01	**5.49**	2.80	1.85
ABCC1	1.09	0.02	0.02	1.15	0.09	0.08	1.03	0.20	0.17	1.11	0.24	0.20	1.19	0.27	0.22	1.00	0.21	0.17	1.21	0.17	0.15	1.41	0.17	0.15
CAT	0.94	0.06	0.05	0.86	0.05	0.05	0.71	0.04	0.03	0.70	0.06	0.06	0.75	0.05	0.05	0.68	0.03	0.03	0.82	0.06	0.05	0.82	0.11	0.10
EPHX1	1.19	0.07	0.07	1.19	0.04	0.04	1.09	0.06	0.05	1.10	0.05	0.05	1.12	0.07	0.07	0.99	0.06	0.06	1.17	0.14	0.13	1.17	0.35	0.27
FTH1	1.24	0.14	0.13	**2.71**	0.46	0.40	**3.02**	0.72	0.58	**3.26**	0.40	0.36	**2.74**	0.48	0.41	**1.89**	4.43	1.32	**2.67**	1.72	1.05	**2.18**	0.29	0.25
G6PD	1.31	0.14	0.12	1.57	0.10	0.09	1.53	0.07	0.07	1.57	0.10	0.09	1.52	0.18	0.16	1.39	0.09	0.09	1.42	0.28	0.23	1.60	0.06	0.06
GCLC	1.35	0.07	0.06	1.44	0.18	0.16	1.70	0.12	0.12	1.65	0.21	0.19	1.78	0.27	0.23	**2.33**	0.19	0.17	**4.51**	0.37	0.34	**4.08**	0.29	0.27
GPX1	0.95	0.07	0.06	0.80	0.04	0.03	0.84	0.10	0.09	**0.60**	0.03	0.02	0.73	0.03	0.03	0.78	0.06	0.06	0.98	0.02	0.02	0.78	0.06	0.06
GSR	1.39	0.23	0.20	1.68	0.09	0.09	**2.03**	0.21	0.19	**1.99**	0.18	0.17	**2.06**	0.23	0.20	**2.45**	0.17	0.16	**2.31**	0.11	0.11	**2.36**	0.14	0.13
GSTP1	1.00	0.04	0.04	1.10	0.06	0.06	1.15	0.07	0.07	1.17	0.07	0.06	1.13	0.05	0.04	1.23	0.09	0.09	1.20	0.04	0.03	1.12	0.06	0.06
KEAP1	1.20	0.20	0.17	1.14	0.20	0.17	0.89	0.21	0.17	0.79	0.10	0.09	0.84	0.13	0.11	**0.61**	0.12	0.10	0.90	0.11	0.10	1.00	0.19	0.16
MT1X	**5.09**	1.79	1.33	**16.50**	4.63	3.62	**19.24**	3.45	2.93	**19.00**	2.17	1.94	**28.47**	3.51	3.12	**32.80**	4.01	3.57	**37.92**	5.41	4.73	**30.18**	2.88	2.63
MT2A	**3.93**	0.23	0.22	**6.58**	0.45	0.42	**7.41**	0.16	0.16	**7.32**	1.29	1.10	**7.89**	0.78	0.71	**7.11**	4.13	2.61	**8.45**	0.85	0.78	**6.90**	0.75	0.68
NAT1	1.16	0.13	0.12	1.57	0.11	0.10	1.84	0.13	0.12	**1.97**	0.12	0.11	1.57	0.10	0.09	1.55	0.04	0.04	0.92	0.16	0.14	0.91	0.13	0.11
NFEL2L	0.98	0.12	0.11	0.95	0.11	0.10	0.90	0.16	0.14	0.86	0.16	0.13	0.90	0.10	0.09	0.87	0.08	0.07	1.00	0.23	0.19	1.08	0.07	0.07
NQO1	1.18	0.03	0.03	1.53	0.04	0.04	1.31	0.12	0.11	1.50	0.06	0.06	1.56	0.10	0.09	1.40	0.04	0.04	1.62	0.10	0.10	**1.80**	0.08	0.08
PRDX1	1.05	0.15	0.13	1.37	0.10	0.09	1.40	0.09	0.08	1.67	0.24	0.21	1.53	0.17	0.15	1.53	0.18	0.16	1.35	0.30	0.25	1.45	0.20	0.18
SEPP1	1.04	0.09	0.08	0.79	0.04	0.04	**0.68**	0.06	0.06	**0.54**	0.12	0.10	**0.45**	0.03	0.03	**0.37**	0.02	0.02	**0.57**	0.14	0.11	**0.52**	0.34	0.20
SLC30A1	1.52	0.58	0.42	**2.47**	1.80	1.04	**3.33**	1.64	1.10	**2.54**	1.79	1.05	**2.69**	0.24	0.22	**3.20**	0.75	0.61	**10.34**	1.13	1.02	**8.13**	0.29	0.28
SOD1	0.96	0.05	0.04	0.98	0.05	0.05	1.31	0.22	0.18	1.26	0.13	0.12	1.18	0.10	0.09	1.55	0.11	0.10	1.38	0.20	0.17	1.19	0.04	0.04
SOD2	0.92	0.03	0.03	0.99	0.06	0.06	0.98	0.09	0.08	1.03	0.05	0.05	0.97	0.04	0.04	0.93	0.04	0.03	0.87	0.06	0.06	0.92	0.02	0.02
SULT1A	1.12	0.19	0.16	1.19	0.10	0.09	1.15	0.16	0.14	0.99	0.10	0.09	0.99	0.11	0.10	0.93	0.05	0.05	1.16	0.14	0.13	0.99	0.23	0.18
TFRC	1.33	0.33	0.26	1.50	0.37	0.30	1.44	0.37	0.29	1.48	0.36	0.29	1.26	0.14	0.13	1.20	0.11	0.10	1.02	0.11	0.10	1.02	0.18	0.15

TXN	1.12	0.19	0.16	1.51	0.16	0.15	1.73	0.45	0.36	**2.01**	0.43	0.36	1.78	0.33	0.28	1.63	0.77	0.52	1.51	0.48	0.36	1.64	0.19	0.17
TXNRD1	1.45	0.12	0.11	**1.80**	0.11	0.10	**2.37**	0.28	0.25	**2.30**	0.24	0.22	**2.46**	0.53	0.44	**3.17**	0.39	0.35	**4.20**	0.51	0.45	**4.38**	0.65	0.56
HMOX1	1.35	0.06	0.06	**22.99**	13.63	8.56	**42.72**	16.08	11.68	**66.43**	17.53	13.87	**62.23**	29.42	19.97	**79.10**	17.14	14.08	**108.78**	8.68	8.04	**161.69**	12.51	11.61
HSPA1A	0.99	0.28	0.22	**66.16**	39.07	24.56	**173.96**	55.85	42.27	**273.36**	32.47	29.02	**160.00**	164.67	81.15	**244.11**	263.94	126.82	**58.80**	73.09	32.59	**150.06**	235.80	91.70
IL8	1.14	0.11	0.10	**2.93**	1.55	1.01	**5.98**	4.41	2.54	**9.78**	4.82	3.23	**6.84**	6.93	3.44	**12.36**	7.02	4.48	**7.45**	3.19	2.23	**13.44**	6.32	4.30
NFKB1	1.09	0.22	0.19	1.03	0.18	0.15	0.82	0.15	0.12	0.76	0.10	0.09	0.86	0.09	0.08	0.67	0.07	0.06	0.88	0.10	0.09	1.01	0.10	0.09
NFKBIA	1.33	0.20	0.17	1.41	0.18	0.16	1.30	0.23	0.20	0.99	0.13	0.12	0.93	0.13	0.11	**0.57**	0.62	0.30	1.02	0.28	0.22	**0.72**	0.57	0.32
NFKB2	1.14	0.27	0.22	1.57	0.19	0.17	1.56	0.35	0.29	1.64	0.31	0.26	1.69	0.43	0.34	1.55	0.23	0.20	1.21	0.61	0.40	1.47	0.14	0.13
CCND1	0.99	0.06	0.06	1.08	0.09	0.08	0.98	0.09	0.08	0.99	0.09	0.08	0.99	0.07	0.06	0.89	0.08	0.07	1.14	0.10	0.09	1.29	0.03	0.03
CDKN1A1	1.08	0.11	0.10	1.10	0.07	0.07	1.14	0.21	0.18	1.08	0.07	0.07	1.16	0.10	0.09	1.19	0.07	0.06	1.30	0.31	0.25	1.11	0.14	0.12
CDKN1B	0.97	0.09	0.08	0.89	0.10	0.09	0.74	0.16	0.13	**0.60**	0.09	0.08	**0.64**	0.14	0.11	**0.45**	0.07	0.06	**0.50**	0.14	0.11	**0.43**	0.21	0.14
CDKN2B	1.01	0.19	0.16	0.96	0.08	0.07	0.99	0.19	0.16	0.99	0.32	0.24	1.11	0.39	0.29	0.95	0.31	0.24	1.21	0.44	0.32	1.51	0.21	0.19
E2F1	1.28	0.06	0.06	0.92	0.04	0.04	0.93	0.17	0.14	**0.69**	0.04	0.04	**0.70**	0.15	0.12	**0.71**	0.17	0.14	**0.69**	0.04	0.04	**0.50**	0.15	0.11
EGFR	1.15	0.08	0.08	0.85	0.01	0.01	0.90	0.13	0.11	0.69	0.03	0.03	0.90	0.22	0.18	0.92	0.10	0.09	1.56	0.63	0.45	**1.50**	0.25	0.21
JUN	0.78	0.18	0.15	**2.15**	0.86	0.61	**4.37**	2.64	1.65	**5.08**	3.46	2.06	**5.75**	4.45	2.51	**9.08**	4.11	2.83	**13.29**	12.43	6.42	**15.35**	15.62	7.74
MAP3K5	1.05	0.11	0.10	0.95	0.09	0.08	0.88	0.09	0.08	0.77	0.09	0.08	0.80	0.04	0.04	0.82	0.01	0.01	0.83	0.07	0.06	0.79	0.09	0.08
MDM2	1.02	0.10	0.09	1.28	0.04	0.04	1.27	0.06	0.06	1.43	0.08	0.08	1.25	0.03	0.03	1.13	0.02	0.02	1.01	0.07	0.06	1.14	0.09	0.08
MYC	1.17	0.17	0.15	0.97	0.14	0.12	0.88	0.20	0.16	0.70	0.10	0.09	0.77	0.10	0.09	0.71	0.11	0.10	1.45	0.07	0.06	1.06	0.47	0.33
PLK3	1.22	0.39	0.30	1.17	0.19	0.17	1.15	0.36	0.28	0.94	0.13	0.11	0.98	0.14	0.12	0.87	0.33	0.24	1.64	0.47	0.37	1.44	0.08	0.07
PPM1D	1.08	0.11	0.10	1.05	0.04	0.04	1.27	0.15	0.13	1.13	0.04	0.04	0.89	0.05	0.05	1.00	0.12	0.11	0.82	0.15	0.12	0.61	0.09	0.08
SIRT2	1.27	0.15	0.14	1.16	0.06	0.06	1.43	0.12	0.11	1.40	0.16	0.14	1.09	0.18	0.15	1.39	0.33	0.26	0.95	0.16	0.14	0.86	0.04	0.04
TP53	0.95	0.11	0.10	0.71	0.10	0.09	**0.57**	0.07	0.06	**0.53**	0.04	0.04	**0.60**	0.07	0.06	**0.50**	0.03	0.03	**0.73**	0.08	0.08	**0.79**	0.07	0.06
VEGFA	1.28	0.18	0.16	1.56	0.02	0.02	1.69	0.20	0.18	1.45	0.11	0.10	1.53	0.08	0.07	0.97	1.62	0.61	1.74	0.28	0.24	1.53	0.13	0.12
APEX1	1.08	0.09	0.09	1.05	0.18	0.15	0.86	0.13	0.11	0.86	0.22	0.18	0.91	0.19	0.16	0.82	0.15	0.13	1.00	0.20	0.17	0.93	0.29	0.22
ATM	1.02	0.22	0.18	0.86	0.05	0.04	0.91	0.06	0.05	0.85	0.06	0.06	0.91	0.08	0.07	0.83	0.04	0.04	0.87	0.10	0.09	1.04	0.22	0.18
ATR	0.97	0.04	0.04	0.88	0.03	0.03	0.96	0.17	0.14	0.80	0.15	0.13	0.85	0.20	0.16	0.94	0.17	0.14	0.98	0.19	0.16	0.76	0.05	0.05
BRCA1	1.05	0.09	0.08	0.91	0.10	0.09	0.92	0.22	0.17	**0.70**	0.13	0.11	**0.69**	0.14	0.12	**0.67**	0.15	0.12	**0.78**	0.09	0.08	**0.58**	0.08	0.07
BRCA2	1.03	0.05	0.04	0.95	0.03	0.03	0.94	0.09	0.09	**0.78**	0.12	0.11	**0.77**	0.20	0.16	**0.71**	0.16	0.13	**0.70**	0.14	0.12	**0.64**	0.11	0.09

DDB1	1.26	0.22	0.19	1.20	0.16	0.14	1.04	0.19	0.16	0.97	0.14	0.12	1.01	0.12	0.10	0.92	0.17	0.14	1.07	0.12	0.11	1.17	0.15	0.13
DDB2	1.16	0.16	0.14	1.10	0.18	0.15	0.84	0.20	0.16	0.72	0.15	0.13	0.60	0.14	0.11	**0.48**	0.21	0.15	**0.49**	0.05	0.05	**0.48**	0.24	0.16
ERCC1	0.92	0.02	0.02	0.95	0.05	0.05	1.12	0.12	0.11	1.13	0.09	0.08	1.09	0.25	0.21	1.39	0.27	0.22	1.19	0.25	0.21	1.25	0.38	0.29
ERCC2	1.16	0.05	0.04	1.08	0.09	0.09	0.90	0.33	0.24	0.93	0.09	0.08	1.03	0.13	0.12	0.95	0.22	0.18	0.96	0.47	0.32	0.97	0.04	0.03
ERCC4	0.87	0.14	0.12	0.84	0.09	0.08	0.71	0.14	0.12	0.66	0.10	0.09	0.72	0.12	0.10	**0.54**	0.06	0.05	**0.56**	0.05	0.04	**0.54**	0.07	0.07
ERCC5	0.96	0.12	0.11	1.01	0.08	0.07	1.04	0.09	0.08	1.18	0.08	0.08	0.90	0.02	0.02	0.89	0.10	0.09	**0.60**	0.07	0.07	0.62	0.09	0.08
LIG1	1.09	0.06	0.05	0.87	0.03	0.03	0.86	0.10	0.09	0.61	0.05	0.05	0.65	0.02	0.02	0.66	0.07	0.06	0.89	0.13	0.11	0.76	0.06	0.05
LIG3	1.26	0.20	0.17	1.00	0.12	0.10	1.09	0.20	0.17	0.88	0.09	0.08	0.89	0.10	0.09	0.99	0.11	0.10	0.90	0.05	0.05	0.77	0.08	0.08
MGMT	1.05	0.17	0.15	1.02	0.22	0.18	0.91	0.16	0.14	0.98	0.14	0.12	0.94	0.19	0.15	0.74	0.16	0.13	0.97	0.14	0.12	1.04	0.28	0.22
MLH1	1.07	0.11	0.10	1.02	0.03	0.03	1.20	0.13	0.11	1.09	0.16	0.14	1.10	0.19	0.16	1.17	0.35	0.27	1.16	0.26	0.21	1.06	0.31	0.24
MSH2	0.84	0.03	0.03	0.89	0.04	0.04	0.85	0.15	0.13	0.83	0.13	0.12	0.80	0.21	0.17	0.72	0.13	0.11	0.69	0.16	0.13	0.66	0.10	0.09
OGG1	1.25	0.26	0.22	1.09	0.19	0.16	1.14	0.25	0.20	0.95	0.22	0.18	0.85	0.14	0.12	0.86	0.19	0.15	0.96	0.20	0.17	0.73	0.17	0.14
PARP1	1.04	0.10	0.09	1.01	0.09	0.09	0.86	0.07	0.07	0.84	0.05	0.05	0.89	0.06	0.05	0.73	0.04	0.04	0.87	0.10	0.09	0.97	0.07	0.07
PCNA	0.90	0.07	0.06	1.02	0.09	0.08	1.03	0.20	0.16	1.05	0.06	0.06	0.92	0.08	0.07	0.93	0.16	0.14	0.75	0.18	0.15	0.69	0.16	0.13
POLB	0.94	0.09	0.08	1.01	0.13	0.11	1.08	0.19	0.16	1.11	0.20	0.17	1.05	0.17	0.15	1.08	0.14	0.13	1.00	0.20	0.16	0.95	0.08	0.07
POLD1	1.21	0.13	0.12	0.95	0.10	0.09	0.93	0.20	0.17	0.69	0.10	0.09	0.78	0.09	0.08	0.76	0.15	0.12	1.01	0.43	0.30	0.80	0.04	0.04
RAD50	1.05	0.04	0.04	0.85	0.04	0.04	0.92	0.11	0.10	0.71	0.07	0.06	0.77	0.10	0.09	0.80	0.08	0.08	0.89	0.10	0.09	0.76	0.06	0.06
RAD51	0.96	0.02	0.02	1.04	0.04	0.04	0.94	0.05	0.05	0.93	0.07	0.06	0.93	0.10	0.09	0.89	0.14	0.12	1.01	0.06	0.06	0.89	0.14	0.12
RRM2B	1.10	0.23	0.19	1.20	0.22	0.18	0.98	0.18	0.15	0.96	0.20	0.17	0.93	0.14	0.12	0.79	0.09	0.08	0.80	0.11	0.10	0.88	0.21	0.17
XPA	0.94	0.03	0.03	0.94	0.01	0.01	0.93	0.16	0.14	0.96	0.08	0.07	0.90	0.15	0.13	0.81	0.09	0.08	0.86	0.21	0.17	0.91	0.12	0.11
XPC	0.96	0.05	0.05	0.96	0.06	0.06	0.82	0.03	0.03	0.85	0.10	0.09	0.85	0.08	0.07	0.71	0.07	0.07	0.69	0.10	0.09	0.78	0.10	0.09
XRCC5	1.05	0.12	0.11	1.02	0.08	0.07	0.95	0.04	0.04	0.98	0.06	0.06	0.98	0.04	0.04	0.89	0.04	0.04	0.95	0.06	0.05	1.04	0.04	0.04
APAF1	1.05	0.20	0.17	0.97	0.09	0.08	0.85	0.16	0.13	0.70	0.06	0.06	**0.76**	0.08	0.07	**0.58**	0.16	0.12	0.85	0.12	0.10	0.70	0.09	0.08
BAX	1.22	0.15	0.14	1.15	0.12	0.11	1.20	0.23	0.19	1.07	0.07	0.06	1.11	0.08	0.07	1.23	0.21	0.18	1.30	0.17	0.15	1.10	0.08	0.08
BBC3	1.03	0.17	0.14	1.08	0.16	0.14	0.98	0.31	0.23	0.88	0.25	0.20	**0.73**	0.42	0.27	**0.72**	0.44	0.27	0.74	0.15	0.13	0.82	0.19	0.16
BCL2	1.32	0.30	0.24	0.96	0.32	0.24	0.94	0.33	0.24	**0.65**	0.16	0.13	**0.72**	0.15	0.12	**0.60**	0.10	0.08	1.04	0.22	0.18	0.86	0.09	0.09
BCL2L1	1.35	0.23	0.20	1.24	0.17	0.15	1.16	0.27	0.22	0.97	0.05	0.05	0.91	0.09	0.08	0.96	0.16	0.14	1.22	0.24	0.20	1.01	0.18	0.15
PMAIP1	0.92	0.12	0.11	1.64	0.17	0.15	**2.64**	0.70	0.55	**3.11**	0.62	0.52	**2.79**	1.02	0.75	**4.08**	0.97	0.78	**3.53**	0.57	0.49	**4.53**	1.39	1.06

TNFRSF10B	1.12	0.11	0.10	1.34	0.18	0.16	1.35	0.31	0.25	1.50	0.37	0.30	**1.70**	0.80	0.55	**1.76**	0.64	0.47	**1.71**	0.69	0.49	**2.21**	0.77	0.57
XIAP	1.21	0.23	0.19	1.29	0.08	0.07	1.56	0.14	0.13	1.61	0.11	0.10	1.49	0.19	0.17	1.72	0.16	0.15	1.26	0.16	0.14	1.45	0.15	0.13

Table A5: mRNA levels in p53-proficient HCT 116 cells: Exposure to sodium selenite (24h:1 µM-5 µM. 8h 5 µM) in combination with 10 µM $CdCl_2$.

	Sodium selenite (24h)									Sodium selenite (24h) + 10 µM $CdCl_2$									Sodium selenite (8h)			Sodium selenite (8h) + 10 µM $CdCl_2$		
	1 µM			3 µM			5 µM			1 µM			3 µM			5 µM			5 µM			5 µM		
	Mean	SD err+	SD err-	**Mean**	SD err+	SD err-	**Mean**	SD err+	SD err-	**Mean**	SD err+	SD err-	**Mean**	SD err+	SD err-	**Mean**	SD err+	SD err-	**Mean**	SD err+	SD err-	**Mean**	SD err+	SD err-
ABCB1	1.06	0.10	0.09	0.98	0.16	0.14	1.63	0.48	0.37	**2.12**	0.89	0.62	**2.08**	1.36	0.82	**1.77**	0.67	0.49	1.68	1.24	0.71	1.16	0.18	0.15
ABCC1	1.06	0.10	0.09	1.17	0.07	0.06	1.21	0.38	0.29	1.13	0.03	0.03	1.17	0.02	0.02	1.25	0.15	0.14	0.93	0.14	0.12	1.03	0.04	0.04
CAT	1.00	0.06	0.06	0.94	0.03	0.03	0.72	0.02	0.02	0.68	0.14	0.11	0.73	0.03	0.03	0.68	0.05	0.05	0.86	0.10	0.09	0.81	0.06	0.06
EPHX1	1.09	0.15	0.13	1.78	0.20	0.18	2.35	0.23	0.21	1.19	0.05	0.05	1.05	0.02	0.02	0.94	0.07	0.07	1.49	0.10	0.09	1.15	0.08	0.07
FTH1	1.08	0.33	0.25	**4.11**	4.06	2.04	**4.86**	5.42	2.56	**2.24**	0.27	0.24	**4.19**	2.65	1.62	**4.17**	1.41	1.06	**2.48**	1.95	1.09	**2.52**	1.31	0.86
G6PD	1.09	0.08	0.07	**2.11**	0.54	0.43	**2.16**	1.06	0.71	1.65	0.24	0.21	**2.18**	0.11	0.10	**2.30**	0.37	0.32	1.43	0.12	0.11	1.40	0.14	0.13
GCLC	1.08	0.10	0.09	**4.35**	1.76	1.25	**5.00**	2.14	1.50	1.61	0.71	0.49	**2.81**	0.18	0.17	**2.60**	0.08	0.08	**4.27**	0.77	0.66	**3.25**	0.38	0.34
GPX1	1.10	0.05	0.05	1.10	0.18	0.15	1.56	0.04	0.04	0.77	0.24	0.18	0.89	0.06	0.05	0.69	0.09	0.08	1.18	0.16	0.14	1.01	0.08	0.08
GSR	1.04	0.14	0.13	1.69	0.15	0.14	**1.97**	0.48	0.38	1.74	0.17	0.15	**2.10**	0.21	0.19	**2.03**	0.10	0.09	1.67	0.20	0.18	1.59	0.08	0.07
GSTP1	1.02	0.00	0.00	1.04	0.03	0.03	1.05	0.10	0.09	1.12	0.08	0.07	1.22	0.03	0.03	1.19	0.14	0.12	1.09	0.05	0.05	1.09	0.06	0.06
KEAP1	1.07	0.07	0.07	1.11	0.07	0.07	1.38	0.50	0.37	0.85	0.41	0.28	1.08	0.24	0.19	1.30	0.11	0.10	1.28	0.24	0.20	1.01	0.08	0.07
MT1X	1.06	0.07	0.07	**2.18**	0.89	0.63	**2.96**	0.96	0.73	**13.44**	1.63	1.46	**15.31**	5.45	4.02	**14.05**	4.53	3.42	1.37	0.17	0.15	**23.94**	4.51	3.80
MT2A	1.04	0.09	0.08	**1.94**	0.42	0.35	**2.93**	0.42	0.37	**5.65**	0.06	0.06	**5.84**	1.10	0.93	**5.76**	1.73	1.33	1.53	0.25	0.22	**5.14**	0.53	0.48
NAT1	0.95	0.04	0.03	0.56	0.04	0.04	0.78	0.08	0.07	1.79	0.67	0.49	1.38	0.42	0.32	1.21	0.16	0.14	0.59	0.09	0.08	0.81	0.04	0.04
NFEL2L	1.00	0.25	0.20	1.41	0.48	0.36	**2.07**	0.39	0.33	0.84	0.08	0.07	0.87	0.12	0.11	0.89	0.06	0.06	1.44	0.52	0.38	0.84	0.06	0.06
NQO1	1.12	0.02	0.02	**2.44**	0.61	0.49	**2.83**	0.95	0.71	1.46	0.18	0.16	1.78	0.09	0.09	**1.98**	0.21	0.19	1.89	0.30	0.26	1.61	0.19	0.17
PRDX1	1.03	0.09	0.08	1.01	0.02	0.02	1.05	0.02	0.02	1.38	0.29	0.24	1.34	0.20	0.17	1.30	0.14	0.13	1.10	0.06	0.05	1.10	0.04	0.04
SEPP1	1.22	0.54	0.37	0.90	0.17	0.14	0.69	0.00	0.00	0.72	0.11	0.09	0.59	0.04	0.03	0.74	0.11	0.10	0.85	0.24	0.18	0.74	0.04	0.04

SLC30A1	0.98	0.08	0.07	1.45	0.57	0.41	**2.06**	0.97	0.66	**3.00**	0.32	0.29	**3.87**	0.27	0.26	**2.91**	0.52	0.44	**1.86**	0.85	0.58	**3.11**	0.65	0.54
SOD1	1.04	0.03	0.03	0.90	0.03	0.03	0.79	0.14	0.12	1.13	0.04	0.04	1.13	0.12	0.11	0.96	0.02	0.02	1.00	0.08	0.07	1.01	0.14	0.13
SOD2	1.01	0.08	0.07	0.86	0.07	0.06	1.09	0.10	0.09	0.93	0.06	0.06	0.87	0.10	0.09	0.88	0.05	0.05	0.95	0.14	0.12	0.86	0.03	0.03
SULT1A	1.06	0.09	0.08	1.10	0.13	0.11	1.06	0.14	0.12	1.06	0.12	0.11	1.66	0.27	0.23	1.50	0.30	0.25	1.17	0.14	0.13	1.07	0.12	0.11
TFRC	1.03	0.15	0.13	1.18	0.10	0.09	1.03	0.27	0.22	1.19	0.18	0.15	1.05	0.06	0.06	0.88	0.13	0.11	1.02	0.02	0.02	0.94	0.03	0.03
TXN	1.04	0.20	0.17	1.29	0.02	0.02	1.83	0.16	0.14	1.53	0.61	0.44	1.36	0.12	0.11	1.43	0.05	0.05	1.29	0.13	0.12	1.14	0.05	0.05
TXNRD1	1.18	0.19	0.16	**4.19**	1.89	1.30	**5.63**	3.27	2.07	**2.07**	0.68	0.51	**4.07**	0.61	0.53	**3.60**	0.50	0.44	**4.85**	2.31	1.57	**3.67**	0.54	0.47
HMOX1	1.07	0.14	0.13	**3.92**	2.44	1.50	**20.26**	20.94	10.30	**53.86**	25.30	17.21	**73.71**	13.88	11.68	**66.07**	18.30	14.33	**9.28**	3.02	2.28	**46.06**	4.25	3.89
HSPA1A	0.97	0.15	0.13	0.76	0.13	0.11	1.20	0.40	0.30	**90.57**	339.43	71.49	**74.48**	220.31	55.66	**30.48**	7.16	5.80	0.90	0.22	0.18	0.90	0.10	0.09
IL8	0.95	0.04	0.04	**13.17**	16.57	7.34	**83.89**	15.65	13.19	**4.15**	2.43	1.53	**5.50**	0.47	0.44	**6.41**	2.00	1.53	**154.53**	419.84	112.96	**2.54**	0.34	0.30
NFKB1	1.05	0.02	0.02	1.05	0.03	0.03	1.65	0.18	0.16	0.83	0.11	0.09	0.71	0.07	0.06	0.79	0.12	0.11	1.18	0.31	0.25	0.77	0.06	0.06
NFKB1A	0.95	0.20	0.17	1.04	0.23	0.19	1.79	0.48	0.38	0.79	0.33	0.23	1.16	0.21	0.18	0.97	0.34	0.25	1.51	0.68	0.47	0.73	0.20	0.16
NFKB2	1.06	0.01	0.01	1.37	0.08	0.08	**3.72**	1.14	0.87	1.67	0.22	0.20	1.81	0.15	0.14	**2.40**	0.54	0.44	**1.95**	1.13	0.71	1.10	0.09	0.08
CCND1	1.04	0.10	0.09	1.14	0.04	0.04	1.65	0.21	0.19	1.05	0.09	0.09	1.17	0.12	0.11	1.34	0.17	0.15	0.97	0.09	0.08	1.07	0.05	0.05
CDKN1A1	1.00	0.16	0.13	**2.41**	1.64	0.98	**9.64**	3.93	2.79	1.00	0.32	0.24	**1.01**	0.22	0.18	1.14	0.14	0.13	**5.75**	5.00	2.67	1.38	0.03	0.03
CDKN1B	1.02	0.19	0.16	1.01	0.09	0.08	1.20	0.41	0.30	0.62	0.03	0.03	0.60	0.10	0.08	0.71	0.03	0.03	0.80	0.20	0.16	0.57	0.02	0.02
CDKN2B	1.14	0.21	0.18	3.27	2.51	1.42	3.62	2.32	1.41	1.11	0.23	0.19	1.28	0.18	0.16	1.45	0.44	0.34	2.34	1.42	0.88	0.85	0.06	0.06
E2F1	1.00	0.14	0.12	0.64	0.18	0.14	0.62	0.05	0.04	0.76	0.44	0.28	0.95	0.11	0.10	0.81	0.10	0.09	1.27	0.04	0.04	0.92	0.04	0.04
EGFR	1.10	0.10	0.09	1.31	0.30	0.24	1.93	0.49	0.39	0.80	0.39	0.26	0.95	0.07	0.07	0.85	0.05	0.05	1.05	0.10	0.09	0.92	0.14	0.12
JUN	0.98	0.48	0.32	**4.16**	1.91	1.31	**9.49**	2.73	2.12	**3.39**	1.89	1.21	**5.92**	0.30	0.28	**4.11**	1.04	0.83	**4.93**	0.52	0.47	**2.60**	0.21	0.19
MAP3K5	1.04	0.11	0.10	1.04	0.13	0.11	1.00	0.07	0.07	0.74	0.17	0.14	0.76	0.03	0.03	0.72	0.08	0.07	0.69	0.12	0.10	0.72	0.08	0.07
MDM2	1.04	0.12	0.11	1.40	0.35	0.28	4.82	2.22	1.52	1.20	0.07	0.07	1.23	0.04	0.04	1.52	0.13	0.12	3.17	2.93	1.52	1.45	0.12	0.11
MYC	0.99	0.14	0.12	0.89	0.08	0.07	1.23	0.09	0.09	0.88	0.23	0.19	0.97	0.14	0.12	0.84	0.07	0.06	1.13	0.02	0.02	1.04	0.13	0.11
PLK3	0.98	0.10	0.09	**2.07**	1.24	0.78	**4.06**	1.52	1.11	0.94	0.50	0.33	1.26	0.07	0.06	1.42	0.38	0.30	**3.86**	2.64	1.57	1.52	0.08	0.07
PPM1D	1.01	0.11	0.10	1.21	0.46	0.33	**3.23**	1.28	0.92	0.90	0.28	0.21	1.09	0.08	0.08	1.03	0.09	0.08	**2.51**	1.95	1.10	1.10	0.08	0.07
SIRT2	0.94	0.21	0.17	1.11	0.39	0.29	1.55	0.28	0.23	1.17	0.35	0.27	1.47	0.03	0.03	1.29	0.15	0.13	0.99	0.16	0.14	0.87	0.06	0.06
TP53	1.06	0.14	0.12	1.65	0.14	0.13	**1.92**	0.50	0.40	0.59	0.06	0.06	0.71	0.01	0.01	0.89	0.05	0.05	1.29	0.18	0.16	0.92	0.04	0.04
VEGFA	1.07	0.20	0.17	**4.40**	3.13	1.83	**5.00**	5.51	2.62	1.21	0.14	0.12	**2.22**	0.98	0.68	**1.92**	0.64	0.48	**3.79**	2.28	1.42	1.64	0.32	0.27

APEX1	1.00	0.02	0.02	0.94	0.05	0.05	1.03	0.02	0.02	0.89	0.10	0.09	0.82	0.09	0.08	0.85	0.11	0.10	0.91	0.07	0.07	0.92	0.05	0.05
ATM	1.20	0.21	0.18	1.68	0.46	0.36	**2.02**	0.83	0.59	0.92	0.01	0.01	0.94	0.04	0.04	1.08	0.11	0.10	1.14	0.45	0.32	0.86	0.07	0.07
ATR	0.98	0.09	0.08	0.88	0.14	0.12	0.85	0.09	0.08	0.76	0.13	0.11	0.83	0.03	0.03	0.72	0.08	0.07	0.83	0.09	0.08	0.89	0.12	0.10
BRCA1	1.09	0.09	0.09	1.08	0.19	0.16	1.18	0.06	0.06	0.78	0.14	0.12	0.87	0.02	0.02	0.84	0.08	0.07	1.18	0.08	0.07	0.92	0.12	0.10
BRCA2	1.09	0.05	0.05	0.80	0.12	0.11	0.77	0.05	0.04	0.82	0.02	0.02	0.74	0.02	0.02	0.72	0.16	0.13	1.03	0.16	0.14	0.84	0.08	0.07
DDB1	1.04	0.10	0.09	1.05	0.05	0.04	1.08	0.25	0.21	1.06	0.21	0.18	1.19	0.09	0.08	1.05	0.16	0.14	0.93	0.08	0.08	1.00	0.03	0.03
DDB2	1.02	0.19	0.16	1.00	0.26	0.20	**2.59**	0.64	0.52	0.74	0.06	0.05	0.68	0.02	0.02	0.70	0.03	0.03	**1.98**	1.28	0.78	0.78	0.02	0.02
ERCC1	1.01	0.02	0.02	1.43	0.40	0.31	**1.94**	0.29	0.25	0.93	0.07	0.07	0.96	0.17	0.14	0.97	0.09	0.08	1.23	0.26	0.22	0.87	0.07	0.07
ERCC2	1.01	0.01	0.01	0.79	0.07	0.06	0.67	0.04	0.03	1.04	0.41	0.30	0.99	0.12	0.11	0.92	0.18	0.15	0.76	0.17	0.14	0.87	0.05	0.05
ERCC4	1.03	0.11	0.10	1.20	0.21	0.18	1.67	0.56	0.42	0.75	0.03	0.03	0.72	0.01	0.01	0.81	0.06	0.06	1.09	0.33	0.26	0.66	0.01	0.01
ERCC5	1.05	0.17	0.15	1.19	0.24	0.20	1.75	0.57	0.43	0.89	0.08	0.08	0.85	0.14	0.12	0.93	0.06	0.06	0.96	0.24	0.19	0.67	0.01	0.01
LIG1	1.05	0.19	0.16	0.74	0.10	0.09	0.74	0.04	0.04	0.66	0.44	0.26	0.89	0.12	0.10	0.74	0.09	0.08	1.05	0.04	0.04	1.00	0.07	0.07
LIG3	1.06	0.13	0.12	1.07	0.14	0.12	1.05	0.22	0.18	0.92	0.31	0.23	1.05	0.09	0.09	1.00	0.03	0.03	0.91	0.06	0.05	0.94	0.07	0.07
MGMT	1.03	0.17	0.14	0.85	0.10	0.09	0.71	0.03	0.03	0.86	0.09	0.08	0.71	0.05	0.05	0.71	0.10	0.08	0.91	0.08	0.07	0.83	0.05	0.05
MLH1	1.07	0.19	0.16	1.70	0.37	0.31	**2.27**	0.81	0.60	0.98	0.20	0.16	1.18	0.05	0.05	1.14	0.09	0.08	1.86	0.47	0.38	1.04	0.21	0.18
MSH2	1.03	0.06	0.06	0.67	0.16	0.13	0.70	0.03	0.03	0.83	0.01	0.01	0.84	0.02	0.02	0.83	0.07	0.07	0.87	0.06	0.05	0.82	0.04	0.04
OGG1	1.00	0.12	0.11	0.81	0.08	0.07	0.77	0.05	0.05	0.93	0.23	0.18	0.85	0.04	0.04	0.83	0.08	0.07	0.85	0.02	0.02	0.90	0.07	0.06
PARP1	1.06	0.00	0.00	0.82	0.10	0.09	0.64	0.12	0.10	0.83	0.17	0.14	0.83	0.03	0.03	0.83	0.08	0.07	0.88	0.12	0.10	0.85	0.04	0.04
PCNA	1.00	0.30	0.23	0.61	0.11	0.09	1.18	0.09	0.08	0.97	0.23	0.19	0.93	0.11	0.10	0.96	0.17	0.14	1.18	0.35	0.27	0.93	0.02	0.02
POLB	0.99	0.04	0.04	1.18	0.20	0.17	1.40	0.32	0.26	1.02	0.01	0.01	0.95	0.05	0.05	0.96	0.03	0.03	1.07	0.17	0.14	0.93	0.08	0.07
POLD1	1.01	0.25	0.20	0.79	0.03	0.03	0.66	0.14	0.11	0.77	0.61	0.34	1.14	0.07	0.06	1.01	0.14	0.13	0.95	0.02	0.02	1.03	0.05	0.05
RAD50	1.06	0.04	0.04	1.30	0.31	0.25	1.53	0.34	0.28	0.74	0.13	0.11	0.80	0.04	0.03	0.78	0.08	0.07	1.09	0.18	0.15	0.87	0.12	0.11
RAD51	1.03	0.04	0.04	0.75	0.23	0.18	0.89	0.12	0.10	1.04	0.17	0.15	1.05	0.07	0.07	1.03	0.03	0.03	1.13	0.07	0.07	1.10	0.02	0.02
RRM2B	1.01	0.03	0.03	1.32	0.34	0.27	**2.60**	0.94	0.69	0.82	0.21	0.16	0.91	0.04	0.03	1.07	0.07	0.06	1.56	0.55	0.41	0.99	0.05	0.04
XPA	1.04	0.25	0.20	1.09	0.11	0.10	1.51	0.19	0.17	0.85	0.08	0.08	0.73	0.07	0.06	0.88	0.03	0.03	1.12	0.23	0.19	0.89	0.04	0.04
XPC	1.06	0.16	0.14	1.20	0.16	0.14	**2.89**	1.34	0.91	0.82	0.05	0.05	0.77	0.02	0.01	0.97	0.07	0.06	**1.85**	1.13	0.70	0.97	0.10	0.09
XRCC5	1.03	0.01	0.01	0.83	0.10	0.09	0.71	0.11	0.09	0.93	0.02	0.02	0.87	0.01	0.01	0.89	0.04	0.04	0.92	0.04	0.04	0.92	0.01	0.01
APAF1	1.05	0.24	0.19	1.03	0.18	0.16	1.08	0.24	0.20	0.91	0.39	0.27	0.92	0.13	0.11	0.92	0.06	0.06	1.29	0.47	0.35	0.93	0.14	0.12

BAX	0.99	0.19	0.16	1.11	0.38	0.29	**2.37**	0.74	0.56	1.03	0.44	0.31	1.36	0.14	0.13	1.18	0.10	0.09	1.48	0.49	0.37	1.23	0.09	0.09
BBC3	1.41	0.01	0.01	**2.73**	0.55	0.45	**6.10**	3.90	2.38	1.30	0.04	0.04	0.87	0.45	0.29	1.22	0.28	0.23	**6.85**	5.15	2.94	**1.31**	0.17	0.15
BCL2	1.02	0.24	0.20	1.02	0.08	0.07	1.27	0.20	0.17	0.71	0.52	0.30	0.95	0.16	0.14	0.95	0.09	0.08	0.86	0.27	0.21	0.86	0.11	0.10
BCL2L1	0.94	0.08	0.07	1.56	0.86	0.55	**2.12**	0.48	0.39	0.95	0.39	0.28	1.34	0.11	0.10	1.24	0.23	0.19	1.05	0.11	0.10	1.01	0.04	0.04
PMAIP1	1.04	0.07	0.07	1.88	0.37	0.31	**3.24**	0.54	0.47	**2.21**	0.26	0.23	**2.46**	0.48	0.40	**2.04**	0.25	0.22	**4.45**	3.61	2.00	1.60	0.19	0.17
TNFRSF10B	0.96	0.10	0.09	**2.80**	1.40	0.93	**4.21**	2.62	1.61	1.27	0.08	0.08	1.46	0.18	0.16	1.63	0.41	0.33	**3.33**	2.00	1.25	1.51	0.03	0.03
XIAP	1.04	0.10	0.09	1.57	0.47	0.36	**2.14**	1.10	0.73	1.24	0.04	0.04	1.31	0.11	0.11	1.26	0.13	0.11	1.20	0.25	0.21	0.97	0.06	0.06

Table A6: mRNA levels in p53-proficient HCT 116 cells: Exposure to selenomethionine (24h: 100 µM-500 µM. 8h 500 µM) in combination with 10 µM $CdCl_2$.

	Selenomethionine (24h)									Selenomethionine (24h) + 10 µM $CdCl_2$									Selenomethionine (8h)			Selenomethionine (24h) + 10 µM $CdCl_2$		
	100 µM			300 µM			500 µM			100 µM			300 µM			500 µM			500 µM			500 µM		
	Mean	SD err+	SD err-	**Mean**	SD err+	SD err-	**Mean**	SD err+	SD err-	**Mean**	SD err+	SD err-	**Mean**	SD err+	SD err-	**Mean**	SD err+	SD err-	**Mean**	SD err+	SD err-	**Mean**	SD err+	SD err-
ABCB1	0.81	0.03	0.03	0.53	0.03	0.03	0.55	0.07	0.06	**2.01**	1.03	0.68	**2.53**	2.04	1.13	**3.24**	3.97	1.78	1.13	0.61	0.40	1.29	0.71	0.46
ABCC1	1.38	0.16	0.14	1.12	0.18	0.16	1.38	0.33	0.27	1.20	0.17	0.15	1.19	0.28	0.23	1.43	0.18	0.16	0.97	0.22	0.18	1.11	0.12	0.11
CAT	0.94	0.00	0.00	0.95	0.05	0.05	1.05	0.12	0.10	0.64	0.09	0.08	0.69	0.05	0.05	0.63	0.07	0.07	0.96	0.10	0.09	0.92	0.05	0.05
EPHX1	1.11	0.29	0.23	1.04	0.23	0.19	1.50	0.49	0.37	0.85	0.06	0.05	1.00	0.19	0.16	1.15	0.16	0.14	1.00	0.04	0.04	1.02	0.06	0.06
FTH1	0.94	0.22	0.18	1.49	2.08	0.87	**3.32**	3.17	1.62	**1.95**	0.52	0.41	**6.32**	5.01	2.79	**2.12**	0.61	0.47	**2.09**	2.25	1.08	**2.23**	0.95	0.67
G6PD	0.94	0.13	0.12	0.77	0.12	0.11	0.95	0.26	0.21	1.35	0.28	0.23	1.44	0.52	0.38	1.65	0.38	0.31	1.04	0.39	0.28	1.19	0.28	0.23
GCLC	0.84	0.01	0.01	1.13	0.22	0.18	1.31	0.41	0.31	1.52	0.21	0.18	**2.08**	0.09	0.09	1.67	0.21	0.19	1.40	2.04	0.83	**2.30**	2.44	1.18
GPX1	0.87	0.05	0.05	0.89	0.14	0.12	0.89	0.18	0.15	0.62	0.21	0.16	0.77	0.03	0.03	0.62	0.02	0.02	1.03	0.21	0.17	0.89	0.09	0.08
GSR	1.04	0.02	0.02	1.07	0.10	0.09	0.99	0.22	0.18	1.62	0.07	0.07	1.64	0.16	0.15	1.47	0.03	0.03	1.25	0.70	0.45	1.45	0.38	0.30
GSTP1	0.88	0.03	0.03	0.86	0.09	0.08	0.87	0.09	0.09	0.98	0.13	0.12	1.12	0.06	0.06	1.04	0.08	0.08	1.02	0.13	0.11	0.98	0.05	0.04
KEAP1	0.90	0.11	0.10	0.66	0.06	0.06	0.73	0.19	0.15	0.62	0.05	0.04	0.46	0.01	0.01	0.48	0.11	0.09	0.66	0.27	0.19	0.69	0.07	0.06
MT1X	0.98	0.01	0.01	1.32	0.44	0.33	1.66	0.80	0.54	**17.89**	4.44	3.55	**51.48**	35.65	21.06	**47.38**	46.51	23.47	**4.32**	22.00	3.61	**11.47**	60.24	9.64
MT2A	1.07	0.38	0.28	1.24	0.47	0.34	1.66	0.71	0.49	**5.45**	0.79	0.69	**12.19**	5.26	3.67	**11.07**	8.66	4.86	**2.31**	3.66	1.41	**3.46**	5.38	2.11

NAT1	0.78	0.01	0.01	0.85	0.13	0.11	1.01	0.14	0.12	**2.03**	0.86	0.61	**2.71**	0.95	0.70	**3.21**	0.76	0.61	0.76	0.07	0.06	0.75	0.15	0.12
NFEL2	1.15	0.16	0.14	0.98	0.25	0.20	1.32	0.38	0.30	0.74	0.04	0.04	0.81	0.11	0.09	0.91	0.15	0.13	1.06	0.16	0.14	1.04	0.13	0.12
NQO1	0.94	0.02	0.02	0.85	0.15	0.12	1.07	0.28	0.22	1.37	0.08	0.08	1.33	0.22	0.19	1.28	0.05	0.05	1.29	0.67	0.44	1.49	0.58	0.42
PRDX1	0.90	0.05	0.04	0.76	0.11	0.09	0.89	0.10	0.09	1.22	0.00	0.00	1.41	0.37	0.29	1.42	0.34	0.28	1.17	0.10	0.10	1.21	0.12	0.11
SEPP1	0.68	0.10	0.09	0.60	0.04	0.04	0.61	0.01	0.01	0.43	0.05	0.05	0.38	0.15	0.11	0.50	0.20	0.14	0.67	0.25	0.18	0.69	0.08	0.07
SLC30A1	0.96	0.02	0.02	1.14	0.24	0.20	1.32	0.41	0.31	**3.57**	0.21	0.20	**5.19**	0.51	0.47	**4.39**	0.13	0.13	**2.28**	4.52	1.52	**4.48**	7.91	2.86
SOD1	0.85	0.02	0.02	0.85	0.11	0.09	0.84	0.06	0.05	0.98	0.10	0.09	1.32	0.41	0.31	1.27	0.51	0.36	1.01	0.14	0.12	0.98	0.07	0.07
SOD2	1.02	0.02	0.02	0.92	0.20	0.17	1.17	0.26	0.21	0.93	0.03	0.03	0.92	0.18	0.15	0.95	0.16	0.14	0.98	0.13	0.11	0.97	0.06	0.06
SULT1A	0.86	0.11	0.10	0.77	0.22	0.17	0.82	0.20	0.16	0.69	0.14	0.11	0.90	0.18	0.15	0.63	0.04	0.03	0.98	0.24	0.19	0.84	0.13	0.11
TFRC	1.11	0.07	0.06	1.06	0.05	0.05	1.01	0.14	0.12	1.26	0.09	0.09	1.38	0.03	0.03	1.31	0.06	0.06	1.07	0.36	0.27	1.03	0.12	0.11
TXN	0.97	0.09	0.08	0.87	0.17	0.15	1.10	0.16	0.14	1.42	0.24	0.20	1.65	0.46	0.36	1.82	0.62	0.46	1.12	0.21	0.18	1.20	0.17	0.15
TXNRD1	1.04	0.05	0.04	1.54	0.17	0.15	1.55	0.29	0.24	**2.18**	0.01	0.01	**3.33**	0.80	0.64	**2.77**	0.45	0.39	**1.90**	2.90	1.15	**2.80**	2.26	1.25
HMOX1	1.20	0.02	0.02	1.32	0.24	0.20	**1.99**	0.78	0.56	**81.48**	52.43	31.90	**129.02**	74.53	47.24	**158.79**	103.47	62.65	**5.13**	53.60	4.68	**24.02**	358.11	22.51
HSPA1A	0.73	0.01	0.01	0.90	0.20	0.16	1.07	0.22	0.19	**39.77**	167.97	32.16	**86.32**	555.66	74.71	**139.09**	1295.40	125.61	1.88	4.21	1.30	**3.39**	8.99	2.46
IL8	1.75	0.01	0.01	**4.81**	0.68	0.60	**7.98**	0.30	0.29	**6.53**	3.38	2.23	**12.37**	3.06	2.45	**16.65**	8.51	5.63	**2.78**	1.99	1.16	**4.04**	2.28	1.46
NFKB1	1.03	0.14	0.13	0.90	0.09	0.08	1.05	0.13	0.12	0.71	0.11	0.10	0.59	0.04	0.04	0.59	0.15	0.12	0.96	0.13	0.12	0.92	0.05	0.05
NFKB1A	0.81	0.09	0.08	0.93	0.39	0.28	1.24	0.54	0.37	0.53	0.38	0.22	0.67	0.16	0.13	0.39	0.21	0.14	0.95	0.06	0.06	0.81	0.23	0.18
NFKB2	1.12	0.30	0.24	1.13	0.03	0.03	1.40	0.22	0.19	1.71	0.29	0.25	2.27	0.50	0.41	2.97	0.73	0.59	0.94	0.30	0.23	0.96	0.09	0.08
CCND1	1.21	0.12	0.11	1.03	0.24	0.20	1.28	0.34	0.27	0.98	0.05	0.05	1.06	0.32	0.25	1.13	0.31	0.24	0.95	0.19	0.16	1.07	0.09	0.09
CDKN1A1	0.91	0.05	0.05	0.96	0.20	0.17	1.18	0.42	0.31	0.86	0.11	0.09	1.31	0.40	0.31	1.47	0.39	0.31	0.81	0.11	0.10	0.75	0.07	0.06
CDKN1B	0.87	0.03	0.03	0.62	0.21	0.15	0.83	0.25	0.19	0.45	0.02	0.02	0.42	0.13	0.10	0.49	0.06	0.06	0.69	0.22	0.16	0.62	0.29	0.20
CDKN2B	**2.06**	0.37	0.31	**2.39**	1.06	0.73	**4.19**	2.63	1.62	1.48	0.11	0.11	**3.33**	1.36	0.96	**4.88**	1.91	1.37	1.65	0.50	0.39	1.75	0.18	0.17
E2F1	0.97	0.02	0.02	1.06	0.15	0.13	0.68	0.13	0.11	0.65	0.13	0.11	**0.58**	0.01	0.01	**0.45**	0.07	0.06	0.95	0.31	0.23	0.78	0.24	0.19
EGFR	1.12	0.07	0.07	1.72	0.18	0.16	1.85	0.39	0.32	0.96	0.07	0.07	1.62	0.32	0.27	1.69	0.13	0.12	1.07	0.37	0.27	1.11	0.12	0.11
JUN	1.19	0.30	0.24	**2.81**	0.34	0.30	**2.90**	0.14	0.13	**4.37**	0.99	0.81	**10.79**	3.30	2.53	**10.94**	3.65	2.74	1.76	2.60	1.05	**3.62**	6.08	2.27
MAP3K5	0.98	0.11	0.10	1.34	0.10	0.09	1.43	0.13	0.12	0.76	0.17	0.14	0.97	0.08	0.08	0.99	0.09	0.08	0.89	0.11	0.10	0.85	0.14	0.12
MDM2	1.04	0.03	0.03	0.93	0.15	0.13	1.19	0.22	0.19	1.11	0.10	0.09	1.16	0.30	0.24	1.38	0.34	0.27	0.73	0.10	0.09	0.80	0.01	0.01
MYC	0.98	0.07	0.06	0.80	0.10	0.09	0.70	0.07	0.07	**0.65**	0.34	0.22	**0.52**	0.04	0.04	**0.35**	0.10	0.08	0.96	0.37	0.27	0.94	0.09	0.08

PLK3	1.27	0.33	0.26	1.43	0.52	0.38	1.80	0.98	0.63	0.97	0.43	0.30	1.86	0.47	0.38	1.89	0.59	0.45	1.05	0.39	0.28	1.03	0.12	0.11
PPM1D	0.86	0.09	0.08	0.99	0.15	0.13	1.00	0.23	0.19	0.83	0.21	0.17	1.10	0.23	0.19	0.91	0.13	0.11	0.80	0.09	0.08	0.72	0.19	0.15
SIRT2	1.15	0.12	0.11	1.40	0.26	0.22	1.58	0.51	0.39	1.28	0.13	0.12	2.07	0.70	0.52	2.27	1.01	0.70	1.05	0.26	0.21	0.97	0.17	0.14
TP53	1.22	0.14	0.13	1.26	0.26	0.22	1.76	0.45	0.36	0.66	0.00	0.00	0.82	0.13	0.11	1.02	0.06	0.06	1.03	0.13	0.12	1.00	0.14	0.12
VEGFA	1.52	0.18	0.16	**2.41**	2.50	1.23	**5.45**	5.29	2.68	1.52	0.08	0.08	**4.68**	3.74	2.08	**3.23**	1.04	0.78	**3.03**	1.68	1.08	**2.84**	1.35	0.92
APEX1	0.82	0.10	0.09	0.64	0.10	0.09	0.73	0.16	0.13	**0.60**	0.13	0.11	**0.49**	0.06	0.05	**0.41**	0.08	0.07	0.97	0.10	0.09	0.88	0.06	0.05
ATM	0.93	0.06	0.06	0.88	0.23	0.18	0.98	0.32	0.24	0.81	0.15	0.13	1.03	0.54	0.36	1.28	0.64	0.43	0.77	0.10	0.09	0.81	0.05	0.05
ATR	0.76	0.04	0.04	0.72	0.16	0.13	0.70	0.10	0.09	0.59	0.21	0.15	0.78	0.18	0.15	0.64	0.17	0.13	0.89	0.09	0.08	0.82	0.12	0.11
BRCA1	1.02	0.03	0.03	1.22	0.13	0.12	0.85	0.06	0.05	0.68	0.18	0.14	0.67	0.04	0.03	0.53	0.07	0.06	0.91	0.10	0.09	0.81	0.28	0.21
BRCA2	1.00	0.02	0.02	0.93	0.09	0.09	0.77	0.04	0.04	0.70	0.06	0.05	0.67	0.11	0.10	0.62	0.03	0.03	0.85	0.15	0.13	0.76	0.21	0.16
DDB1	1.00	0.17	0.15	0.95	0.11	0.10	0.92	0.14	0.12	0.94	0.08	0.07	0.85	0.01	0.01	0.83	0.13	0.12	1.03	0.29	0.22	1.04	0.07	0.06
DDB2	1.07	0.47	0.33	**0.68**	0.10	0.09	**0.78**	0.14	0.12	**0.55**	0.11	0.09	**0.41**	0.04	0.04	**0.40**	0.08	0.07	**0.73**	0.14	0.12	**0.60**	0.21	0.16
ERCC1	1.04	0.08	0.08	1.27	0.38	0.29	1.73	0.56	0.42	1.06	0.06	0.06	**2.05**	0.89	0.62	**2.29**	1.23	0.80	1.02	0.08	0.08	1.01	0.04	0.03
ERCC2	1.08	0.18	0.16	0.87	0.10	0.09	0.93	0.26	0.20	0.96	0.01	0.01	0.97	0.17	0.15	1.11	0.13	0.12	1.00	0.45	0.31	0.89	0.06	0.06
ERCC4	0.83	0.00	0.00	0.73	0.20	0.16	1.01	0.37	0.27	**0.54**	0.02	0.02	**0.65**	0.20	0.15	**0.74**	0.22	0.17	**0.65**	0.25	0.18	**0.60**	0.19	0.14
ERCC5	1.04	0.06	0.06	0.89	0.23	0.18	1.24	0.46	0.33	0.77	0.13	0.11	1.32	0.98	0.56	1.91	2.02	0.98	0.79	0.21	0.17	0.73	0.21	0.16
LIG1	0.89	0.09	0.08	**0.77**	0.08	0.07	**0.55**	0.02	0.02	**0.57**	0.24	0.17	**0.60**	0.05	0.05	**0.48**	0.03	0.03	0.96	0.40	0.28	0.87	0.20	0.16
LIG3	0.87	0.01	0.01	0.87	0.15	0.13	0.88	0.20	0.16	0.70	0.08	0.07	0.87	0.26	0.20	0.88	0.21	0.17	0.81	0.18	0.14	0.76	0.10	0.09
MGMT	1.06	0.18	0.15	0.74	0.22	0.17	1.01	0.20	0.17	0.75	0.01	0.01	0.78	0.25	0.19	0.90	0.21	0.17	0.97	0.10	0.09	0.89	0.06	0.05
MLH1	1.37	0.05	0.05	**2.19**	0.34	0.29	**2.15**	0.44	0.37	1.30	0.05	0.05	**2.52**	1.07	0.75	**2.58**	0.99	0.72	1.26	0.17	0.15	1.28	0.34	0.27
MSH2	0.70	0.03	0.03	**0.47**	0.06	0.05	**0.44**	0.02	0.02	**0.49**	0.08	0.07	**0.34**	0.04	0.04	**0.29**	0.02	0.02	0.76	0.17	0.14	0.67	0.16	0.13
OGG1	0.94	0.06	0.06	0.92	0.14	0.12	0.90	0.18	0.15	0.72	0.30	0.21	0.88	0.22	0.18	0.79	0.17	0.14	0.96	0.12	0.11	0.83	0.24	0.19
PARP1	0.95	0.04	0.04	0.77	0.06	0.06	0.83	0.11	0.10	0.78	0.04	0.04	0.70	0.11	0.09	0.74	0.07	0.06	0.97	0.23	0.18	0.96	0.02	0.02
PCNA	0.84	0.04	0.04	**0.51**	0.06	0.05	**0.48**	0.02	0.02	0.69	0.02	0.02	**0.41**	0.03	0.03	**0.34**	0.08	0.06	0.86	0.14	0.12	0.86	0.13	0.11
POLB	0.96	0.01	0.01	1.00	0.31	0.24	1.37	0.40	0.31	0.99	0.05	0.05	1.24	0.34	0.27	1.34	0.31	0.25	1.16	0.13	0.12	1.11	0.11	0.10
POLD1	0.94	0.06	0.05	0.87	0.07	0.07	**0.65**	0.07	0.06	0.68	0.22	0.17	0.82	0.19	0.16	**0.69**	0.11	0.10	1.00	0.69	0.41	0.95	0.16	0.13
RAD50	0.90	0.08	0.07	0.98	0.20	0.17	1.02	0.21	0.18	0.65	0.11	0.10	0.86	0.12	0.10	0.78	0.09	0.08	0.92	0.03	0.03	0.89	0.18	0.15
RAD51	0.99	0.03	0.03	0.99	0.12	0.11	0.75	0.12	0.11	0.89	0.21	0.17	0.60	0.19	0.15	0.49	0.22	0.15	1.15	0.18	0.15	1.10	0.04	0.04

RRM2B	0.90	0.04	0.03	0.93	0.13	0.11	1.23	0.33	0.26	0.74	0.01	0.01	0.67	0.06	0.05	0.73	0.14	0.12	0.83	0.14	0.12	0.84	0.12	0.10
XPA	0.86	0.06	0.06	0.65	0.18	0.14	0.90	0.26	0.20	0.69	0.05	0.05	0.99	0.41	0.29	1.20	0.74	0.46	0.92	0.13	0.12	0.92	0.08	0.07
XPC	0.94	0.12	0.11	0.74	0.14	0.12	0.99	0.33	0.25	0.73	0.08	0.07	0.82	0.19	0.15	1.08	0.27	0.21	0.67	0.14	0.12	0.68	0.05	0.05
XRCC5	0.89	0.06	0.06	0.69	0.08	0.07	0.70	0.09	0.08	0.83	0.05	0.05	0.65	0.07	0.06	0.61	0.03	0.02	0.99	0.12	0.11	1.00	0.05	0.04
APAF1	0.92	0.13	0.12	1.03	0.09	0.08	0.91	0.12	0.10	0.74	0.20	0.16	0.71	0.08	0.07	0.63	0.13	0.11	0.95	0.24	0.19	0.93	0.15	0.13
BAX	0.82	0.01	0.01	0.81	0.23	0.18	0.86	0.30	0.22	0.89	0.29	0.22	1.23	0.58	0.40	1.18	0.55	0.37	0.88	0.33	0.24	0.86	0.04	0.04
BBC3	1.19	0.00	0.00	1.45	0.20	0.18	1.47	0.34	0.28	1.10	0.02	0.02	1.14	0.33	0.26	1.82	0.62	0.46	0.94	0.16	0.14	0.97	0.10	0.09
BCL2	0.86	0.12	0.10	0.94	0.07	0.06	0.77	0.10	0.09	**0.57**	0.36	0.22	**0.56**	0.16	0.13	**0.55**	0.05	0.05	0.89	0.32	0.24	0.99	0.17	0.15
BCL2L1	1.28	0.37	0.29	1.39	0.35	0.28	1.58	0.54	0.40	0.93	0.40	0.28	1.32	0.19	0.17	1.19	0.04	0.04	1.12	0.52	0.35	1.08	0.14	0.12
PMAIP1	1.38	0.09	0.08	1.87	0.22	0.20	**2.10**	0.29	0.26	**3.16**	0.11	0.11	**4.01**	0.95	0.77	**4.12**	0.67	0.58	**1.85**	0.84	0.58	**2.47**	1.02	0.72
TNFRSF10B	1.31	0.29	0.24	1.79	0.34	0.28	**2.74**	1.10	0.78	1.59	0.82	0.54	**3.03**	0.83	0.65	**3.94**	1.33	0.99	**1.22**	0.58	0.39	1.48	0.33	0.27
XIAP	1.02	0.07	0.06	1.31	0.30	0.25	1.64	0.43	0.34	1.49	0.35	0.29	2.02	0.67	0.50	2.19	0.56	0.45	1.04	0.16	0.14	1.10	0.15	0.13

Table A7: mRNA levels in p53-deficient HCT 116 cells: Exposure to cadmium chloride (24h: 5 µM-50 µM)

	$CdCl_2$ (24 h)								
	5 µM			10 µM			50 µM		
	Mean	SD err+	SD err-	**Mean**	SD err+	SD err-	**Mean**	SD err+	SD err-
ABCB1	1.19	0.04	0.04	1.80	0.30	0.26	**3.11**	0.30	0.28
ABCC1	1.07	0.00	0.00	1.14	0.16	0.14	1.16	0.08	0.07
CAT	0.93	0.05	0.05	0.89	0.04	0.04	0.82	0.04	0.04
EPHX1	1.10	0.08	0.08	1.13	0.05	0.05	1.13	0.01	0.01
FTH1	**1.94**	0.57	0.44	**2.16**	0.63	0.49	**2.90**	0.43	0.37
G6PD	1.51	0.09	0.09	1.61	0.35	0.29	1.89	0.19	0.17
GCLC	1.28	0.20	0.18	1.53	0.19	0.17	1.60	0.02	0.02
GPX1	0.88	0.01	0.01	0.90	0.07	0.07	0.91	0.04	0.04
GSR	1.23	0.16	0.14	1.45	0.03	0.03	1.57	0.00	0.00
GSTP1	1.04	0.05	0.04	1.16	0.05	0.05	1.16	0.01	0.01
KEAP1	1.15	0.04	0.04	1.15	0.24	0.20	1.08	0.09	0.08
MT1X	**18.18**	3.23	2.75	**19.75**	5.28	4.17	**25.06**	2.36	2.15
MT2A	**4.94**	0.57	0.51	**5.22**	0.49	0.45	**5.69**	0.23	0.23
NAT1	1.18	0.17	0.15	1.42	0.31	0.26	**1.92**	0.09	0.08
NFEL2L	0.91	0.06	0.05	0.93	0.05	0.05	0.96	0.02	0.02
NQO1	1.63	0.04	0.04	1.62	0.26	0.22	1.76	0.11	0.10
PRDX1	1.23	0.02	0.02	1.29	0.08	0.08	1.51	0.02	0.02
SEPP1	0.86	0.03	0.03	0.73	0.04	0.04	0.66	0.02	0.02
SLC30A1	**3.73**	0.58	0.50	**3.78**	0.49	0.43	**3.79**	0.26	0.24
SOD1	1.04	0.09	0.08	1.13	0.15	0.13	1.24	0.10	0.09
SOD2	1.01	0.02	0.02	1.01	0.06	0.05	1.07	0.06	0.05
SULT1A	0.96	0.15	0.13	1.12	0.04	0.04	0.97	0.02	0.02
TFRC	1.07	0.04	0.04	1.24	0.06	0.06	1.27	0.04	0.04
TXN	1.18	0.01	0.01	1.31	0.03	0.03	1.53	0.03	0.03
TXNRD1	1.61	0.36	0.29	**1.88**	0.32	0.27	**2.53**	0.06	0.06
HMOX1	**8.13**	3.44	2.42	**22.42**	11.17	7.45	**46.08**	5.97	5.28
HSPA1A	**72.34**	41.29	26.29	**202.03**	442.09	138.66	**909.98**	51.68	48.90
IL8	1.25	0.20	0.17	**1.93**	0.41	0.34	**2.80**	0.19	0.18
NFKB1	0.96	0.02	0.02	0.99	0.07	0.07	0.90	0.03	0.03
NFKB1A	0.88	0.15	0.13	1.07	0.16	0.14	0.98	0.10	0.09
NFKB2	1.31	0.05	0.04	1.47	0.40	0.32	1.68	0.06	0.06
CCND1	1.00	0.06	0.06	1.07	0.07	0.07	1.18	0.07	0.07
CDKN1A1	1.20	0.14	0.13	1.22	0.26	0.21	1.39	0.07	0.07
CDKN1B	0.92	0.02	0.02	0.89	0.07	0.07	0.93	0.10	0.09
CDKN2B	1.15	0.01	0.01	1.29	0.25	0.21	1.34	0.08	0.08
E2F1	0.96	0.14	0.12	0.89	0.04	0.04	0.81	0.03	0.02
EGFR	1.08	0.15	0.13	1.13	0.16	0.14	1.25	0.04	0.04
JUN	1.50	0.39	0.31	**2.03**	1.08	0.70	**3.55**	0.13	0.13

MAP3K5	1.00	0.06	0.05	1.01	0.05	0.05	0.97	0.00	0.00
MDM2	1.00	0.01	0.01	1.08	0.07	0.07	1.14	0.09	0.09
MYC	0.87	0.05	0.05	0.88	0.03	0.03	0.76	0.00	0.00
PLK3	1.14	0.09	0.08	1.16	0.14	0.12	1.06	0.01	0.01
PPM1D	0.91	0.10	0.09	1.05	0.09	0.08	1.16	0.09	0.08
SIRT2	1.22	0.18	0.16	1.27	0.28	0.23	1.57	0.03	0.03
TP53	0.81	0.02	0.02	0.84	0.03	0.03	0.67	0.01	0.01
VEGFA	1.16	0.14	0.13	1.28	0.20	0.18	1.43	0.10	0.09
APEX1	0.94	0.01	0.01	0.94	0.07	0.07	0.79	0.02	0.02
ATM	0.91	0.09	0.08	1.10	0.07	0.06	1.15	0.06	0.06
ATR	1.03	0.12	0.10	1.00	0.12	0.11	0.98	0.07	0.06
BRCA1	0.92	0.10	0.09	0.98	0.09	0.08	0.92	0.07	0.07
BRCA2	0.95	0.08	0.07	1.04	0.04	0.04	1.01	0.00	0.00
DDB1	1.02	0.05	0.05	1.13	0.08	0.08	1.09	0.01	0.01
DDB2	**0.90**	0.02	0.02	**0.87**	0.09	0.08	**0.72**	0.05	0.04
ERCC1	1.03	0.07	0.06	1.05	0.08	0.08	1.11	0.02	0.02
ERCC2	1.21	0.10	0.09	1.17	0.22	0.19	1.17	0.05	0.04
ERCC4	0.86	0.03	0.03	0.91	0.03	0.03	0.87	0.11	0.10
ERCC5	0.98	0.06	0.05	1.13	0.10	0.09	1.32	0.13	0.12
LIG1	0.91	0.09	0.08	0.94	0.03	0.03	0.88	0.02	0.02
LIG3	1.01	0.09	0.09	1.02	0.04	0.04	1.08	0.02	0.02
MGMT	0.92	0.11	0.10	0.99	0.05	0.04	0.94	0.01	0.01
MLH1	1.09	0.25	0.20	1.30	0.09	0.09	1.35	0.01	0.01
MSH2	0.93	0.03	0.03	0.90	0.02	0.02	0.88	0.04	0.04
OGG1	1.07	0.11	0.10	1.09	0.09	0.08	1.13	0.09	0.08
PARP1	0.98	0.04	0.03	0.93	0.10	0.09	0.91	0.09	0.08
PCNA	0.93	0.01	0.01	0.93	0.06	0.06	0.95	0.03	0.03
POLB	1.00	0.02	0.02	1.02	0.03	0.03	1.03	0.02	0.02
POLD1	1.11	0.18	0.15	1.11	0.14	0.12	1.09	0.09	0.08
RAD50	0.88	0.09	0.08	0.98	0.09	0.08	0.90	0.03	0.03
RAD51	1.06	0.03	0.03	1.08	0.02	0.01	0.99	0.02	0.02
RRM2B	0.99	0.01	0.01	0.99	0.07	0.07	0.91	0.03	0.03
XPA	0.89	0.06	0.06	0.93	0.08	0.07	0.92	0.09	0.08
XPC	0.95	0.01	0.01	1.00	0.10	0.09	1.03	0.14	0.12
XRCC5	1.03	0.02	0.02	1.05	0.09	0.08	1.02	0.07	0.06
APAF1	1.11	0.20	0.17	1.19	0.09	0.08	1.18	0.04	0.04
BAX	1.00	0.10	0.09	1.07	0.04	0.04	1.03	0.05	0.04
BBC3	0.94	0.04	0.04	1.32	0.10	0.09	1.16	0.19	0.17
BCL2	0.99	0.12	0.11	0.96	0.03	0.03	0.86	0.04	0.03
BCL2L1	1.23	0.21	0.18	1.14	0.14	0.13	1.29	0.10	0.09
PMAIP1	1.28	0.14	0.13	1.48	0.32	0.26	**1.88**	0.08	0.08
TNFRSF10B	1.01	0.04	0.04	1.10	0.13	0.12	1.10	0.10	0.09
XIAP	1.13	0.10	0.09	1.23	0.13	0.12	1.40	0.03	0.03

Table A8: mRNA levels in p53-deficient HCT 116 cells: Exposure to sodium selenite (24h; 5 µM) or selenomethionine (24h; 500 µM) in combination with 10 µM $CdCl_2$.

	Sodium selenite 5 µM (24h)			Sodium selenite 5 µM + 10 µM $CdCl_2$ (24h)			Selenomethionine 500 µM (24h)			Selenomethionine 500 µM + 10 µM CdCl2 (24h)		
	Mean	SD err+	SD err-	**Mean**	SD err+	SD err-	**Mean**	SD err+	SD err-	**Mean**	SD err+	SD err-
ABCB1	1.09	0.08	0.07	1.19	0.13	0.12	0.59	0.03	0.03	1.07	0.47	0.32
ABCC1	1.12	0.07	0.06	1.02	0.11	0.10	1.35	0.19	0.17	1.08	0.16	0.14
CAT	0.87	0.17	0.15	0.82	0.08	0.07	1.05	0.03	0.03	0.86	0.14	0.12
EPHX1	1.49	0.20	0.18	1.15	0.10	0.10	1.55	0.19	0.17	1.24	0.15	0.13
FTH1	**4.65**	2.47	1.61	**2.17**	3.15	1.29	**3.65**	2.92	1.62	**3.96**	3.50	1.86
G6PD	1.65	0.26	0.23	1.74	0.76	0.53	0.80	0.13	0.11	1.10	0.49	0.34
GCLC	**3.66**	3.51	1.79	**2.75**	0.28	0.25	1.47	0.26	0.22	**2.23**	0.41	0.35
GPX1	1.10	0.07	0.07	0.89	0.08	0.07	1.09	0.22	0.18	0.74	0.11	0.10
GSR	1.79	0.86	0.58	1.65	0.39	0.32	0.87	0.14	0.12	1.41	0.44	0.34
GSTP1	1.03	0.05	0.05	1.06	0.08	0.07	0.99	0.08	0.07	1.13	0.14	0.12
KEAP1	1.31	0.15	0.14	1.10	0.34	0.26	0.82	0.18	0.15	0.65	0.15	0.12
MT1X	1.25	0.55	0.38	**8.17**	4.23	2.79	**2.19**	0.56	0.45	**57.46**	24.36	17.11
MT2A	1.37	0.45	0.34	**3.84**	0.43	0.39	**2.43**	0.49	0.41	**8.50**	1.12	0.99
NAT1	0.65	0.18	0.14	0.85	0.02	0.02	1.02	0.15	0.13	**2.05**	1.23	0.77
NFEL2L	1.69	0.62	0.45	1.09	0.05	0.04	1.57	0.31	0.26	1.28	0.17	0.15
NQO1	**2.19**	1.19	0.77	**2.08**	0.50	0.40	1.02	0.21	0.18	1.47	0.44	0.34
PRDX1	1.01	0.04	0.04	1.22	0.09	0.08	0.89	0.06	0.06	1.27	0.23	0.20
SEPP1	1.10	0.23	0.19	1.03	0.02	0.02	1.01	0.21	0.18	0.52	0.03	0.03
SLC30A1	1.55	0.54	0.40	**2.28**	1.40	0.87	1.48	0.31	0.25	**7.60**	1.76	1.43
SOD1	0.98	0.14	0.12	1.08	0.18	0.15	0.88	0.11	0.10	1.15	0.15	0.13
SOD2	0.83	0.01	0.01	0.80	0.07	0.06	1.24	0.22	0.19	0.97	0.15	0.13
SULT1A	1.04	0.09	0.09	0.96	0.19	0.16	1.03	0.28	0.22	0.60	0.23	0.17
TFRC	0.93	0.24	0.19	0.82	0.05	0.05	0.92	0.01	0.01	0.92	0.22	0.18
TXN	1.55	0.41	0.32	1.55	0.17	0.16	1.09	0.10	0.10	1.77	0.49	0.38
TXNRD1	**4.18**	4.24	2.10	**3.38**	1.21	0.89	1.74	0.63	0.46	**3.14**	1.42	0.98
HMOX1	**8.47**	17.22	5.68	**21.78**	15.90	9.19	**2.79**	0.59	0.49	**67.93**	29.17	20.41
HSPA1A	0.94	0.07	0.06	**24.33**	14.38	9.04	1.19	0.11	0.10	**98.75**	385.45	78.61
IL8	**73.86**	59.55	32.97	**5.13**	1.56	1.19	**9.90**	2.54	2.02	**11.13**	4.41	3.16
NFKB1	1.06	0.11	0.10	0.68	0.05	0.05	1.00	0.11	0.10	0.68	0.08	0.07
NFKBIA	1.35	0.62	0.43	0.67	0.08	0.07	1.30	0.35	0.27	0.75	0.30	0.22
NFKB2	1.62	0.55	0.41	1.33	0.52	0.37	1.64	0.33	0.27	1.77	0.67	0.49
CCND1	0.94	0.18	0.15	0.87	0.03	0.03	0.91	0.26	0.20	0.74	0.14	0.12
CDKN1A1	**2.69**	2.80	1.37	1.59	0.55	0.41	**3.02**	1.16	0.84	**3.44**	1.47	1.03
CDKN1B	1.19	0.07	0.07	0.76	0.03	0.03	0.91	0.27	0.21	**0.53**	0.15	0.12
CDKN2B	1.11	0.15	0.13	0.94	0.09	0.08	**1.99**	0.44	0.36	**1.80**	0.45	0.36
E2F1	0.71	0.24	0.18	0.75	0.09	0.08	0.74	0.16	0.13	0.50	0.11	0.09
EGFR	1.31	0.44	0.33	0.97	0.11	0.10	1.91	0.47	0.38	1.74	0.56	0.43

JUN	**3.68**	1.42	1.03	**1.94**	1.08	0.69	**2.81**	0.51	0.43	**4.53**	1.73	1.25
MAP3K5	0.82	0.12	0.11	0.79	0.07	0.06	1.03	0.11	0.10	0.78	0.10	0.09
MDM2	1.31	0.19	0.16	1.08	0.07	0.07	1.39	0.16	0.14	1.13	0.22	0.19
MYC	1.19	0.13	0.12	0.94	0.01	0.01	0.93	0.11	0.10	0.55	0.14	0.11
PLK3	1.55	0.41	0.32	1.23	0.14	0.12	**2.91**	1.00	0.74	**2.19**	0.63	0.49
PPM1D	1.01	0.20	0.17	0.91	0.11	0.10	1.04	0.21	0.17	0.99	0.26	0.21
SIRT2	0.92	0.14	0.12	1.16	0.21	0.18	1.68	0.47	0.37	1.76	0.77	0.53
TP53	1.84	0.31	0.26	1.21	0.06	0.06	**2.51**	0.14	0.13	1.45	0.12	0.11
APEX1	0.85	0.04	0.04	0.84	0.05	0.04	0.80	0.07	0.07	0.63	0.04	0.04
ATM	1.42	0.04	0.04	1.20	0.05	0.05	1.10	0.23	0.19	0.92	0.25	0.20
ATR	0.87	0.10	0.09	0.90	0.22	0.18	0.83	0.20	0.16	0.79	0.06	0.06
BRCA1	1.24	0.18	0.16	1.09	0.10	0.10	1.22	0.15	0.13	0.90	0.12	0.11
BRCA2	1.12	0.11	0.10	1.00	0.08	0.08	1.15	0.13	0.12	0.82	0.13	0.12
DDB1	0.99	0.25	0.20	0.93	0.06	0.06	1.01	0.10	0.09	0.95	0.15	0.13
DDB2	0.87	0.27	0.20	0.77	0.07	0.06	1.23	0.03	0.03	0.80	0.03	0.03
ERCC1	1.10	0.17	0.15	0.92	0.02	0.02	1.66	0.32	0.27	1.79	0.57	0.43
ERCC2	0.66	0.32	0.21	0.77	0.11	0.09	0.94	0.10	0.09	0.87	0.25	0.20
ERCC4	1.12	0.11	0.10	0.83	0.01	0.01	0.90	0.22	0.18	0.60	0.17	0.14
ERCC5	1.17	0.07	0.06	1.02	0.02	0.02	1.35	0.22	0.19	1.21	0.40	0.30
LIG1	0.89	0.13	0.11	0.87	0.09	0.08	0.74	0.23	0.17	0.58	0.12	0.10
LIG3	0.95	0.17	0.14	0.92	0.05	0.04	0.82	0.16	0.13	0.66	0.15	0.12
MGMT	0.93	0.18	0.15	0.83	0.15	0.13	1.19	0.08	0.08	0.91	0.02	0.02
MLH1	1.56	0.30	0.25	1.35	0.13	0.12	**2.32**	0.50	0.41	**2.30**	0.46	0.38
MSH2	0.86	0.10	0.09	0.85	0.06	0.05	0.43	0.04	0.04	0.33	0.02	0.02
OGG1	0.76	0.10	0.09	0.89	0.04	0.04	1.10	0.32	0.25	1.00	0.27	0.21
PARP1	0.81	0.15	0.13	0.73	0.04	0.04	0.80	0.07	0.07	0.62	0.06	0.06
PCNA	0.78	0.22	0.17	0.88	0.17	0.14	**0.55**	0.05	0.05	**0.46**	0.07	0.06
POLB	1.01	0.13	0.11	0.93	0.03	0.03	1.25	0.37	0.28	1.17	0.22	0.19
POLD1	0.78	0.17	0.14	0.86	0.24	0.19	0.76	0.22	0.17	0.70	0.22	0.17
RAD50	1.22	0.15	0.13	1.04	0.11	0.10	1.13	0.24	0.20	0.89	0.17	0.14
RAD51	0.88	0.10	0.09	0.98	0.03	0.03	0.82	0.03	0.03	0.74	0.14	0.12
RRM2B	1.12	0.10	0.09	0.90	0.06	0.05	1.37	0.17	0.15	0.96	0.14	0.12
XPA	1.14	0.03	0.03	0.97	0.12	0.11	0.96	0.10	0.09	0.91	0.20	0.17
XPC	1.15	0.16	0.14	0.91	0.10	0.09	1.18	0.09	0.08	0.92	0.15	0.13
XRCC5	0.91	0.13	0.11	0.85	0.07	0.06	0.72	0.12	0.10	0.60	0.15	0.12
APAF1	0.83	0.11	0.10	0.98	0.05	0.05	1.06	0.25	0.20	0.89	0.24	0.19
BAX	0.94	0.28	0.22	0.97	0.06	0.06	1.22	0.39	0.30	1.02	0.33	0.25
BBC3	**5.75**	2.63	1.81	**2.33**	0.70	0.54	**5.66**	0.87	0.75	**4.02**	1.64	1.17
BCL2	1.00	0.21	0.18	0.94	0.11	0.10	0.78	0.29	0.21	0.54	0.17	0.13
BCL2L1	1.11	0.36	0.27	1.10	0.24	0.20	**2.08**	0.31	0.27	1.88	0.37	0.31
PMAIP1	**1.96**	0.52	0.41	1.53	0.18	0.16	**2.13**	0.63	0.48	**2.85**	0.62	0.51
TNFRSF10B	**2.63**	1.04	0.74	1.55	0.14	0.13	**3.51**	0.25	0.23	**3.05**	0.49	0.43
XIAP	1.40	0.42	0.33	1.07	0.24	0.19	1.71	0.49	0.38	1.78	0.73	0.52

9.6.2 Enzymatic activities of catalase and SOD

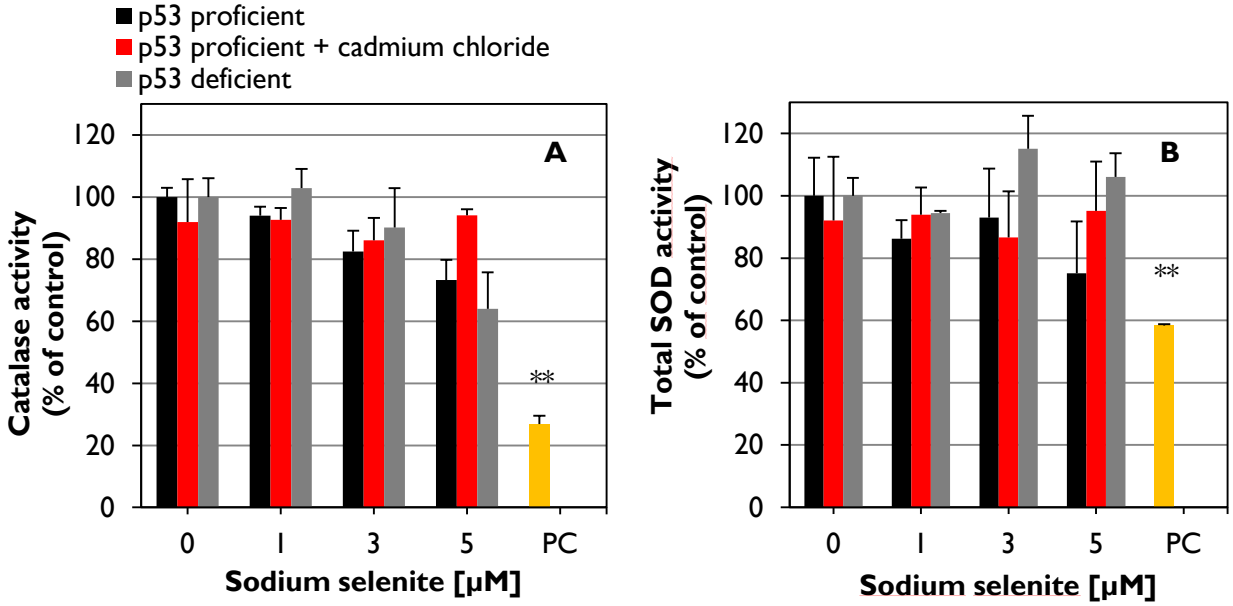

Figure A1: Impact of sodium selenite in the combination with cadmium chloride on (A) CAT enzyme activity and (B) SOD enzyme activity in p53-proficient and p53-deficient HCT116 cells after 24 h incubation. 50 mM sodium azide (6 h) served as CAT positive control. CAT activity was determined by detection of decomposition of H_2O_2 at 240 nm. 50 mM diethyldithiocarbamate (DDC)(6 h) served as SOD positive control. Total SOD activity was determined by detection of superoxide radicals generated by xanthine oxidase and hypoxanthine, whereby SOD dismutates the superoxide radical (WST-1). Mean values ± SD of three independent experiments are shown.

9.6.3 ROS detection

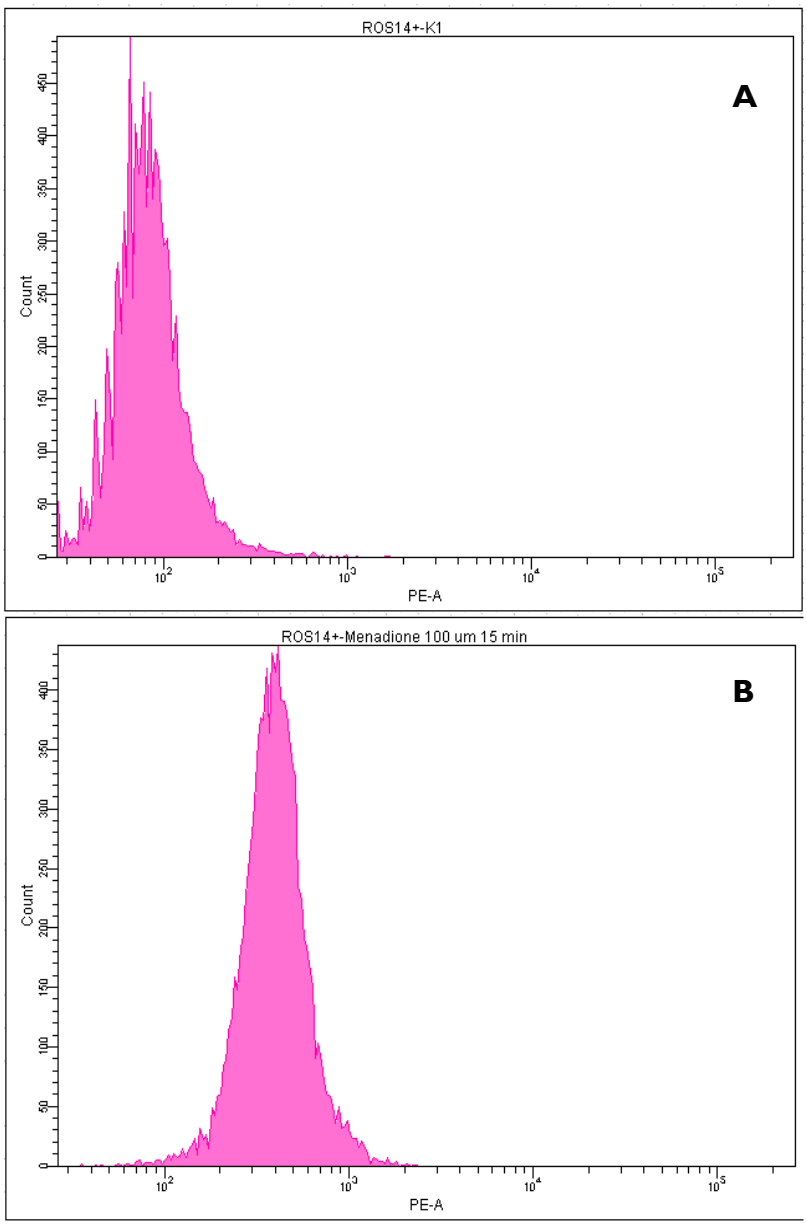

Figure A2: Example of histograms depicting increased PE signal and thereby oxidized DHE, indicating increased superoxide production in (A) untreated p53-proficient HCT116 control cells and (B) 15 min 100 µM menadione-treated cells.

9.6.4 Cell cycle distribution

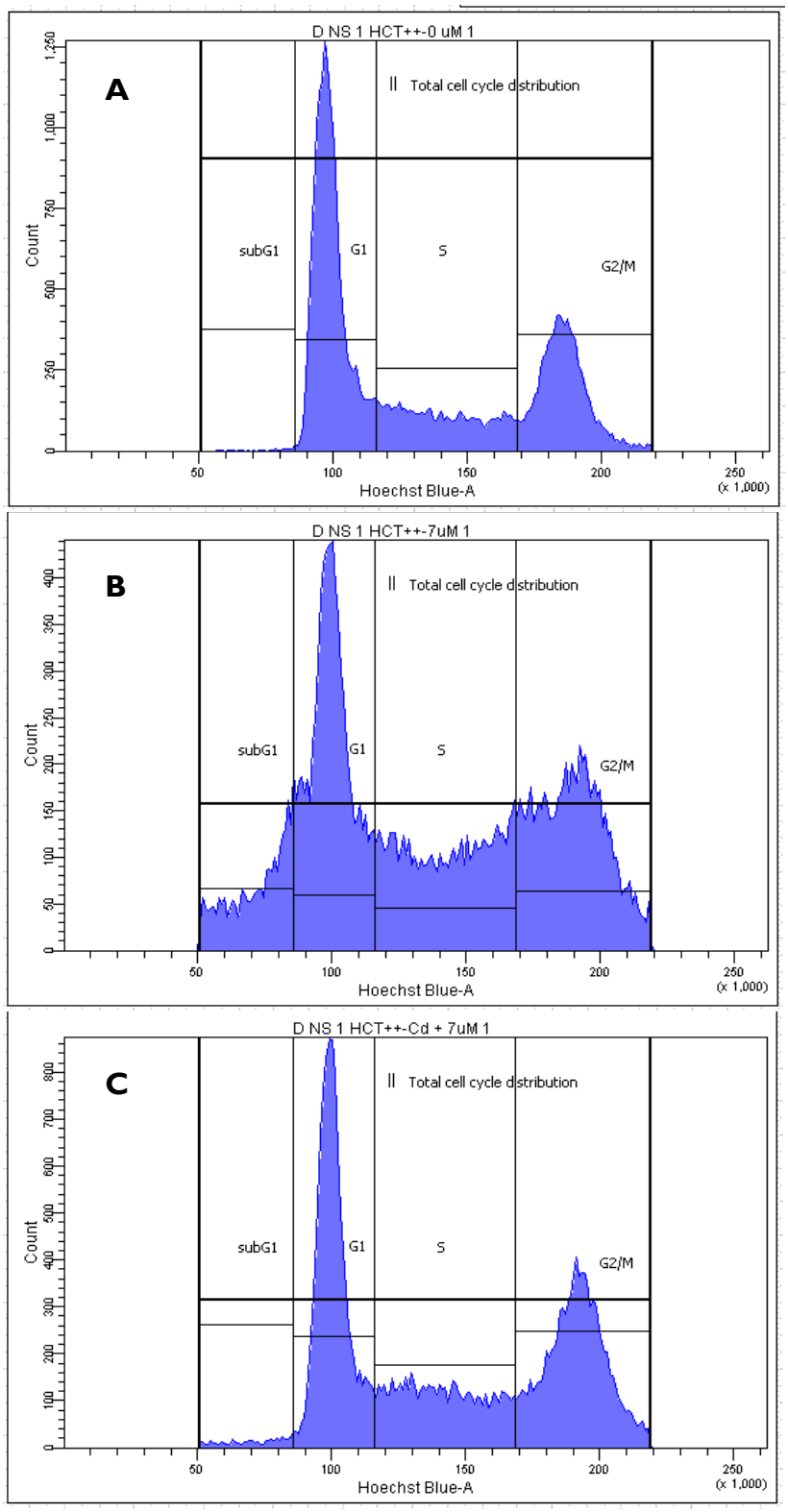

Figure A3: Cell cycle distribution depicted as histograms in (A) untreated p53-proficient HCT116 control cells, (B) sodium selenite treated cells (7 µM, 24 h) and (C) 24 h co-incubation with 10 µM cadmium chloride and 7 µM sodium selenite co-treated cells

9.6.5 Cell death analysis

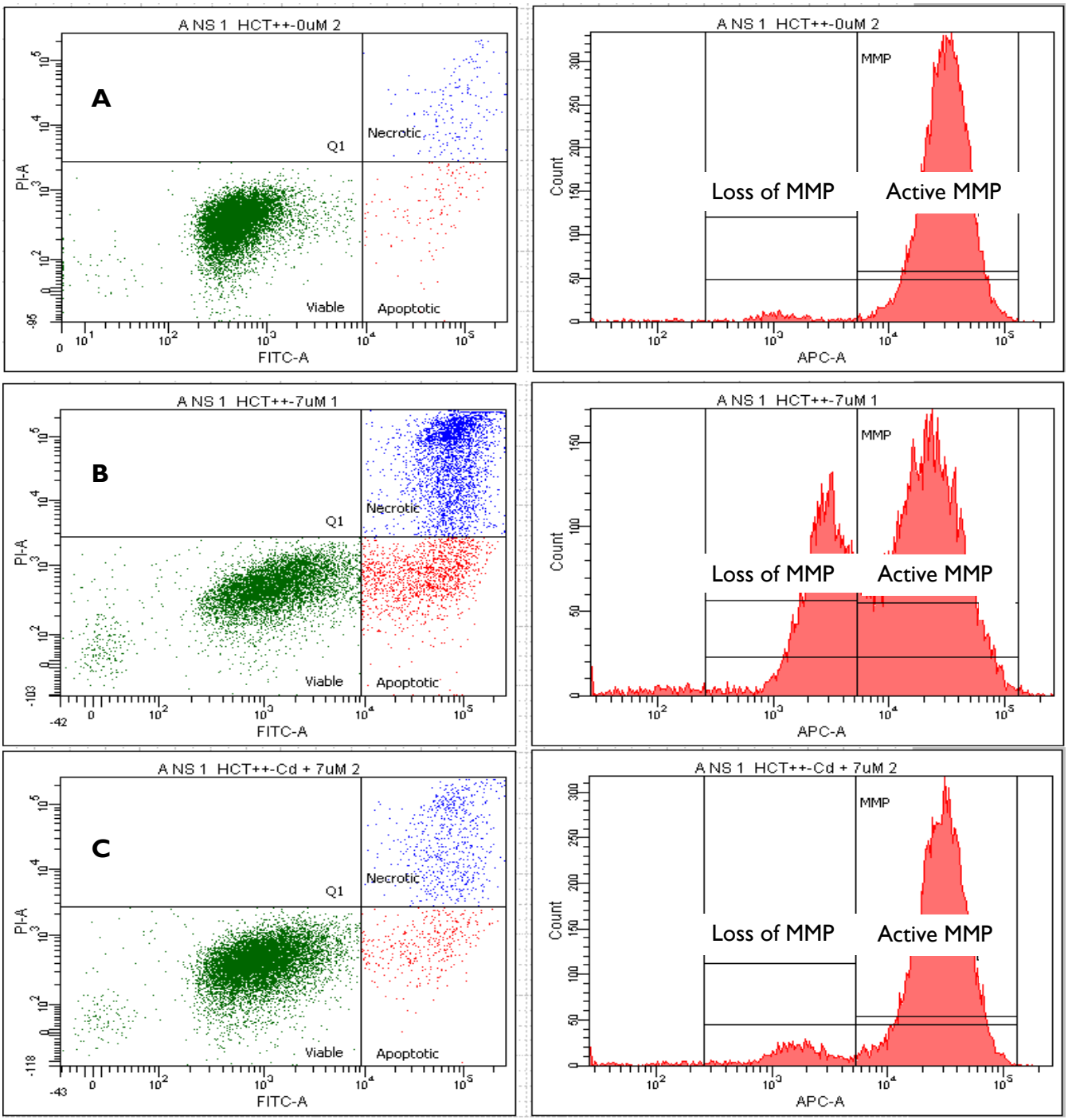

Figure A4: Example of scatter plots of propidium iodide (PI) and Annexin V-FITC stained cell populations as well as histograms displaying changes in mitochondrial membrane potential in (A) untreated p53-proficient HCT116 control cells, (B) sodium selenite treated cells (7 µM, 24 h) and (C) with sodium selenite (7 µM) and cadmium chloride (10 µM) 24 h co-incubation

10 Publication list

Publications

- B. M. Fischer, D. Neumann, A. L. Piberger, S. F. Risnes,, A. Hartwig. "*Gene expression profiling to assess the impact of chemical substances on genomic stability: Use of high throughput RT-qPCR*". Paper submission to BMC Genomics.

- S.F. Risnes, A. Hartwig. "*Differential cellular effects of sodium selenite and selenomethionine in HCT116 cells: Involvement of tumor suppressor protein p53*". Paper in preparation

- S.F. Risnes, A. Hartwig. "*Cadmium inhibits p53-mediated apoptosis induced by sodium selenite in HCT116 cells*". Paper in preparation

Published abstracts

- S. F. Risnes, A. Hartwig (2015). *Impact of cadmium on antioxidant enzymes in HCT116 cells and protective interaction by selenium.* Perspectives in Science. 3 (1–4), 55.

Oral conference presentations

- South West Regional Association of the Food Chemistry Society (LChG, section in German Chemical Society (GDCh), 2013 19. - 2 0. March 2013 in Karlsruhe, Germany, "*Inhibition of selenite-induced apoptosis by cadmium in HCT116 cells",* S. F. Risnes, V. Klaus, A. Collins, A. Hartwig

Conference poster presentations

- 42nd Annual Meeting European Environmental Mutagen Society (EEMS), 16. - 20. September 2012 Warshaw, Poland, "*Impact of cadmium on apoptosis induced by different selenium compounds in HCT116 cells",* S. F. Risnes, V. Klaus, A. Collins, A. Hartwig

- Selen2012 Workshop, 8. – 9. October 2012 in Karlsruhe, Germany, "*Impact of cadmium on apoptosis induced by different selenium compounds in HCT116 cells",* S. F. Risnes, V. Klaus, A. Collins, A. Hartwig

- 28th Annual Meeting of German Society for Minerals and Trace Elements Society (GMS), 11. – 13. October 2012 in Karlsruhe, Germany, "*Impact of cadmium on apoptosis induced by different selenium compounds in HCT116 cells",* S. F. Risnes, V. Klaus, A. Collins, A. Hartwig

- Toxicology Net-BW Symposium 2012, 23. November 2012 in Karlsruhe, Germany; "*Cadmium is inhibiting selenite-induced apoptosis in human colon cancer cells",* S. F. Risnes, V. Klaus, A. Collins, A. Hartwig

- 10th International Symposium on Selenium in Biology and Medicine (SELENIUM 2013), 14. - 18. September 2013 in Berlin, Germany, "*Impact of cadmium on antioxidant enzymes in HCT116 cells and protective interaction by selenium",* S. F. Risnes, A. Hartwig

- 29th Annual Meeting of the German Society for Minerals and Trace Elements Society (GMS), 13. – 15. September 2013 in Berlin, Germany "*Impact of cadmium on antioxidant enzymes in HCT116 cells and protective interaction by selenium",* S. F. Risnes, A. Hartwig

- 43rd Annual Meeting of the German Chemical Society (GDCh), 22. – 24. September 2014 in Gießen, Germany, "*Global gene expression responses to different selenium species in mammalian cells" ,* S. F. Risnes, A. Hartwig

Poster award

- Best Poster Award at the 29th Annual Meeting of the German Society for Minerals and Trace Elements Society (GMS), 13. – 15. September 2013 in Berlin, Germany "*Impact of cadmium on antioxidant enzymes in HCT116 cells and protective interaction by selenium",* S. F. Risnes, A. Hartwig

11 Acknowledgements

I would first of all express my very sincere thanks to Professor Andrea Hartwig for the supervision during my entire doctorate. Thank you for providing me with the opportunity to continue the exciting topic I started during my master thesis, thank you for your patience and your support.

Sincere thanks goes to Professor Mirko Bunzel for kindly agreeing to act as second examiner of my dissertation.

I wish to thank my all fellow colleagues in both working groups of Professors Hartwig and Bunzel, especially I owe my cordial thanks: to Beate, Betty, Judith, Rachel and Rebecca. For all good advice, support and co-operation in the lab. For the love, humor and laughter, but also sorrow, and of course for all the food we have shared. For the friendships we have developed. Rachel, thanks for breaking language barriers together, for the early jogs, for the birthday celebrations. Simply, thank you for your friendship. Beate and Rachel, thank you for taking your precious time to proof-read and edit my thesis in order to achieve flawless grammar. I am truly grateful. To Liza, my long-term office partner and my Scrabble contestant, thank you for the time in Karlsruhe. To Elena and Barbara, who have always had an open door and ear for me. To Matze, thank you for your contagious mood. I am also very thankful to my three diploma students Dorothee, Julia and Jennifer. Thank you for the good work and time we have spent together. Doro, thank you for the little time together as office partners, and of course for proof-reading my dissertation's abstract in German. To Sonya, thank you for being you. You brighten the day.

A huge gratitude goes to my beloved family, who has expanded over the years: to my father Bent and my siblings Bent Andre, Edvard, Julie, Michael, Lina, and nonetheless my partner-in-crime and doppelganger, namely my twin sister Louise. Thank you for your support and understanding of my choice of life path in Germany. To all of my dear funny, lovely and curious nephews and nieces, Jesper, Bo Herman, Albert, Dennis, Signe, Maja, Hilde and Lissie-to-come. To my finest almost-son Jens, who carries the genes of his mother and me. I love you all. Our wonderful mother would have been so proud of us!

To my closest friends, Idunn, Mari, Hedda, and naturally Louise. I truly treasure our long lasting friendship. The Fives must go on!

Last, but not least, to my brand-new husband and love of my life. Without your love, support and comfort, I would be lost. Looking forward to continuing our amazing journey!